Deciphering the Roles of the HCMV Chemokine Receptors in Viral Latency & Reactivation

Samuel Medica

A DISSERTATION

Submitted to the Department of Molecular Microbiology and Immunology

Oregon Health and Science University

School of Medicine

In Partial Fulfillment of the Requirements for the Degree of Doctor of Philosophy

November 7th, 2025

“Every single day, in every walk of life, ordinary people do extraordinary things.”

-Jim Valvano

Dissertation Advisory Committee

Daniel N. Streblow, Ph.D., *Dissertation Research Advisor*

Alec J. Hirsch, Ph.D., *Member & Chair*

Meaghan H. Hancock, Ph.D., *Member*

Braden T. Lobingier, Ph.D., *Member*

Patrizia Caposio, Ph.D., *External Member*

I. Table of Contents

II. Common Abbreviations

Abv	Abbreviation		**Abv2**	Abbreviation2
mya	Million years ago		**TRL**	Terminal repeat long
HSV	Herpes simplex virus		**TRS**	Terminal repeat short
EBV	Epstein-Barr Virus		**IRL**	Internal repeat long
HCMV	Human cytomegalovirus		**IRS**	Internal repeat short
HHV	Human herpesvirus		**ORF**	Open reading frame
KSHV	Kaposi's sarcoma-associated herpesvirus		**PDGFR**	Platelet-derived growth factor receptor
FDA	Food and Drug Administration		**TGFβR**	Transforming growth factor β receptor
HPC	Hematopoietic progenitor cell		**NRP2**	Neuropilin 2
KS	Kaposi's sarcoma		**MIEP**	Major immediate early promotor
HIV	Human immunodeficiency virus		**IE**	Immediate early
AIDS	Acquired immunodeficiency syndrome		**oriLyt**	Lytic origin of DNA replication
ART	Antiretroviral therapy		**NLS**	Nuclear localization signal
HLA	Human leukocyte antigen		**VAC**	Viral assembly compartment
UL	Unique long		**TGN**	Trans Golgi network
US	Unique short		**EGFR**	Epidermal growth factor receptor
gX	Glycoprotein-X		**TNFR1**	Tumor necrosis factor receptor 1
VLP	Virus like particle		**PI3K**	phosphatidylinositol 3-kinase
MVA	Modified vaccinia Ankara		**dpi**	Days post-infection
NEIP	Non-infectious Enveloped Particle		**MAPK**	Mitogen-activated protein kinases
MCP	Major capsid protein		**NFκB**	nuclear factor kappa-light-chain-enhancer of activated B cells

mCP	Minor capsid protein		**STAT**	Signal Transducer and Activator of Transcription
mCBP	Minor capsid binding protein		**NO**	Nitric oxide
SCP	Smallest capsid protein		**Flt3**	Fms-like tyrosine kinase 3
GRK	G protein-coupled receptor kinases		**IER5**	Immediate early response 5
NRF1	Nuclear respiratory factor 1		**LUNA**	Latency -associated transcript
ARE	Antioxidant response element		**CREB**	cAMP response element-binding protein
NFAT	Nuclear factor of activated T cells		**EGR1**	Early growth response 1
GM-CSF	Granulocyte-macrophage colony stimulating factor		**GPCR**	G protein-coupled receptor
G-CSF	Granulocyte colony stimulating factor		**CCKR**	Conventional chemokine receptor
hESC	Human embryonic stem cell		**ACKR**	Atypical Chemokine receptor
huNSG	Humanized NOD/SCID/IL2Rγ^{null}		**TM**	Transmembrane
huBLT	Humanized bone marrow/liver/thymus		**GEF**	guanine nucleotide exchange factor
RGS	Regulator of G-protein signaling		**PKA**	Protein kinase A
DAG	Diacylglycerol		**IP3**	Inositol trisphosphate
RGS	Regulator of G-protein signaling			

III. Dedication

This body of work is the product of many years filled with good times, failures, bad jokes, laughter, struggle, learning experiences, growth, and perseverance.

First and foremost, I would like to thank my parents, Denise and Paul Medica. Thank you for making sacrifices to provide me with all the love, support, and opportunity I'll ever need.

To my mentor, Dan Streblow, thank you for teaching me "the game," for your patience, and for always keeping me looking on the bright side of life. I'll never forget the fun times we've shared both in and outside of graduate school. I'm truly grateful for the countless lessons about science and life, and for your mentorship over the past five years.

To my committee members, Meaghan Hancock, Alec Hirsch, Braden Lobingier, and Patrizia Caposio, thank you for your guidance and support.

To my co-defendants in the Streblow Laboratory, Mike Denton, Craig Kreklywich, Whitney Weber, Hannah Jaeger, Gauthami Sulgey, Adam Mayo, Lydia Pung, Zach Streblow, Takeshi Ando, Patsy Smith, Brenden Bartsch, Brayden Graves, and Pam Streblow, thank you for helping and guiding me along the way. It truly takes a village, and each of you contributed in your own unique way.

To the PPG team, thank you for your advice and helpful feedback throughout this journey.

To all my friends at the VGTI, especially Nicole Diggins and Aaron Dirck, thank you for your advice, guidance, and patience in helping me along the way.

Finally, to my fellow students in the PBMS 2021 cohort, thanks for all the rounds of golf, great trips, and cold pints.

IV. Abstract

Human cytomegalovirus (HCMV) is a pervasive β-herpesvirus that establishes lifelong persistence within the host by adopting a latent state in hematopoietic progenitor cells (HPCs). Periodic reactivation from latency poses significant risks to immunocompromised individuals and contributes to HCMV-associated disease, yet the viral and host mechanisms governing this process remain incompletely defined. Among HCMV's gene products, a subset of virally encoded G protein-coupled receptors (vGPCRs) have emerged as critical regulators of latency and reactivation. This dissertation investigates the molecular signaling properties, interactomes, and functional consequences of two vGPCRs, US28 and UL78, in order to delineate how HCMV manipulates host pathways to persist and reactivate from latent infection.

In the first study, proximity-dependent labeling was employed to comprehensively define the US28 interactome during both latent and lytic infection. These analyses revealed that US28 signaling converges upon RhoA and EGFR transduction cascades and identified RhoGEFs as essential intermediates. Pharmacological inhibition of RhoGEFs abrogated viral reactivation in $CD34^+$ HPCs and in a humanized mouse model, underscoring their necessity for HCMV persistence. This work not only expanded the catalog of US28-associated proteins but also established the utility of proximity labeling approaches to dissect dynamic viral signaling complexes.

The second study focused on mechanistic determinants of US28 signaling. Through mutational analysis of the third intracellular loop, specific residues (S218, K223, R225) were identified as critical for coupling to multiple Gα isoforms and for activating MAPK and RhoA signal transduction pathways. Mutations at these sites selectively impaired signaling without disrupting receptor localization or internalization, thereby uncoupling structural determinants of function from receptor trafficking. Functionally, these signaling-deficient mutants failed to support efficient reactivation from latency in vitro and in vivo. Together, these findings define discrete molecular features of US28 that are indispensable for viral reactivation and highlight candidate targets for therapeutic intervention.

The third study extended this analysis to UL78, a vGPCR with previously undefined roles in infection. Using recombinant viruses, we demonstrated that UL78 is essential for reactivation and requires intact $G\alpha_i$ coupling via a conserved DRL motif. Proximity-dependent labeling identified several nuclear-localized proteins, including nuclear pore complex proteins, transcriptional regulators, and viral gene products. Orthogonal approaches confirmed a subset of UL78 localizes to the nucleus during infection, suggesting novel roles for this receptor in regulating viral genome accessibility and transcription. These findings reveal UL78 as an unexpected nuclear signaling scaffold that contributes to the orchestration of reactivation.

Collectively, this dissertation establishes that the HCMV vGPCRs US28 and UL78 exploit distinct but complementary signaling modalities to control latency and reactivation in progenitor cells. By delineating their interactomes, signaling mechanisms, and functional requirements, these studies advance our understanding of HCMV pathogenesis and provide a foundation for the development of targeted antiviral strategies

Chapter 1: Introduction

Section 1.1: Preface – Herpesviridae

The order of *Herpesvirales* consists of large double-stranded DNA viruses, which are among the oldest and most evolutionarily successful viruses studied. Families include *Alloherpesviridae* (infecting frogs and fish), *Malacoherpesviridae* (infecting mollusks), and *Herpesviridae* (infecting birds, reptiles, and mammals). The latter encompasses over 150 viruses spread across three subfamilies including the α-, β-, and γ-herpesviruses. Generally, subfamilies are categorized based on host tropism, replication kinetics, and genetic similarity. Virions for all subfamilies are typically 200 – 250 nanometers (nm) in diameter and consist of a double-stranded DNA genome of approximately 110 – 235 kilobases (kb) in size packaged within an icosahedral capsid, an inner proteinaceous layer called the tegument, and an exterior lipid envelope, which houses numerous glycoproteins (1). Evolutionary divergence amongst the three subfamilies likely occurred between 180 – 210 million years ago (mya), however this date is tentative with some estimates being closer to 400 mya (2). The common ancestor to the three subfamilies contributed 43 genes that are positionally conserved and are often associated with the core viral replication machinery (3). Although the family of *Herpesviridae* is quite large, there are only nine viruses known to routinely infect humans: herpes simplex virus 1 and 2 (HSV-1 and HSV-2), varicella zoster virus (VZV), Epstein-Barr virus (EBV), human cytomegalovirus (HCMV), human herpesviruses 6A and 6B (HHV-6A and HHV-6B), human herpesvirus 7 (HHV-7), and Kaposi's sarcoma-associated herpesvirus (KSHV) (1). In rare circumstances the macaque Cercopithecine herpesvirus 1, also known as B-Virus, has been shown to infect humans leading to life threatening encephalitis (4). Despite a robust and sustained immune response against herpesviruses, primary infection cannot be cleared due to the ability of these viruses to establish life-long latent infections within their respective hosts (5). During the latent phase of infection, no new virions are produced, and the infection lies dormant, however, viral reactivation events are quite common and are often preceded by immunosuppression, inflammation, or stress. Consequently, global seroprevalence for members of the *Herpesviridae* family is quite high making these viruses amongst the most clinically relevant pathogens.

1.1.1 α-Herpesviruses

The α-herpesviruses relevant to human health are HSV-1 (HHV-1), HSV-2 (HHV-2), and VZV (HHV-3). All are characterized by a relatively short replication cycle where they infect mucocutaneous epithelial cells resulting in the formation of large multinucleated cells (6,7). After primary infection, these viruses enter peripheral neurons and travel retrogradely to the cell bodies, where they establish life-long latent infections (8). Clinically, HSV-1 is primarily associated with oral lesions and encephalitis, whereas HSV-2 is associated with genital infections. HSV-1 typically establishes latent infections in the trigeminal ganglia sensory neurons located at the base of the brain (9). These neurons innervate the oral epithelium allowing for periodic reactivation events producing characteristic oral lesions. Similarly, HSV-2 establishes latent infections within the sacral ganglia of the spine where viral reactivation leads to the formation of genital lesions (10). Seroprevalence for HSV-1 and HSV-2 are estimated to be 67% and 13%, respectively, with increasing seroprevalence in developing nations (11). Currently, there are no Federal and Drug Administration (FDA)-approved vaccines against HSV-1 or HSV-2; however, ongoing efforts have focused on subunit-based vaccines against the viral glycoprotein gD2, live-attenuated vaccines, and mRNA vaccines (12–14). Primary infection with VZV is proven to be the etiological cause of chickenpox. During primary infection, VZV can infect T-lymphocytes, neurons, and epithelial cells. Infection of the latter is responsible for skin lesions which assist in transmitting the virus to new hosts (7). Following the establishment of a latent infection within the dorsal root ganglia and waning immunity to primary infection, VZV reactivation events produce a painful skin rash called shingles typically occurring in individuals over the age of 50 (15). VZV is the only herpesvirus with an FDA-approved vaccine. Children typically receive two doses of a live-attenuated vaccine that is 95% effective at preventing subsequent infection while adults over the age of 50 receive a subunit-based vaccine against the viral glycoprotein gE, which is over 90% effective at preventing shingles (16,17).

1.1.2 β-Herpesviruses

Characterized by long replicative cycles, large genomes, strict species tropism, and extensive immune evasion capabilities; the β-herpesviruses that infect humans are: HCMV (HHV-5), HHV-

6A and -6B, and HHV-7 (18). Primary infection of HCMV in immunocompetent individuals is typically asymptomatic but can result in symptoms similar to mononucleosis. HCMV remains the most common congenital infection and the leading cause of developmental deficits in newborn infants (19). Excluding vertical transmission, the virus is typically spread through direct contact with bodily fluids. The global seroprevalence rate of HCMV has been estimated to be above 90%, making it among the most widespread pathogens (20). HCMV is capable of efficiently replicating in fibroblasts, epithelial cells, smooth muscle cells, and endothelial cells (21,22). Following primary infection, HCMV establishes latent infections within the bone marrow in $CD34^+$ hematopoietic progenitor cells (HPCs) and in circulating $CD14^+$ monocytes (23). Upon cellular differentiation of these cells, HCMV can reactivate causing health complications in immunocompromised individuals often leading to severe morbidity and mortality (this topic is covered in more detail in sections 1.2 – 1.4). There is no approved vaccine against HCMV, however, multiple candidates are in clinical trials utilizing live-attenuated, mRNA, and subunit-based vaccine platforms (24,25). HHV-6 and HHV-7 are commonly referred to as the roseoloviruses and are the cause of sixth disease; a febrile illness common in infants, which manifests through fever and rash symptoms subsiding after seven days. Nearly all individuals will be infected with either HHV-6 and/or HHV-7 by the age of 5 years and these viruses establish latent infections within T-lymphocytes and $CD34^+$ HPCs (26). Viral latency is partly achieved by integration of the viral genome into host telomeres. Integration into germline cells occurs with a frequency of 1% and results in inherited chromosomally integrated infection (27). Subsequent reactivation of the roseoloviruses is poorly understood but has been associated with systemic consequences including encephalitis and meningitis in immunocompromised hosts. Additionally, the roseoloviruses have been tangentially associated with several other diseases such as infertility, multiple sclerosis, cancer, thyroiditis, epilepsy, and chronic fatigue syndrome. There are currently no clinical trials for vaccines against HHV-6 or HHV-7, however, promising research is underway examining the efficacy of a tetrameric subunit-based vaccine against the glycoprotein complex (gH/gL/gQ1/gQ2) of HHV-6 (28).

1.1.3 γ-Herpesviruses

The γ-herpesviruses that infect humans are EBV (HHV-4) and KSHV (HHV-8). Both of these viruses share an extremely restricted host range, slow replication cycle, and strong oncogenic potential (29). For EBV specifically, primary infection occurs in epithelial cells and B-lymphocytes and is cause of infectious mononucleosis, which manifests as fever, fatigue, swollen lymph nodes, and general illness (30). Following EBV primary infection, latency is established in B-lymphocytes where periodic reactivation events cause acute illness resembling the symptoms associated with primary infection (31). During latent infection in cultured cells, EBV can immortalize B-lymphocytes leading to their prolonged lifespan and conferring indefinite cell division (32). The transforming potential of EBV makes it a significant contributor to the development of various cancers such as Burkitt's lymphoma, Hodgkin's lymphoma, non-Hodgkin's lymphoma, and nasopharyngeal carcinoma (33). The incidence of EBV-associated cancer is especially prevalent in immunocompromised individuals. Additionally, EBV infection has been associated with multiple sclerosis, although a direct link between the two remains poorly understood (34). Similar to the β-herpesviruses, seroprevalence to EBV is greater than 80% with most individuals contracting the disease during childhood or early adolescence (35). No approved vaccine against EBV exists, but there are two current clinical trials evaluating the efficacy of mRNA- and nanoparticle-based vaccines aimed at preventing primary EBV infection and an additional therapeutic vaccine aimed at ameliorating symptoms (36–38). KSHV is implicated in several significant diseases such as Kaposi's sarcoma (KS) and the lymphoproliferative disorder Multicentric Castleman Disease (39). Primary infection is the result of direct contact with bodily fluids during which the virus preferentially infects B-lymphocytes, epithelial cells, endothelial cells, and monocytes (40). Similar to EBV, KSHV undergoes latent infections within B-lymphocytes (40,41). KS, which disproportionally effects individuals who have contracted human immunodeficiency virus (HIV)/acquired immunodeficiency syndrome (AIDS), manifests itself as a vascular tumor that presents purplish skin lesions and can also involve mucous membranes or internal organs such as the gastrointestinal tract or lungs leading to life-threatening complications (42). The seroprevalence of KSHV is highly dependent on geographical location and other socioeconomic factors. In the United States, seroprevalence hovers between 3 – 7%,

however, this number can reach greater than 40% in Sub-Saharan Africa (43,44). Despite its significant impact on human health, research on a vaccine against KSHV limited, primarily due to the lack of a suitable animal model for testing candidate approaches.

Section 1.2: Human Cytomegalovirus – "The Silent Burden"

1.2.1 Seroprevalence and Epidemiology of HCMV

Described as "the silent burden", HCMV is a ubiquitous pathogen affecting people of all ages across the globe (45). In adults, global seroprevalence is estimated to be between 45 – 100% with variance across geographical regions, socioeconomic status, and existing risk factors. In adults living in the United States or Canada, seroprevalence hovers around 54%, which is in stark contrast to adults living in Latin America where the incidence rate reaches greater than 95% (46,47). In all instances, seroprevalence is higher in women of childbearing age than in men. Most individuals are infected with HCMV during infancy, acquiring infection from contaminated breast milk or through contact with other infected children. Transmission occurring later in life is typically associated with sexual contact, blood transfusions, organ transplantation, and contact with infected children. Because HCMV infection cannot be cleared by the immune system, seroprevalence increases steadily with age due to cumulative exposures over time. Socioeconomic status, crowded living conditions, and limited access to healthcare are strongly associated with earlier and more frequent HCMV exposure. In immunocompetent populations, primary infection of HCMV is typically subclinical but can result in viremia, fever, fatigue, and transient bone marrow suppression (48–50). In immunocompromised populations, HCMV infection can lead to severe disease manifesting several symptoms such as leukopenia, malaise, arthralgia, retinitis, organ inflammation, and in extreme cases end-stage organ failure (51–53).

1.2.2 Congenital HCMV Infection

HCMV remains the most common global congenital infection, with an estimated incidence of approximately 0.5%. In utero transmission can occur during primary infection, superinfection (reinfection with a new strain), or during viral reactivation; however, primary maternal infection

carries the highest risk for fetal transmission and severe outcomes (54). While most infants born with a congenital HCMV infection are asymptomatic at birth, about 10–15% of these children develop long-term sequelae such as sensorineural hearing loss, neurodevelopmental delay, and vision impairment (54,55). Symptomatic neonates may present symptoms such as jaundice, petechiae, hepatosplenomegaly, microcephaly, or intrauterine growth restriction. Up to 90% of symptomatic neonates will experience a lasting disability (54,55). The timing of maternal CMV infection during pregnancy greatly influences the risk of vertical transmission and severity of clinical outcomes. The incidence of vertical transmission increases with gestational age; however, severe disease is most often restricted to infection during the first trimester of pregnancy (56,57). Brain injury induced by CMV congenital infection may be the result of uncontrolled viral replication, immune-mediated damage by cytotoxic $CD8^+$ T-lymphocytes, and fetal hypoxia in the presence of placental damage (58). Antiviral therapy may improve outcomes in symptomatic infants, but no curative treatment exists. Preventive strategies focus on hygiene measures during pregnancy, particularly for seronegative women, as no licensed vaccine is currently available to prevent congenital transmission.

1.2.3 HCMV Infection in AIDS Patients

HCMV is a significant opportunistic pathogen in HIV^+ individuals living with AIDS, particularly in the context of advanced immunosuppression. In patients with untreated or late-stage AIDS, profound $CD4^+$ T-cell depletion impairs immune control of latent HCMV, leading to viral reactivation and end-organ disease (59). The most frequent manifestation was HCMV retinitis, a progressive necrotizing retinal infection that could lead to irreversible vision loss if untreated (52,60). Other manifestations include esophagitis, colitis, pneumonitis, and encephalitis. The risk of HCMV-associated disease increases significantly when $CD4^+$ counts fall below 50 cells per µL (61). With the introduction of antiretroviral therapy (ART), the incidence of HCMV disease has declined substantially due to improved immune reconstitution. However, HCMV remains a serious threat in individuals with delayed diagnosis, poor ART adherence, or virologic failure. Management includes antiviral therapy with agents such as ganciclovir or valganciclovir, as well

as effective HIV suppression to restore immune function. Continued vigilance is required in immunocompromised populations to prevent disease progression.

1.2.4 Transplant Recipients and HCMV Infection

HCMV infection represents one of the most substantial infectious pathogens in transplant medicine, contributing significantly to morbidity and mortality in both solid organ and stem cell allograft transplant recipients. Transplant recipients are vulnerable to HCMV infection via primary infection, super infection, and reactivation from latent infection. Donor seropositive to recipient seronegative combinations are the highest risk for HCMV-associated complications (62). HCMV promotes chronic rejection, reduces graft and patient survival, and increases the incidence of tissue invasive disease including pneumonitis, colitis, hepatitis, and retinitis (63). Notably, HCMV pneumonia remains a major concern with fatality rates reaching 50% despite antiviral therapy (64). Cardiac grafts are especially susceptible, with HCMV infection contributing to reduced graft survival and the development of transplant vascular sclerosis. Graft vasculature serves as a primary target for HCMV-mediated injury, and elevated cytokine levels, particularly interleukin-6, have been correlated with HCMV-associated disease in bone marrow transplant recipients (65,66). These effects are intensified by human leukocyte antigen (HLA) mismatches between donor and recipient. Ongoing research is focused on improving diagnostic techniques, developing less toxic antiviral agents, and advancing vaccine candidates to reduce the burden of HCMV. Until more effective therapeutics exist, effective HCMV management remains integral to improving outcomes in transplant recipients.

1.2.5 HCMV Infection and Incidence of Cancer

HCMV has been increasingly implicated in the development and progression of several malignancies, though its role remains controversial and not definitively causal. HCMV is not classified as an oncogenic virus; however, it exhibits several oncomodulatory properties that may contribute to tumorigenesis, particularly in immunocompromised individuals. HCMV DNA, proteins, and transcripts have been detected in various tumor tissues, including glioblastoma, colorectal cancer, breast cancer, and prostate cancer (67). The virus can modulate key cellular

pathways involved in proliferation, apoptosis, angiogenesis, and immune evasion. Multiple hypotheses have been proposed to elucidate the role of HCMV in cancer development. One proposed mechanism is the "hit and run" hypothesis, in which HCMV initiates cellular transformation but is not required for the maintenance of the malignant phenotype (68,69). An alternative framework characterizes HCMV's involvement in cancer as "oncomodulation," wherein the virus does not directly transform cells but instead enhances the malignant potential of already-transformed cells (70). While evidence supports a strong association between HCMV and certain cancers, further research is needed to determine whether HCMV acts as a true cofactor in oncogenesis or as an opportunistic passenger exploiting the tumor environment.

Section 1.3: Therapeutics and Prophylactics Against Human Cytomegalovirus

1.3.1 FDA-Approved Antivirals and Therapeutics

Even though development of effective antivirals against HCMV began more than three decades ago, there are only five FDA-approved antivirals used to treat and/or prevent CMV associated disease. Broadly, they can be broken up into three categories: polymerase-targeting agents, terminase inhibitors, and kinase inhibitors. Ganciclovir, administered intravenously, and its oral prodrug valganciclovir represent the cornerstone of HCMV therapy (71). Both small molecules require phosphorylation by the viral kinase (UL79), followed by conversion to the active triphosphate form, which inhibits the viral DNA polymerase (UL54) via chain termination (71,72). Valganciclovir's favorable oral bioavailability has made it the preferred agent for prophylaxis in high-risk solid organ transplant recipients, as well as for the treatment of CMV viremia and end-organ disease (73,74). Foscarnet and Cidofovir, a pyrophosphate analog and a nucleoside analog, respectively, directly inhibit UL54 polymerase via chain termination without requiring prior activation (75,76). Foscarnet and Cidofovir usage is limited to CMV retinitis in AIDS, although both retain a role as salvage therapies in resistant or refractory transplant-associated disease (77,78). Despite their widespread usage, all the polymerase-targeting agents are plagued by adverse side effects such as myelosuppression, neutropenia, anemia, thrombocytopenia, and multiple organ

toxicity (79–83). Maribavir is an orally bioavailable inhibitor of the viral UL97 kinase, however, its mechanism differs fundamentally from ganciclovir. Maribavir binds to the ATP binding domain of UL79 to disrupt DNA processing, encapsidation, and egress (84). Letermovir represents a novel inhibitor of the HCMV terminase complex, targeting UL56 with contributions from UL51 and UL89 (85–87). By blocking DNA cleavage and packaging, Letermovir acts independently of DNA polymerase-based replication, which suggests it could be used in combination with the other antivirals directed against HCMV. Unlike the polymerase inhibitors, Maribavir and Letermovir do not cause myelosuppression, and adverse effects are primarily gastrointestinal (88,89). The current therapeutic landscape against HCMV emphasizes a tiered approach. Polymerase-acting agents remain the standard first-line therapeutics for treatment; however, toxicity and resistance are frequent limitations. Letermovir has redefined primary prophylaxis, particularly in hematopoietic stem cell and kidney transplantation, by reducing CMV burden without hematologic suppression but the barrier to resistance with this antiviral is low. Finally, maribavir offers an oral and well-tolerated therapy for refractory or resistant infection, filling a long-standing therapeutic gap.

1.3.2 Vaccines

Vaccination offers a proactive strategy for mitigating CMV-associated disease, particularly congenital CMV and post-transplant complications. Yet, herpesviruses pose unique challenges to vaccine development, as sterilizing immunity is rarely achieved and reinfection with a new isolate has been documented in many individuals. To date, VZV remains the only human herpesvirus for which an effective vaccine exists (90). For HCMV, the hurdles of a large and complex genome, genetic diversity, frequent reinfection, latency, and an arsenal of immune evasion genes have hindered progress toward a licensed vaccine. Nevertheless, a wide array of vaccine platforms are under active investigation, reflecting growing optimism in the field. These include live-attenuated HCMV strains, viral-vectored vaccines, glycoprotein B (gB) subunit vaccines, DNA-based vaccines encoding pp65, gB, or IE1, mRNA-based vaccines, virus-like particle (VLP) vaccines, and dense body vaccines.

Live-attenuated vaccine candidates were among the earliest tested in clinical trials. The laboratory-adapted strain AD169, attenuated by extensive passage in fibroblasts, was evaluated as a subcutaneous or intradermal vaccine (91). Subcutaneous immunization elicited neutralizing antibody responses, whereas intradermal administration did not (92). Building on these results, a derivative of AD169 with a repaired pentameric complex and an engineered FKBP-destabilization domain on viral proteins IE1, IE2, and UL51 ("V160") was shown to induce neutralizing antibodies in preclinical models. Moreover, V160 induced robust $CD4^+$ and $CD8^+$ T-cell responses in multiple animal models (93). In a phase II trial, V160 conferred approximately 42% efficacy against primary HCMV infection and elicited memory B-cell responses, although antibody titers were lower than those seen in naturally infected individuals (94). The Towne strain, another attenuated isolate, has similarly been evaluated. Although Towne vaccination induced neutralizing antibodies and T-cell responses, antibody titers were consistently lower than those from natural infection (95). Recombinant Towne–Toledo chimeras improved immunogenicity to some degree, but antibody levels again fell short of protective benchmarks (96). Importantly, despite suboptimal efficacy, safety profiles of these live-attenuated candidates were favorable, with no reports of severe adverse events (91,93,95,96).

Attention has since shifted toward viral envelope glycoprotein complexes, which are the primary targets of neutralizing antibodies. Chief among these are gB and the pentameric complex. The viral fusogen, gB, is required for entry into all cell types. The pentameric complex is essential for infection of epithelial, endothelial, and myeloid lineage cells. Clinical trials of gB subunit vaccines demonstrated partial protection, with efficacy ranging from 40–50% in seronegative adolescents and postpartum women (97). However, neutralizing antibody titers were lower than those achieved after natural infection. Four doses of a purified gB vaccine were required to achieve equivalent antibody responses over the course of one year (98). More recent vector-based approaches incorporating the pentamer have shown superior immunogenicity in animal models. For example, a Modified Vaccinia Ankara (MVA) vector encoding the complete pentamer elicited markedly higher neutralizing titers in mice and rhesus macaques compared to gB or gH/gL alone (99,100).

Current vaccine development increasingly emphasizes multivalent platforms. Moderna's mRNA-1647 vaccine, encoding both gB and the pentameric complex, has advanced to phase III clinical trials (24,101). Early studies indicate robust induction of both neutralizing and Fc-mediated functions, including antibody-dependent cellular cytotoxicity and phagocytosis. Parallel efforts, such as the Triplex MVA vector vaccine encoding pp65, IE1, and IE2, have demonstrated efficacy in transplant settings by reducing viremia and improving outcomes (102–104). Together, these data suggest that combining gB with pentameric components, and eliciting both antibody and T-cell responses, may be critical for achieving durable protection.

Section 1.4: The Complex Biology of Human Cytomegalovirus

1.4.1 Viron Structure and Composition

A mature HCMV infectious particle is spherical, approximately 200 nm in diameter, and comprised of four main components: the envelope, tegument, capsid, and viral genome **(Fig. 1.1)** (48). Additional byproducts of infection include noninfectious enveloped particles (NIEPs), which lack the only viral genome, and dense bodies, which differ in structure and composition when compared to mature virions (105,106). NIEPs arise due to errors during DNA packaging within the nucleus whereas dense bodies are the result of errors in virion formation and lack a capsid. Because both NIEPs and dense bodies are enveloped with viral proteins, both are highly immunogenic and may contribute to manipulation of the host immune response (107–110).

Figure[1.1] HCMV Genome and Virion Structure

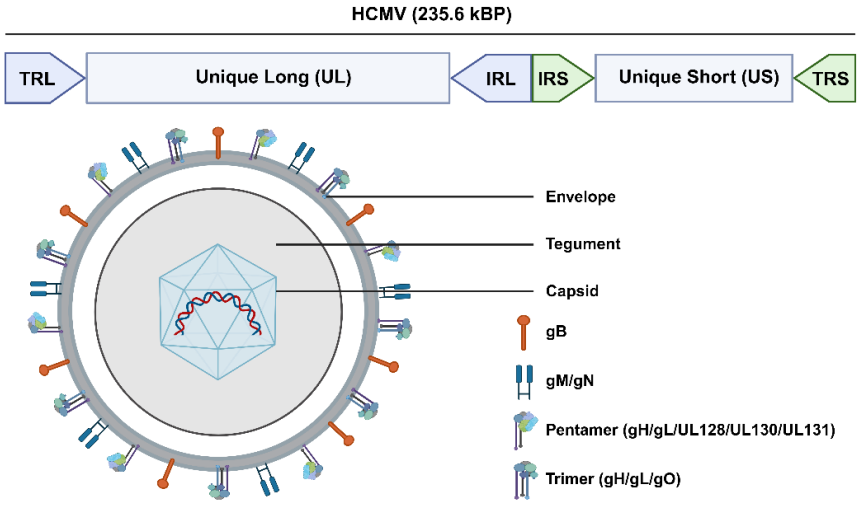

[1.1] **Figure Legend**

HCMV genome organization and virion composition. Created in BioRender. Medica, S. (2025) https://BioRender.com/ck50rtb

The envelope of HCMV is a lipid bilayer originating from the Trans Golgi Network (TGN) and endoplasmic reticulum. The exact lipid composition of the viral envelope is dependent on the host cell type, however, studies have shown that saturated very long chain fatty acids are crucial for proper formation and infectivity of viral particles (111,112). Embedded within the viral envelope are 19 viral glycoproteins that mediate several processes but are most commonly associated with viral entry (113). Three glycoprotein complexes have been characterized as critical mediators of viral entry: glycoproteins M and N (gM/gN – UL100/UL73), glycoproteins H and L (gH/gL – UL75/UL116) which complex themselves with additional viral glycoproteins gO (UL74) and UL128/130/131, and glycoprotein B (gB – UL55) (21,114).

The tegument layer of HCMV consists of a heterogenous and multifunctional proteinaceous layer that exists between the envelope and capsid. Proteomic analysis of the tegument layer of HCMV has identified over 70 viral proteins that represent over 40% of the overall virion mass (113,115). Generally, tegument proteins can be broadly divided into two categories: structural components that contribute to virion integrity, and functional effectors that reprogram the host cell

immediately upon infection. This dichotomy can be illustrated by the differing functions of the tegument proteins UL99 (pp28), which facilitates secondary envelopment, and UL83 (pp65), which interferes with innate immune sensing by blocking interferon-inducible responses and modulating natural killer (NK) cell recognition (116,117). The specific function of each individual tegument protein remains poorly understood, and continued investigation into tegument composition and function will likely provide key insights into the pathogenesis of HCMV.

The HCMV capsid conforms to the canonical herpesvirus morphology, exhibiting T=16 icosahedral symmetry (118). It measures roughly 130 nm in diameter and is constructed from approximately 150 hexons and 11 pentons, organized around a single portal vertex (119). The major capsid protein (MCP – UL86) forms the bulk of this structure, assembling into hexamers and pentamers that constitute the repeating units of the capsid shell (113,115). Stabilization of the lattice is provided by the minor capsid protein (mCP – UL85), minor capsid binding protein (mCBP – UL46), and the smallest capsid protein (SCP – UL48.5), which bridge the gaps between MCP subunits (115). Located at a unique vertex, the portal complex is formed by a dodecameric ring of UL104 proteins and functions as the entry and exit site for viral DNA (120). The resulting architecture is highly stable, designed to withstand the internal pressure exerted by the densely packed viral genomic DNA.

The HCMV genome is comprised of double stranded DNA and is approximately 236 kilobases in length, making it the largest of all human herpesviruses **(Fig. 1.1)** (121). In total, the genome is capable of encoding well over 200 viral proteins, several microRNAs, and non-coding RNAs (113,122). The genome is subdivided into two main sections, unique long (UL) and unique short (US), and is flanked by internal and terminal repeat regions (TRL, IRL, IRS, and TRS). The UL region of the genome contains approximately 132 protein coding open reading frames (ORFs) while the US region has only 34. Several of these ORFs can be lost with subsequent passaging in a laboratory setting as there are only 45 genes considered to be essential for viral replication in fibroblasts (123). Within the virion, the genome exists as linear; once inside the host cell, 3’ overhangs present at the end of the genome facilitate circularization into an episome (124).

1.4.2 The Lytic Replication Cycle of HCMV

HCMV can productively infect numerous cell types including fibroblasts, epithelial cells, endothelial cells, monocytes, macrophages, dendritic cells, smooth muscle cells, and HPCs (21,22). Consequently, viremia can occur in most organs of the body. The lytic lifecycle of HCMV consists of entry, uncoating and trafficking to the nucleus, viral gene expression, genome replication, capsid assembly and packaging, nuclear egress, tegumentation, envelopment, and egress. These processes rely on a cascade of defined temporal gene expression events that are classified as immediate early, early, and late events **(Fig. 1.2)**. A summary of these events can be found below.

Figure[1.2]

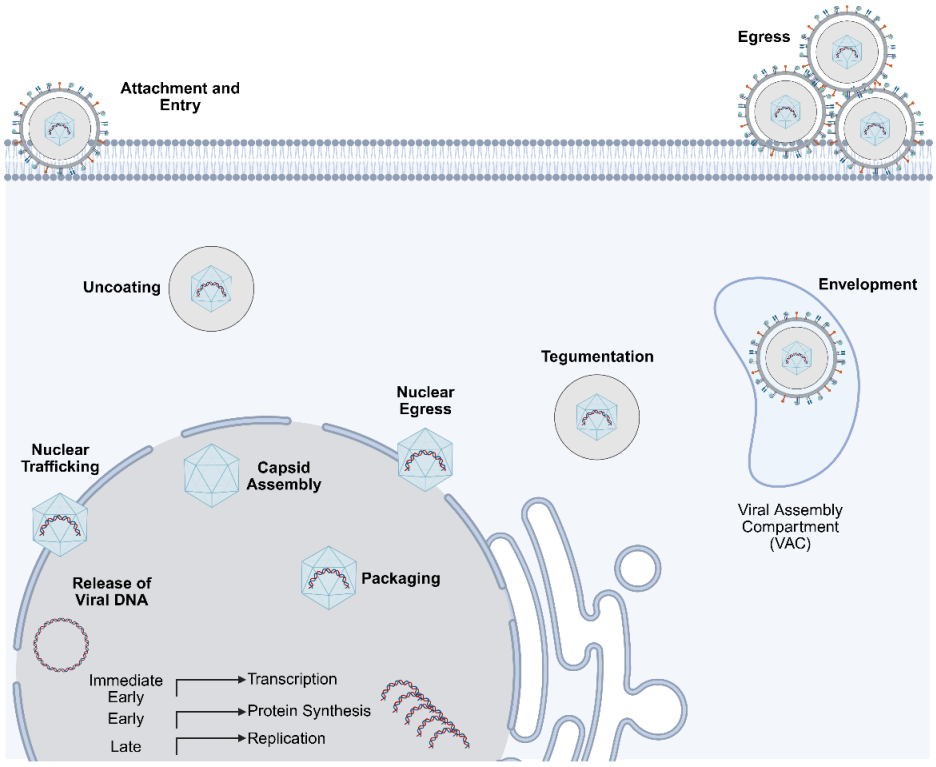

[1.2] Figure Legend

HCMV lytic replication cycle. Created in BioRender. Medica, S. (2025) *https://BioRender.com/ck50rtb*

I. Viral Entry

HCMV enters host cells through a complex, multistep process involving both viral envelope glycoproteins and host cell surface receptors. Entry is cell type-dependent and generally occurs

via either direct membrane fusion or endocytosis, followed by fusion with endosomal membranes. The initial phases of viral entry involves tethering of the virion heparin sulfate proteoglycans mediated by the gM/gN complex and gB (125–127). Once tethered, one of two gH/gL complexes will facilitate formal attachment. The complex of gH/gL is common amongst all human herpesviruses and acts as a scaffold for additional viral proteins that are involved in cell type-specific entry. The trimer, comprised of gH/gL/gO, is essential for entry into fibroblasts, and mediates high-affinity interactions with host cell surface receptors including platelet derived growth factor receptor α (PDGFRα) and transforming growth factor β receptor (TGFβR) (21,128). Entry via the trimer is typically associated with pH-independent membrane fusion (129). The gH/gL/UL128/UL130/UL131 pentamer complex is required for efficient entry into epithelial cells, endothelial cells, monocytes, and macrophages. Pentamer binds to the neuropilin 2 receptor (NRP2) and CD147 (130–134) and directs entry through endocytosis and a low pH-mediated fusion process (135,136). Engagement of the trimer or pentamer to the corresponding cellular receptors results in recruitment of gB and an irreversible conformational change that mediates either entry mechanism (137,138).

II. Uncoating and Nuclear Trafficking

Following membrane fusion, the viral capsid and tegument proteins are released into the host cell cytoplasm, which initiates the uncoating process involving the partial disassembly of the tegument layer to expose the underlying capsid while retaining essential regulatory proteins. For example, select tegument proteins modulate cellular responses, including UL83 (pp65), US7, and US8, which function to suppress innate immune responses (116,139). Other tegument proteins, including UL32 (pp150), UL96, and UL47, help stabilize the capsid and mediate interactions with host trafficking machinery (140,141). The intact capsid is then transported along microtubules toward the nucleus using the host cell's dynein-dynactin motor complex (142). This retrograde movement enables efficient delivery of the viral genome to the nuclear periphery. The capsid docks at a nuclear pore complex (NPC), where further uncoating occurs. A coordinated interaction between the capsid and components of the NPC facilitates the release of viral DNA into the nucleus. The genome is then circularized and initiates the viral replication cycle. This

spatially and temporally regulated trafficking process ensures that the viral genome is protected from cytoplasmic immune sensors and that infection proceeds efficiently in permissive cells.

III. Immediate Early Functions and DNA Replication

Inside the newly infected cell nucleus, the viral genome is circularized at the 3' overhangs into an episome and is immediately attacked by host restriction factors (124). Chromatin reorganization proteins such as PML nuclear bodies and Daxx histone deacetylases act on the viral genome in an attempt to silence gene expression from the major immediate early promoter (MIEP) (143–145). This repression is alleviated in part by the nuclear-localized tegument protein UL82, which functions to interact with Daxx resulting in proteasomal degradation (146). Nascent UL123 transcripts are translated into IE1 (IE72) proteins, which further liberate the viral genome by deconstructing PML nuclear bodies allowing for efficient viral transcription to take place (147). UL122 (IE2; IE86) serves as the master regulator of viral gene synthesis and transcription (148–150). In addition to stimulating viral transcription, IE2 functions to stimulate the transcription of E2F responsive genes resulting in S-phase transition of the host cell thereby allowing for the accumulation of enzymes and dNTPs required for efficient viral genome replication (151–153). At the cis-acting origin of replication (oriLyt), genome replication proceeds via a rolling circle method mediated by IE2 and UL84 (154,155). Six viral proteins comprise the core DNA replication machinery: UL54 (viral polymerase), UL44 (polymerase processivity factor), UL105 (helicase), UL70 (primase), UL102 (primase-helicase processivity factor), and UL57 (ssDNA binding protein). In addition to the core six, UL112/UL113 (recruitment phosphoproteins) and UL114 (glycosylase) are required for efficient genome replication (156–161). The activity of these proteins facilitates continuous strand-displacement synthesis that results in the formation of numerous concatemeric viral genomes, which serve as substrates for packaging into progeny capsids.

IV. Capsid Assembly, Packaging, and Nuclear Egress

Following viral DNA replication, sufficient late gene expression, and protein translation, capsid assembly and DNA packaging within nuclear replication compartments are coordinated in a highly ordered and energy-dependent process. Capsid formation initiates within the cytoplasm

of infected host cells beginning with the synthesis of the MCP (UL86), the mCP(UL85), the mCBP (UL46), and the SCP (UL48.5) (162–165). The precursor assembly protein (UL80), containing a nuclear localization signal (NLS), will bind to the procapsid to stabilize its formation and shuttle it to the nucleus (166). While nuclear assembly of capsid precursors remains incompletely characterized in HCMV, studies of HSV suggest that capsid, portal, and scaffolding proteins likely follow a conserved assembly pathway. Within the infected cell nucleus, newly synthesized concatemeric viral DNA is packaged into mature capsids through the portal complex (UL104) mediated by the heterotrimeric terminase complex consisting of the large subunit UL56, the nuclease/ATPase subunit UL89, and the recently identified cofactor UL51 in an ATP-dependent manner (162,167). Following nuclear assembly and DNA packaging, viral capsids undergo primary envelopment at the inner nuclear membrane and transit into the perinuclear space, after which they are de-enveloped by fusion with the outer nuclear membrane to access the cytoplasm (168,169). Nuclear egress is mediated by the UL50-UL53 nuclear egress complex in coordination with UL97, which reorganizes the nuclear lamina to facilitate capsid release (170).

V. Tegumentation and Viral Egress

The remaining assembly steps to produce a mature virion take place within the cytoplasmic virion assembly compartment (VAC), a structure derived from CMV-induced remodeling of the endosecretory pathway. Within this compartment, tegument and envelope proteins accumulate at the trans-Golgi network (TGN) and the microtubule organizing center, where tegumentation and secondary envelopment proceed in a manner dependent on UL47 and UL48 (113,171,172). Following tegumentation and secondary envelopment within the endosecretory pathway, virion-containing vesicles are trafficked to the plasma membrane, where fusion of the vesicular and cellular membranes mediates viral egress. This step is critically dependent on the tegument protein UL103, whose absence disrupts the release of both dense bodies and cell-free virions (173).

1.4.3 HCMV Latency and Reactivation

During primary infection, HCMV targets a broad range of cell types, giving rise to diverse infection outcomes within the host. In fibroblasts, the virus undergoes efficient replication before being

eventually cleared. In endothelial and epithelial cells, it establishes a persistent, low-level infection that can lead to intermittent viral shedding over months or even years (174,175). Bone marrow resident $CD34^+$ HPCs and circulating $CD14^+$ monocytes are capable of maintaining viral genomes in a non-replicative state, thereby serving as latent reservoirs in HCMV infected individuals (176–178). The transition between viral latency and reactivation is governed by both host and viral factors that either repress or promote lytic gene expression and are explicitly linked to cellular differentiation down the myeloid lineage (179,180). Central to the interplay between latent and productive infection is regulation of the MIEP, which drives expression of IE genes necessary for initiating lytic replication (181–183). During latency, MIEP activity is repressed by epigenetic mechanisms, viral proteins, and microRNAs often acting in concert with one another to achieve transcriptional silencing.

Amongst the most well studied viral factors that drive MIEP silencing are members of the ULb' polycistronic region spanning ORFs UL133 – UL138. The most well characterized of these is UL138, which is expressed as three unique transcripts and proteins that function to interface with epidermal growth factor receptor (EGFR) and tumor necrosis factor receptor-1 (TNFR1) signal transduction to promote heterochromatinization of the viral genome. This process is achieved in part by sustaining EGFR signal transduction resulting in the inhibition of histone demethylases at the MIEP (184–186). Two of the five alternatively spliced isoforms from the related UL136 locus, UL136p19 and UL136p23, reinforce epigenetic silencing of the MIEP by modulating phosphoinositide 3-kinase γ (PI3K)–Akt signal transduction. However, the exact mechanism of action is context dependent and poorly understood (187). The differential functions of UL136 in latency and reactivation suggest that UL136 is likely to function in concert with other members of the ULb' locus. Similar to UL136, UL133 acts in conjunction with UL138 and UL136 isoforms to coordinate epigenetic silencing of the MIEP (188,189). The precise molecular mechanism of UL133 is currently unknown, however, specific bursts in expression at two and five days post-infection (dpi) suggest that UL133 may serve as a modulator of UL138 and UL136 activity promoting a cellular environment conducive to silencing of the MIEP and the establishment of a latent infection (190).

Several viral proteins outside of the ULb' locus also contribute to the establishment of latency. The most well characterized are the viral chemokine receptor US28 (reviewed further in section 1.6.3) and the secreted protein UL7. Both of these proteins function to hijack host cell signal transduction networks to promote the establishment of viral latency. Specific to establishing a latent infection, US28 has been shown to attenuate mitogen-activated protein kinases (MAPKs) and nuclear factor kappa-B (NFκB) signal transduction in latently infected cells, which may suppress MIEP transcription (191,192,192). This attenuation appears to be dependent on ligand binding and signaling potential as mutations within US28 that disrupt either of these processes result in an inability to establish or maintain a latent infection (192,193). Additionally, this requirement appears to be independent of the upstream US27 ORF, which is transcribed with US28 (194). Beyond direct attenuation of signaling pathways that stimulate transcription from the MIEP, constitutive US28 signal transduction contributes to other processes that promote the establishment of a latent infection. In $CD34^+$ HPCs, US28 signaling results in the activation of signal transducer and activator of transcription 3 (STAT3), which has been shown to promote the differentiation of HPCs into an immunosuppressive monocyte subset (195). In turn, this monocyte subset generates a high level of nitric oxide (NO) to silence HCMV IE transcription and promote viral latency (195). The secreted viral protein glycoprotein UL7 has also been shown to play an indirect role in the establishment of latent infection; serving as a ligand for the FMS-like tyrosine kinase 3 (Flt-3) receptor (196). Upon binding to Flt-3, UL7 mediated activation of the extracellular signal-related kinase (ERK) signal transduction pathway results in the phosphorylation and sequestration of forkhead box O3 (FOXO3) to the cytoplasm where it is unable to stimulate transcription from the MIEP (197). Importantly, both US28 and UL7 play dual roles in establishing a latent infection and the capacity to reactivate underscoring the timing, cell specific nature, and manipulation host signal transduction networks.

Several virally encoded microRNAs also significantly contribute to the establishment and maintenance of latent infection by modulating both host and viral gene expression by direct or indirect mechanisms. For instance, miR-UL112 directly targets the UL123 transcript encoding IE1,

limiting its expression and reducing viral DNA replication, while also diminishing cytotoxic T cell recognition (198,199). Additional viral transcripts, including UL112/UL113 and UL120/UL121, are also subject to miR-UL112 regulation, underscoring its broad influence (200). This contrasts with the indirect control of IE gene expression by miR-UL148D, which targets immediate early response 5 (IER5) reducing its expression thereby maintaining CDC25B levels, which activate cyclin-dependent kinase (CDK-1) to suppress transcription of UL123 (201). Other viral microRNAs, such as miR-US5-1, have dual roles in the establishment and maintenance of latent infection by targeting transcription factors that stimulate expression from the MIEP while simultaneously targeting host proapoptotic proteins. Specifically, miR-US5-1 directly inhibits expression of the transcription factor FOXO3 and the proapoptotic protein BCL2L11 (202). Another example of this dual control is miR-US25-1, which targets the small GTPase RhoA which is required for $CD34^+$ HPC self-renewal, proliferation, and hematopoiesis while also inhibiting viral DNA synthesis through a multiple mechanisms (203,204). Cooperatively, HCMV miRNAs function as multifunctional regulators that silence viral IE gene expression, manipulate cellular signaling and apoptosis, and preserve viral episomes, ensuring successful establishment and long-term maintenance of latency in hematopoietic progenitors.

Despite significant research regarding the factors which govern viral reactivation, the precise molecular mechanisms behind these processes are still unclear. To date, seven viral genes and at least three viral microRNAs have been identified as factors required for HCMV reactivation in myeloid lineage cells (193,196,205–211). Many of these viral factors have dual roles in latency establishment and cell type-specific functions that are highly context dependent in regard to host cell type and replication status. Members of the RL11 gene family, UL7 and UL8, have both been shown to be required for efficient viral reactivation through distinct mechanisms. By binding Flt-3 as a ligand, UL7 stimulates PI3K-Akt and MAPK signal transduction to induce cellular differentiation in both $CD34^+$ HPCs and $CD14^+$ monocytes facilitating efficient reactivation (196). Alternatively, the membrane bound UL8 transcribed from the same locus is capable of interacting with components of the Wnt/β-catenin pathway through its PDZ domain; however, the exact mechanism by which UL8 facilitates viral reactivation is still under investigation (205).

Two viral genes within the ULb' region contribute to viral reactivation by distinct mechanisms, and both are transcribed from polycistronic loci. The UL135 locus produces two transcripts: the predominant 308 amino acid isoform M21 and a shorter soluble isoform initiating at M97 (187,212). Generally, both isoforms of UL135 function to alleviate the repressive effects of UL138. Mechanistically, UL135 interacts with host proteins to regulate EGFR signal transduction. Specifically, the interactions with adapter proteins Abi-1, Abi-2, CIN85, and CD2AP helps UL135 recruit the Cbl ubiquitin ligase to target EGFR for degradation (209,213–215). Additionally, UL135 directly stimulates IE2 gene expression through its interaction with the viral kinase UL97 and it has been shown that removal of UL135 results in impaired UL97 function (216,217). The other locus within the ULb' region of the CMV genome which contributes to viral reactivation are the three UL136 isoforms: UL136p25, UL136p26, and UL136p33 (187,212). Similar to the latency promoting isoforms of UL135, the exact mechanism by which UL136 facilitates viral reactivation remains poorly understood, however, distinct patterns during late gene expression suggest that UL136 functions as a regulatory switch by modulating the balance between UL135- and UL138-driven outcomes during infection (218).

The latency-associated transcript (LUNA), encoded within the UL81–82 locus, is expressed during latent infection in $CD34^+$ hematopoietic progenitor cells and monocytes, and is required for efficient reactivation of HCMV (207,219). Unlike viral proteins that directly regulate IE gene expression, LUNA functions to prepare the latent viral genome for reentry into the lytic cycle. Mechanistically, LUNA possesses deSUMOylase activity, targeting host chromatin-associated proteins such as PML and Sp100 that reinforce repression of the MIEP (219). By removing SUMO modifications from these host proteins, LUNA disrupts the integrity of PML nuclear bodies, which are critical for maintaining viral genome silencing. This activity reduces the repressive chromatin environment surrounding the MIEP, thereby permitting transcriptional activation of IE genes upon receipt of differentiation or stress signals.

Three chemokine receptors encoded by HCMV have been shown to play major roles during viral reactivation. UL33 shares homology with the host chemokine receptors CCR1 and CCR5 and is expressed during latent infection and required for viral reactivation. Through coupling to $G\alpha_q$ and downstream phosphorylation of cyclic AMP-responsive element-binding protein (CREB), UL33 is able to indirectly drive expression from the MIEP (210). This activity appears to be signaling dependent as viruses harboring mutations in UL33 that disrupt G-protein coupling activity are unable to reactivate (210). UL33 is classified as an orphan receptor with no known ligand binding partner. Therefore, it is unknown whether ligand binding or constitutive signaling is responsible for CREB phosphorylation (220,221). Despite being integral for establishing a latent infection, US28 also functions to promote viral reactivation underscoring its context dependent and promiscuous signaling capacity (192,193,222). Several studies have shown the requirement for US28 during viral reactivation. Specifically, US28 couples to $G\alpha_{12}$ isoforms to activate Rho guanine nucleotide exchange factors (GEFs) and downstream RhoA to facilitate efficient viral reactivation (206). This activity appears to be ligand binding and signaling dependent. Mutation of residues within the third intracellular loop of US28 that facilitate signal transduction and G protein coupling have impaired viral reactivation (223). Whether this phenomenon is dependent on stimulating viral transcription or inducing cellular differentiation remains an area of ongoing research; however, it is well established that US28 signaling activity induces cellular differentiation towards the myeloid linage (193). Outside of stimulating RhoA signal transduction, US28 constitutively activates phospholipase C (PLC)-β signal transduction to promote monocyte adhesion at the site of atherosclerotic plaques (224,225). The pro-inflammatory environment generated by these plaques provides a potential mechanism for macrophage differentiation suggesting a further role in viral dissemination (226,227). Recently, it's been demonstrated UL78 is required for efficient viral reactivation through its interaction with $G\alpha_i$ (228,229). Moreover, UL78 appears to translocate to the nuclear envelope during viral infection through an undefined mechanism (229). A ligand binding partner, signaling capacity, and a precise mechanism for the requirement of UL78 in viral reactivation remains to be elucidated.

A subset of virally encoded microRNAs contributes to viral reactivation, oftentimes, in a cooperative manner. One key regulator is miR-US22, which targets the transcription factor early growth response-1 (EGR-1). By modulating EGR-1 expression, miR-US22 disrupts EGFR/MEK/ERK signaling and attenuates expression of UL138, a latency-associated gene that stabilizes EGFR signaling and reinforces a feed-forward loop critical for latency maintenance (230,231). Notably, miR-US22 is not expressed during latency but is re-expressed upon reactivation, suggesting it helps dismantle the EGFR–UL138 loop to promote exit from latency, though this requires further validation (230). In addition, miR-US5-2 indirectly influences this axis by targeting the EGFR adaptor protein GAB1, thereby modulating EGR-1 and UL138 expression, though its role in reactivation remains less defined (232). Together, these findings highlight EGFR signaling as a key molecular switch controlling the balance between latency and reactivation. Recent studies have highlighted the cooperative nature of the HCMV microRNAs where it's been shown that miR-UL36, miR-UL112 and miR-UL148D act synergistically to downregulate Akt expression and attenuate downstream signaling, resulting in the activation of FOXO3 and enhanced internal promoter-driven IE transcription in $CD34^+$ HPCs (211).

HCMV latency exemplifies a finely tuned equilibrium between viral repression and host biology. By examining viral determinants, transcriptional and epigenetic regulation, and host signaling as interconnected processes, a more holistic understanding of latency emerges. This integrated perspective not only clarifies how HCMV persists within hematopoietic reservoirs but also guides future strategies to prevent reactivation and mitigate disease. Bridging these mechanisms is key to elucidating the intricacies of HCMV latency and moving toward effective control of this lifelong infection.

Section 1.5: Chemokines and Their Receptors

1.5.1 Chemokines – Classification, Structure, and Function

Chemokines constitute a large family of small, secreted proteins that play essential roles in leukocyte trafficking, tissue homeostasis, and immune surveillance. They are classified within the

chemotactic cytokine superfamily and are broadly responsible for directing the migration of immune cells to sites of inflammation, infection, or tissue injury (233). Beyond their classical role in chemotaxis, chemokines are also implicated in processes such as angiogenesis, hematopoiesis, and organ development, thereby serving as key regulators of both immune modulation and viral infection (234).

Chemokines are relatively small molecules ranging from 8–12 kDa in size. Structurally, all chemokines are characterized by a tertiary fold stabilized by two disulfide bonds between conserved cysteine residues (235). Based on the arrangement of their first two cysteines, chemokines are subdivided into four major subfamilies: CC, CXC, XC, and CX_3C **(Fig. 1.3)** (236).

Figure[1.3]

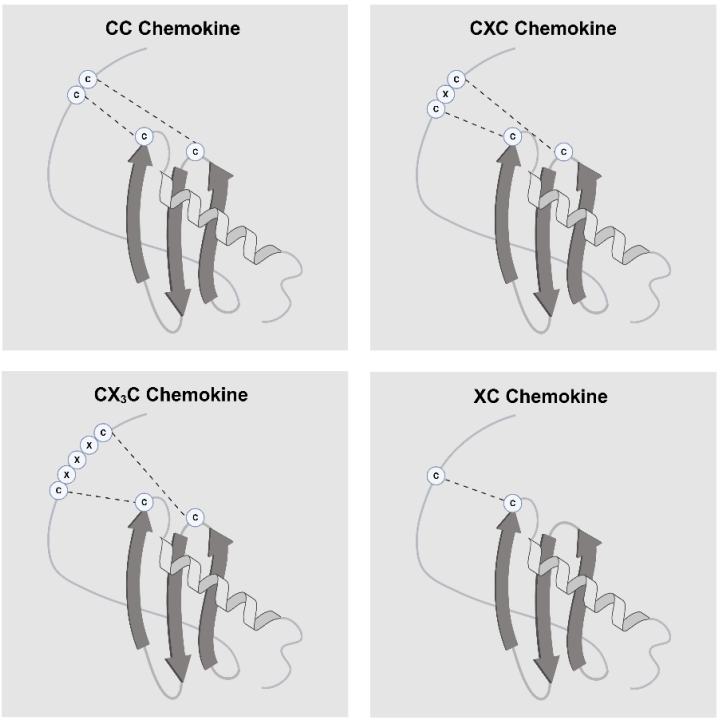

[1.3] **Figure Legend**

Chemokine structure and classification. Created in BioRender. Medica, S. (2025) https://BioRender.com/09271r5.

Of the four chemokine subfamilies, the CC group is the largest consisting of 27 members. The CXC chemokines, containing 17 members, are further stratified by the presence or absence of a glutamic acid-leucine-arginine motif (ERL-motif) that directs neutrophil migration and

angiogenesis (237). CXC chemokines lacking the ERL-motif have been demonstrated to exhibit angiostatic properties (237). The XC and CX_3C chemokine families are comparatively small, with only a limited number of identified members. In mammals, the XC family is represented by two chemokines, lymphotactin-α and -β (XCL1/XCL2), which contain a single conserved cysteine residue (238,239). Despite the absence of the typical pair of cysteines, this structural feature is sufficient to stabilize the characteristic chemokine fold and enable receptor engagement. The CX_3C family is represented by a single member, CX_3CL1 (fractalkine), in which the first two cysteine residues are separated by three amino acids (238). Fractalkine is unique in existing in two distinct forms: a soluble, secreted isoform and a membrane-bound form anchored on the surface of cells such as endothelial cells (238,240). Fractalkine has been implicated in diverse pathological processes, particularly within the context of inflammatory diseases (240).

Functionally, chemokines are broadly categorized as either inflammatory or homeostatic. Inflammatory chemokines are induced in response to infection, vaccination, cancer, or tissue damage and direct the migration of effector immune cells, including neutrophils, monocytes, and activated T lymphocytes, to sites of pathology. By contrast, homeostatic chemokines are constitutively expressed in specific tissues, where they regulate basal leukocyte trafficking necessary for immune surveillance and tissue integrity. For example, the CXCL12–CXCR4 axis is essential for hematopoietic stem cell homing and retention within the bone marrow niche, while CCL19 and CCL21 orchestrate lymphocyte migration to secondary lymphoid organs (241–243).

1.5.2 Chemokine Receptors – Classification, Structure, and Function

The biological functions of chemokines are principally mediated through their interaction with chemokine receptors that belong to the superfamily of Class A (Rhodopsin-like) G protein–coupled receptors (GPCRs) (244,245). These receptors share the canonical seven-transmembrane α-helical structure with an extracellular N-terminus that mediates ligand binding and specificity. Disulfide bridges within the extracellular loops help to stabilize the barrel structure allowing the intracellular loops to interact with G proteins **(Fig. 1.4)**. The GPCR C' terminal tail engages signaling molecules and mediates receptor recycling (246). To date, nearly 20 functional

chemokine receptors have been identified in humans, and they are designated according to the chemokine subfamily to which their primary ligands belong (237). The chemokine receptor structural and functional diversity provides specificity to the chemokine system while maintaining a level of redundancy that ensures robustness in immune cell recruitment.

Chemokine receptors are broadly divided into two categories: conventional chemokine receptors (cCKRs) and atypical chemokine receptors (ACKRs) (237,247). cCKRs are responsible for canonical signaling that drives chemotaxis and cellular activation. In contrast, ACKRs generally lack the capacity to signal through G proteins but instead function as chemokine scavengers or transporters, shaping chemokine gradients and modulating immune cell positioning (248). For instance, ACKR1 (also known as DARC) is expressed on erythrocytes and endothelial cells, where it binds multiple chemokines and regulates their bioavailability (249). Such receptors highlight the complexity of chemokine biology, extending beyond direct cell migration to include the fine-tuning of chemokine distribution.

The expression patterns of chemokine receptors provide an additional layer of specificity to immune regulation. Distinct leukocyte subsets express unique repertoires of chemokine receptors that guide their trafficking to appropriate tissues. For example, CCR7 directs naïve T cells and dendritic cells to secondary lymphoid organs through its interaction with CCL19 and CCL21, while CXCR5 mediates B cell migration into lymphoid follicles (250–252). Similarly, effector T cells upregulate receptors such as CXCR3 and CCR5, enabling their recruitment to inflamed tissues (253). These patterns underscore the central role of chemokine receptors in both homeostatic and inflammatory contexts.

Dysregulation of chemokine receptor function has profound implications for disease pathogenesis. Aberrant receptor expression or signaling contributes to chronic inflammatory diseases, autoimmune disorders, tumor metastasis, and exacerbate the effects of viral infections (254–256). For example, HIV exploits CCR5 and CXCR4 as co-receptors for cell entry, while certain viruses encode viral chemokine receptor homologs to manipulate host immune responses

(257,258). These findings have spurred intense interest in targeting chemokine receptors therapeutically. Antagonists of CCR5, such as maraviroc, have been successfully developed for HIV treatment, and additional receptor-targeted therapies are under investigation for cancer and inflammatory diseases (259,260).

1.5.3 The Chemokine Signaling Axis

The interaction between chemokines and their receptors initiates classical GPCR signaling cascades through interaction with heterotrimeric G protein complexes consisting of α, β, and γ subunits **(Fig. 1.4)** (237).

Figure[1.4]

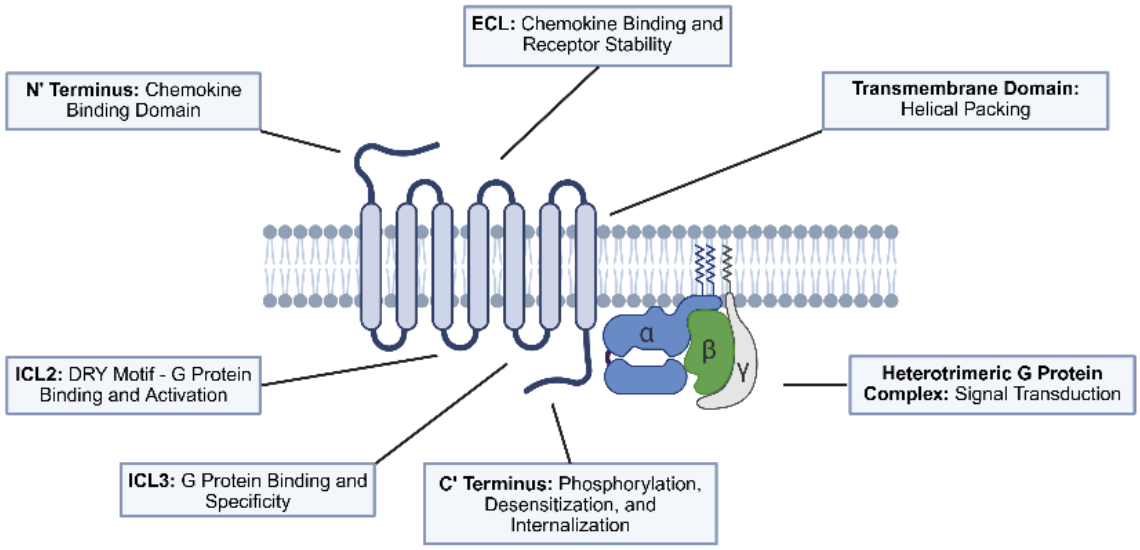

[1.4] **Figure Legend**

Schematic representation of a chemokine receptor and heterotrimeric G-protein complex with critical functional domains. Created in BioRender. Medica, S. (2025) https://BioRender.com/12zqow2

In the resting or inactive state, chemokine receptors are stabilized via an ionic lock between transmembrane domains (TM) two and six. Specifically, these interactions are mediated by an aspartic acid-arginine-tyrosine motif (DRY-motif) located at the base of TM2 and negatively

charged amino acids in TM6 such as aspartic acid and glutamic acid (261). Upon chemokine binding at the N' terminus, a conformational change in the extracellular and transmembrane domains of the receptor propagate to the cytoplasmic side, breaking the ionic lock and allowing the receptor to function as a guanine nucleotide exchange factor (GEF) (246). The receptor will catalyze the exchange of GDP for GTP on the Gα subunit resulting in dissociation of Gα from the Gβγ dimer, liberating both components to engage downstream effectors. Importantly, mutations in the DRY motif can profoundly alter receptor signaling. Substitutions within this sequence often disrupt efficient G protein coupling but do not always affect recycling other G protein independent functions (262).

Once dissociated, Gα and Gβγ subunits are free to regulate effector signal transduction pathways that shape cellular behavior in a G protein and cell-type specific manner. Gα subunits can be classified into one of four families that are generally dependent on the signal transduction pathways that they regulate **(Table 1.1)**.

Table[1.1]

G Protein	Isoforms	Effector
$G\alpha_s$	$G\alpha_s$ $G\alpha_{sXL}$ $G\alpha_{olf}$	Adenylyl Cyclase Src Tyrosine Kinases
$G\alpha_{i/o}$	$G\alpha_{i1\text{-}3}$ $G\alpha_o$ $G\alpha_z$ $G\alpha_t$ $G\alpha_g$	Adenylyl Cyclase Phosphodiesterase
$G\alpha_{q/11}$	$G\alpha_q$ $G\alpha_{11}$ $G\alpha_{14}$ $G\alpha_{15/16}$	Phospholipase Cβ
$G\alpha_{12/13}$	$G\alpha_{12}$ $G\alpha_{13}$	Rho Guanine Exchange Factors
Gβγ	Gβ (1-5) Gγ (1-13)	Adenylyl Cyclase PI3K-Akt Ca^{2+} and K^+ GRK (Recruit)

[1.4] Figure Legend

Table of G-protein isoforms with stimulated (green) or repressed (red) signal transduction properties. Created in BioRender. Medica, S. (2025) https://BioRender.com/12zqow2

$G\alpha_s$ is primarily associated with stimulation of adenylate cyclase and cyclic AMP production from ATP resulting in the activation of protein kinase A (PKA). $G\alpha_{i/o}$ counteracts the activity of $G\alpha_s$ resulting in a decrease in cyclic AMP production and inhibition of PKA. $G\alpha_{q/11}$ stimulates the membrane bound PLC-β which regulates inositol triphosphate (IP3) and diacylglycerol (DAG) accumulation to regulate calcium flux. $G\alpha_{12/13}$ are broadly associated with Rho GTPase signal transduction mediating cytoskeletal remodeling and cellular migration (263,264). The Gβγ dimer also plays a central role in chemokine receptor signaling via activation of the PI3K–Akt signal

transduction pathway to promote cell survival and polarity (265,266). The simultaneous activation of Gα- and Gβγ-mediated pathways allows for coordinated control over motility, adhesion, and survival. Signal termination is achieved when intrinsic GTPase activity of Gα hydrolyzes GTP back to GDP in a process facilitated by regulators of G protein signaling (RGS proteins) (267). This restores the inactive heterotrimer and resets the receptor complex.

Chemokine receptor desensitization and internalization is mediated by G protein–coupled receptor kinases (GRKs) and β-arrestins, which provide a means to regulate the magnitude and duration of chemokine signaling. GRKs function to phosphorylate tyrosine and serine residues within the intracellular C' terminal tail of chemokine receptors. Phosphorylation serves as a docking site for β-arrestins, which sterically hinder further coupling of the receptor to heterotrimeric G protein complexes and initiate the recruitment of internalization machinery, thereby terminating classical G protein–mediated signaling (268,269). Beyond uncoupling, β-arrestins also initiate alternative signaling cascades, including those involving MAPKs and Akt, reflecting the biased signaling potential of desensitized receptors (270). Importantly, β-arrestin binding also links chemokine receptors to the endocytic machinery where they will be internalized via clathrin- or caveolin-dependent mechanisms (271). Once internalized, receptors are trafficked to early endosomes where they face one of two fates: recycling or degradation.

In the recycling pathway, receptors are dephosphorylated and returned to the plasma membrane, restoring surface expression and resensitizing the cell to chemokine stimulation. This rapid recycling is particularly important in immune cells such as T lymphocytes and neutrophils, which must continually sense and respond to chemokine gradients during migration (271). Alternatively, receptors may be sorted to lysosomes for degradation, a process that reduces receptor availability at the cell surface and contributes to long-term desensitization. The balance between recycling and degradation is influenced by the identity of the receptor, the specific ligand, and the cellular context. For example, CCR5 and CXCR4 both can undergo rapid recycling and lysosomal degradation, with the latter favored during prolonged or high-intensity stimulation (272).

Section 1.6: Molecular Mimicry of Human Cytomegalovirus

HCMV has co-evolved with its host over millions of years, developing an extensive arsenal of immune evasion strategies that allow it to persist for life in the face of robust host defenses. Central to this success is the virus's capacity for molecular mimicry, whereby viral proteins structurally and functionally resemble host molecules, enabling subversion of immune surveillance while maintaining viral replication. These strategies act at multiple layers of the immune system including targeting innate recognition, adaptive effector functions, and the establishment of long-term viral latency. A subset of these processes are discussed below.

1.6.1 Chemokines Encoded by HCMV

In addition to modulating the host chemokine signaling axis, HCMV encodes its own chemokines to modulate host immune responses. These viral chemokines include UL146, UL147A, UL128, and UL130 and represent a critical component of the virus's immune modulatory arsenal. The most extensively studied of these molecules are the CXC chemokine homologs UL146 and UL147A, which are most closely similar to CXCL1 and CXCL2, respectively (273). UL146 exhibits strong functional homology to host ELR^+ CXC chemokines such as CXCL8 (IL-8), and UL146 binds to CXCR1 and CXCR2 with high affinity. This interaction promotes intracellular calcium flux and the chemotaxis of neutrophils, which is suspected to serve as a trojan horse for viral dissemination given its abundance in circulation and ability to infiltrate tissues (274). UL146 also activates neutrophil effector functions, including degranulation and oxidative burst, but paradoxically may benefit the virus by fueling local inflammation and creating a permissive environment for viral replication and spread (275). UL147A is less well characterized, however, preliminary studies suggest overlapping activities with UL146, functioning to inhibit the responses of natural killer cells (276). Interestingly, both UL146 and UL147A are among the most genetically diverse loci in clinical HCMV isolates, implying strong selective pressures to maintain their immunomodulatory roles (277).

The viral CC chemokines UL128 and UL130, homologous to CCL1 and CCL2 respectively, are expressed as components of the HCMV pentameric glycoprotein complex (gH/gL/UL128–131), which is essential for viral entry into epithelial and endothelial cells (21). Beyond this structural role, these viral chemokine-like proteins retain sequence similarity to host CC chemokines and are thought to contribute to immune modulation. For example, UL128 has been implicated in attracting monocytes, which are key reservoirs for HCMV latency and dissemination (278). UL130, likewise, may influence monocyte and dendritic cell trafficking, further promoting infection of immune cell subsets that support viral persistence (279). Although their chemotactic activity is less well defined compared to UL146, these proteins highlight how HCMV integrates chemokine mimicry into both entry and immune evasion strategies.

1.2.2 Chemokine Receptors Encoded by HCMV – The Fab Four

Like related β- and γ-herpesviruses, HCMV encodes GPCRs with homology to host chemokine receptors that play major roles in viral pathogenesis. These viral GPCRs are expressed at different timepoints post infection and contribute to diverse processes, including immune evasion, manipulation of host signaling, and regulation of latency and reactivation. While most share some degree of homology, each receptor displays distinct properties and functions **(Table 1.2)**.

Table[1.2]

	Homology	Ligand	G-Protein	Function
UL33 	CCR1	Unknown	$G\alpha_{q/11}$ $G\alpha_{i/o}$ $G\alpha_{12/13}$	Activates CREB, PLC-β
UL78 	CXCR1	Unknown	Unknown	Unknown
US27 	CCR1 CX_3CR1	Unknown	$G\alpha_{q/11}$	Activates PI3K, NRF1, ARE
US28 	CCR1 CCR5 CX_3CR1	CCL2 (MCP-1) CCL3 (MIP-1α) CCL4 (MIP-1β) CCL5 (RANTES) CCL7(MCP-3) CX_3CL1(Fractalkine)	$G\alpha_{q/11}$ $G\alpha_{i/o}$ $G\alpha_{12/13}$	Activates SRE/ ELK1, SRF, NFκB, STAT3, NFAT, TCF

[1.2] Table Legend

Table and functionality of the chemokine receptor homologs encoded by HCMV. Created in BioRender. Medica, S. (2025) https://BioRender.com/ihiprnb

Conserved in all β-herpesviruses, UL33 shares approximately 25% sequence homology to the host CCR1 chemokine receptor and is packaged into the mature virion (113). In epithelial cells lines and fibroblasts, it is expressed with late kinetics at 48 hours post-infection (280). While dispensable for replication in fibroblasts, UL33 appears to be required for efficient viral gene expression and virion production in more clinically relevant epithelial cell lines (280). UL33 is unique amongst the HCMV-encoded chemokine receptors, as it is the only vGPCR that is comprised of multiple spliced exons to form the full-length mRNA. During infection, UL33 localizes to endocytic compartments, viral membranes, and the plasma membrane (281). UL33

is classified as an orphan receptor with no known ligand binding partner but does exhibit a high degree of constitutive activity (221). Several studies have examined the signaling potential of UL33 where it was demonstrated to signal through $G\alpha_q$, $G\alpha_i$, and $G\alpha_s$ isoforms (220,282). Downstream signaling mediated by UL33 typically activates both the PLC-β and adenylyl cyclase signal transduction pathways and has been linked to viral dissemination via both extracellular and cell-to-cell means through an unknown mechanism (221). While the precise role for UL33 in viral pathogenesis remains an area of ongoing study, it's been demonstrated that UL33 signal transduction through $G\alpha_s$ is capable of facilitating CREB activation and subsequent transcription from the MIEP to enhance immergence from latent infection (210). In addition to its roles in viral reactivation and viral dissemination, UL33 stimulates several signal transduction pathways involved in inflammation, proliferation, angiogenesis, and has been implicated in tumorigenesis (221).

The least well characterized of the HCMV chemokine receptors is UL78, which is expressed with early kinetics in fibroblasts (283). Homology to host chemokine receptors is quite limited with the most closely related being CXCR1 to which UL78 shows approximately 5% homology (284). Like UL33, UL78 is classified as an orphan receptor with no known ligand binding partner. To date, no robust constitutive signaling capacity has been demonstrated for UL78, however, the crystal structure of UL78 binding to $G\alpha_i$ was recently solved (285). Despite being dispensable for viral replication in fibroblasts, deletion of UL78 has been shown to slightly delay IE protein accumulation in more clinically relevant epithelial cell lines (286). Localization studies in infected fibroblasts reveal that UL78 is predominantly retained within intracellular compartments, particularly the endoplasmic reticulum, Golgi apparatus, and perinuclear space (229,287). In transiently transfected cells, UL78 has been shown to interface with the host and viral chemokine receptors CCR5, CXCR4, and US28 to modulate surface expression and signal transduction (288,289). Importantly, a recent study examining the latent transcriptome in primary $CD34^+$ HPCs identified that UL78 is expressed during latent infection (290,291).

The US27 gene product exhibits many features of chemokine receptors including a moderate degree of sequence homology with CCR1 and CX_3CR1 (292). US27 is classified as a late protein

only showing detectable protein expression after DNA synthesis. Results from subcellular localization studies indicate that US27 predominantly resides in intracellular vesicles, the Golgi apparatus, and the plasma membrane where it is rapidly internalized (287). Removal of the US27 ORF from HCMV results in a minor growth defect in epithelial and fibroblast cells and has been linked to impaired extracellular shedding (293). In transiently transfected cells, US27 augments the mRNA and protein levels of CXCR4, leading to greater calcium flux and migration to CXCL12 (294). Like UL78, US27 has been shown to form heterodimers CCR5, CXCR4, and US28 to augment surface expression and signal transduction (288,289). While no ligand for US27 has been identified, robust signal transduction capabilities have been identified for US27. Specifically, US27 couples to Gβγ to stimulate PI3K-Akt signal transduction resulting in the activation of nuclear respiratory factor-1 (NRF-1) and the transcription of genes under the control of the antioxidant response element (ARE) (295). Additionally, the presence of US27 has been associated with increased proliferative abilities in transiently transfected cells suggesting a potential role during viral latency and reactivation, however, no direct study has recapitulated these results during infection (293).

Among the four chemokine receptors encoded by HCMV, US28 is the most extensively studied. US28 shares homology to multiple host chemokine receptors including CCR1, CCR5, and CX_3CR1 (292,296,297). Unsurprisingly, US28 is equally diverse regarding the specific ligands to which it binds. Known ligand binding partners include: CCL2, CCL3, CCL4, CCL5, CCL7, and CX_3CL1 (227,298,299). During infection, US28 localizes to plasma membrane where it is continuously internalized within endocytic vesicles (300). US28 signaling is both constitutive and ligand dependent with differential signal transduction capabilities dependent on the specific bound ligand. Constitutive US28 signal transduction has traditionally associated with coupling to $G\alpha_q$ to stimulate PLC-β and PI3K-Akt pathways to activate transcription factors such as nuclear factor of activated T-cells (NFAT) and NFκB (301). Upon binding to CCL2 or CCL5, US28 signal transduction induces calcium flux and subsequent MAPK activation whereas binding to CCL5 stimulates coupling to $G\alpha_{12/13}$ to activate Rho and focal adhesion kinase (FAK), promoting actin rearrangements and chemotaxis (297,302–304). By contrast, CX_3CL1 binding prevents $G\alpha_q$ coupling, thereby inhibiting PLC-β and NFκB signaling (227,305,306). Importantly, US28

transcripts and protein are expressed during both lytic and latent replication, and its activity is essential for the establishment and maintenance of latency and the capacity to reactivate (291). During the establishment of latency, US28 suppresses NFκB signaling, thereby reducing transcription from the MIEP (192,222). This repression depends on both ligand binding and signaling capacity, as mutations that impair either function prevent the virus from establishing or maintaining latency (193). In the context of reactivation, US28 engages $G\alpha_{12}$ proteins to activate RhoGEFs and downstream RhoA to promote efficient viral reemergence (206). While it remains unresolved whether this mechanism acts directly on viral transcription or indirectly through promoting cellular differentiation, it is clear that US28 signaling drives differentiation along the myeloid lineage, a process tightly linked to reactivation (193). Additionally, US28 capable of interfacing with several canonical signal transduction pathways to activate transcription factors such as NFAT, CREB, NF-κB, ELK/SRE, STAT3, SRF, and TCF/LEF which have been shown to bind the MIEP (282,307–310). Outside of viral latency and reactivation, US28 has been demonstrated to be necessary and sufficient for the migration of infected macrophages and vascular smooth muscle cells (vSMCs) (303). US28 induced migration is ligand dependent and cell-type specific. In vSMCs, migration is stimulated by CC chemokine binding but inhibited by the CX_3CL1, whereas in macrophages the opposite occurs, with CX_3CL1 promoting US28-mediated migration (227,306). This process requires coupling to $G\alpha_{12/13}$ proteins and involves downstream signaling through Src and FAK (304). Finally, US28 has been demonstrated to have immunomodulatory properties, specifically as a chemokine scavenging protein. One such study noted that the supernatants of fibroblast cultures infected with a US28 null virus exhibited an increase in CC chemokine concentration when compared to infection with a wildtype virus (311). The in vivo relevancy of these observations remains to be determined.

Together, the HCMV-encoded vGPCR contributes uniquely to viral persistence, balancing host immune evasion, modulation of signaling, and control of the latency–reactivation switch. Ongoing work will be essential to fully define how these receptors cooperate during infection and whether they can be targeted therapeutically to disrupt lifelong HCMV persistence.

1.6.3 HCMV Encoded MHC and Cytokine Impersonators

CMV encodes several immune-modulatory proteins that interfere, or mimic MHC-I function, the best characterized from this group is UL18. Although UL18 adopts an overall MHC-I like structure, it shares only ~25% sequence identity with classical MHC-I molecules (312). Functionally, UL18 binds to the inhibitory receptor LILRB1 on NK cells and is capable of presenting peptides in a manner similar to host MHC-I (313). The protein is heavily glycosylated, containing 13 potential N-linked glycosylation sites, which shield much of its surface with carbohydrate groups. This extensive glycosylation restricts most protein–protein interactions, leaving only its ability to engage LILRB1. Early studies suggested UL18 broadly blocked NK cell killing; however, later work revealed a more complex role. Specifically, LILRB1^{+} NK cells are inhibited when encountering UL18-expressing fibroblasts, whereas LILRB1^{-} NK cells are instead activated (313). Notably, UL18 is expressed with late kinetics, appearing around 72 hours post-infection, and is not required for viral replication in vitro (314). Beyond UL18, HCMV encodes additional modulators of MHC-I pathways. US3 prevents MHC-I molecules from leaving the endoplasmic reticulum, leading to perinuclear accumulation of MHC-I heavy chains, while US6 inhibits antigen presentation by binding to TAP and blocking peptide transport (315,316). Interestingly, UL18 has been shown to interact with US6, restoring TAP activity for peptide loading onto UL18 itself while continuing to block loading of host MHC-I molecules (317).

HCMV encodes a viral homolog of IL-10 (cmvIL-10), produced from the UL111A gene, which mimics host IL-10 function despite limited sequence homology (318). By binding the IL-10 receptor complex and activating Jak1/Tyk2–STAT3 signaling, cmvIL-10 suppresses proinflammatory cytokine production, downregulates MHC-II expression, and inhibits T cell activation, thereby dampening antiviral immunity (319). During productive infection, cmvIL-10 skews macrophages and dendritic cells toward a tolerogenic phenotype, while alternatively spliced latency-associated isoforms (LAcmvIL-10) are expressed in CD34^{+} progenitor cells (320). These isoforms retain immune-suppressive activity and additionally enhance progenitor survival, supporting maintenance of latent reservoirs. Deletion or neutralization of cmvIL-10 leads to heightened immune responses and reduced viral persistence, emphasizing its role as a key viral

cytokine that co-opts host immunoregulatory pathways to promote both immune evasion and lifelong latency (321).

Section 1.7: Models for the Study of Human Cytomegalovirus Latency and Reactivation

1.7.1 CD34$^+$ Hematopoietic Progenitor Cells – "The Gold Standard"

CD34$^+$ HPCs represent the natural in vivo reservoir of latent virus, harboring HCMV genomes in an episomal transcriptionally restricted state, and are considered the gold standard model for experimentally studying HCMV latency (177,178). Isolated from bone marrow, cord blood, or fetal liver, they represent a heterogeneous pool of cells ranging from early progenitors to lineage-committed precursors and are permissive to latent infection. Long term culture involves a transwell system where CD34$^+$ HPCs are cultured above a stromal cell support layer to maintain progenitor stemness (322). This system recapitulates key hallmarks of latency such as reduced viral transcription, progressive loss of detectable genomes, and a lack of infectious virion production (323). Differentiation down the myeloid lineage triggers reactivation; a rare event occurring in approximately 1 in 10,000 cells (324). Reactivation is driven by the addition of cytokines such as granulocyte colony stimulating factor (G-CSF) and granulocyte-macrophage-colony stimulating factor (GM-CSF) underscoring the link between hematopoietic maturation and viral control (325). Importantly, findings in CD34$^+$ HPCs such as roles for viral genes that regulate latency and host pathways involved in chromatin modifications have been validated in humanized mouse models, reinforcing their physiological relevance (325). Limitations of the model include donor variability, limited availability of bone marrow– or cord blood–derived cells, and challenges with genetic manipulation. Mobilized peripheral blood stem cells and fetal liver HPCs offer alternatives, though each introduces confounding factors. To overcome these hurdles, embryonic stem cell (hESC)–derived HPC models have been developed that recapitulate latency and reactivation, allow scalable and reproducible culture, and support higher frequencies of reactivation of 1 in approximately 300 cells (326). This system addresses donor heterogeneity

and limited material, providing an emerging platform to dissect host–virus interactions during latency with greater resolution.

1.7.2 CD14$^+$ Monocytes Recapitulate Aspects of HCMV Latency

Monocytes are central to the dissemination and persistence of HCMV, both as latent reservoirs and as vehicles for viral spread (327). Following primary infection at mucosal surfaces, monocytes subsequently traffic to the bone marrow, where they may transfer infection to CD34$^+$ HPCs. Infected monocytes exhibit enhanced adhesion, cytoskeletal remodeling, and motility, enabling extravasation into tissues where they differentiate into macrophages (328). This differentiation not only establishes long-lived tissue reservoirs but also provides a trigger for viral reactivation. Like CD34$^+$ HPCs, monocytes are a heterogeneous population, broadly classified into classical, intermediate, and nonclassical subsets, each with distinct immunological roles. HCMV infection appears to bias differentiation toward proinflammatory macrophage-like states, though whether the virus selectively infects subpopulations or drives specific fates remains unresolved (329). Transcriptomic analyses suggest that latency in monocytes is not transcriptionally silent but marked by delayed and restricted gene expression. Viral factors such as US28, UL7, and LUNA regulate monocyte-to-macrophage differentiation, latency, and reactivation, often by manipulating MAPK and AKT signaling pathways (193,205,219). Entry of HCMV into monocytes involves viral glycoproteins (e.g., gB, pentamer complex) engaging host receptors such as EGFR and integrins, which activate signaling cascades that enhance cell survival, motility, and long-term differentiation. In vitro infection of primary monocytes is characterized by delayed nuclear entry and gene expression, with viral transcription becoming detectable only after differentiation into macrophages (136,330,331). Tumor-derived myelomonocytic cell lines, particularly THP-1 cells, have been widely used to dissect molecular mechanisms of latency, including silencing and re-expression of immediate early genes. While these models lack robust reactivation potential, they have been invaluable in identifying viral promoters, host transcription factors, and signaling pathways involved in latency control (332). Ultimately, validation in primary CD14$^+$ monocytes remains essential, as these primary cells better reflect the complex biology of HCMV persistence in vivo.

1.7.3 Humanized Mouse Models of HCMV Infection

The strict species specificity of HCMV has limited the development of conventional animal models, making humanized mice the most relevant in vivo system. In the huNSG model, NOD-scid-IL2Rγ^{null} mice were engrafted with human CD34^{+} HPCs. These mice reconstituted human myeloid cells at physiologically relevant levels, permitting HCMV infection following inoculation with infected fibroblasts (333,334). Viral DNA can subsequently detected in organs repopulated with human hematopoietic cells (179). Treatment with G-CSF and the CXCR4 inhibitor AMD3100 enhanced mobilization of infected cells into peripheral tissues, with viral transcripts and proteins localizing specifically to human monocytes and macrophages (179). This model also recapitulated clinical observations of cell-associated transmission, as transplantation of stem cells from seropositive donors transmitted infection to seronegative huNSG mice. A major limitation of huNSG mice is their incomplete immune reconstitution, lacking functional B cells, T cells, and dendritic cells. To address this, the huBLT model was developed by engrafting human bone marrow, liver, and thymus tissue into NOD-scid-IL2Rγ^{null} mice (335). huBLT mice display more complete immune reconstitution, including functional CD4^{+} and CD8^{+} T cells, NK cells, and antibody responses. In this context, HCMV infection elicits human T-cell immunity and HCMV-neutralizing antibodies, while G-CSF treatment stimulates viral reactivation and dissemination to peripheral tissues (335). Humanized mouse models have been instrumental in validating viral and host determinants of latency and reactivation, as well as probing the role of viral gene products in hematopoietic differentiation. Variable engraftment efficiency, heterogeneous human-to-mouse cell ratios, and species-specific differences in cytokine signaling complicate interpretation. Despite these challenges, these models uniquely enable in vivo studies of HCMV within a human cellular and immune environment, providing an essential platform for mechanistic research and preclinical evaluation of therapies.

1.7.4 Comparative Animal Models: MCMV, RCMV, and RhCMV

Because HCMV is strictly species-specific, related animal cytomegaloviruses have been essential for uncovering conserved mechanisms of latency and reactivation. Among these, murine

cytomegalovirus (MCMV) is the most widely studied. MCMV establishes latency in the spleen, bone marrow, and salivary glands, recapitulating many aspects of HCMV biology, including genome silencing and reactivation upon immune suppression (336–338). The availability of genetic tools, inbred mouse strains, and robust immunological assays has made MCMV invaluable for dissecting host–virus interactions. Nevertheless, differences in viral gene content and immune modulation limit its direct applicability to HCMV (339).

Rat cytomegalovirus (RCMV) has been used less extensively but provides complementary insights. Like HCMV, RCMV persists in monocytes and endothelial cells and exhibits immune evasion strategies that parallel those of its human counterpart (340–342). Its utility lies particularly in comparative immunology, though fewer reagents and genetic tools constrain widespread adoption relative to MCMV.

Rhesus macaque cytomegalovirus (RhCMV) is the most physiologically relevant nonhuman primate model, closely resembling HCMV in genome organization, immune evasion genes, and pathogenesis. RhCMV infection establishes latency, persistence, and reactivation that mirror human infection (343–345). Importantly, RhCMV-based vectors have been leveraged for vaccine development, demonstrating potent protection in simian immunodeficiency virus challenge models (346–348). These findings highlight RhCMV's translational significance. However, the cost, ethical considerations, and logistical demands of seronegative nonhuman primate research limit broad use.

Together, these animal models provide critical perspectives on conserved and divergent features of CMV latency. MCMV offers experimental tractability, RCMV expands comparative approaches, and RhCMV provides the closest surrogate to HCMV. When used in combination with humanized mouse and primary cell systems, these models form an indispensable toolkit for advancing our understanding of CMV biology and for informing antiviral and vaccine development.

Chapter 2: Proximity-Dependent Mapping of the HCMV US28 Interactome Identifies RhoGEF Signaling as a Requirement for Efficient Viral Reactivation

Samuel Medica[1], Lindsey B. Crawford[1*], Michael Denton[1], Chan-Ki Min[2], Taylor A. Jones[1], Timothy Alexander[1], Christopher J. Parkins[1], Nicole L. Diggins[1], Gabriel J. Streblow[1], Adam T. Mayo[1], Craig N. Kreklywich[1], Patricia Smith[1], Sophia Jeng[3], Shannon McWeeney[3], Meaghan H. Hancock[1], Andrew Yurochko[2], Michael S. Cohen[4], Patrizia Caposio[1], and Daniel N. Streblow[1,5]

[1] Vaccine and Gene Therapy Institute, Oregon Health and Science University, Beaverton, Oregon, USA

[2] Department of Microbiology & Immunology, Center for Molecular & Tumor Virology, Louisiana State University Health Sciences Center-Shreveport, Shreveport, LA 71130, USA

[3] Department of Bioinformatics and Computational Biology, Oregon Health and Science University, Portland, Oregon, USA

[4] Department of Chemical Physiology and Biochemistry, Oregon Health and Science University, Portland, Oregon, USA

[5] Division of Pathobiology and Immunology, Oregon National Primate Research Center, Beaverton, Oregon, USA

***** Current affiliation: Department of Biochemistry, University of Nebraska – Lincoln, Lincoln, Nebraska, USA

PLoS pathogens. 2023 Oct 2;19(10):e1011682.

Doi: 10.1371/journal.ppat.1011682

Section 2.1: Abstract

Human cytomegalovirus (HCMV) encodes multiple putative G protein-coupled receptors (GPCRs). The constitutively active GPCR US28 functions as a viral chemokine receptor and is expressed during both latent and lytic phases of virus infection. US28 actively promotes cellular migration, transformation, and plays a major role in mediating viral latency and reactivation; however, knowledge about the interaction partners involved in these processes is still incomplete. Herein, we utilized a proximity-dependent biotinylating enzyme (TurboID) to characterize the US28 interactome when expressed in isolation, and during both latent ($CD34^+$ hematopoietic progenitor cells) and lytic (fibroblasts) HCMV infection. Our analyses indicate that the US28 signalosome converges with RhoA and EGFR signal transduction pathways, sharing multiple mediators that are major actors in processes such as cellular proliferation and differentiation. Integral members of the US28 signaling complex were validated in functional assays by immunoblot and small-molecule inhibitors. Importantly, we identified RhoGEFs as key US28 signaling intermediaries. In vitro latency and reactivation assays utilizing primary $CD34^+$ hematopoietic progenitor cells (HPCs) treated with the small-molecule inhibitors Rhosin or Y16 indicated that US28 – RhoGEF interactions are required for efficient viral reactivation. These findings were recapitulated in vivo using a humanized mouse model where inhibition of RhoGEFs resulted in a failure of the virus to reactivate. Together, our data identifies multiple new proteins in the US28 interactome that play major roles in viral latency and reactivation, highlights the utility of proximity-sensor labeling to characterize protein interactomes, and provides insight into targets for the development of novel anti-HCMV therapeutics.

Section 2.2: Author Summary

Human cytomegalovirus (HCMV) continues to be amongst the most prevalent viral infections worldwide. Primary infection of HCMV is often asymptomatic and results in the establishment of latency within cells of myeloid lineage. Once latency is established, the virus will persist throughout the host's lifetime. Subsequent viral reactivation events can pose life-threatening health complications for the immunocompromised population; including transplant recipients

and AIDS patients. Many factors have been shown to mediate the switch from latent to lytic HCMV infection such as signal transduction through the viral G protein-coupled receptor (vGPCR) US28. In the present report, we utilize proximity-dependent labeling coupled with mass spectrometry to identify host and viral proteins proximal to US28. Our analysis indicates significant overlap between US28 and the EGFR and RhoA signaling pathways. We further explored the relationship between US28 and the RhoA signal transduction pathway to identify RhoGEFs as an important member of the US28 signalosome. Our data indicates that ablation of RhoGEF activity significantly attenuates US28 signaling. Furthermore, we show that pharmacological inhibition of RhoGEFs results in an inability of the virus to efficiently reactivate in vitro and in vivo. These findings reveal previously unknown US28 interactors, which play an integral role in the facilitation of viral reactivation and provide the first example of specific cellular factors being implicated in US28 function and viral reactivation in vivo.

Section 2.3: Introduction

Human cytomegalovirus (HCMV) is the largest member of the β-herpesvirus family and infects the majority of the world population (349,350). The virus persists as a lifelong infection through latency establishment in hematopoietic progenitor cells (HPCs) located in the bone marrow (187). Latently infected monocytes generated from these HPCs are thought to be the cellular reservoir from which the virus disseminates to other tissues of the body (177,178,351). Viral reactivation events pose a major risk during solid organ and bone marrow transplantation and can lead to CMV-associated disease including organ failure and graft rejection (352–359). Several cellular signaling pathways have been implicated to be involved with HCMV latency and reactivation, including EGFR, PI3K/AKT, MAPK, TGF-β, Src, ERK, Rho, and Wnt pathways (225,307,309,310,360–363); however, the exact signaling mechanisms that contribute to the establishment of latency and potential to reactivate remain unclear. Moreover, current FDA-approved HCMV antivirals often have toxic effects and primarily target late phases of viral replication when clinical manifestations are already present. Therefore, in order to discover additional treatment options for HCMV, it is crucial that we elucidate the molecular mechanisms mediating viral latency and reactivation.

HCMV encodes four putative G protein-coupled receptors (GPCRs) with homology to cellular chemokine receptors; however, US28 has been the most extensively characterized to date. US28 is expressed in infected human peripheral blood cells during periods of latency and during reactivation episodes (364–366). US28 signaling results in the activation of multiple transcription factors involved in cellular proliferation, differentiation, and migration; including nuclear factor of activated T cells (NF-AT), cAMP-response element binding protein (CREB), nuclear factor kappa-light chain enhancer of activated B cells (NF-κB), serum response factor (SRF), signal transducer and activator of transcription 3 (STAT3), and β-catenin (225,307,309,310,360–363). We, and others, have previously demonstrated that US28 is required for HCMV reactivation in latently infected $CD34^+$ HPCs and that US28 drives cellular differentiation down the myeloid lineage in HCMV-infected $CD34^+$ HPCs (191–193). Additionally, our previous studies show that US28 is required for both the maintenance of viral latency and the capacity to reactivate in vivo utilizing a humanized mouse model (193). Combined, these data indicate that US28 is required for latency/reactivation in vitro and in vivo; however, the specific cellular signaling pathways involved have yet to be defined.

US28 uniquely binds both CC chemokines (RANTES, MCP-1, MIP-1α) and CX_3C-chemokines (Fractalkine) (367–369). Depending on the ligand stimulus and infected cell type, US28 signaling can result in the activation of multiple signaling transduction pathways. For instance, US28 coupling with $G\alpha_{12/13}$ proteins, and subsequent activation of RhoA and downstream effector Rho-associated kinase (ROCK) is critical for promoting actin reorganization and cellular migration in infected smooth muscle cells and monocytes (227,370). Cell migration, differentiation, and other cellular processes are tightly regulated in part by activation of Rho GTPases, which are in turn regulated by Rho guanine nucleotide exchange factors (RhoGEFs) (371,372). GEFs provide a direct link between the activation of RhoA and the cell-surface receptors for growth factors (i.e., EGFR), cytokines and chemokines (i.e., RANTES, MCP-1, MIP-1α), and G protein-coupled receptors (i.e., US28). Because cellular differentiation and migration are essential for the switch from latent to lytic HCMV infection, RhoGEFs may serve as key regulators of cellular signaling pathways involved in viral latency and reactivation. However, it is difficult to determine the consequences of US28

signaling without a complete understanding of the protein interactions that occur during signal transduction.

In the current study, we utilized an unbiased proximity-dependent labeling enzyme (TurboID) to characterize proteins that are proximal to US28 in multiple relevant cell models. Our proteomic analysis identified multiple novel proteins involved in US28 signal transduction. We further explored the relationship between US28 and the RhoA signal transduction pathway to identify RhoGEFs as important facilitators of viral reactivation. Our data indicates that ablation of RhoGEF activity, via pharmacological inhibition, attenuates US28 signaling activity. Furthermore, we show that inhibition of RhoGEFs, via the small-molecule inhibitors Rhosin and Y16, impedes efficient viral reactivation in primary $CD34^+$ HPCs. Utilizing a humanized NSG mouse model, we show that treatment with Rhosin resulted in failure of the virus to reactivate. Collectively, our data demonstrates that RhoGEFs are integral components of the US28 signalosome and are required for efficient viral reactivation.

Section 2.4: Results

2.4.1 Characterization of US28-TurboID Constructs

Our understanding of US28 signaling pathways and the proteins that act in concert with US28 is still incomplete. To characterize how US28 signaling influences latency, reactivation, and lytic infection, we took an unbiased approach to determine interactors within the US28 signalosome. By affixing TurboID to the C' terminal tail of US28, we developed a system to assess the US28 interactome directly in living cells. Expression of the HA-tagged US28-TurboID protein (HA-US28-BT), at the expected size, was verified by immunoblot after transfection into HEK293M cells **(Fig. 2.1A).** We chose to use HEK293M cells because of their efficient transfectability and prior use in US28 functional assays. Next, we examined the capability of HA-US28 and HA-US28-BT to transcriptionally activate the reporter elements SRE and SRF in transiently transfected HEK293M cells. In the absence of any exogenous ligands, transfected HA-US28 and HA-US28-BT were able to stimulate $G\alpha_{q/11}$ and downstream SRE at levels several-fold above transfection with the empty pcDNA3.1 vector alone **(Fig. 2.1B)**. In a similar manner, transfected HA-US28 and HA-US28-BT

induced activation of $G\alpha_{12/13}$ and downstream RhoA signaling as measured via SRF reporter element activation **(Fig. 2.1C)**. To confirm that addition of TurboID does not alter localization of US28, we performed immunofluorescence imaging analysis on human fibroblasts transfected with HA-US28 and HA-US28-BT. No discernable difference in localization was observed between the two constructs **(Fig. 2.1D).** Together, these results show that HA-US28-BT is efficiently expressed in HEK293M cells and that the addition of TurboID to US28 does not impact signaling activity or localization.

Figure[2.1] Expression, Signaling, and Localization of US28 BioID Constructs

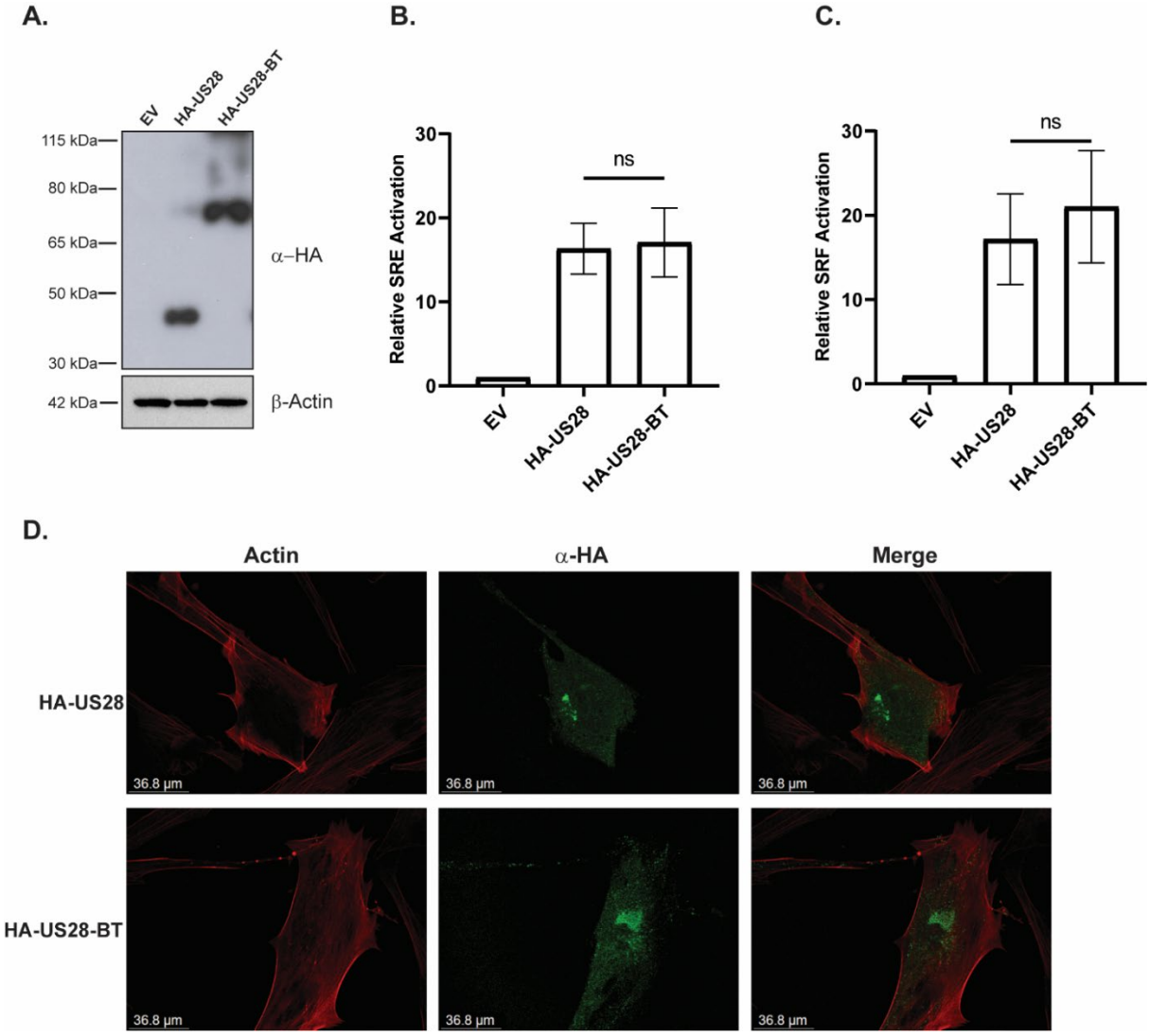

[2.1] Figure legend

(A) HEK293M cells were transfected with pcDNA3.1-HA-US28 (HA-US28), pcDNA3.1-HA-US28-TurboID (HA-US28-BT), or the empty pcDNA3.1 vector (EV). Lysates were harvested 24 hours post-transfection and expression was

confirmed via immunoblot using an anti-HA antibody (n = 3, representative blot shown). **(B & C)** HEK293M cells were transfected with HA-US28, HA-US28-BT, or the empty pcDNA3.1 vector (EV) along with Renilla and luciferase reporter plasmids for **(B)** SRE or **(C)** SRF. At 18 hours post-transfection, media was exchanged with serum-free DMEM. Luciferase activity was measured using the Dual-Luciferase Reporter Assay System (Promega) at 6 hours post-media exchange. Error bars represent the standard error of the mean between triplicate experiments. Statistical significance was calculated by one-way ANOVA followed by Tukey's multiple comparisons test between experimental groups. (**D)** NHDF cells were seeded onto coverslips and transfected with either HA-US28 or HA-US28-BT. At 48 hours post-transfection, cells were fixed, permeabilized, and stained overnight against HA (green) and phalloidin (actin-red) (n = 2, representative images shown).

2.4.2 Identification of the US28 Interactome

Next, we sought to confirm that our system could efficiently label proteins within the US28 interactome, including those with transient or short-lived interactions **(Fig. 2.2A).** We chose to use HEK293M cells for initial characterization of the interactome before validating results in infected cells. To this end, HEK293M cells were transfected with HA-US28 and HA-US28-BT. At 18 hours post transfection, the culture medium was supplemented with biotin and lysates harvested six hours thereafter. The resulting tagged proteins were purified via streptavidin mediated bead-based precipitation. One quarter of the same purified protein lysate used for mass spectrometry was analyzed to verify input and control conditions. Coomassie staining verified comparable protein content in HA-US28 and HA-US28-BT transfected whole cell lysates **(Fig. 2.2B, right: Whole Lysate).** Moreover, appreciable amounts of protein were only detectable in cells transfected with HA-US28-BT after streptavidin-mediated purification and pulldown of biotinylated proteins **(Fig. 2.2B, left: SA-PD)**. Further analysis by immunoblot using HRP-conjugated streptavidin confirms efficient labeling **(Fig. 2.2B, left: SA-PD)** and specific pulldown **(Fig. 2.2B, right: Unbound)**. While transient transfection in established cell lines is a tractable model for initial studies, the differential cellular signaling events that occur during the course of infection are not accurately captured in these systems. To characterize the host and viral proteins that interact with US28 during infection, we engineered a recombinant virus using the TB40/E-GFP backbone and affixing the TurboID enzyme onto the C' terminal tail of US28 (TB40/E-GFP-US28-BT). NHDF or human embryonic stem cell (hESC) -derived $CD34^+$ HPCs were mock infected, or infected with TB40/E-GFP or TB40/E-GFP-US28-BT at a MOI of 2. In NHDF experiments, the culture medium was supplemented with biotin at 3-days post infection (dpi) and cell lysates were

harvested six hours thereafter. CD34^{+} HPCs were cultured in conditions that promote latent infection as previously described (193). At 14-dpi, the culture medium was supplemented with biotin and cells were incubated overnight prior to cell lysis. Viral infection and efficient biotin ligation were confirmed in whole cell lysates derived from NHDFs via immunoblot using HRP-conjugated streptavidin and antibodies directed against HCMV pUL44 and TurboID **(Fig. 2.2C).** Similar results were obtained using whole cell lysates derived from CD34^{+} HPCs **(Fig. 2.2D).** The resulting interacting proteins for all three in vitro models were purified via streptavidin bead-based precipitation and analyzed by liquid chromatography tandem mass spectrometry (LC-MS/MS).

Figure[2.2] Labeling and Purification of Transfected and Infected Lysates

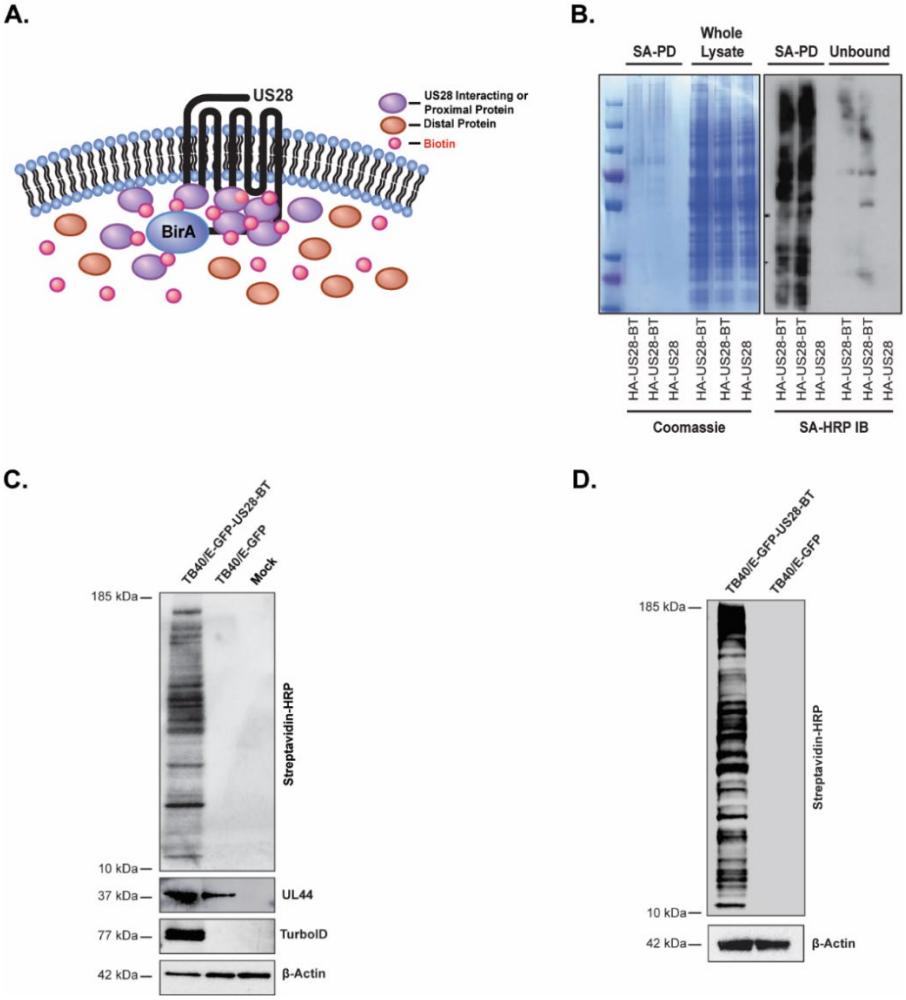

[2.2] Figure legend

(A) Experimental outline of US28-TurboID labeling in cells. Interacting or proximal proteins (purple) are tagged with biotin (red) while distal proteins (orange) remain untagged. Tagged proteins are purified and analyzed by

mass spectrometry to identify proteins that are in close proximity to US28. **(B)** HEK293M cells were transfected with pcDNA3.1-HA-US28-BT (HA-US28-BT) or pcDNA3.1-HA-US28 (HA-US28). At 18 hours post-transfection the cell culture medium was supplemented with biotin (50µg/mL) for 6 hrs. Tagged proteins were bound to NeutrAvidin beads and incubated overnight prior to extensive washing, trypsin digestion, and formic acid treatment. Protein content, purification, and efficient labeling were confirmed by Coomassie staining and streptavidin-specific immunoblot (n = 2, representative images shown). **(C)** NHDF cells or **(D)** $CD34^+$ HPCs were infected with TB40/E-GFP-US28-BT or TB40/E-GFP at a MOI of 2. At 3 dpi, the cell culture medium was supplemented with biotin (50µg/mL) for 6 hrs. Labeling and infection were confirmed by immunoblot on whole cell lysates using the indicated primary antibodies. Purified proteins were analyzed by mass spectrometry for protein identification (n = 3, representative blot shown).

2.4.3 US28 Signals Through Multiple Pathways Including RhoGEFs

Hits from our proteomic analysis were refined by excluding proteins that were identified as likely contaminants based on comparison to the CRAPome database (373). Our revised list included 984, 1,054, and 843 host proteins which were in close proximity to US28 in HEK293M, NHDF, and $CD34^+$ HPC datasets, respectively. To examine the cellular signaling pathways whose components were in close proximity to US28, we used the pathway analysis tool Reactome (374) to identify significantly enriched signal transduction pathways **(Fig. 2.3A-C & Data S2.1-3)**. Our analysis indicated enrichment of proteins that are members of multiple cellular signaling pathways contributing to membrane trafficking, cellular metabolism, differentiation, and cellular migration. Consistent with other studies, our pathway analysis of the US28 signaling complex in all three cell culture models demonstrates significant overlap between US28 and the RhoA signaling pathway (227,305,370,375). While we identified EphA2 in the US28 interactome during proximity-dependent labeling in NHDFs, which was consistent with previous reports (222,375), we did not detect this cellular protein tyrosine signaling molecule in the US28 interactome in $CD34^+$ HPCs but we did consistently detect Src **(Fig. 2.4A)** (304). Because we have previously shown that US28 signaling stimulates $G\alpha_{12/13}$ activity (370), we decided to further explore US28 – RhoA interactions using the STRING database to map identified interactors and their downstream effectors. Interestingly, Rho-specific guanine nucleotide exchange factors (GEFs) responsible for activation of RhoA, were highly enriched in the US28 proximity labeling in all three cell types/conditions **(Fig. 2.3D-F)**.

Figure[2.3] Network Analysis of the US28 Interactome

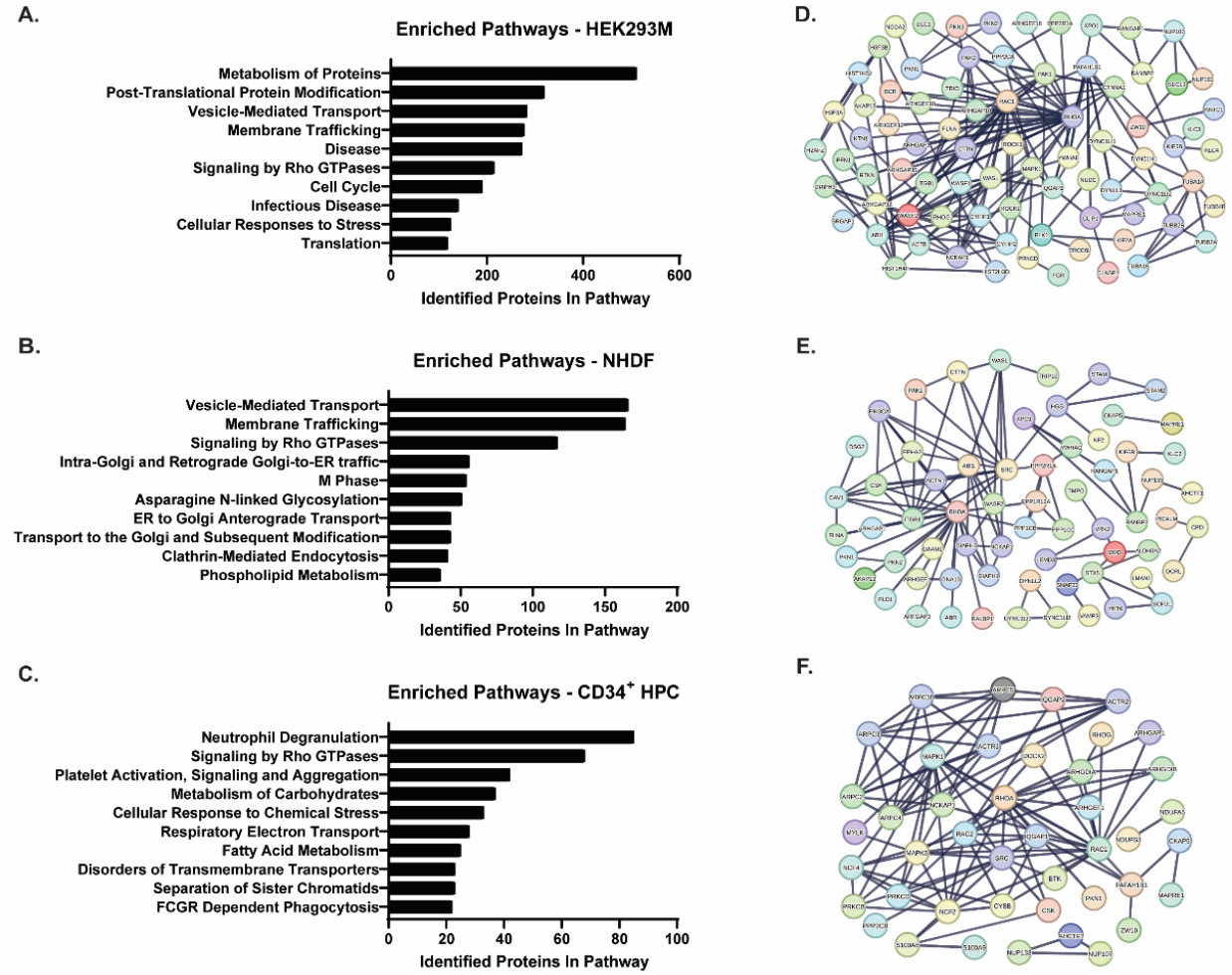

[2.3] Figure legend

Proteins within the US28 interactome were identified via LC-MS/MS and analyzed using Reactome and STRING software tools. **(A-C)** Proteins identified by LC-MS/MS were analyzed using Reactome for **(A)** HEK293M cells transfected with pcDNA3.1-HA-US28-BT, **(B)** NHDFs infected with TB40/E-GFP-US28-BT, and **(C)** CD34$^+$ HPCs infected with TB40/E-GFP-US28-BT. Significantly enriched pathways and the number of associated proteins were plotted using GraphPad Prism 9.0 software. **(D-F)** STRING network analysis of the US28 interactome identified RhoGEFs as members of the US28 interactome in **(D)** HEK293M cells transfected with pcDNA3.1-HA-US28-BT, **(E)** NHDFs infected with TB40/E-GFP-US28-BT, and **(F)** CD34$^+$ HPCs infected with TB40/E-GFP-US28-BT.

In addition to host proteins, we also identified several viral proteins that are potential interaction partners of US28 during both latent and lytic infection. In cellular lysates obtained from infected NHDFs, we identified 28 viral proteins that may interact with US28 **(Fig. 2.4B & Table 2.1)**.

Figure[2.4] Comparison of the US28 – Rho GTPase Specific Interactomes During Latent and Lytic Infection

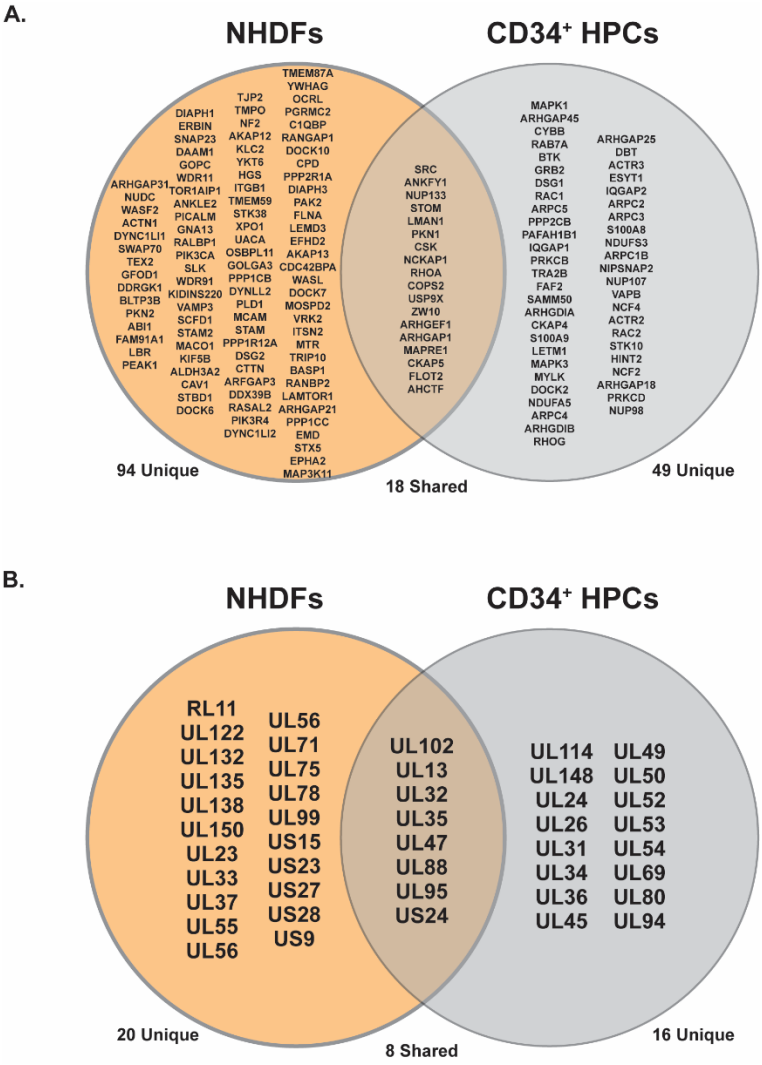

[2.4] Figure legend

(A) Candidate host US28 interaction partners specific to Rho GTPase signaling were compared between NHDFs and latently infected CD34⁺ HPCs. **(B)** Candidate viral US28 interaction partners were compared between NHDFs and latently infected CD34⁺ HPCs.

Interestingly, several viral GPCRs (UL33, UL78, and US27), glycoproteins (UL55, UL75, UL132, and US9), and tegument proteins (UL23, UL35, UL47, UL71, UL88, US23, and US24) were shown to be in close proximity to US28. These data would suggest that, during late lytic replication conditions, US28 is associated with the viral assembly compartment. In lysates obtained from latently infected CD34⁺ HPCs, we identified 24 viral proteins that interact with, or are within close proximity, to US28 **(Fig. 2.4B & Table 2.2)**.

Table[2.1]

Protein	Description	q-Value	PEP Score	# Peptides	PSMs	AAs	kDa
RL11	Unknown	0.000	10.46	2	4	234	26.6
UL102	Primase-Associated Factor	0.000	46.53	10	50	874	94
UL122	Major Immediate-Early Transactivator	0.000	39.93	8	47	564	61
UL13	Mitochondria MICOS stabilizer	0.000	93.84	17	84	473	54.5
UL132	Glycoprotein; Formation of Assembly Compartment	0.000	183.35	19	278	270	29.7
UL135	Viral reactivation	0.000	60.26	11	55	308	33.3
UL138	Viral latency	0.000	18.21	4	16	169	19.3
UL150	Viral Entry	0.000	39.99	6	35	328	35.1
UL23	Tegument Protein; Particle Infectivity	0.000	9.35	3	5	284	32.9
UL32	Tegument Phosphoprotein	0.000	137.07	26	112	1049	112.7
UL33	Viral G Protein-Coupled Receptor	0.000	48.70	6	45	411	46
UL35	Tegument Protein; Particle Infectivity	0.000	18.93	4	16	641	72.6
UL37	Viral Mitochondrion-Localized Inhibitor of Apoptosis	0.000	5.87	2	12	202	23.2
UL47	Tegument Protein; Particle Infectivity	0.000	46.53	11	26	983	110
UL55	Glycoprotein B (gB); Viral Entry	0.000	77.01	11	62	907	101.9
UL56	Viral DNA packaging	0.000	69.53	13	44	850	95.7
UL71	Tegument Protein; Particle Infectivity	0.000	191.64	28	252	361	39.8
UL75	Glycoprotein H (gH); Viral Infectivity	0.000	26.19	6	19	743	84.4
UL78	Viral G Protein-Coupled Receptor	0.000	26.47	5	21	431	47.3
UL88	Tegument Protein	0.000	45.67	12	38	429	47.7
UL95	Late Gene Expression	0.000	27.94	4	16	531	57.2
UL99	Tegument Phosphoprotein	0.000	6.88	2	9	190	20.9
US15	Tegument Protein	0.000	4.72	2	5	262	29.1
US23	Tegument Protein, Viral Transactivator	0.000	8.35	2	9	592	68.9

US24	Unknown	0.000	27.78	7	15	501	58
US27	Viral G Protein-Coupled Receptor	0.001	3.94	2	9	361	41.9
US28	Viral G Protein-Coupled Receptor	0.000	42.58	8	43	354	41
US9	Glycoprotein, blocks IFN signaling	0.000	7.02	3	7	247	28

[2.1] Table legend

Viral Proteins Within the US28 Interactome in Infected NHDF cells

Table[2.2]

Protein	Description	q-Value	PEP Score	# Peptides	PSMs	AAs	MW (kDa)
UL102	Primase-Associated Factor	0.000	15.977	6	11	874	94
UL114	DNA Repair	0.000	18.776	4	6	250	28.3
UL13	Mitochondria MICOS Stabilizer	0.000	3.643	2	2	473	54.5
UL148	Chaperone Protein	0.000	11.065	5	14	316	36.4
UL24	Unknown	0.000	10.054	3	5	300	34.2
UL26	Tegument Protein	0.000	10.021	4	8	222	24.9
UL31	Innate Immune Evasion	0.000	32.035	11	17	595	65.6
UL32	Tegument Phosphoprotein	0.000	24.99	8	12	1049	112.7
UL34	Transcriptional Repressor	0.000	32.069	7	19	407	45.4
UL35	Tegument Protein; Particle Infectivity	0.000	43.213	12	20	641	72.6
UL36	Tegument Protein	0.000	19.365	6	13	453	52.2
UL45	Unknown	0.000	30.066	12	16	906	101.7
UL47	Tegument Protein; Particle Infectivity	0.000	15.556	4	6	983	110
UL49	Viral Pre-Initiation Complex	0.000	4.307	2	3	570	63.7
UL50	Viral Egress	0.000	39.422	12	22	400	43.2
UL52	Capsid Localization	0.000	11.506	4	8	667	74.1
UL53	Viral Egress	0.000	3.265	2	2	376	42.3
UL54	Viral Polymerase	0.000	7.739	3	4	1242	137.1
UL69	Transcriptional Activator	0.000	21.081	6	13	741	82.3
UL80	Scaffold Protein	0.000	13.709	5	10	708	73.7
UL88	Tegument Protein	0.000	8.695	3	6	429	47.7
UL94	Viral Egress	0.000	17.437	5	16	345	38.2

UL95	Late Gene Expression	0.000	8.086	3	5	531	57.2
US24	Tegument Protein	0.000	12.056	4	4	501	58

2.2 Table legend

Viral Proteins Within the US28 Interactome in Latently Infected CD34$^+$ HPCs.

In In contrast to our analysis in infected NHDFs, proteins within the latency (CD34$^+$ HPC) dataset were involved in immune evasion (UL31) and gene expression (UL34, UL102, UL54, UL69, and UL95). A comparison between US28 interactomes in infected NHDFs and CD34$^+$ HPCs yielded 18 shared host and 8 shared viral proteins **(Fig. 2.4).** Previous pulldown analyses of the US28 interactome identified 47 HCMV proteins in lysates from human fibroblasts and of these we detected 28 in NHDFs during lytic replication (375). An additional 10 viral proteins were identified in our proximity labeling in CD34$^+$ HPCs that were unique to this cell type but overlapped with those reported previously (375). Interestingly, UL69 was the most highly represented viral protein in our CD34$^+$ HPC US28 interactome, we also detected the UL69 interacting protein Suppressor of Ty 6 and other elongation factors associated with UL69 (376) but not the mRNA export protein U2AF65 (377) indicating that US28 may form a complex linked with UL69. Thus, our US28 proximity labeling results largely overlap with the viral and cellular proteins reported previously, and we demonstrate a consistent intersection of US28 and the Rho signaling pathways during both latent and lytic phases of the virus lifecycle.

2.4.4 Inhibition of RhoGEFs Attenuates US28 Signaling

To validate our analyses, we took a multifaceted approach to confirm select cellular interaction partners of US28, and to examine the effects of these interactions on US28 signaling. First, we confirmed the association of previously identified host proteins that interact with US28. Our group, and others, have shown that US28 interacts with Src and ERK mediating several signal transduction events (227,303–305). The presence of newly identified interactors PDZ-RhoGEF, p115-RhoGEF, and ROCK1, as well as the known interactors (Src and ERK), were validated by traditional immunoblot following streptavidin pulldown on lysates harvested from NHDF cells infected with TB40/E-GFP-US28-BT **(Fig. 2.5A)**. Next, to examine the effects of RhoGEF interactions on US28 signaling, we identified two small-molecule compounds inhibiting various aspects of RhoGEF signaling. The small molecule inhibitors, Rhosin and Y16, sterically block RhoA interactions with associated GEFs (378,379), and inhibited RhoA activation in a dose-dependent

manner **(Fig. S2.1A)**. In US28 signaling assays, treatment with either Rhosin or Y16 lead to a 70-72% and 53-60% reduction in US28-mediated activation of the SRF reporter element, respectively **(Fig. 2.5B)**. Taken together, these results indicate a robust association between US28 and the RhoA signaling pathway during both lytic and latent phases of the viral lifecycle.

Figure[2.5] Validation of US28 Interactome Analysis

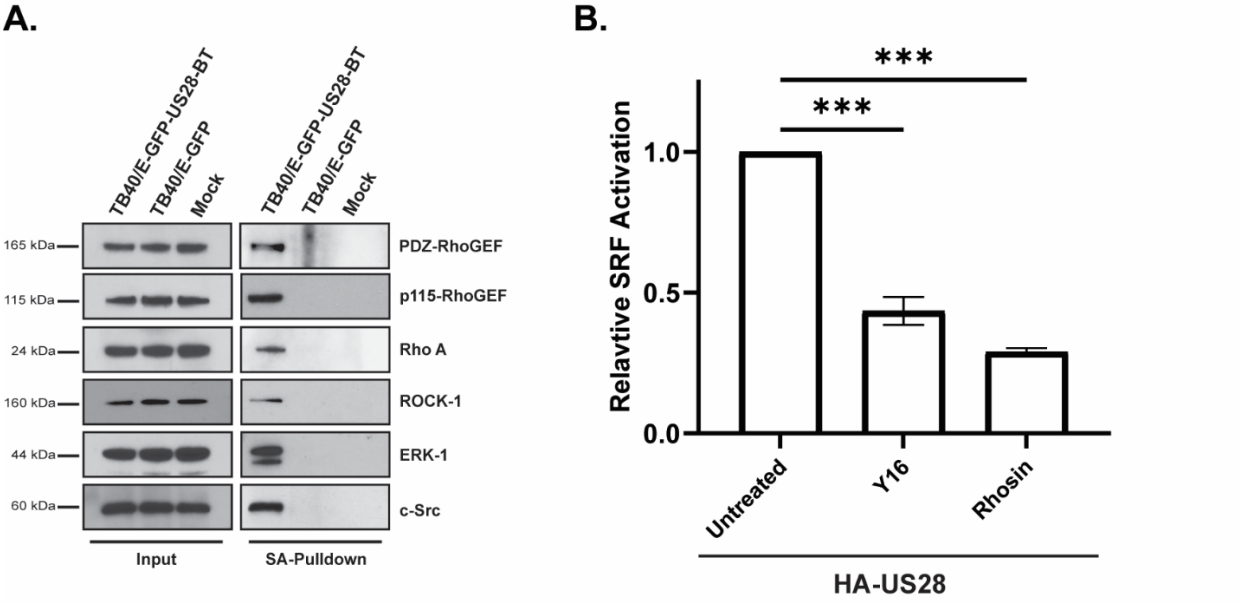

[2.5] Figure legend

(A) NHDF cells were mock infected, or infected with TB40/E-GFP-US28-BT or TB40/E-GFP at a MOI of 2. At 3 DPI, the cell culture medium was supplemented with biotin (50µg/mL) for 6 hrs. Lysates were harvested and tagged proteins were bound to NeutrAvidin beads and incubated overnight prior to extensive washing. The presence of indicated proteins was confirmed via traditional immunoblot using the indicated primary antibodies (n = 3, representative blots shown). **(B)** HEK293M cells were transfected with pcDNA3.1-HA-US28 (HA-US28) or the empty pcDNA3.1 vector along with Renilla and SRF reporter plasmids. At 18 hours post-transfection, media was changed to serum-free DMEM supplemented with Rhosin (5µM) or Y16 (5µM). Luciferase activity was measured using the Dual-Luciferase Reporter Assay System (Promega) 6 hours post-media replacement. Error bars represent the standard error of the mean between triplicate experiments and statistical significance was calculated by one-way ANOVA followed by Tukey's multiple comparisons test between experimental groups. *P* values are listed for significant comparisons where *** $P < 0.001$.

2.4.5 RhoGEFs are Required for Efficient Reactivation of From Latency

Because we identified and validated RhoGEFs in all our US28 interactome models, we examined the extent of RhoGEF involvement in viral latency and reactivation. To this end, we further characterized the pharmacological inhibitors Rhosin and Y16. In vitro cytotoxicity experiments

for both compounds showed limited to no deleterious effects on cell survival at 72 hours post-treatment in NHDFs and $CD34^+$ HPCs (**Fig. S2.1B,C)**. In addition to cytotoxicity experiments, we confirmed that neither Rhosin nor Y16 influenced viral replication in fibroblasts using the reporter virus TB40/E-GFP-gHnLuc, which expresses nano-luciferase under the rhesus cytomegalovirus gH viral promoter. Results from this experiment showed no significant effect on viral replication at concentrations as high as 40μM when compared to untreated control cells and cells treated with the HCMV antiviral Foscarnet, which demonstrated robust antiviral activity **(Fig. S2.1D)**.

To determine if RhoGEF activity is required for reactivation of HCMV in progenitor cells, $CD34^+$ HPCs were isolated from four independent primary donors, infected with TB40/E-GFP, and cultured to establish latency as previously described (193). Confirmation that RhoGEFs targeted by Rhosin and Y16 were sufficiently expressed in our $CD34^+$ HPC system was accomplished by RT-qPCR in uninfected cells **(Fig. S2.2)**. To block RhoGEF interactions during reactivation, latently infected HPCs were plated on a fibroblast layer in reactivation supportive media containing either Rhosin or Y16. The establishment of latency was confirmed in each donor by virus production under conditions that promote reactivation combined with the absence of infectious virus particles in latently infected cells (pre-reactivation). Treatment with Rhosin, to block RhoA interaction with upstream GEFs, results in a 36-49% decrease in the amount of virus produced during reactivation **(Fig. 2.6 & S2.3).** Using Y16 to target RhoA – LARG, p115-RhoGEF, and PDZ-RhoGEF interactions, results in a comparable (31-47%) decrease in the amount of virus produced during reactivation **(Fig. 2.6 & S2.3)**. Together, these data show that RhoGEF activity is required for efficient viral reactivation in $CD34^+$ HPCs.

Figure[2.6] RhoGEF Interactions Contribute to Reactivation

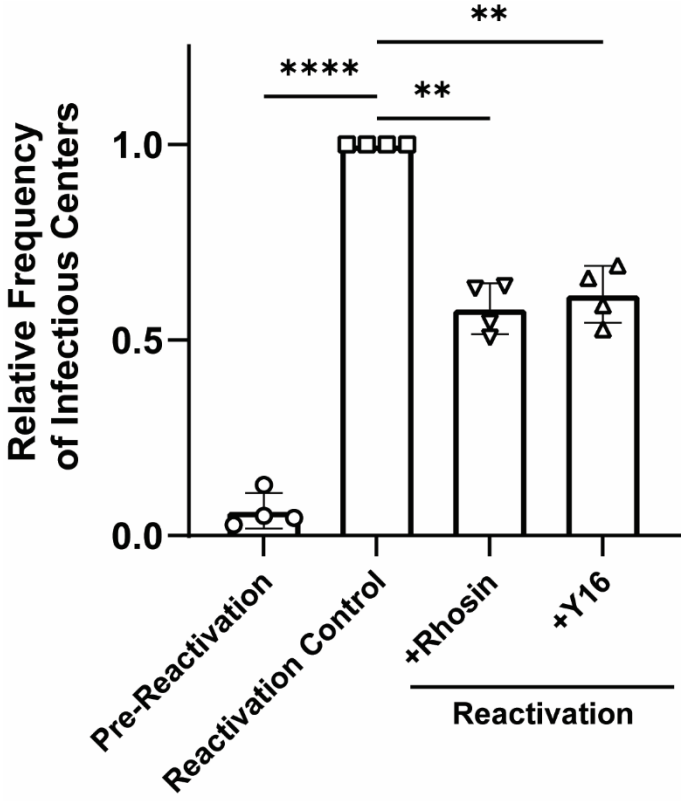

[2.6] Figure legend

Primary CD34⁺ hematopoietic progenitor cells (HPCs) isolated from four independent donors were infected with TB40/E-GFP (WT-HCMV), and then FACS isolated for viable, CD34⁺, GFP⁺ HPCs at 2 dpi as previously described (193). Infected HPCs were cultured on stromal cell support for 12 days to establish latency and equivalent populations of HPCs were co-cultured in supportive media on a fibroblast layer to reactivate virus as previously described (193). Samples were treated with the RhoGEF inhibitors Rhosin (10nM) or Y16 (10nM) at the time of reactivation, and the reactivation frequency was compared to untreated controls (reactivation). Reactivation was measured as the frequency of infectious centers determined at 3 weeks post-plating for all groups. Data is shown as the average fold change in infectious centers, as compared to the reactivation group, for four independent donors. Samples were compared by two-way ANOVA followed by Tukey's multiple comparisons test between experimental groups. *P* values are listed for significant comparisons where ** $P < 0.005$ and **** $P < 0.0001$.

2.4.6 RhoGEFs Contribute to Viral Reactivation In Vivo

To confirm that US28-mediated activation of RhoGEFs influences viral reactivation in vivo, we employed a humanized NSG (huNSG) mouse model previously developed by our group (179). In this experiment, huNSG mice were engrafted with human CD34⁺ HPCs and infected via intraperitoneal injection of TB40/E-GFP-infected fibroblasts as previously described (193).

Because the efficacy of Rhosin was greater than that of Y16 in multiple in vitro models, we decided to proceed with only Rhosin for in vivo experiments. At 8 weeks post-infection, latently-infected huNSG mice were treated with 40mg/kg Rhosin (N=5) or DMSO (N=10). To stimulate viral reactivation, animals in the experimental group were treated with granulocyte-colony-stimulating factor (G-CSF) and AMD3100 (N=5 Rhosin treated, and N=5 DMSO treated) while the remaining mice (N=5 DMSO treated) were left untreated as a control for latency maintenance. One-week post mobilization, spleen tissues were harvested and HCMV viral load was determined by qPCR. Treatment with Rhosin during reactivation resulted in a 73% decrease in viral load, as measured by copies of HCMV viral genomes, when compared with the reactivated but untreated animals **(Fig. 2.7).** Additionally, huNSG mice receiving Rhosin showed comparable viral loads to latently infected animals **(Fig. 2.7).** This data demonstrates that US28-RhoGEF interactions contribute to viral reactivation in an in vivo setting in the background of complex-multicellular interaction partners and highlights the potential of Rhosin to block HCMV reactivation.

Figure[2.7] Rhosin Inhibits Reactivation In Vivo

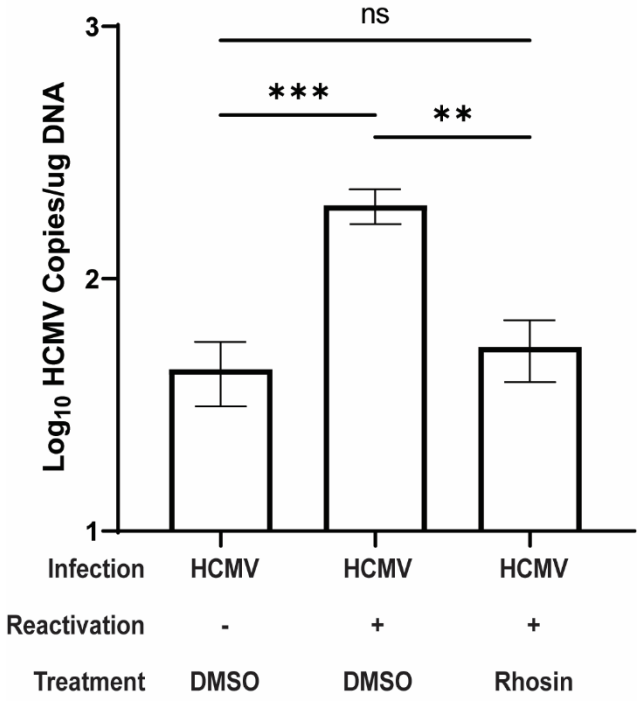

[2.7] Figure legend

Humanized NSG (huNSG) mice were infected with TB40/E-GFP as previously described (179,193). After human cell engraftment and viral infection, animals were placed into one of three treatment groups (N=5 each). At 8

weeks post-infection, one group of huNSG mice (N=5) was treated with 40mg/kg Rhosin, and the remaining two groups were treated with a comparable volume of DMSO diluent. In parallel, two-thirds of the mice were treated with G-CSF to induce viral reactivation (N=5 Rhosin treated and N=5 DMSO treated). Control, latently-infected mice were treated with DMSO but not G-CSF. At 1-week post-treatment (post-reactivation), mice were euthanized, and spleen tissues were harvested. Total DNA was extracted using DNAzol, and HCMV viral load was determined by qPCR from two tissue sections per mouse. Error bars represent the standard error of the mean between the average DNA copies per huNSG mouse (N=5 mice per group). All samples were compared by two-way ANOVA followed by Tukey's multiple comparisons test between experimental groups. *P* values are listed for significant comparisons where ** $P < 0.005$ and *** $P < 0.001$.

Section 2.5: Discussion

The HCMV-encoded chemokine receptor US28 influences several phases of the HCMV lifecycle, including latency and reactivation; however, the exact mechanisms through which US28 functions remains unclear. In the present report, we utilized a proximity-dependent biotinylating enzyme (TurboID) to characterize the US28 interactome under latent and lytic infection modes and focused our study on exploring the role of RhoA and RhoGEFs as an important US28 signaling intermediary. We further explored the relationship between US28 and RhoGEFs in vitro where inhibition of RhoGEFs, via the small-molecule compounds Rhosin and Y16, resulted in a substantial decrease in US28-mediated activation of RhoA. Viral latency and reactivation assays utilizing $CD34^+$ HPCs indicated that blocking US28 – RhoGEF signaling pathway results in a significant reduction in infectious virus after exposure to conditions that induce viral reactivation. These findings were recapitulated in a humanized NSG mouse model where treatment with Rhosin prevented the virus from efficiently reactivating. Collectively, our findings indicate that the US28-RhoGEF signaling pathway is required for efficient viral reactivation and provides insight into targets for the development of novel anti-HCMV therapeutics.

Classical approaches for the identification of protein-protein interactions have several limitations including altering the cell state or disturbing protein secondary structure (380–382). Herein, we circumvent these issues by making use of an unbiased biotin ligase system to examine the proteins which directly bind or are in close proximity to US28. Fusing the TurboID enzyme to the C' terminal tail of US28 did not negatively impact signaling in transfected HEK293M cells as

measured by SRE and SRF luciferase reporter assays, nor did it appear to alter US28 localization. Our results highlight the utility of BioID-based systems as an efficacious method for characterizing the complete US28 interactome including weak, transient, and indirect interactions. While our findings are consistent with other published US28 proximity labeling studies (222,304,375), they represent a significant advancement by comparing US28 interactomes between three unique models including transiently transfected cells, lytically infected fibroblasts, and latently infected $CD34^+$ HPCs.

Our group, and others, have previously shown that US28 regulates several cellular processes by binding unique host chemokines (CC vs. CX_3C) and activating a number of signaling intermediates (Src, FAK, Pyk2, PLC, IP_3, Ras, ERK, PKC, Calmodulin, and RhoA) (225,303–305,307,309,310,360–363,370). Consistent with our previous findings, proteomic analyses performed here identified several of these signaling intermediates emphasizing the validity of our BioID system. Interestingly, RhoGEFs were enriched in all three cell culture models. GEFs are responsible for catalyzing the dissociation of GDP from GTPases and provide a direct link between US28 signaling and the downstream RhoA activation cascade. Several studies have implicated RhoA in aspects of the HCMV lifecycle with differential effects dependent on the infected cell type and chemokine stimulus. For instance, in latently infected $CD34^+$ HPCs, HCMV miR-US25-1 targets RhoA for downregulation to inhibit cytokinesis and assist in maintaining the viral genome (383). However, during lytic infection, US28-mediated RhoA signaling facilitates smooth muscle cell migration in response to RANTES (227). Given these differential effects, we chose to further investigate the role that US28-mediated RhoGEF signaling has on viral reactivation.

We confirmed the physical interaction between US28 and several proteins from our proteomic analysis using a streptavidin bead-based pulldown procedure and traditional immunoblot. To further validate the association between US28 signaling and RhoGEFs, we identified two pharmacological inhibitors of RhoGEFs. Treatment with the small-molecules Rhosin or Y16, both of which target RhoGEF-RhoA interactions, resulted in a significant decrease in US28 signaling in HEK293M cells. Surprisingly, the inhibitory effects of Rhosin treatment were greater than that of Y16 despite targeting similar protein-protein interactions. We hypothesize that this differential

effect is largely due to the mechanistic differences between how the two compounds function. Y16 directly blocks the activation of LARG (ARHGEF12), p115-RhoGEF (ARHGEF1), and PDZ-RhoGEF (ARHGEF11) but not any additional activators of RhoA (378). Alternatively, Rhosin blocks the entirety of RhoGEF-RhoA interactions by directly binding to two adjacent shallow grooves on the surface of RhoA required for GEF interaction (379). Therefore, it may be possible that US28 facilitates activation of the RhoA signaling pathway through multiple GEF-RhoA interactions and that greater inhibition of US28 activation of RhoGEFs may be achieved using both compounds synergistically.

Primary $CD34^+$ HPCs are the gold standard for in vitro modeling of HCMV latency and reactivation (384). Furthermore, huNSG mice represent the only animal model capable of supporting HCMV infection and we have shown that huNSG mice engrafted with human $CD34^+$ HPCs to be a reliable and robust model of both latent and lytic infection (179). Similar to results obtained utilizing a recombinant virus lacking US28 (193), pharmacological inhibition of US28-mediated RhoGEF signaling resulted in a failure of the virus to efficiently reactivate in vitro and in vivo. We hypothesize that the observed reduction in infectious virus and viral load is due to inhibition of reactivation pathways or an inability of progenitor cells to efficiently traffic out of the bone marrow. This hypothesis is not without precedent as multiple studies have shown RhoGEFs to be required for cellular migration and differentiation in bone marrow-derived cells and macrophages (385–387). Therefore, these findings provide a direct link to US28-mediated viral reactivation through the RhoA signaling pathway. It is also possible that RhoGEFs interact with other viral proteins such as UL33 and UL78 during viral reactivation. However, these viral GPCRs have not yet been shown to mediate signaling through the RhoA pathway.

The viral GPCR US28 plays an integral role in the pathogenesis of HCMV, establishing differential signaling networks dependent on the presence or absence of bound ligand and the infected cell type. The findings of this study reveal previously unknown US28 interactors which play a crucial role in the facilitation of viral reactivation. To our knowledge, this is the first time specific cellular factors have been implicated in US28-mediated viral reactivation in vivo. Additional studies characterizing the US28 interactome in multiple cell types will be required to gain a more

comprehensive understanding of the multi-faceted ways in which US28 influences viral latency and reactivation.

Section 2.6: Materials & Methods

Plasmids

Turbo ID was kindly provided by Dr. Alice Ting (388). US28 and US28-TurboID, containing an in-frame C' terminal fusion with TurboID, were PCR amplified and cloned into pcDNA3.1(-) (Invitrogen). The PCR fragments were flanked by 5' EcoRI and a 3' HindIII restriction enzyme sites. All clones were transformed into TOP10 Escherichia coli cells (Invitrogen) and confirmed by sequencing. Reporter plasmids pRL-SV40 *Renilla* luciferase (*R*luc), pGL4.33(luc2P/SRE/Hygro) and pGL4.34(luc2P/SRF-RE/Hygro) containing SRE and SRF responsive elements driving luciferase expression were purchased from Promega.

Cells and Virus

Normal human dermal fibroblasts (ATCC No. PCS-201-010) and human embryonic kidney (HEK) 293M cells (Microbix) were cultured in Dulbecco's modified Eagle's medium (DMEM) supplemented with 10% fetal bovine serum (FBS), penicillin, streptomycin, and glutamine and maintained at 37°C and 5% CO_2. The HCMV strain TB40/E-GFP that constitutively expresses green fluorescent protein under the SV40 promoter (130) was amplified in NHDFs. Infectious virus was determined by limiting dilution plaque assays. The HCMV TB40/E-GFP bacterial artificial chromosome (BAC) was used in a two-step recombination protocol to either replace UL13 with a gH-nLuc reporter cassette (TB40/E-GFP-gHnLuc) or to add an in-frame fusion of TurboID with the C'terminal tail of US28 (TB40/E-GFP-US28-BT) (193). Following the rescue and expansion of HCMV recombinants, virus preparations were aliquoted and stored at -80°C. Viral manipulations were confirmed by sequencing. Nano Luciferase activity under the rhesus CMV gH promoter was confirmed and shown to be sensitive to Foscarnet treatment. TurboID expression and activity was confirmed by immunoblotting and biotin labeling.

Signaling Reporter Assays

HEK293M cells were plated at $3x10^4$ cells per well in 96-well, white-walled culture dishes. Cells were co-transfected with 50ng pcDNA3.1(-) control, or pcDNA3.1-HA-US28 or HA-US28-TurboID

along with 10ng of pRL-SV40 (*R*luc) and 50ng pGL4 firefly luciferase reporter vectors (SRE and SRF) using Fugene4K (Promega). At 18 hours post transfection growth medium was replaced with serum-free DMEM with or without small-molecule inhibitors at the indicated concentrations. Luciferase activity was measured in triplicate wells using the Dual Luciferase Reporter Assay System (Promega) at 6 hours post media replacement. Briefly, cell medium was removed and 20µL of passive lysis buffer was added to each well. The 96-well plate was placed at -20° C for 30 minutes followed by a 15-minute agitation at room temperature. Luciferase assay reagent was reconstituted and 50µL was injected per well in a Promega GloMax Navigator luminometer for luminescence detection. Assay results were transferred to an Excel spreadsheet, normalized to *Renilla* expression, set relative to the empty vector, and analyzed using GraphPad Prism 9.0 software.

Proximity-Dependent Labeling

For HEK293M experiments, three 10cm cell culture dishes containing 70-80% confluent monolayers of cells were transiently transfected with pcDNA3.1-HA-US28 and pcDNA3.1-HA-US28-TurboID. At 18 hours post transfection, HEK293M cells were incubated for 6h in complete media supplemented with 50µg/mL biotin. For NHDF experiments, three 10cm cell culture dishes containing 70-80% confluent monolayers of cells were infected at a MOI of 2 with either TB40/E-GFP-US28-TurboID, TB40/E-GFP, or mock infected. Three days post infection, cells were incubated for 6h in complete media supplemented with 50µg/mL biotin. In both experiments, cells were scraped, pelleted at 4°C and washed three times with PBS. Cells were lysed in RIPA buffer (50mM Tris pH 8, 150mM NaCl, 1% triton x-100, 0.1% SDS) and 1x Halt protease inhibitor cocktail (ThermoFisher) and centrifuged at 10,000 relative centrifugal force at 4°C. Supernatants were incubated with 250µL Pierce NeutrAvidin Agarose beads (ThermoFisher) overnight at 4°C while rotating. Beads were collected and washed twice for 5 min at 25°C (all subsequent steps at 25°C) in 500µL urea wash buffer (PBS pH 7.4, 4M urea). This was repeated three times with wash buffer 2 (PBS pH 7.4, 1% triton x-100), two times with 50mM fresh ammonium bicarbonate and twice with PBS. Bound proteins were removed from the agarose beads with 50µL Laemmli SDS-sample buffer at 42°C. Twenty-five percent of the sample was reserved for visualizing separated proteins by colloidal Coomassie blue staining and standard immunoblotting. The remaining 75%

of the sample (for analysis by mass spectrometry) was washed an additional two times in 50mM ammonium bicarbonate and then resuspended in 268µL 50mM ammonium bicarbonate and incubated on a 70°C heat block for 10 min with agitation. The samples were immediately treated with 132µL 6M urea and then cooled to room temperature before adding 2.5µL of fresh 0.5M TCEP (Tris(2-carboxyethyl) phosphine hydrochloride; Sigma) and incubated for 30min at room temperature, followed by adding 9µL of fresh 0.5M iodoacetamide and incubating in the dark for another 30 min at room temperature. The samples were then subjected to tryptic digestion by adding 3.7µL 10mM $CaCl_2$ followed by 20µL of 0.1µg/µL sequencing grade trypsin and incubated overnight at 37°C with rotation. Twenty microliters of formic acid were then added to the eluate and stored at -80°C until LC-MS/MS analysis. Samples were desalted using ZipTip C18 (Millipore, Billerica, MA) and eluted with 70% acetonitrile/0.1% TFA (Trifluoracetic acid; Sigma) and the desalted material dried in a speed vac. On bead tryptic digests were analyzed by the Fred Hutchinson Proteomics Core Facility (Seattle, WA).

Orbitrap Fusion LC/MS-MS

Desalted samples were brought up in 2% acetonitrile in 0.1% formic acid (12µL) and 10µL of sample analyzed by LC/ESI MS/MS with a ThermoScientific Easy-nLC II nano HPLC system (Thermo Scientific, Waltham, MA) coupled to a tribrid Orbitrap Fusion mass spectrometer (Thermo Scientific, Waltham, MA). Peptide separations were performed on a reversed-phase column (75 µm × 400 mm) packed with Magic C18AQ (5-µm 100Å resin; Michrom Bioresources, Bruker, Billerica, MA) directly mounted on the electrospray ion source. A 90-minute gradient from 7% to 28% acetonitrile in 0.1% formic acid at a flow rate of 300nL/minute was used for chromatographic separations. The heated capillary temperature was set to 300°C and a static spray voltage of 2100 V was applied to the electrospray tip. The Orbitrap Fusion instrument was operated in the data-dependent mode, switching automatically between MS survey scans in the Orbitrap (AGC target value 500,000, resolution 120,000, and maximum injection time 50 milliseconds) with MS/MS spectra acquisition in the linear ion trap using quadrupole isolation. A 2 second cycle time was selected between master full scans in the Fourier-transform (FT) and the ions selected for fragmentation in the HCD cell by higher-energy collisional dissociation with a normalized collision

energy of 27%. Selected ions were dynamically excluded for 30 seconds and exclusion mass by mass width +/- 10 ppm.

Data analysis was performed using Proteome Discoverer 2.2 (Thermo Scientific, San Jose, CA). The data were searched against Uniprot Human and CRAPome (373) data repositories (>25% cutoff). Trypsin was set as the enzyme with maximum missed cleavages set to 2. The precursor ion tolerance was set to 10 ppm and the fragment ion tolerance was set to 0.6 Da. Variable modifications included oxidation on methionine (+15.995 Da), carbamidomethyl on cysteine (+57.021 Da), and acetylation on protein N-terminus (+42.011 Da). Data were searched using Sequest HT (389). All search results were run through Percolator for scoring (390).

Pathway Analysis

Reactome pathway analysis software was used to evaluate proteomic data and identify significantly enriched pathways using the default analysis settings (374). Significantly impacted canonical pathways were also explored using STRING pathway mapping web browser tools to identify and predict additional interactors (391).

Immunoblot

Cell lysates were harvested in RIPA buffer supplemented with HALT protease inhibitor and stored at -20°C. Proteins were separated on a 4-12% SDS-PAGE gel and blotted on PVDF membranes. Immunoblots were performed using antibodies directed against HA (sc-7392, Santa Cruz Biotechnology), p115 RhoGEF (sc-74565, Santa Cruz Biotechnology), ROCK1 (sc-5562, Santa Cruz Biotechnology), c-Src (sc18, Santa Cruz Biotechnology), □-actin-HRP (sc-47778, Santa Cruz Biotechnology), endothelial cell growth factor receptor (EGFR; Cell Signaling; D3881), Streptavidin-HRP (Thermo Scientific; 21130), UL44 (CA006-100, Virusys), and TurboID (AS204440, Agrisera) and if required, with the appropriate HRP conjugated secondary antibodies (anti-mouse sc-25409 and anti-rabbit sc-2357).

Microscopy

NHDFs ($1.0x10^5$) were added to each microscope coverslip and maintained at 37°C and 5% CO_2. NHDFs were transfected with 1µg of either HA-US28 or HA-US28-BT using Lipofectamine 2000 according to manufacturer's instructions. At 16 hours, cells were fixed with 4%

paraformaldehyde in PBS, permeabilized in 0.25% Triton-X100 in PBS, and blocked with 2% bovine serum albumin 0.1% Triton-X100 in PBS. Cells were stained with HA tag monoclonal antibody coupled with Alexa Fluor 488 (1:1,000 dilution; ThermoFisher) and Phalloidin-Alex Fluor 647 (1:1,000 dilution; ThermoFisher) in blocking buffer. Coverslips were washed with PBS and mounted using Fluoromount-G. Images were captured with a Leica Stellaris 8 confocal microscope using Leica Application Suite X software version 4.5.0 (Leica Microsystems).

Quantitative RT-qPCR

RhoGEF gene expression was confirmed by real-time RT-PCR using primer and probe sets for ARHGEF1 (4448892; Hs00180327_m1), ARHGEF11 (4448892; Hs01064532_m1), and ARHGEF12 (4448892; Hs00209661_m1) available from Thermo Fisher Scientific. Total RNA was isolated using Trizol (Thermo Fisher Scientific) from normal human dermal fibroblasts (NHDF) and $CD34^+$ hemopoietic progenitor cells (HPCs). The RNA was treated with EZ-DNAse (Thermo Fisher Scientific). cDNA was generated using Superscript IV (Invitrogen) and analyzed by RT-PCR using TaqMan Fast Advanced Master Mix and a QuantStudio 7 Flex Real-Time PCR system. Cycle threshold values were calculated using QuantStudio Design software (392).

Limiting Dilution HCMV Latency and Reactivation Assay

Latency and reactivation was monitored in long-term cultures of $CD34^+$ HPCs using methods as previously detailed (335,384). Primary $CD34^+$ hematopoietic progenitor cells (HPCs) were isolated using magnetic bead separation (Miltenyi Biotech) and viably frozen as previously described (335). $CD34^+$ HPCs were thawed and recovered overnight in stem cell media, and infected with TB40/E-GFP at a multiplicity of infection (MOI) equal to 3 for 48 hours prior to isolation by fluorescence activated cell sorting (FACS) using a FACSAria (BD FACS Aria equipped with 488, 633 and 405nm lasers, running FACS DIVA software) in order to obtain a pure population of viable GFP^+ $CD34^+$ HPCs as previously described (335,384). The cells were then co-cultured in transwell culture dishes above monolayers of irradiated M2-10B4 and S1/S1 stromal cells. At 14 days post infection (dpi), HPCs were serially diluted in RPMI-1640 medium containing 20% FBS, 2mM L-glutamine, 100U/mL penicillin, 100µg/mL streptomycin, 15ng/mL granulocyte-colony stimulating factor (G-CSF), and 15ng/mL granulocyte-macrophage colony stimulating factor (GM-CSF) and overlaid onto confluent monolayers of NHDFs cultured in 96-well plates. To quantify the levels of

pre-reactivation infectious virus, a fraction of the HPC cultures were mechanically disrupted and lysates were serially diluted and then added to NHDFs cultured in 96-well plates. Cell cultures were microscopically visualized for the presence of GFP^+ weekly, for up to 4 weeks, to assess the reactivation frequency from latently infected cells and the presence of preformed infectious virus by extreme limiting dilution assay (ELDA) (384).

Cellular Cytotoxicity Assay

Compound cytotoxicity was measured following the CellTiter-Glo luminescent cell viability assay (Promega). Briefly, one day prior to the assay, black walled 96-well plates (Corning) were seeded with NHDFs at $1.5x10^4$ cells per well in 50µL. Compounds, starting at a concentration of 40µM, were diluted 1:2 with DMEM supplemented with 5% FBS and 1X PSG. A total of 50µL of diluted compound was added to triplicate wells of the 96-well plate. At 72h following compound addition, 50µL of CellTiter-Glo substrate was added to each well, followed by 2 min on an orbital rocker and a 10 min incubation. The luminescence of each well was measured using a Promega GloMax Navigator luminometer. Well luminescence, indicative of the number of living cells per well, was converted to percent cell viability in Microsoft excel, by dividing luminescence values in experimental wells by the value in control wells containing untreated cells and multiplying by 100. These values used to calculate compound 50% cellular cytotoxicity (CC_{50}) values by nonlinear regression analysis of graphs with compound concentration in log plotted versus cell viability, using GraphPad Prism 9.0 Software.

$CD34^+$ HPCs were differentiated from WA01 human embryonic stem cells using a commercial feeder-free hematopoietic differentiation kit (STEMdiff Heme, Stem Cell Technologies) according to the manufacturer's directions. HPCs were cultured in SFEMII with 10% BIT serum replacement, stem cell cytokines (stem cell factor, FLT3L, IL-3, and IL-6 (PeproTech)), and penicillin/streptomycin, along with increasing concentrations of Rhosin, Y16, or DMSO (control) in triplicate for 5 days. Colorimetric assay (WST-1 based, Roche) was used to perform the cytotoxicity assay according to the manufacturer's directions. Absorbance (ʎ420) values were background subtracted from media alone and normalized to DMSO control.

HCMV nLuc Assay

The antiviral activity of Rhosin (Tocris Bioscience) and Y16 (Calbiochem) was measured using the reporter virus TB40/E-GFP-gHnLuc that expresses nanoluciferase under the gH late viral promoter. NHDF cells ($1.5x10^4$ cells/well) were plated in 96-well plates 24 hours prior to start of the assay. Compounds, starting at a concentration of 40µM, were diluted 1:2 with DMEM supplemented with 5% FBS and 1X PSG. Cells were treated with Rhosin, Y16, Foscarnet (positive antiviral control) or DMSO in triplicate and infected with HCMV TB40/E-gHnLuc (MOI = 0.3 PFU/cell). At 72 hpi, 50µL Nano-Glo Luciferase Assay reagent (Promega) was added to each well, followed by 2 min on an orbital rocker and a 10 min incubation. Luminescence was measured using a GloMax Navigator Luminometer. Results were graphed using Graphpad Prism 9.0 software.

RhoA Activation Assay

NHDFs were plated in 10-cm dishes ($2.0x10^6$ per well) 24 hours prior to treatment with the indicated concentrations of Rhosin, Y16, or an equivalent amount of DMSO (untreated control), diluted in serum-free DMEM for 24 hours. The cells were subsequently stimulated with media containing 10% fetal bovine serum for 15 minutes. Cells were washed once with PBS and lysed in a buffer containing 25 mM Tris-HCl, 150 mM NaCl, 5 mM $MgCl_2$, 1% NP-40, and 5% glycerol. Lysates were clarified by centrifugation at 4°C and protein concentrations were normalized using the Qubit™ Protein BR Assay Kit (Invitrogen). Proteins were isolated using the Active Rho Pulldown and Detection kit (Thermo Scientific) according to the manufacturer's recommendations. The total amount of active RhoA was assessed via immunoblot using the indicated primary antibodies. Quantification shows the relative expression of RhoA bound to GTP compared to untreated lysates and normalized to levels of beta actin.

HCMV Infection of Humanized Mice

Mouse procedures were performed in accordance with approved Institutional Animal Care and Use Committee (IACUC) protocols under the recommendations of the American Association for Accreditation of Laboratory Animal Care (AAALAC). Mice were housed in the Vaccine & Gene Therapy Institute at Oregon Health & Science University vivarium using microisolator cages and fed sterile food and water *ad litem*. For this experiment, humanized mice were generated by

irradiating NOD.Cg-*Prkdc*^{scid}*IL2R*γ^{tm1Wjl}/SzJ (NSG) mice (Jackson Laboratories) by sublethal irradiation of 0- to 3-day-old neonates at 75 cGy using a ^{137}Cs gamma irradiation source. The irradiated animals were reconstituted by intrahepatic injection of 1x10^5 human CD34$^+$ HPCs as described previously (193). Peripheral blood was collected every 4 weeks beginning at week 8 post-injection to assess human cell engraftment using flow cytometry. 16 weeks post engraftment, mice were distributed to experimental groups normalized for engraftment success as determined by percentage human CD45$^+$ lymphocytes in the periphery. Humanized mice were dosed with 1 ml of 4% thioglycolate (Brewer's medium; BD) by intraperitoneal (i.p.) injection and then injected i.p. with two T150 flasks of HCMV TB40/E-GFP-infected NHDFs. At 8 weeks post-infection, the animals were divided into three groups. Two groups of latently infected mice were treated with 100 µl of Neupogen (G-CSF; 300 mg/ml; Amgen) by subcutaneous pump and 125µg of AMD3100 administered by i.p. injection to mobilize progenitor cells and promote HCMV reactivation (193,335). One of the reactivation groups received 40mg/kg Rhosin HCl resuspended in a final volume of 100µL DMSO and the other group was treated with an equivalent amount of DMSO for 7 days by IP injection. The third group of latently infected mice did not receive the reactivation cocktail but was treated with DMSO to serve as comparators for viral levels during latency. At 1-week post mobilization, the mice were euthanized via CO_2 administration according to AAALAC euthanasia guidelines, and then blood, bone marrow, spleen, and liver tissues were collected for further analysis.

Quantitative Detection of HCMV Viral DNA

Total DNA was extracted from portions of mouse spleen using DNAzol (ThermoFisher) and primers and probe recognizing HCMV UL141 were used to quantify viral genomes by quantitative real-time PCR as previously described (193). Dilutions of purified HCMV BAC DNA were used to create a standard curve. A 1 µg sample of total DNA was added to each reaction well of TaqMan FastAdvance PCR master mix (Applied Biosystems) and samples were analyzed in triplicate on a StepOnePlus TaqMan PCR machine (Applied Biosystems) with an initial activation at 50°C for 2 min and 95°C for 20 s, followed by 40 cycles of 1 s at 95°C and 20 s at 60°C. TaqMan results were analyzed using ABI StepOne software and graphed using Prism 9.0 software.

Section 2.7: Acknowledgements

This work was supported by a grant from the National Institutes of Health NIAID (P01 AI127335).

Section 2.8: Supplemental Figures

Figure[S2.1] Characterization of RhoGEF Inhibitors Rhosin and Y16

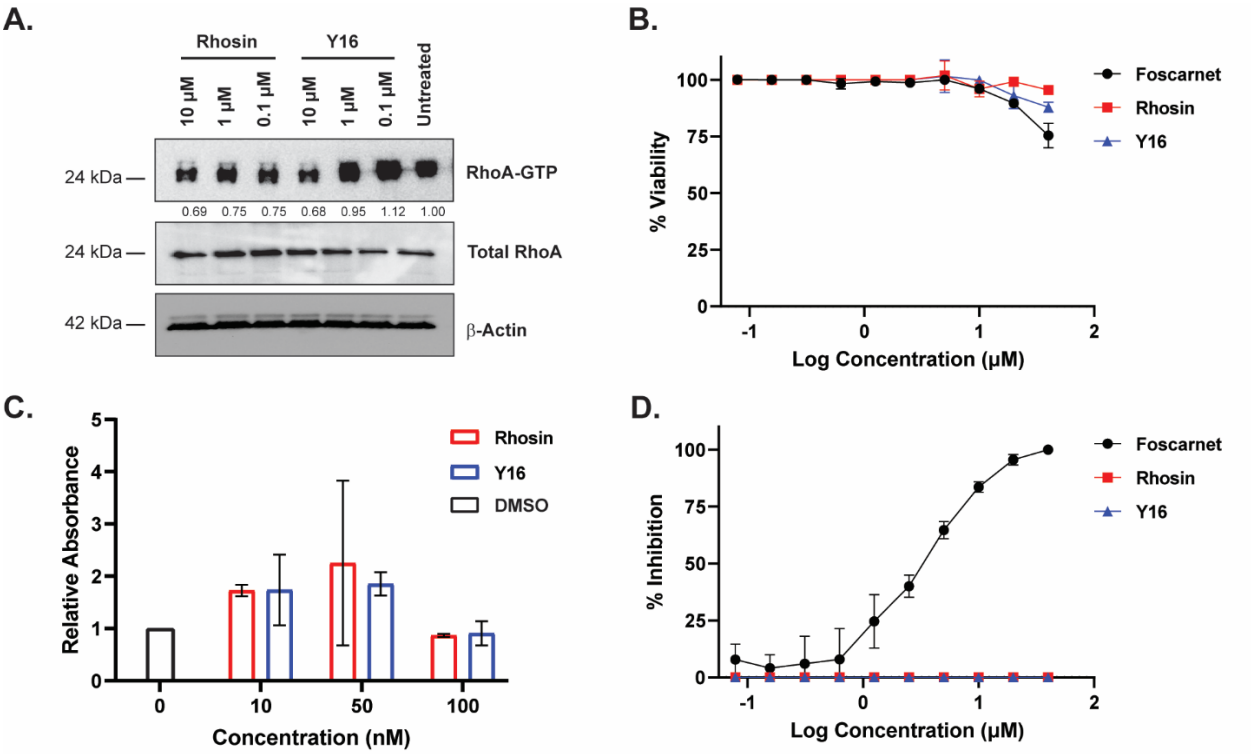

[S2.1] Figure legend

(A) NHDF cells were treated at the indicated concentrations of Rhosin and Y16 for 24 hours in serum-free media. 24 hours post addition, cells were stimulated with 10% fetal calf serum for 15 minutes. Lysates were harvested and subjected to GST-Rhotekin pulldown according to the manufacturer's recommendations (Thermo Fisher). RhoA activation was assessed via immunoblot using the indicated primary antibodies. Quantification shows the relative expression of RhoA bound to GTP compared to β-actin and normalized to untreated lysates (n = 3, representative blot shown). **(B)** To measure the cytotoxic effects of Foscarnet, Rhosin, and Y16, NHDF cells were treated with dilutions of inhibitors ranging from 40 to 0.078µM or DMSO alone. At 72 hours post-treatment the cells were analyzed using the CellTiter-Glo luminescent cell viability assay according to the manufacturer's (Promega) recommendation. Data is plotted as cell viability relative to the DMSO-treated control cells. Concentrations of the indicated compounds were Log_{10} transformed, and error bars are representative of the standard error of the mean between triplicate experiments. **(C)** $CD34^+$ HPCs were cultured in SFEMII with 10% BIT

serum replacement, stem cell cytokines (stem cell factor [SCF], FLT3L, IL-3, IL-6 [PeproTech]), and penicillin/streptomycin, along with increasing concentrations of Rhosin, Y16, or DMSO (control) in triplicate for 5 days. Colorimetric assay (WST-1 based, Roche) was used to perform the cytotoxicity assay according to the manufacturer's directions. Absorbance (ʎ420) values were background subtracted from media alone and normalized to DMSO control. Error bars represent the standard deviation from two separate experiments. Statistical significance was determined using two-way ANOVA followed by Tukey's multiple comparisons test between experimental groups. **(D)** To investigate the potential antiviral activity of Rhosin and Y16, NHDF cells were pretreated for one hour with 2-fold serial dilutions of inhibitor, ranging from 40 to 0.078µM or DMSO. Treated cells were infected with TB40/E-GFP-gHnLuc at a MOI equal to 0.3. Foscarnet-treated cells were used as a positive control. After 72 hrs incubation, luminescence was quantified using the Nano-Glo Luciferase assay system and measured on a GloMax Navigator microplate reader according to the manufacturer's (Promega) recommendations. Data is plotted as percent inhibition relative to the cells treated with DMSO. Concentrations of the indicated compounds were Log_{10} transformed, and error bars are representative of the standard error of the mean between triplicate experiments.

Figure[S2.2] RhoGEF Expression in NHDF and CD34+ HPCs

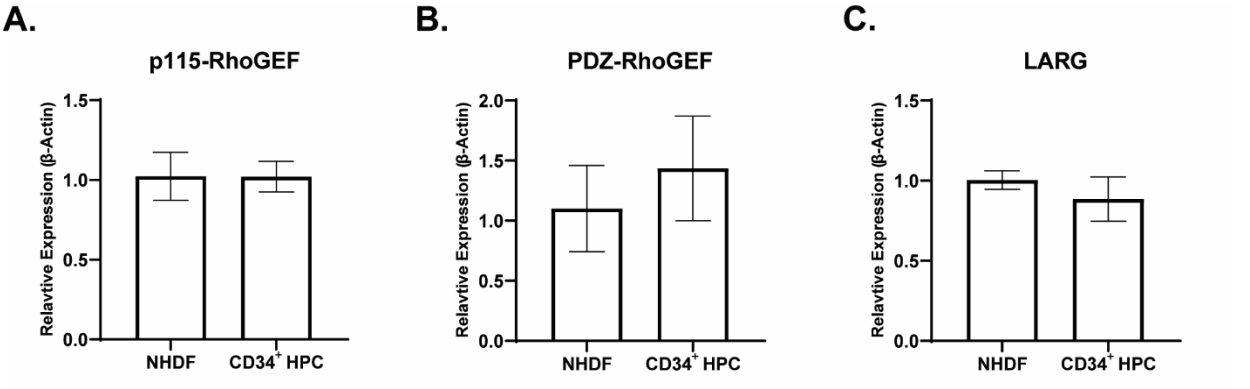

[S2.2] Figure legend

Total RNA from uninfected primary $CD34^+$ HPCs (n = 5) and NHDF (n = 3) was obtained using a phenol-chloroform extraction method. Relative expression of **(A)** ARHGEF1 (p115-RhoGEF), **(B)** ARHGEF11 (PDZ-RhoGEF), and **(C)** ARHGEF12 (LARG) was calculated via RT-qPCR relative to β-Actin using the delta-delta CT method.

Figure[S2.3] RhoGEF Interactions Contribute to HCMV Reactivation

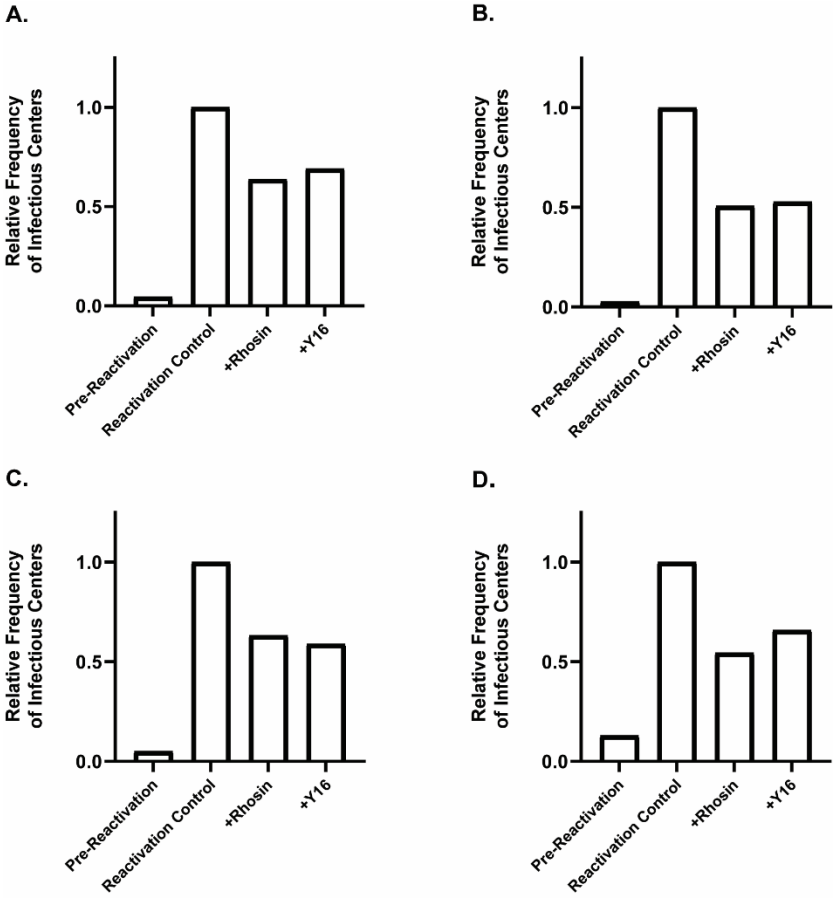

[S2.3] Figure legend

(A-D) Representative replicates for experiments performed in Fig 2.6. Primary $CD34^+$ HPCs isolated from four independent donors infected with TB40/E-GFP (WT-HCMV) were FACS isolated for viable, $CD34^+$, GFP^+ HPCs at 2 dpi as previously described. Infected HPCs were cultured on stromal cell support for 12 days to establish latency and equivalent populations of HPCs were co-cultured in supportive media on a fibroblast layer to reactivate virus as previously described. Samples were treated with the RhoGEF inhibitors Rhosin (10nM) or Y16 (10nM) at the time of reactivation and the reactivation frequency was compared to untreated controls (reactivation). Reactivation was measured as the frequency of infectious centers determined at 3 weeks post-plating for all groups.

Section 2.9: Data Availability

All data and supplementary material associated with this manuscript is available within the main publication. Doi: 10.1371/journal.ppat.1011682

Chapter 3: Third Intracellular Loop of HCMV US28 Is Necessary for Signaling and Viral Reactivation

Samuel Medica[a,b], Michael Denton[a], Nicole L. Diggins[a], Olivia Kramer-Hansen[c], Lindsey B. Crawford[a,*], Adam T. Mayo[a], Wilma D. Perez[a], Michael A. Daily[a], Christopher J. Parkins[a], Luke E. Slind[a], Lydia J. Pung[a], Whitney C. Weber[a,b], Hannah K. Jaeger[a], Zachary J. Streblow[a], Gauthami Sulgey[a], Craig N. Kreklywich[a], Timothy Alexander[a], Mette M. Rosenkilde[c], Patrizia Caposio[a], Meaghan H. Hancock[a], & Daniel N. Streblow[a,b,d,#]

[a] Vaccine and Gene Therapy Institute, Oregon Health and Science University, Beaverton, Oregon, USA

[b] Department of Molecular Microbiology and Immunology, Oregon Health and Science University, Portland, Oregon, USA

[c] Department of Biomedical Sciences Molecular Pharmacology, University of Copenhagen, Copenhagen, Denmark

[d] Division of Pathobiology and Immunology, Oregon National Primate Research Center, Beaverton, Oregon, USA

* Current affiliation: Department of Biochemistry, University of Nebraska – Lincoln, Lincoln, Nebraska, USA

Journal of virology. 2025 Jan 31;99(1):e01801-24

Doi: 10.1128/jvi.01801-24

Section 3.1: Abstract

The HCMV encoded chemokine receptor US28 plays a critical role in viral pathogenesis, mediating several processes such as cellular migration, differentiation, transformation, and viral latency and reactivation. Despite significant research examining the signal transduction pathways utilized by US28, the precise mechanism by which US28 activates these pathways remains unclear. We performed a mutational analysis of US28 to identify signaling domains that are critical for functional activities. Our results indicate that specific residues within the third intracellular loop (ICL3) of US28 are major determinants of G-protein coupling and downstream signaling activity. Alanine substitutions at positions S218, K223, and R225 attenuated US28-mediated activation of MAPK and RhoA signal transduction pathways. Furthermore, we show that mutations at positions S218, K223, or R225 result in impaired coupling to multiple Gα isoforms. However, these substitutions did not affect US28 plasma membrane localization nor the receptor internalization rate. Utilizing $CD34^+$ HPC models, we demonstrate that attenuation of US28 signaling via mutation of residues within the ICL3 region results in an inability of the virus to efficiently reactivate from latency. These results were recapitulated in vivo, utilizing a humanized mouse model of HCMV infection. Together, our results provide new insights into the mechanism by which US28 manipulates host signaling networks to mediate viral latency and reactivation. Results reported here will guide the development of targeted therapies to prevent HCMV-associated disease.

Section 3.2: Importance

Human cytomegalovirus (HCMV) is a β-herpesvirus that infects between 44 – 100% of the world population. Primary infection is typically asymptomatic and results in the establishment of latent infection within $CD34^+$ hematopoietic progenitor cells (HPCs). However, reactivation from latent infection remains a significant cause of morbidity and mortality in immunocompromised individuals. The viral chemokine receptor US28 influences various cellular processes crucial for viral latency and reactivation, yet the precise mechanism by which US28 functions remains unclear. Through mutational analysis, we identified key residues within the third intracellular loop (ICL3) of US28 that govern G-protein coupling, downstream signaling, and viral reactivation

in vitro and in vivo. These findings offer novel insights into how US28 manipulates host signaling networks to regulate HCMV latency and reactivation and expand our understanding of HCMV pathogenesis.

Section 3.3: Introduction

Human cytomegalovirus (HCMV) is an opportunistic pathogen that infects a large proportion of the world's population (349). HCMV remains the most common congenital infection and causes severe neurological and developmental deficits in neonates (54). Furthermore, HCMV infection is a significant cause of morbidity and mortality in organ transplant recipients and otherwise immunocompromised populations (393). Primary infection with HCMV is typically asymptomatic and results in the establishment of viral latency within $CD34^+$ hematopoietic progenitor cell (HPC) and $CD14^+$ monocyte reservoirs (187). During latent infection, the HCMV genome exists in a quiescent state limiting gene expression to evade detection by the host immune system (394). During viral reactivation, differentiated macrophages and dendritic cells generated from these reservoirs disseminate the virus throughout the host (395,396). Despite significant research examining the cues governing the switch from latent to lytic infection, the specific molecular mechanisms mediating these processes remain unclear. To date, no FDA-approved vaccine against HCMV exists and current antiviral regimens often have severe adverse side effects (64,397,398). Moreover, these therapeutic agents only act during lytic infection when clinical manifestations are already present and promote the evolution of drug-resistant HCMV strains. Therefore, to facilitate the advancement of new therapies targeting HCMV, it is imperative to clarify the precise cellular and viral mechanisms responsible for mediating HCMV latency and reactivation.

G protein-coupled receptors (GPCRs) represent the most abundant and diverse family of membrane-bound proteins in the human genome and are targets for over one-third of FDA-approved pharmaceuticals (399). GPCRs are characterized as containing an extracellular N-terminal domain, seven alpha-helical transmembrane domains, and an intracellular C-terminal domain (400,401). Extracellular loops formed by the transmembrane domains assist with facilitating ligand binding while the intracellular loops, primarily intracellular loops two and three

(ICL2/3), are paramount for G protein-coupling and selectivity (246,402). Upon interfacing with extracellular ligands, GPCRs undergo conformational changes allowing them to couple with cognate heterotrimeric G protein complexes consisting of α-, β-, and γ-subunits. GPCRs act as guanine nucleotide exchange factors (GEFs) catalyzing the exchange of GDP for GTP on the Gα subunit. Once bound to GTP, the α-subunit dissociates from the βγ-subunits to activate downstream signal transduction effectors and ultimately alter gene expression. The exact cellular signal transduction cascades initiated by G-proteins are dependent on cell type, GPCR class, ligand specificity, and activated Gα isoform. Gα proteins are broadly organized into four families: $G\alpha_s$, $G\alpha_{i/o}$, $G\alpha_{q/11}$, and $G\alpha_{12/13}$ based on their structural composition and signaling characteristics (263,400). Together, GPCR – G protein interactions, and downstream signaling, are responsible for modifying nearly all facets of cellular processes relating to metabolism, cellular migration, proliferation, and cytoskeletal remodeling.

HCMV encodes four putative GPCRs including US28, which exhibits homology to the host CC-chemokine receptors CCR1 and CCR5 (296,367). US28 is expressed with early kinetics and is packaged into the mature virion (191,302). Within infected cells, US28 is primarily localized to intracellular multivesicular bodies and is continuously internalized from the cell surface via both β-arrestin and clathrin-mediated mechanisms (300,403–405). US28 binds both CC and CX_3C chemokines and is capable of coupling to multiple Gα isoforms including $G\alpha_{q/11}$, $G\alpha_{i/o}$, and $G\alpha_{12/13}$ subfamilies (284,296,303,406,407). Dependent on the infected cell type and interacting G-protein, US28 is capable of interfacing with several canonical signal transduction pathways to activate transcription factors such as NFAT, CREB, NF-κB, ELK/SRE, STAT3, SRF, and TCF/LEF (225,307,309,310,360,361). For instance, in arterial smooth muscle cells, binding of CCL2 or CCL5 to US28 stimulates cellular migration, whereas binding of CX_3CL1 blocks this effect (303). A reverse of this ligand-specific phenotype was observed in macrophages wherein CX_3CL1 promoted migration and CC ligands blocked it, highlighting the cell type-specific effector functions of US28. Within $CD34^+$ HPCs, US28 drives cellular differentiation down the myeloid lineage through an undefined mechanism (193). Importantly, US28 is expressed during both latent and lytic phases of the viral lifecycle and ligand-dependent signaling is essential for the

establishment of latent infection and for viral reactivation; however, the exact mechanisms by which US28 facilitates these processes remain unclear (192–194,206,222).

In the present study, we conducted a mutational analysis of US28 aimed at identifying crucial motifs essential for signaling and functional capabilities. Our findings reveal that specific residues within the US28 ICL3 play a pivotal role in determining G-protein coupling and downstream signaling activity. Notably, mutations at positions S218, K223, and R225 led to diminished US28-mediated activation of mitogen-activated protein (MAP) kinase and RhoA signal transduction. Moreover, we observed that alanine substitution at positions S218, K223, and R225 significantly impaired the coupling of US28 to multiple Gα isoforms, while having no impact on its plasma membrane localization nor internalization kinetics. Furthermore, we illustrate that the attenuation of US28 G-protein coupling and downstream signaling hampers the virus's ability to efficiently reactivate in $CD34^+$ HPCs. Importantly, these findings were replicated in vivo using a humanized mouse model of HCMV infection. Collectively, our results contribute novel insights into the mechanism through which US28 influences host signaling networks to orchestrate the complex interplay between latent and lytic infection. The findings of this study will be integral for the development of novel therapeutics preventing HCMV-associated disease.

Section 3.4: Results

3.4.1 Activation of $Ga_{q/11}$ and Downstream Signal Transduction Effectors is Required for Efficient Viral Reactivation

Previous studies have shown that US28 is capable of activating the $G\alpha_{q/11}$ family of G-proteins to stimulate several signal transduction cascades such as MAPK, NF-κB, and PLC-β (225,227,408). Importantly, many of these signal transduction pathways play an integral role in the establishment of viral latency or the capacity to reactivate (409–413). To understand how the activation of $G\alpha_{q/11}$ influences viral latency and reactivation, we identified YM-254890, a selective inhibitor of the $G\alpha_{q/11}$ family of G-proteins (414). Treatment with YM-254890 in primary human fibroblasts showed minimal cytotoxic effects at 72 hours post-treatment at concentrations up to 10μM **(Fig. S3.1A)**. Moreover, treatment of HCMV-infected fibroblasts with YM-254890 exhibited no discernable effects on lytic viral replication as measured via nano-luciferase (nLuc) reporter

assay and by limiting dilution plaque assays **(Fig. S3.1B,C)**. To evaluate the effects of YM-254890 on US28 signaling activity, we performed luciferase reporter assays in transiently transfected HEK-293 cells monitoring US28-mediated activation of MAPK signaling. Treatment with YM-254890 resulted in dose-dependent inhibition of US28-mediated activation of the SRE reporter element **(Fig. S3.1D)** suggesting that inhibiting US28 – $G\alpha_{q/11}$ signaling blocks US28-mediated MAPK activation.

To determine whether $G\alpha_{q/11}$ activation affects the establishment of viral latency or capability of the virus to reactivate, we infected human embryonic stem cell (hESC)-derived $CD34^+$ HPCs with HCMV TB40/E-GFP (323,326). Infected $CD34^+$ HPCs were isolated via FACS and cultured above a murine stromal support layer under conditions that favor latent infection. At the time of initial plating, the cell culture media was supplemented with 1μM of YM-254890 or an equivalent amount of vehicle (DMSO). At 14 days post-infection (DPI), half of the HPCs were lysed (pre-reactivation) and the remaining cells were treated with granulocyte-macrophage colony stimulating factor (GM-CSF) and granulocyte colony stimulating factor (G-CSF) to induce cellular differentiation and viral reactivation. Cells and lysates were plated over a monolayer of fibroblasts to perform an extreme limiting dilution assay (ELDA) assessing the frequency of infectious centers up to three weeks post-plating (384). Comparable levels of virus were present in YM-254890-treated versus vehicle-treated latently infected cells (pre-reactivation) indicating that $G\alpha_{q/11}$ signal transduction has minimal effect on the establishment of viral latency **(Fig. 3.1A, Fig. S3.2)**. In contrast, treatment with YM-254890 resulted in a significant decrease in the ability of the virus to efficiently reactivate **(Fig. 3.1A, Fig. S3.2)**. Because an observed deficit in viral reactivation can be due to an inability to maintain viral genomes throughout the latency establishment period, we quantified HCMV genomes at the end of latent infection via quantitative PCR. Results from these experiments confirmed that inhibition of $G\alpha_{q/11}$ signal transduction causes a true reactivation deficit since a comparable number of viral genomes were present in YM-254890 and DMSO-treated cells **(Fig. 3.1B)**. Together these results indicate that activation of $G\alpha_{q/11}$, through US28 or other mechanisms, is required for efficient HCMV reactivation in $CD34^+$ HPCs.

Figure[3.1] Activation of $G\alpha_{q/11}$ is Required for Efficient Reactivation

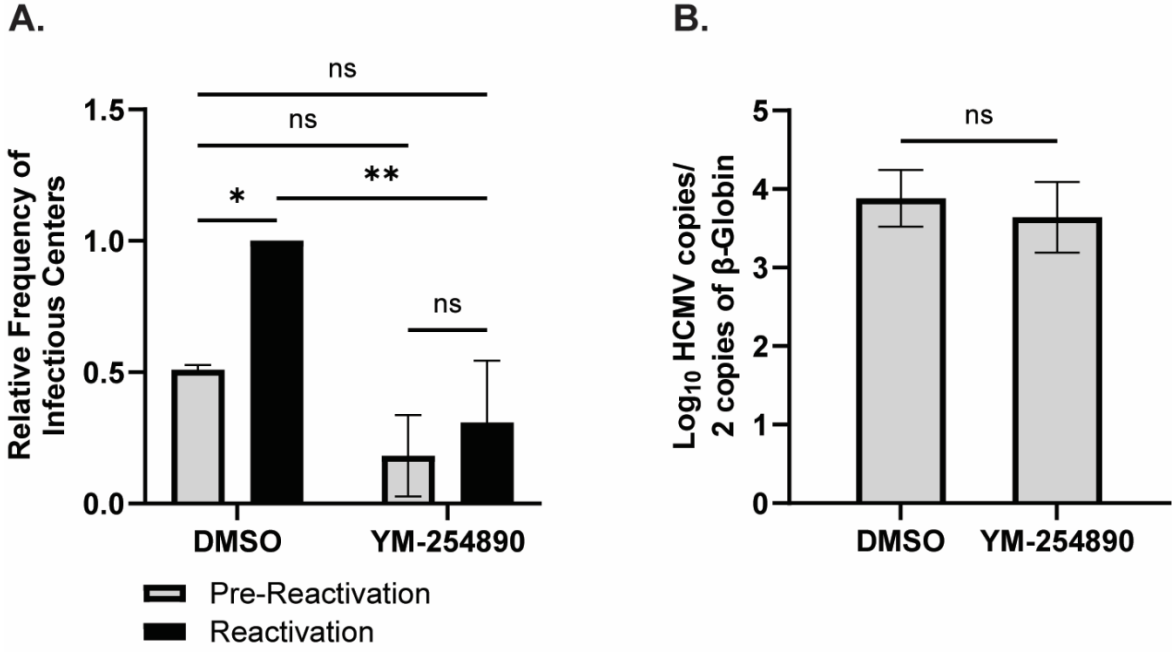

[3.1] Figure legend

hESC-derived CD34⁺ HPCs were infected with TB40/E-GFP at a MOI of 2 for 48 hours. Cells were FACS isolated for viable CD34⁺/GFP⁺ HPCs and were cultured above a murine stromal cell support layer for 12 days to establish latent infection. Cells were treated with 1 µM YM-254890 ($G\alpha_{q/11}$ inhibitor) or an equivalent amount of DMSO throughout the latency culture. **(A)** At 14-DPI, half of the cells were treated with reactivation cocktail and plated onto a fibroblast monolayer, the other half of the cells were lysed and used to infect fibroblasts directly (pre-reactivation control). Reactivation was assessed by the frequency of infectious centers as determined via ELDA (415,416) at 3 weeks post-plating. Data is shown as fold change in infectious centers, as compared to the reactivation group, for triplicate experiments. Error bars represent the standard error of the mean and statistical significance was calculated using two-way ANOVA followed by Tukey's post-hoc analysis *(*p < 0.05 / **p < 0.01).* **(B)** At 14-DPI**,** total DNA was harvested from infected CD34⁺ HPCs and viral genomes were quantified via qPCR using primers and probes specific for the viral UL141 gene. Viral genomes were normalized to total cell number using human β-globin as a reference gene. Data represents the mean Log_{10} transformed values for triplicate experiments. Error bars represent the standard error of the mean and statistical significance was calculated using a student's t-test.

3.4.2 Mutations in the Third Intracellular Loop of US28 Decrease Signaling Activities Despite Maintaining Similar Localization and Internalization

Next, we sought to identify regions of US28 that are required for propagating downstream signaling activity. Because the third intracellular loop (ICL3) between transmembrane domains five and six is a major determinant of G protein coupling in other class A GPCRs (417–422), we

generated alanine substitutions for basic and polar residues within this region (S218, S220, K223, and R225). The wild type and ICL3 mutant constructs contained an in-frame N' terminal 11 amino acid HiBiT tag to quantify protein production and surface expression **(Fig. 3.2A)**.

Figure[3.2] Mutational Analysis of the US28 ICL3 Identifies Residues Required for Signaling Activity

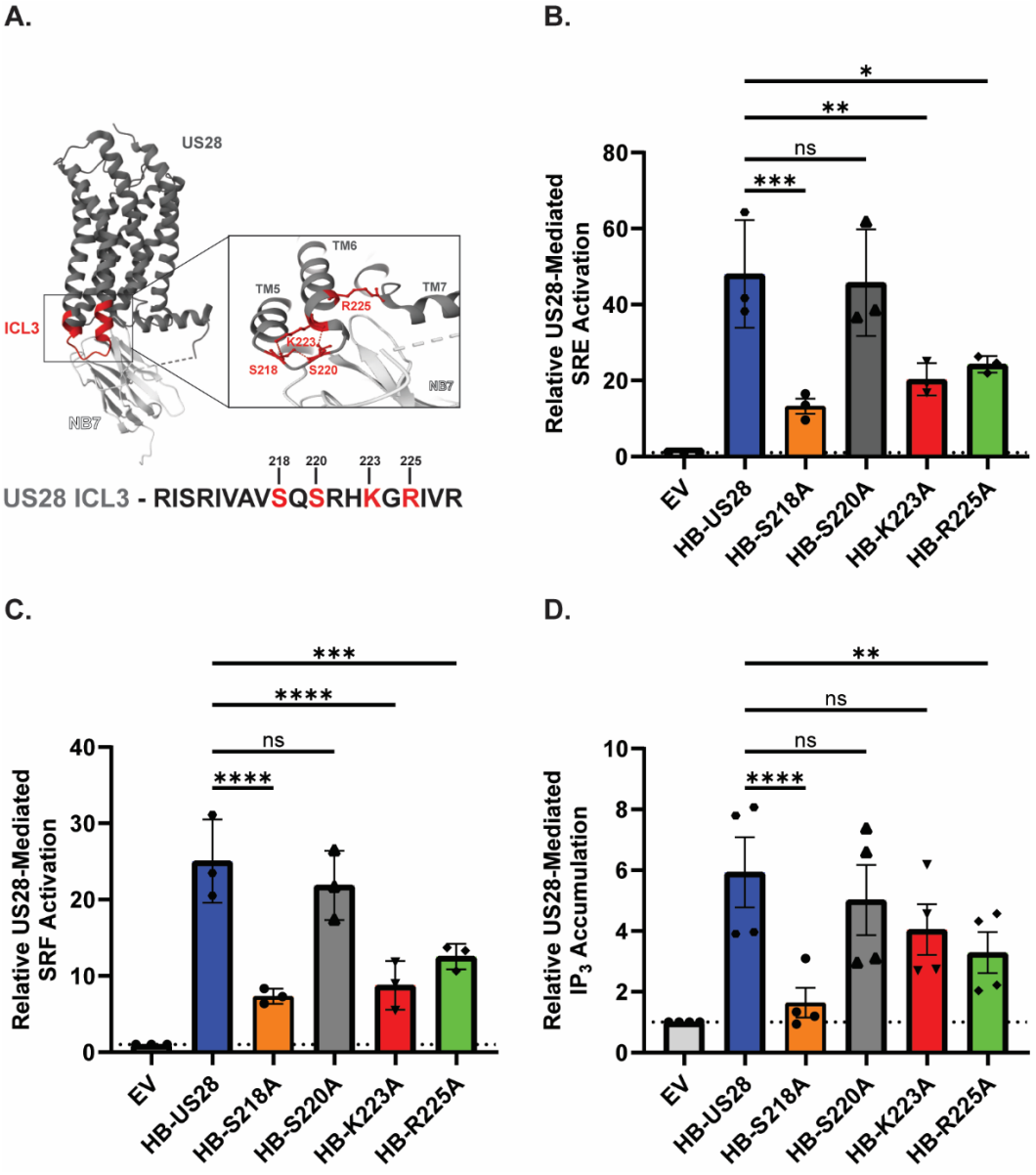

[3.2] Figure legend

(A) Structural representation of the third intracellular loop of US28 with alanine substituted residues denoted in red. Adapted from (423) **(B & C)** HEK-293 cells were transfected with the indicated constructs along with Renilla and Firefly luciferase reporter plasmids for SRE **(B)** or SRF **(C)**. At 18 hours post-transfection, media was exchanged with serum-free DMEM. Luciferase activity was measured using the Dual-Luciferase Reporter Assay System (Promega) at 6 hours post-media exchange. Data is shown as fold change relative to transfection with the empty

vector for triplicate experiments. Error bars represent the standard error of the mean. Statistical significance was calculated by one-way ANOVA followed by Dunnett's multiple comparison post-hoc analysis (*p < 0.05, **p < 0.01, ***p < 0.001 / ****p < 0.0001). **(D)** HEK-293 cells were transfected with the indicated constructs or the empty vector (EV) and incubated with tritium labeled myo-inositol. At 48 hours post-transfection, cells were washed and incubated with LiCl prior to cell lysis. Lysates were incubated with SPA-YSi beads for 8 hours and scintillation was measured. Data is plotted as the fold change relative to transfection with the empty vector for quadruplicate experiments. Error bars represent the standard error of the mean. Statistical significance was calculated by one-way ANOVA followed by Dunnett's multiple comparison post-hoc analysis (**p < 0.01 / ****p < 0.0001).

Equivalent expression and membrane localization of each mutant construct was verified by immunoblot and HiBiT detection assay in transiently transfected HEK-293 cells **(Fig. S3.3)**. To examine the effects of these mutations on known US28 signal transduction pathways, we conducted luciferase reporter assays monitoring US28-mediated activation of MAPK and RhoA signaling (206,370,424). Alanine substitution at positions S218, K223, and R225 significantly reduced US28-mediated activation of MAPK as indicated by a reduction in luminescence driven by the SRE reporter element **(Fig. 3.2B)**. In a similar manner, the same three mutants exhibited decreased US28-mediated activation of RhoA as indicated by a reduction in luminescence driven by the SRF reporter element **(Fig. 3.2C)**. No significant effect was observed regarding alanine substitution at position S220 for either MAPK or RhoA signal transduction **(Fig. 3.2B,C)**. Results from these experiments were further confirmed by immunoblot monitoring ERK phosphorylation and RhoA activation **(Fig. S3.4)**. Because US28 signals through phospholipase C (PLC), we performed scintillation proximity assays to monitor accumulation of the downstream signaling intermediary inositol triphosphate (IP_3) for the US28 mutants (224). Interestingly, results from these experiments showed that only alanine substitutions at S218 and R225 showed a significant reduction **(Fig. 3.2D)**. Because a decrease in signaling activity could be associated with aberrations in receptor internalization, we monitored the real-time internalization kinetics for each of our constructs via a FRET-based assay. To this end, we engineered an in-frame SNAP-tag on the N' terminus of the wild-type US28 and the ICL3 mutant receptors. In this assay, the SNAP tag serves as the energy donor and exogenous fluorescein as the energy acceptor. Following optimization of the transfection conditions to achieve comparable donor signal for each of the constructs **(Fig. S3.5)**, the real-time internalization experimental data show that mutations in the ICL3 region do not alter the internalization kinetics of US28 **(Fig. 3.3)**. Together, these findings

suggest that specific residues within the ICL3 region of US28 are required for signal transduction but not for receptor localization or internalization.

Figure[3.3] Mutations in the ICL3 Region of US28 Do Not Affect Receptor Internalization Kinetics

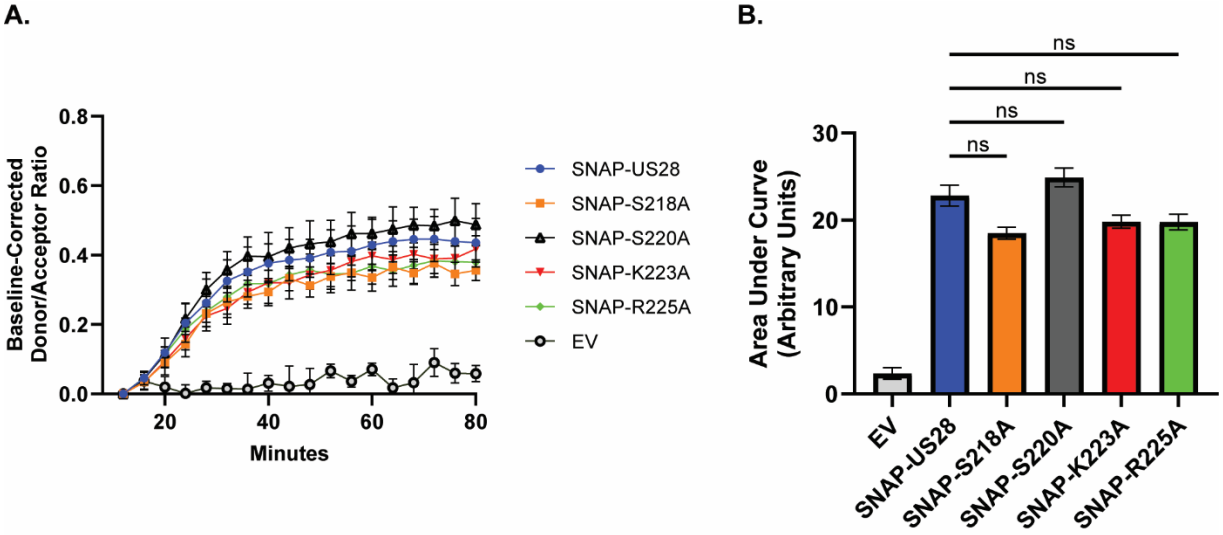

[3.3] Figure legend

(A) HEK-293 cells were transfected with the indicated SNAP-US28 constructs or the empty vector (EV). At 48 hours post-transfection, cells were treated with SNAP-Lumi4-Tb (donor) for one hour prior to washing. Fluorescein (acceptor) was added to the appropriate wells and internalization kinetics were measured for 80 minutes. Data is plotted as the baseline corrected donor/acceptor ratio (abs 615/520 nm). Error bars represent the standard error of the mean for triplicate experiments. **(B)** The area under the curve was calculated and plotted for each profile. Error bars represent the standard error of the mean between triplicate experiments. Statistical significance was calculated using one-way ANOVA followed by Dunnett's multiple comparison post-hoc analysis.

3.4.3 Third Intracellular Loop of US28 Is Necessary for G-Protein Coupling

To further understand the reduction in US28 signaling activity observed with mutation at residues S218, K223, and R225, we assessed the ability of our mutant constructs to efficiently couple with heterotrimeric G-protein complexes. To this end, we made use of a nLuc-based complementation assay measuring real-time interactions that was described previously by Laschet and colleagues (425). In this system, the C' terminus of the GPCR is linked in frame to one of three NanoBiT subunits (HiBiT, SmBiT, or the native natural peptide [NP]) while the Gα subunit is genetically fused to the complementing Large Bit (LgBiT) (425). We chose to use natural peptide as our NanoBiT as it provides an optimal balance between interaction affinity/reversibility and strength

of signal (425). Consequently, we engineered an in-frame natural peptide-tag on the C' terminus of the wild-type US28 receptor followed by site-directed mutagenesis substituting alanine at positions S218, S220, K223, and R225. As a negative control, we generated a construct with substitutions in the canonical G protein-coupling domain of US28 ($DRY_{128-130}$ – $AAA_{128-130}$) located at the base of TM3. Mutations within this region prevent US28 coupling to respective heterotrimeric G-protein complexes rendering the receptor "signaling dead" (192,296,306,361,426). Equivalent expression of each construct was verified by immunoblot in transiently transfected HEK-293 cells **(Fig. S3.6)**. In live cell GPCR interaction assays with LgBiT-$G\alpha_{i1}$, -$G\alpha_q$, and -$G\alpha_{12}$, US28 mutations at positions S218, K223, and R225 exhibited significantly impaired G-protein coupling to multiple different Gα isoforms when compared to the wild-type US28-NP construct **(Fig. 3.4)**.

Figure[3.4] US28 ICL3 Mutants Exhibit Impaired G – Protein Coupling

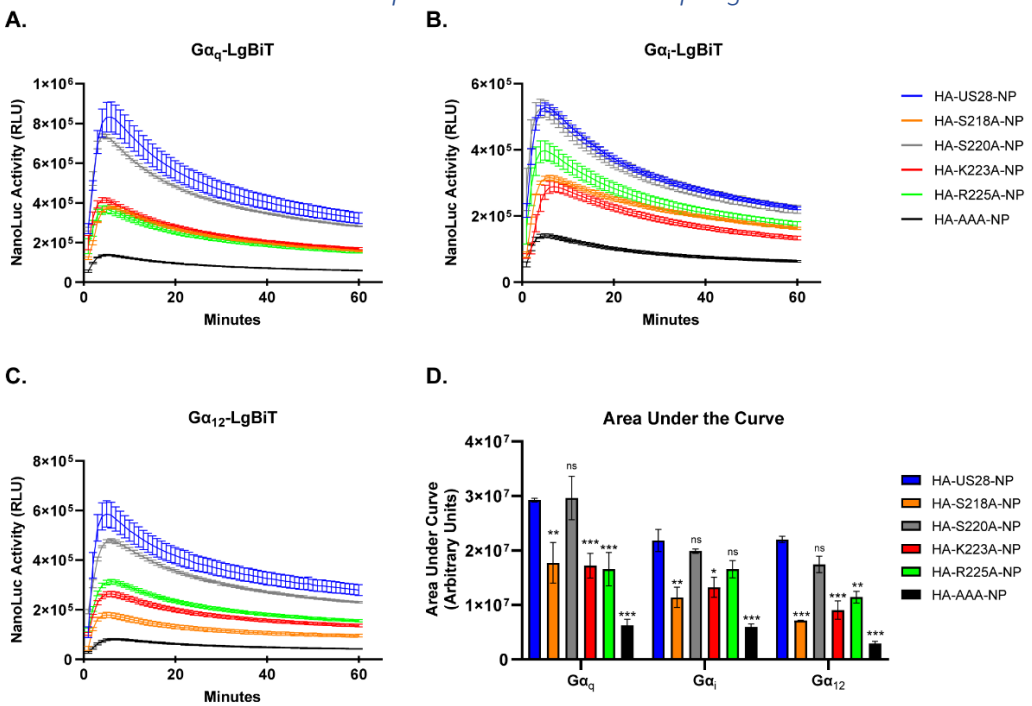

[3.4] Figure legend

HEK-293 cells were transfected with the indicated natural peptide-tagged US28 constructs or the empty vector (EV) and LgBiT tagged **(A)** $G\alpha_q$, **(B)** $G\alpha_i$, or **(C)** $G\alpha_{12}$. At 18 hours post-transfection, media was exchanged with serum-free DMEM. At 6 hours post media replacement; luciferase activity was monitored for 60 minutes using the Nano-Glo Live Cell Assay System (Promega). Error bars represent the standard error of the mean between technical triplicates. **(D)** The area under the curve was calculated for each profile and plotted. Error bars represent

the standard error of the mean between triplicate experiments. Statistical significance was calculated using two-way ANOVA followed by Dunnett's multiple comparison post-hoc analysis *(*p < 0.05 / **p < 0.01 / ***p < 0.001).*

The attenuation of G-protein coupling for all mutants was not as severe as complete alanine substitution of the DRY motif located in the second intracellular loop, and no significant difference was observed regarding mutation at position S220 **(Fig. 3.4)**. Interestingly, despite observing a non-significant difference in scintillation proximity assays, we observed a decrease in the ability of the K223 mutant to couple with $G\alpha_q$ isoforms. Together, these data indicate that mutation at specific residues within the ICL3 region of US28 results in an inability to efficiently couple with respective G-proteins, consequently attenuating US28 signaling activity.

3.4.4 Mutations in HCMV US28 ICL3 Fail to Efficiently Reactivate from Latent Infection in $CD34^+$ HPCs

While transient transfection in established cell lines is a reliable and tractable model for studying the effects of viral chemokine signaling in isolation, the complexities of viral infection are not accurately captured in these systems. To monitor the effects of US28-ICL3 mutations within the context of infection, we generated recombinant viruses using the HCMV TB40/E-GFP backbone and engineering the HiBiT tag onto the N' terminus of US28 followed by alanine substitutions at positions K223 and R225 (TB40/E-GFP-HB-US28, TB40/E-GFP-HB-US28-K223A, and TB40/E-GFP-HB-US28-R225A), as both of these mutations, when compared to wild type US28, have reduced signaling and G-protein coupling activities but retain expression and localization. To determine the growth kinetics of our recombinant viruses, we performed both single and multistep growth analysis in primary human fibroblasts. All three recombinant viruses exhibited similar replication kinetics to the parental virus confirming previous reports that US28 is not required for viral replication in fibroblasts **(Fig. 3.5A,B)** (225,302,311,427). Moreover, recombinant viruses exhibited similar immediate early, early, and late viral protein expression, including US28, at multiple time points post-infection **(Fig. 3.5C)**. To assess whether point mutations alter US28 localization within the context of infection, we performed HiBiT surface vs. total expression assays in infected human fibroblasts. Consistent with localization and internalization experiments conducted in transiently transfected cells **(Fig. 3.3, Fig. S3.4)**, no detectable difference in surface

expression was observed between the three recombinant viruses indicating that mutations within the ICL3 region do not significantly affect subcellular localization of US28 **(Fig. 3.5D)**.

Figure[3.5] Characterization of US28 ICL3 Recombinant Viruses

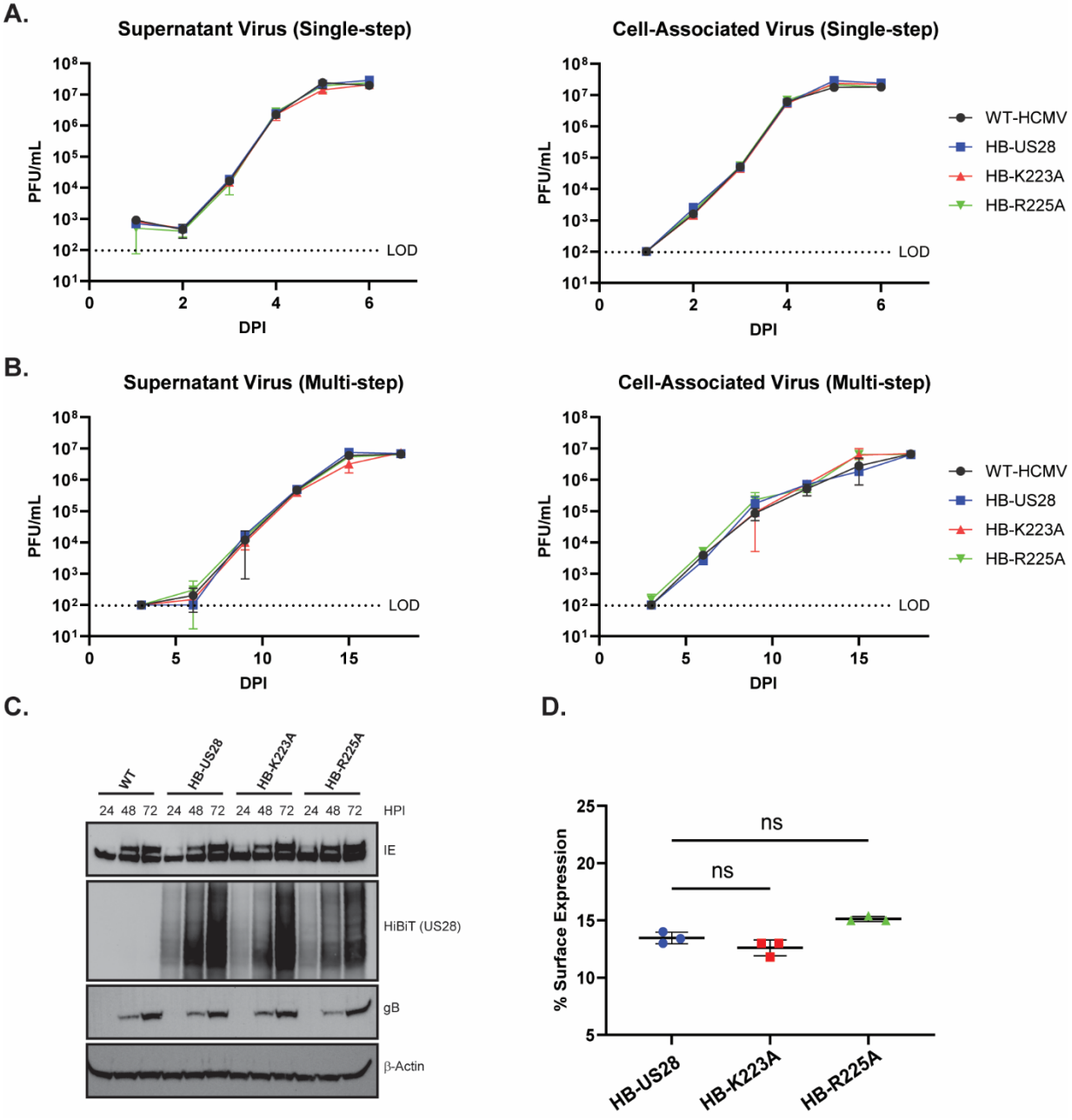

[3.5] Figure legend

NHDF cells were infected with the indicated viruses at a MOI of **(A)** 3 or **(B)** 0.01. Supernatant and cell-associated virus were harvested at the indicated timepoints post-infection and titered using confluent monolayers of NHDFs. Error bars represent the standard error of the mean between biological triplicates. **(C)**. NHDFs were infected with the indicated viruses at a MOI of 2 and lysates were harvested at the indicated time points post-infection. The

presence of indicated proteins was confirmed via traditional immunoblot using the indicated primary antibodies or the Nano-Glo HiBiT Blotting System (Promega). Representative blot shown from triplicate experiments. **(D)** NHDFs were infected with the indicated HiBiT-US28 tagged viruses at a MOI of 2. At 3 days post-infection, total and surface expression was assessed using the Nano-Glo HiBiT Lytic and Extracellular Detection Systems (Promega). Error bars represent the standard error of the mean between triplicate experiments. Statistical significance was calculated by one-way ANOVA followed by Dunnett's multiple comparison post-hoc analysis.

Since US28-mediated signaling plays a major role in the establishment of viral latency and the capacity to reactivate (192,193,222), we hypothesized that US28-ICL3 recombinant viruses with impaired G-protein coupling may exhibit an inability to establish latent infection or deficiencies in their ability to reactivate. To test this hypothesis, we infected both primary and hESC-derived $CD34^+$ HPCs with HCMV TB40/E-GFP, HCMV TB40/E-GFP-HB-US28-K223A (HCMV HB-K223A), and/or HCMV TB40/E-GFP-HB-US28-R225A (HCMV HB-R225A) (326,384). Infected $CD34^+$ HPCs were isolated via FACS and cultured above a murine stromal support layer under conditions that favor latent infection. At 14-DPI, the frequency of infectious centers was assessed via ELDA, as previously described (323,384). In both primary and hESC-derived $CD34^+$ HPCs infected with HCMV HB-K223A or HCMV HB-R225A, we observed deficits in the ability of the virus to efficiently reactivate from latent infection when compared with wild-type infected cells **(Fig. 3.6A, Fig. S3.7)**. To assess whether loss of genomes could explain the reactivation defect observed with either of the recombinant viruses containing ICL3 mutations, we quantified viral genome copies from infected hESC-derived $CD34^+$ HPCs at the beginning and end of latent infection via quantitative PCR. A comparable number of viral genomes were present in cells infected with WT-HCMV and recombinant viruses with mutations in the ICL3 region of US28, suggesting a reactivation defect occurs with these mutants **(Fig. 3.6B,C)**. Together, these results indicate that US28 G-protein coupling and downstream signaling play an integral role in the viral reactivation process in $CD34^+$ HPCs.

Figure[3.6] US28 ICL3 Mutants Fail to Efficiently Reactivate from Latent Infection

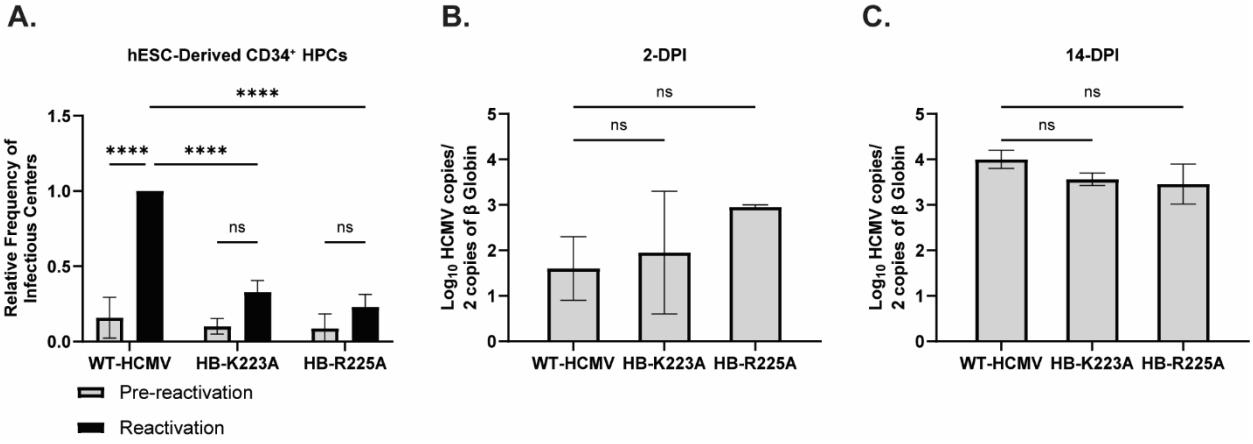

[3.6] Figure legend

(A) hESC-derived CD34⁺ HPCs were infected with HCMV TB40/E-GFP (WT-HCMV), HCMV TB40/E-GFP-HB-US28-K223A (HB-K223A), and/or HCMV TB40/E-GFP-HB-US28-R225A (HB-R225A) at a MOI of 3 for 48 hours. Cells were FACS isolated for viable, CD34⁺ /GFP⁺ HPCs and were cultured above a stromal cell support layer for 12 days to establish latent infection. At 14-DPI, half of the cells were treated with reactivation cocktail and plated onto a fibroblast monolayer, the other half of the cells were lysed and used to infect fibroblasts directly (pre-reactivation control). Reactivation was assessed by the frequency of infectious centers as determined via ELDA (415,416) at 3 weeks post-plating. Data is shown as fold change in infectious centers, as compared to the WT reactivation group, for triplicate experiments. Error bars represent the standard error of the mean and statistical significance was calculated using two-way ANOVA followed by Tukey's post-hoc analysis *(****$p < 0.0001$).* **(B)** At 2-DPI and **(C)** 14-DPI**,** total DNA was harvested from infected CD34⁺ HPCs and viral genomes were quantified via qPCR using primers and probes specific for the viral UL141 gene. Viral genomes were normalized to total cell number using human β-globin as a reference gene. Data is shown as the mean Log_{10} transformed values for triplicate experiments. Error bars represent the standard error of the mean and statistical significance was calculated by one-way ANOVA followed by Dunnett's multiple comparison post-hoc analysis.

3.4.5 US28 Third Intracellular Loop Mutations Affect Viral Reactivation in vivo

To further examine the impact of attenuating US28 G-protein interactions on viral reactivation, we utilized a humanized NOD-scid IL2Rγc^{null} (huNSG) mouse model of HCMV infection (179). In these experiments, huNSG mice received engraftment of cord blood-derived CD34⁺ HPCs and, at five weeks post engraftment, were infected with HCMV TB40/E-GFP (WT-HCMV) or HCMV TB40/E HB-K223A by intraperitoneal injection of infected fibroblasts (179). At four weeks post-infection, half of the latently infected huNSG mice were treated with a reactivation cocktail consisting of G-CSF and the CXCR4 antagonist AMD3100 to induce cellular differentiation and

mobilization. One-week post-mobilization, spleen and liver tissue were harvested from all animals, and viral genome copies, indicative of viral reactivation, were assessed via quantitative PCR probing. Comparable viral loads in liver and spleen tissues were observed for animals latently infected with HCMV HB-K223A and WT-HCMV **(Fig. 3.7A,B)**. This finding demonstrates that HCMV HB-K223A can establish latency in humanized mice to WT levels, mirroring our findings in $CD34^+$ HPCs. In contrast, animals infected with HCMV HB-K223A that received reactivation stimulus showed a significant reduction in viral genome copies in both liver and spleen tissues compared to WT-HCMV infected animals **(Fig. 3.7A,B**), indicating that the virus has a reactivation defect in vivo. Together, these results confirm that protein-protein interactions mediated by the third intracellular loop of US28 are not required for the establishment or maintenance of latent infection but are required for HCMV reactivation both in vitro and in vivo.

Figure[3.7] US28 ICL3 Mutants Fail to Efficiently Reactivate from Latent Infection in Humanized Mice

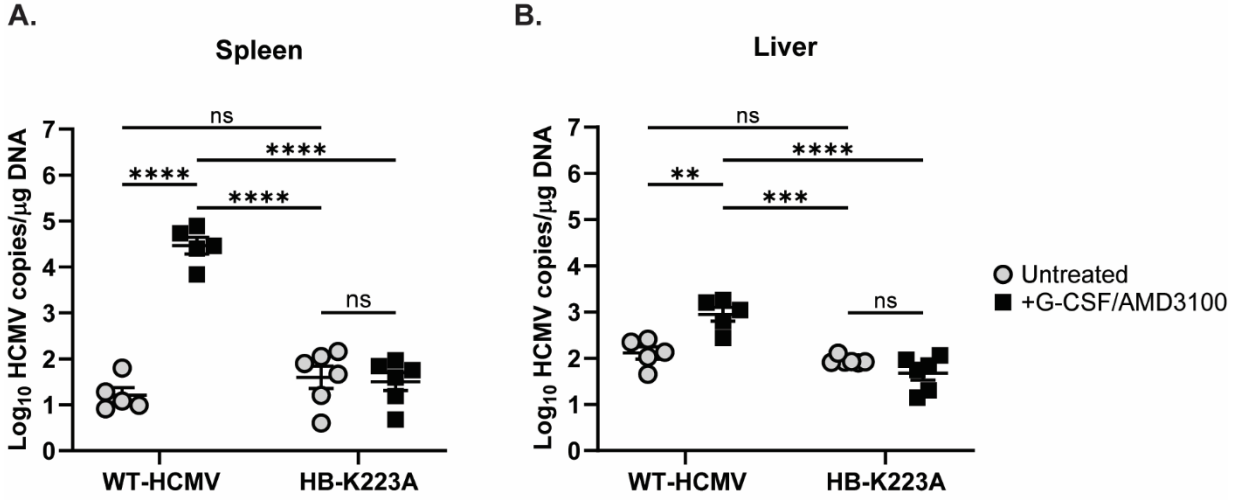

[3.7] Figure legend

Humanized NSG (huNSG) mice were infected via intraperitoneal injection of NHDFs infected with HCMV TB40/E-GFP (WT-HCMV) or HCMV TB40/E-GFP-HB-US28-K223A (HB-K223A) (179,193). At 4 weeks post-infection, half of the of the mice in each infection group were treated with G-CSF and AMD3100 to induce viral reactivation. Control, latently infected mice were treated with DMSO. At 1-week post-treatment, mice were euthanized prior to harvesting **(A)** spleen and **(B)** liver tissues. Total DNA was extracted using DNAzol, and HCMV viral load was determined by qPCR from two tissue sections per mouse. Error bars represent the standard error of the mean between the average DNA copies per huNSG mouse (n=5 mice per group). All samples were compared by two-way ANOVA followed by Tukey's multiple comparisons test between experimental groups *(**p < 0.01 / ***p < 0.001 / ****p < 0.0001).*

Section 3.5: Discussion

While a growing number of studies have examined signal transduction through the viral chemokine receptor US28, the specific mechanism by which US28 initiates these signaling cascades remains unclear. In the present report, we conduct a mutational analysis of the third intracellular loop (ICL3) of US28 to identify residues that are integral for G protein coupling, downstream signaling, and viral reactivation. Our results indicate that alanine substitutions at positions S218, K223, and R225 significantly attenuate US28-mediated activation of mitogen-activated protein (MAP) kinase and RhoA signal transduction pathways. Furthermore, we show that mutations at positions S218, K223, and R225 result in impaired coupling to multiple Gα isoforms, including $G\alpha_{i/o}$, $G\alpha_{q/11}$, and $G\alpha_{12/13}$, despite maintaining normal surface expression and internalization kinetics. Utilizing primary- and hESC-derived $CD34^+$ HPCs, we show that recombinant viruses with mutations in the ICL3 region of US28 fail to efficiently reactivate from latent infection. These results were further confirmed in a humanized mouse model of HCMV infection where recombinant viruses established and maintained latent infection but did not reactivate post-mobilization. Taken together, our results identify novel residues within the ICL3 region of US28 that are required for G-protein coupling, downstream signaling activity, and viral reactivation from latency in hematopoietic progenitor cells.

Mounting evidence into the mechanism of rhodopsin-like receptor coupling to cognate Gα subunits indicates that specific residues at the base of TM3 and TM6 (ICL2/3) are major determinants of G-protein coupling and specificity (418–422,428). For instance, a recent study examining autoregulation of the β_2 adrenergic receptor (β_2AR) found that residues within the third intracellular loop participate in ionic interactions to stabilize weakly coupled G-proteins allowing them to efficiently interface with the β_2AR receptor (420). Consistent with these findings, our results indicate that mutation of polar and charged residues within the ICL3 region of US28 results in deficient G-protein coupling and downstream signaling activity. We show that the observed reduction in G-protein coupling and signaling are independent of subcellular localization as receptors harboring mutations in the ICL3 region exhibit normal internalization kinetics **(Fig. 3.3)**. Interestingly, we did not observe any significant difference in signal

transduction or G-protein coupling with regard mutation at position S220 **(Fig. 3.2,3.4)**. This result would suggest that this residue may be occluded from interacting with heterotrimeric G-protein complexes and not participate in coupling but may have additional functional purposes. Furthermore, we note that the K223 residue is important for US28 coupling to $G\alpha_{q/11}$ isoforms, but we observe no effect with this mutant in IP_3 accumulation experiments **(Fig. 3.2,3.4)**. We surmise that this may be due to differences in assay sensitivity and/or residual activity as we did not observe a complete loss of coupling activity. The observed deficit in G-protein coupling for other US28 ICL3 mutant constructs was not as severe as results obtained by mutation of the canonical G-protein coupling domain located in the second intracellular loop, and no specific effect was observed when examining different Gα isoforms **(Fig. 3.4)**. These results would suggest that residues within the ICL3 region of US28 may mediate secondary interactions with G-proteins irrespective of classification, or that they are required for stabilizing the active conformation of US28. These hypotheses are not without basis as a recent publication authored by De Groof et al. showed similar attenuation of G-protein coupling utilizing intrabodies recognizing the ICL3 region of US28 (429). Results reported here confirm these findings and suggest that the ICL3 region is integral for US28 – G protein interactions. Further structural and biochemical research examining the constitutive and ligand-induced signal transduction will be required to delineate the specific role of this region in relation to signal transduction.

Despite being dispensable for viral replication in fibroblasts **(Fig. 3.5)**, the functional consequences of US28 downstream signaling are cell-type specific, with differential effects observed dependent on the infected cell type. Importantly, previous work indicates that US28 is expressed during both latent and lytic phases of the viral lifecycle and that US28 is required for both the maintenance of latent infection and the capacity to reactivate (191–194,222,291). Recently, our group published a study describing US28-mediated activation of RhoA to enhance emergence out of latent infection, and that pharmacologic inhibition of US28-mediated RhoA signaling blocks viral reactivation in vitro and in vivo (206). Similarly, results reported here validate that US28 signaling activity is required for viral reactivation in vitro and in vivo, and identifies novel motifs required for US28 signaling activity. Despite showing that $G\alpha_{q/11}$ signal transduction is important for viral reactivation **(Fig. 3.1)** and that mutation of K223 results in no

significant change in IP_3 accumulation **(Fig. 3.2)**, we observed a deficit in the ability of this virus to reactivate from latent infection in vitro and in vivo **(Fig. 3.6,3.7)**. Moreover, none of the mutations within the ICL3 region of US28 completely abrogated coupling to heterotrimeric G-protein complexes **(Fig. 3.4)** yet still exhibited an inability to reactivate from latent infection. These results suggest that, in addition to stimulating PCL-β activity, US28 is modulating viral latency and reactivation through multiple signal transduction pathways concurrently and that these signaling events are not all or nothing perse. Therefore, it is likely that a receptor as promiscuous as US28 serves a multipurpose function in regard to HCMV latency and reactivation, acting as a rheostat for the fine tuning of cell signaling networks altering the cellular microenvironment in favor of the virus.

Contradictory to previous well conducted studies regarding the requirement of US28 to maintain latent infection within cells of myeloid lineage (191,194,430), we did not observe any deficits in the ability of our recombinant viruses to establish or maintain a latent infection. We suggest that incongruencies reported here could be to differences in cell source or recombinant virus construction. Previous studies have utilized recombinant viruses lacking the complete US28 ORF while viruses used here are only deficient in receptor function. Moreover, $CD34^+$ HPCs represent a heterogeneous population of cells with distinct differences dependent on the source from which they are harvested (23,326,431). While we made use of hESC- and primary fetal liver-derived HPCs in this study, cord blood-derived $CD34^+$ HPCs likely have subtle genetic and morphological differences which may explain inconsistencies in results reported elsewhere. An in-depth comparison of different HCMV latency models would certainly be of great value to the field but is nonetheless outside the scope of the current study.

The γ-herpesviruses, Epstein Barr Virus (EBV) and Kaposi Sarcoma Herpesvirus (KSHV), encode their own respective viral GPCRs: BILF1 and ORF74, respectively. Despite exhibiting a low degree of sequence similarity to US28, the ICL3 region of these vGPCRs contain several polar and charged residues that have been implicated to be important for G-protein coupling (432–434). EBV-BILF1 and KSHV-ORF74 are important for immune evasion, modulation of cellular proliferation, transformation, and regulation of cellular signal transduction (435–439). Results reported here

provide insights into the functional importance of the ICL3 region of these vGPCRs and have highlighted its potential as a therapeutic target for developing novel antiviral strategies aimed at disrupting viral GPCR signaling pathways. Future research focusing on the detailed molecular interactions within the ICL3 region of EBV-BILF1 and KSHV-ORF74 will be crucial for unraveling the precise mechanisms underlying viral pathogenesis and for informing the development of targeted therapies against gamma herpesvirus-associated diseases.

US28 is notable for its ability to interact with multiple Gα isoforms and initiate diverse signaling cascades, influencing various cellular processes crucial for viral pathogenesis. Because of its substantial role in viral latency and reactivation, there has been interest in developing novel therapeutics targeting US28. To date, these candidate therapeutics encompass multiple different mechanisms of action including small molecule antagonists and inverse agonists, fusion toxin-protein molecular trojan horse chimeras, and single domain nanobodies targeting US28 (440). One such US28-specific intrabody, VUN103, was shown to bind the second and third intracellular loops of US28 to displace $G\alpha_q$ and prevent constitutive US28-mediated activation of STAT3, NF-κB, and NFAT (429). Consistent with these findings, results reported here indicate that the third intracellular loop of US28 is a major determinant of G-protein coupling and is required for downstream signaling. To our knowledge, this is the first study to investigate the ICL3 region of US28 as pertaining to viral latency and reactivation. Our findings will guide future studies aiming to develop novel therapeutics against HCMV-associated disease.

Section 3.6: Materials & Methods

Plasmids

US28-NP was generated by cloning the Natural Peptide (NP) tag (GVTGWRLCERILA) in-frame with the C-term of US28. HB-US28 was generated by cloning the HiBiT (HB) tag (VSGWRLFKKIS) in-frame with the N-term of US28. Primers used for generating plasmid constructs are listed in **Table S3.1**. Fragments were PCR amplified and cloned into the pcDNA3.1-vector. Mutations in the third intracellular loop of US28 were generated by site-directed mutagenesis, substituting alanine for the indicated amino acid using the Q5 Mutagenesis Kit (NEB) following the manufacturer's recommended procedure. All constructs were confirmed by sequencing and transformed into

TOP10 Escherichia coli cells (Invitrogen). Large-BiT tagged Gα subunits were kindly provided by Julien Hanson (Addgene plasmid ID: 134359, 134360, 134364, and 134363) (425). Reporter plasmids pRL-SV40 Renilla luciferase (Rluc), pGL4.33[luc2P/SRE/Hygro], and pGL4.34[luc2P/SRF-RE/Hygro] containing SRE and SRF responsive elements driving luciferase expression were purchased from Promega.

Cells and Virus

Normal human dermal fibroblasts (NHDFs) were obtained from ATCC (PCS-201-010), and human embryonic kidney (HEK) -293 cells were obtained from Microbix. Both cell types were maintained in Dulbecco's modified Eagle's medium (DMEM), 10% FBS, streptomycin, penicillin, and glutamine at 37°C and 5% CO_2. M2-10B4 and S1/S1 stromal cells were obtained from Stem Cell Technologies and cultured as previously described (384). WA01 human embryonic stem cells (hESCs) were obtained from the WiCell Research Institute – National Stem Cell Bank and were cultured as previously described (323,441). The HCMV strain TB40/E-GFP, which constitutively expresses green fluorescent protein under the SV40 promoter (442), was amplified in NHDFs as previously described (196,202,443). Recombinant US28 mutant viruses were generated using a two-step recombineering procedure (415) utilizing the HCMV TB40/E-GFP bacterial artificial chromosome (BAC) (442). Viral constructs were confirmed by next-generation sequencing prior to plaque purification and clonal expansion. Viral titers were determined via plaque assay on NHDF cells and aliquots stored at -80°C. For viral growth analyses, single-step growth curves were carried out at a multiplicity of infection (MOI) of 3.0 PFU/mL, and multi-step growth curves were carried out at a MOI of 0.01 PFU/mL. Supernatant and cell-associated virus were harvested at multiple time points post-infection and titered via limiting dilution plaque assay on NHDF cells.

Immunoblot

Cell lysates were harvested using RIPA Lysis Buffer (Santa-Cruz Biotechnology) supplemented with HALT protease inhibitor (Thermo-Fisher Scientific). Proteins were separated on a 4-12% SDS-PAGE gel and transferred onto PVDF membranes. Immunoblots were performed using antibodies directed against β-Actin (sc-47778, Santa-Cruz Biotechnology), HCMV IE1/IE2 (MAB8131, Millipore-Sigma), HA (sc-7392, Santa-Cruz Biotechnology), HCMV gB (sc-69742, Santa-Cruz Biotechnology), P-p44/42 MAPK T202/Y204 (4370S, Cell Signaling Technology), p44/42 MAPK

(9102S, Cell Signaling Technology), Rho (1862332, Thermo Scientific), and, if required, the appropriate HRP-conjugated secondary antibody (sc-525409). HiBiT-tagged proteins were visualized using the Nano-Glo HiBiT Blotting System (Promega).

Cytotoxicity Assay

Compound cytotoxicity was determined using the CellTiter-Glo kit (Promega) (444). Briefly, NHDF cells were seeded into treated black 96-well plates at a density of $1.5x10^4$ cells per well. The following day, cells were treated with compound at the indicated concentration or an equivalent amount of DMSO (vehicle) in triplicate. At 72 hours post-treatment, cellular cytotoxicity was assessed by adding 100 µL of assay reagent to each well and incubating for 10 minutes with agitation per the manufacturer's recommendation. Luminescence was measured using a Promega GloMax Navigator luminometer. Well luminescence, indicative of the number of living cells per well, was converted to percent cell viability in Microsoft Excel by dividing luminescence values in experimental wells by the value in control wells containing untreated cells and multiplying by 100. Values obtained were used to calculate 50% cellular cytotoxicity (CC_{50}) by nonlinear regression analysis within GraphPad Prism 10.0 software.

HCMV-gHnLUC Viral Replication Assay

To assess the effects of the indicated compounds on viral replication we used our TB40/E-gHnLUC reporter virus assay as previously described (206). Briefly, NHDF cells were seeded into treated black 96-well plates at a density of $1.5x10^4$ cells per well. The following day, cells were treated with compound at the indicated concentration or an equivalent amount of DMSO (vehicle) in triplicate and were infected with TB40/E-gHnLUC at a multiplicity of infection (MOI) of 0.3. At 72 hours post-infection, viral replication was assessed using the Nano-Glo Luciferase Assay kit (Promega) as previously described (206). Luminescence was measured using a Promega GloMax Navigator luminometer. Well luminescence, indicative of viral growth, was converted into percent inhibition in Microsoft Excel by dividing luminescence values in experimental wells by the value in control wells containing untreated cells and multiplying by 100. The resulting values were used to calculate the 50% inhibitory concentration (IC_{50}) by nonlinear regression within GraphPad Prism 10.0 software.

Luciferase Reporter Assay

Reporter assays were conducted as previously described (203) using the Dual Luciferase Assay Kit (Promega). Briefly, HEK-293 cells were seeded into treated black 96-well plates at a density of $3.0x10^4$ cells per well. The following day, cells were co-transfected in triplicate with the indicated US28 construct and/or the empty pcDNA3.1 vector, the indicated FireFly luciferase reporter element, and the Renilla luciferase reporter element using Fugene4K (Promega) following the manufacturers recommended protocol. At 18 hours post-transfection, the growth medium was replaced with serum-free DMEM with or without small-molecule inhibitors at the indicated concentrations. At 6 hours post media replacement, cell culture medium was removed and 20 µL of Passive Lysis Buffer (Promega) was added to each well. Plates were incubated for 20 minutes with agitation at room temperature. Luciferase assay reagents were reconstituted and 100 µL was injected per well in a Promega GloMax Navigator luminometer. Assay results were transferred to a Microsoft Excel spreadsheet, normalized to Renilla luciferase, and analyzed using GraphPad Prism 10.0 software.

Scintillation Proximity Assay

IP_3 accumulation assays were conducted as previously described (445). Briefly, HEK-293 cells were seeded into 96-well plates pre-treated with poly-D-lysine at a density of $3.5x10^4$ cells per well. The following day, cells were transfected in duplicate with 20 ng of the indicated US28 construct and/or the empty pcDNA3.1 vector using Lipofectamine 2000 (Thermo-Fisher Scientific). At 24 hours post-transfection, the culture medium was aspirated and replaced with 0.1 mL media supplemented with 0.5 µL of 1 mCi/mL [3H]myo-inositol. Following 24 h incubation, cells were treated as follows: the medium was aspirated, and wells were washed twice with Hanks' Balanced Salt Solution (HBSS, Gibco). 100 µL of HBSS buffer containing 10 mM LiCl was added to each well and incubated for 90 min at 37 ℃. After incubation, the plates were put on ice, the medium was aspirated and 40 µL of 10 mM formic acid were added to each well to lyse the cells. The [^{3}H]IPs in the formic acid cell lysates were thereafter quantified by Ysi-poly-D-Lys-coated SPA beads Briefly, 35 µL of lysate were transferred to a new white 96-well plate and mixed with 60 µL of SPA-YSi (PerkinElmer) bead solution (12.5 mg/mL) Plates were sealed, agitated for at least 30 min and centrifuged. SPA beads were allowed to settle and react with the extract for

8 h before radioactivity was determined using a MicroBeta2® (2450-0060, Perkin Elmer). All determinations were made in duplicate.

FRET-Based Real-Time Internalization Assay

The internalization kinetics of wild-type and ICL3 US28 mutant constructs were assessed as previously described (446). Briefly, HEK-293 cells were transiently transfected with the indicated constructs and/or the empty vector (SNAP-FRT) using Lipofectamine 2000 (Thermo-Fisher Scientific) according to the manufacturer's recommendation. At 48 hours post-transfection, cells were incubated with Tag-Lite SNAP-Lumi4Tb (donor) [Cisbio, SSNPTBD] for 1 hour at 4°C. Afterward, cells were washed four times with HBSS. Following washing, 20 µL of reconstituted fluorescein-O'-acetic acid (acceptor) [Sigma-Aldrich, catalog no. 88596] was added to each well. Internalization was measured for 80 minutes utilizing a PerkinElmer EnVision 2104 Multilabel Reader using the following settings: 340 nm (excitation), 520 nm (acceptor), and 615 nm (donor). Results are presented as the baseline corrected ratio of donor over acceptor emissions (615/520 nm). To compare internalization across constructs, the area under the curve (AUC) was calculated as described previously (447). Assay results were plotted in GraphPad Prism 10.0 software.

Live Cell G-Protein Coupling Assay

US28 ICL3 mutant G-protein coupling was assessed as previously described (425) using the Nano-Glo Live Cell Assay system (Promega). Briefly, HEK-293 cells were seeded into treated black 96-well plates at a density of $3.0x10^4$ cells per well. The following day, cells were co-transfected in triplicate with a 1:1 ratio of the indicated US28-NP construct and/or the empty pcDNA3.1 vector, and Large BiT linked Gα subunit using Fugene4K (Promega) following the manufacturer's recommended procedure. At 18 hours post-transfection, the growth medium was replaced with Opti-MEM media (Thermo Fisher Scientific). At 6 hours post media replacement, 25 µL of reconstituted Nano-Glo Live Cell assay reagent was added to each well, and plates were briefly incubated with agitation. Luminescence, indicative of US28 – G protein coupling, was measured using a Promega GloMax Navigator luminometer. Assay results were transferred to a Microsoft Excel spreadsheet, backgrounds subtracted and plotted in GraphPad Prism 10.0 software.

HiBiT Surface Expression Assay

NHDF or HEK-293 cells were seeded into cell culture-treated black 96-well plates at a density of $1.5x10^4$ cells per well. The following day, triplicate wells were infected with the indicated HiBiT-tagged US28 recombinant viruses at a MOI of 1.0 or transfected with the indicated HiBiT-tagged US28 pcDNA3.1(-) constructs. At 72 hours post-infection or 24 hours post transfection, surface vs. total HiBiT expression was evaluated using the Nano-Glo HiBiT Extracellular and Lytic Detection kits (Promega) following the manufacturer's recommended procedure. Luminescence was measured using a Promega GloMax Navigator luminometer. Assay results were transferred to a Microsoft Excel spreadsheet, background subtracted, normalized to the HiBiT control protein, and % surface expression was determined by using the ratio of extracellular vs lytic luminescence. Results were analyzed using GraphPad Prism 10.0 software.

Active Rho Pulldown and Detection Assay

GST-Rhotekin pulldown was performed as previously described (206). Briefly, HEK-293 cells were seeded into treated 10cm dishes at a density of $3.0x10^5$ cells/mL. The following day, cells were co-transfected with the indicated US28 constructs or the empty pcDNA3.1 vector using Fugene4K (Promega) following the manufacturers recommended protocol. At 24 hours post-transfection, the growth medium was replaced with serum-free DMEM, and cells were cultured for an additional 24 hours. Cells were washed once with PBS and lysed in a buffer containing 25 mM Tris-HCl, 150 mM NaCl, 5 mM $MgCl_2$, 1% NP-40, and 5% glycerol. Lysates were clarified by centrifugation at 4°C and protein concentrations were normalized using the Qubit Protein BR Assay Kit (Invitrogen). Proteins were isolated using the Active Rho Pulldown and Detection kit (Thermo Scientific) according to the manufacturer's recommendations. The total amount of active RhoA was assessed via immunoblot using the indicated primary antibodies. Quantification shows the relative expression of RhoA bound to GTP normalized against the loading control (beta-actin) and compared to transfection with the wild type US28 receptor.

HCMV Latency and Reactivation Assay

hESC-derived $CD34^+$ HPCs were differentiated from WA01 human embryonic stem cells using the commercial STEMdiff Heme feeder-free hematopoietic differentiation kit (Stem Cell Technologies) as previously described (205,323,326). Primary $CD34^+$ HPCs were isolated from

deidentified donors using magnetic bead separation (Miltenyi Biotech) as previously described (193,335). HPCs were cultured in SFEMII with 10% BIT serum replacement, stem cell cytokines (stem cell factor, FLT3L, IL-3, and IL-6 [PeproTech]), and penicillin/streptomycin as previously described (193,203,323,326,335,384). $CD34^+$ HPCs were infected with the indicated viruses at a MOI of 2 for 48 hours prior to isolation by fluorescence-activated cell sorting (FACS) using a FACSAria (BD FACS Aria equipped with 488, 633, and 405 nm lasers, running FACS DIVA software) in order to obtain a pure population of viable GFP^+, $CD34^+$, HPCs as previously described (335,384). Infected cells were co-cultured in transwell culture dishes above monolayers of irradiated M2-10B4 and S1/S1 stromal cells. At 14 days post-infection, HPCs were serially diluted in RPMI-1640 medium containing 20% FBS, 2 mM L-glutamine, 100 U/mL penicillin, 100 µg/mL streptomycin, 15 ng/mL granulocyte-colony stimulating factor (G-CSF), and 15 ng/mL granulocyte-macrophage colony-stimulating factor (GM-CSF) and overlaid onto confluent monolayers of NHDFs cultured in 96-well plates. To quantify the levels of pre-reactivation infectious virus, a fraction of the HPC cultures were mechanically disrupted and lysates were serially diluted and then added to NHDFs cultured in 96-well plates. Cell cultures were microscopically visualized for the presence of GFP^+ weekly, for up to 4 weeks, to assess the reactivation frequency from latently infected cells and the presence of preformed infectious virus by extreme limiting dilution assay (384,416).

HCMV Infection of Humanized Mice

Mouse procedures were performed in accordance with approved Institutional Animal Care and Use Committee (IACUC) protocol 0922 under the recommendations of the American Association for Accreditation of Laboratory Animal Care (AAALAC). Mice were housed in the Vaccine & Gene Therapy Institute at Oregon Health & Science University vivarium using microisolator cages and fed sterile food and water ad litem. Both sexes of animals were used. Humanized mice were generated by irradiating NOD.Cg-PrkdcscidIL2Rγtm1Wjl/SzJ (NSG) mice (Jackson Laboratories) by sublethal irradiation of seven- to ten-week-old mice (250 cGy by 137Cs γ-irradiation). The irradiated animals were reconstituted by tail vein injection of $1x10^5$ human cord blood-derived $CD34^+$ HPCs as described previously (179). At four weeks post-engraftment, mice were distributed to experimental groups normalized for engraftment success as determined by the

percentage of human $CD45^+$ lymphocytes in the periphery. Humanized mice were dosed with 1 mL of 4% thioglycolate (Brewer's medium; BD) by intraperitoneal (i.p.) injection and then injected i.p. with approximately 10^5 PFU of cell-associated virus per mouse with the indicated viruses. At four weeks post-infection, the animals were divided into two groups. One group of latently infected mice were treated with 100 µL of Neupogen (G-CSF; 300 mg/mL; Amgen) by subcutaneous pump and 125 µg of AMD3100 administered by i.p. injection to mobilize progenitor cells and promote HCMV reactivation (193,448). At 1-week post mobilization, the mice were euthanized via CO_2 administration according to AAALAC euthanasia guidelines, and then blood, bone marrow, spleen, and liver tissues were collected for further analysis.

Viral DNA Quantification

Primers and probes recognizing HCMV UL141 were used to quantify viral genomes by quantitative real-time PCR (193). Briefly, total DNA was extracted from portions of mouse spleen and liver using DNAzol (ThermoFisher) according to the manufacturer's recommendations. Dilutions of purified HCMV BAC DNA were used to create a standard curve. A 1 µg sample of total DNA was added to each reaction well of TaqMan FastAdvance PCR master mix (Applied Biosystems) and samples were analyzed in triplicate on a StepOnePlus TaqMan PCR machine (Applied Biosystems) with an initial activation at 50°C for 2 min and 95°C for 20 s, followed by 40 cycles of 1 s at 95°C and 20 s at 60°C. TaqMan results were analyzed using ABI StepOne software and graphed using GraphPad Prism 10.0 software.

Section 3.7: Acknowledgements

This work was supported by grant P01 AI127335 from the National Institute of Allergy and Infectious Diseases, National Institutes of Health (NIH), awarded to D.N.S. S.M. is supported by National Institutes of Health (NIH) T32AI170496-01A1. M.H.H. and P.C. are supported by National Institutes of Health R37 AI21640 and P01 AI127335. The funder had no role in study design, data collection and analysis, decision to publish, or preparation of the manuscript.

Author Contributions: S.M., N.L.D., O.K-H., L.B.C., M.M.R., M.H.H., P.C., and D.N.S. designed research; S.M., M.D., N.L.D., L.B.C., O.K.-H., L.J.P., W.D.P., M.A.D., C.J.P., L.E.S., W.C.W., H.K.J.,

Z.J.S., G.S., A.T.D., C.N.K., T.A., M.H.H., and P.C. performed research; S.M., N.L.D., L.B.C., M.M.R., M.H.H., P.C., and D.N.S. analyzed data; and S.M., M.D., N.L.D., O.K-H., M.M.R., M.H.H., and D.N.S. wrote the paper with input from all authors. The authors declare no competing interest.

Section 3.8: Supplemental Figures

Figure[S3.1] Characterization of the Gαq/11 Inhibitor YM-254890

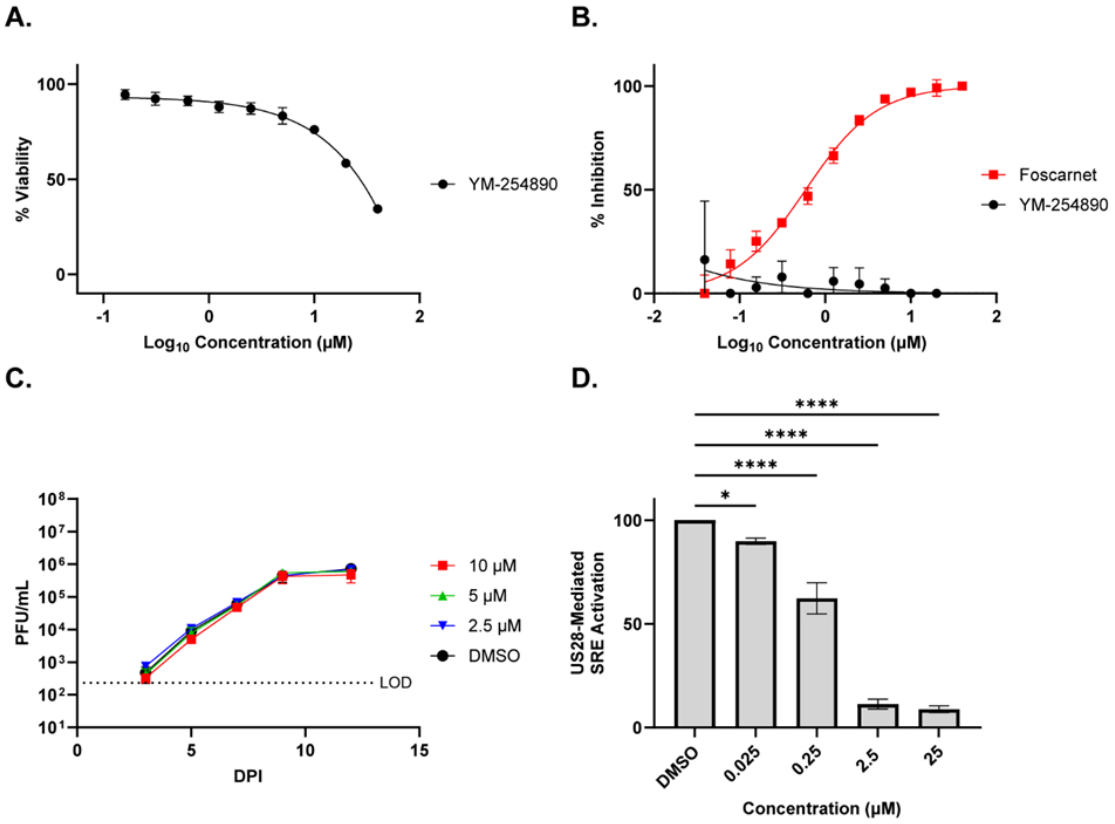

[S3.1] Figure legend

(A) NHDFs were treated with the indicated concentration of YM-254890 or an equivalent amount of DMSO (vehicle). At 3 days post-treatment, cellular viability was assessed using the CellTiter-Glo assay system (Promega). Concentrations of YM-254890 were Log_{10} transformed, and data is plotted as percent viability relative to the cells treated with vehicle alone. Error bars represent the standard error of the mean between triplicate experiments. **(B)** NHDFs were treated with the indicated concentrations of YM-254890, Foscarnet, or an equivalent amount of DMSO (vehicle) followed by infection with TB40/E-gHnLUC at a MOI of 0.3. At 3 days post-infection, luminescence was quantified using the Nano-Glo luciferase assay system (Promega). Concentrations of the indicated compounds were Log_{10} transformed and plotted as percent inhibition relative to the cells treated with vehicle alone. Error bars are representative of the standard error of the mean between triplicate experiments. **(C)** NHDFs were treated with the indicated concentration of YM-254890 and infected with the TB40/E-GFP (WT-HCMV) at a MOI of 0.01. Supernatant virus was harvested at the indicated timepoints post-infection and tittered over an

NHDF monolayer. Error bars represent the standard error of the mean between biological duplicates. **(D)** HEK-293 cells were transfected with HiBiT tagged US28 or the empty pcDNA3.1 vector along with Renilla and SRE reporter plasmids. At 18 hours post-transfection, the media was changed to serum-free DMEM supplemented with the indicated concentrations of YM-254890. Luciferase activity was measured using the Dual-Luciferase Reporter assay system (Promega) 6 hours post-media replacement. Error bars represent the standard error of the mean between triplicate experiments. Statistical significance was calculated by one-way ANOVA followed by Dunnett's multiple comparisons test between experimental groups *(*p < 0.05 / ****p < 0.0001).*

Figure[S3.2] Replicate Experiments for YM-254890 Latency Assays

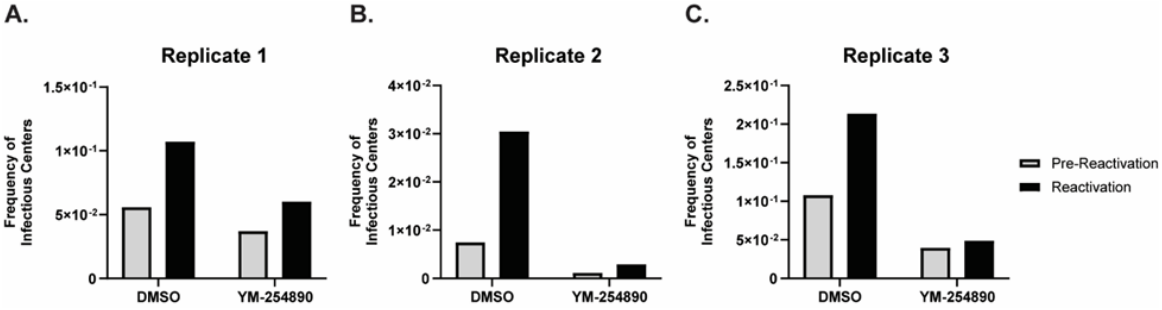

[S3.2] Figure legend

hESC-derived CD34⁺ HPCs were infected with TB40/E-GFP at a MOI of 2 for 48 hours. Cells were FACS isolated for viable CD34⁺/GFP⁺ HPCs and were cultured above a murine stromal cell support layer for 12 days to establish latent infection. Cells were treated with 1 µM YM-254890 ($G\alpha_{q/11}$ inhibitor) or an equivalent amount of DMSO throughout the latency culture. **(A – C)** At 14-DPI, half of the cells were treated with reactivation cocktail and plated onto a fibroblast monolayer, the other half of the cells were lysed and used to infect fibroblasts directly (pre-reactivation control). Reactivation was assessed by the frequency of infectious centers as determined via ELDA (87,95) at 3 weeks post-plating.

Figure[S3.3] HiBiT Tagged US28 ICL3 Mutant Constructs are Efficiently Expressed

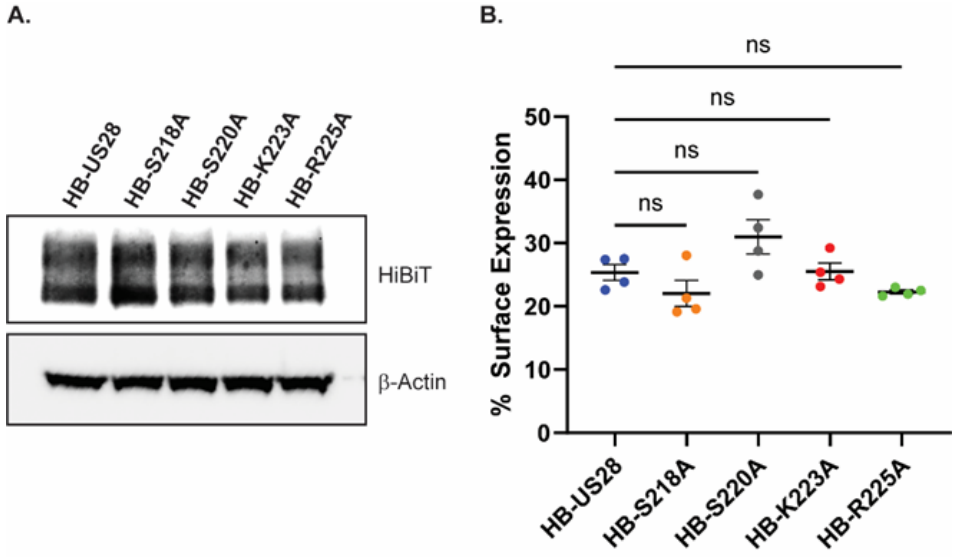

S3.3 Figure legend

(A) HEK-293 cells were transfected with the indicated HiBiT-tagged US28 constructs. Expression was confirmed via immunoblot using the indicated antibodies and the Nano-Glo HiBiT Blotting System (Promega) on whole lysates harvested 48 hours post-transfection. Representative blot shown from triplicate experiments. **(B)** HEK-293 cells were transfected with the indicated HiBiT-US28 tagged constructs or the empty vector. At 24 hours post-transfection, total and surface expression was assessed using the Nano-Glo HiBiT Lytic and Extracellular Detection Systems (Promega). Error bars represent the standard error of the mean between triplicate experiments. Statistical significance was calculated by one-way ANOVA followed by Dunnett's multiple comparison post-hoc analysis.

Figure S3.4 HiBiT Tagged US28 ICL3 Mutant Constructs Exhibit Attenuated MAPK and RhoA Signal Transduction

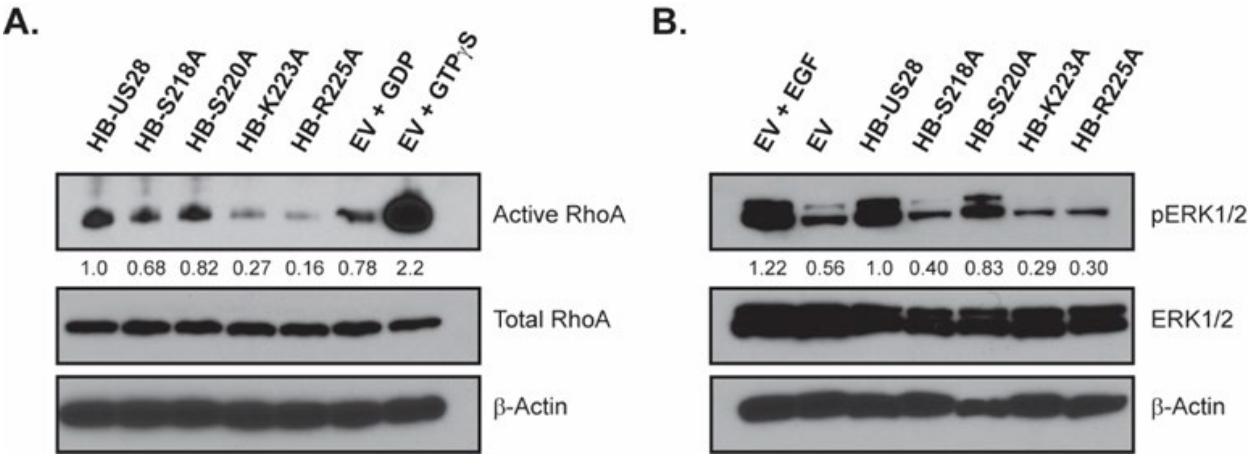

S3.4 Figure legend

(A) HEK-293 cells were transfected with the indicated HiBiT-tagged US28 constructs or the empty vector. At 24 hours post-transfection, cell culture media was exchanged to serum-free DMEM for an additional 24 hours prior to harvesting whole cell lysates. Lysates were subjected to GST-Rhotekin pulldown kit according to the manufacturer's (ThermoFisher) recommendations. RhoA activation was assessed via immunoblot using the indicated primary antibodies. Quantification shows the relative expression of RhoA bound to GTP normalized against β-actin and set relative to transfection with the wild type US28 receptor. Representative blot shown from triplicate experiments. **(B)** HEK-293 cells were transfected with the indicated HiBiT-tagged US28 constructs or the empty vector. At 24 hours post-transfection, cell culture media was exchanged to serum-free DMEM for an additional 24 hours prior to harvesting whole cell lysates. ERK phosphorylation was assessed via immunoblot using the indicated primary antibodies. Quantification shows the relative expression of phosphorylated ERK normalized against β-actin and set relative to transfection with the wild type US28 receptor. Representative blot shown from triplicate experiments.

Figure[S3.5] Optimization of SNAP-tagged US28 Construct Transfection Conditions

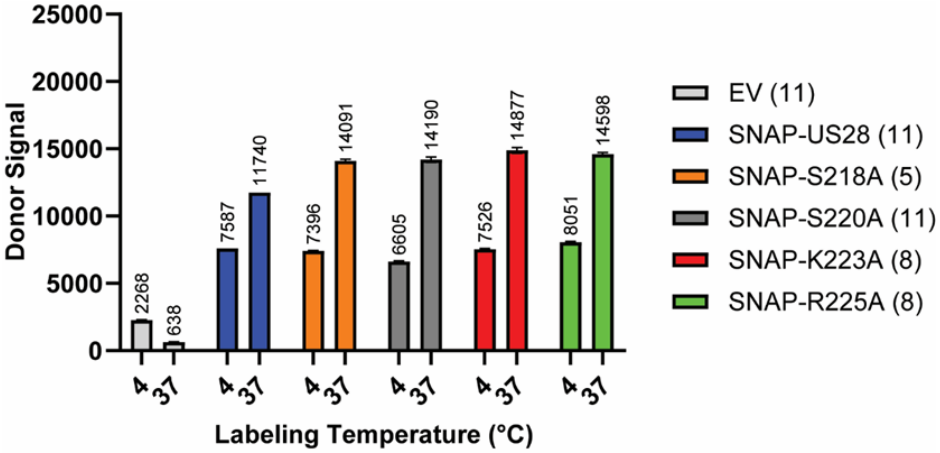

[S3.5] Figure legend

HEK-293 cells were transfected with the indicated SNAP-US28 constructs or the empty vector (EV). At 48 hours post-transfection, cells were treated with SNAP-Lumi4-Tb (donor) for one hour prior to washing. Fluorescein was added to the appropriate wells and internalization kinetics were measured for 80 minutes. Data is plotted as the baseline corrected donor signal intensity.

Figure[S3.6] Natural Peptide Tagged US28 ICL3 Mutant Constructs are Efficiently Expressed

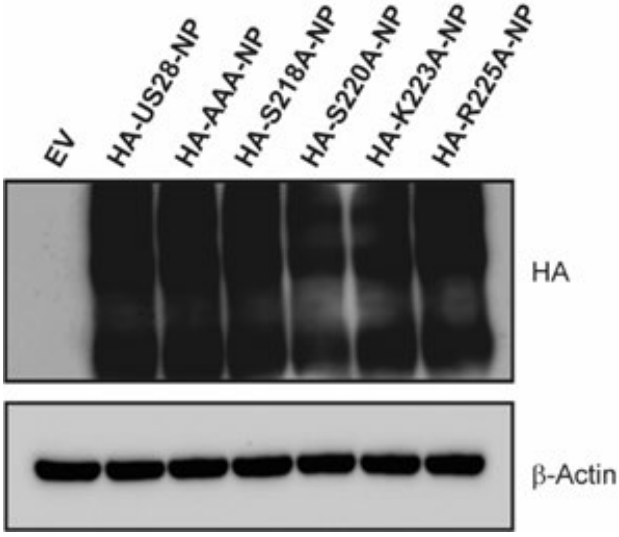

[S3.6] Figure legend

HEK-293 cells were transfected with the indicated HA-tagged US28 constructs. Expression was confirmed via immunoblot using the indicated antibodies on whole lysates harvested at 48 hours post-transfection. Representative blot shown from triplicate experiments.

Figure[S3.7] Replicate Experiments for US28-ICL3 Latency Assays

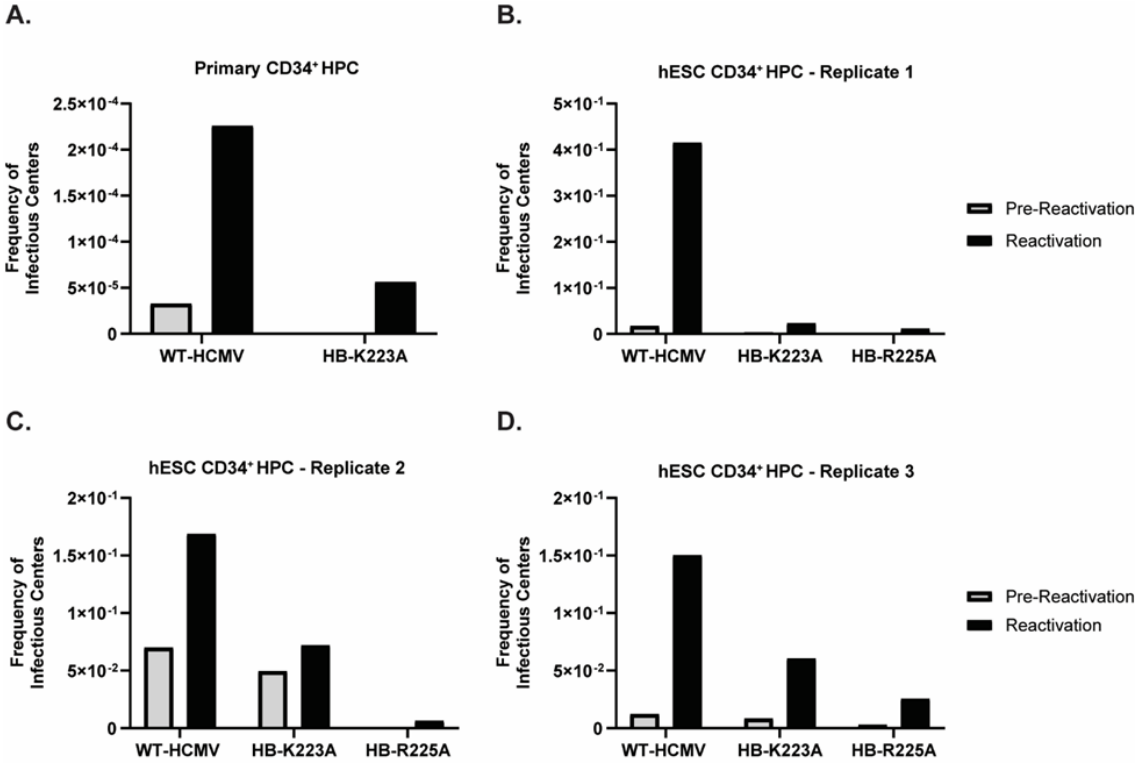

[S3.7] Figure legend

(A) Primary or hESC-derived **(B – D)** CD34$^+$ HPCs were infected with HCMV TB40/E-GFP (WT-HCMV), HCMV TB40/E-GFP-HB-US28-K223A (HB-K223A), and/or HCMV TB40/E-GFP-HB-US28-R225A (HB-R225A) at a MOI of 3 **(A)** or 2 **(B – D)** for 48 hours. Cells were FACS isolated for viable, CD34$^+$ /GFP$^+$ HPCs and were cultured above a stromal cell support layer for 12 days to establish latent infection. At 14-DPI, half of the cells were treated with reactivation cocktail and plated onto a fibroblast monolayer, the other half of the cells were lysed and used to infect fibroblasts directly (pre-reactivation control). Reactivation was assessed by the frequency of infectious centers as determined via ELDA at 3 weeks post-plating.

Section 3.9: Data Availability

All data and supplementary material associated with this manuscript is available within the main publication. Doi: 10.1128/jvi.01801-24

Chapter 4: Human Cytomegalovirus UL78 is a Nuclear-Localized GPCR Necessary for Efficient Reactivation from Latent Infection in CD34$^+$ Hematopoietic Progenitor Cells

Samuel Medica[a*], Nicole L. Diggins[a*], Michael Denton[a], Rebekah L. Turner[a], Lydia J. Pung[a], Adam T. Mayo[a], Olivia Kramer-Hansen[b], Jennifer Mitchell[a], Luke Slind[a], Linh K. Nguyen[a], Teresa A. Beechwood[a], Gauthami Sulgey[a], Craig N. Kreklywich[a], Daniel Malouli[a], Mette M. Rosenkilde[b], Patrizia Caposio[a], Daniel N. Streblow[a], & Meaghan H. Hancock[a]

[a] Vaccine & Gene Therapy Institute, Oregon Health & Science University, Beaverton, Oregon, USA

[b] Department of Biomedical Sciences Molecular Pharmacology, University of Copenhagen, Copenhagen, Denmark

* These authors contributed equally to this work

Journal of Virology. 2025 Oct 8:e01402-25.

Doi: 10.1128/jvi.01402-25

Section 4.1: Abstract

Human cytomegalovirus (HCMV) is a ubiquitous pathogen that persists throughout the lifetime of the host due to the establishment of latency. HCMV encodes four putative G protein-coupled receptors (GPCRs): US27, US28, UL33, and UL78. A definitive role for UL78 in HCMV infection has yet to be elucidated. Utilizing an in vitro $CD34^+$ hematopoietic progenitor cell (HPC) model, we demonstrate that a recombinant virus lacking UL78 protein expression fails to efficiently reactivate from latent infection. Furthermore, we show that UL78 preferentially couples to the $G\alpha_i$ family of G proteins and that a recombinant HCMV containing mutations in the UL78 G protein-coupling DRL motif also fails to reactivate from latent infection. Together our findings indicate that $G\alpha_i$ coupling is important for UL78 function during reactivation in latently infected $CD34^+$ HPCs. To better understand the role of UL78, we conducted proteomic analyses in HCMV-UL78-TurboID infected fibroblasts and $CD34^+$ HPCs undergoing reactivation from latency. Congruent with our coupling data, we found $G\alpha_i$ was the only heterotrimeric $G\alpha$ protein in proximity to UL78. Pathway analysis of the UL78 interactome revealed proteins associated with membrane trafficking, signaling, and the nuclear pore complex as enriched in both cell types. In addition, the UL78 interactome contained viral proteins with nuclear localization including viral transcription and DNA replication machinery. Nuclear localization of UL78 was validated using cell fractionation, immunofluorescence microscopy, and proteomic analysis of isolated nuclei. Together, our results provide novel insights into the localization and function of UL78, previously unknown to contribute to reactivation from latent infection.

Section 4.2: Importance

Primary HCMV infection is typically asymptomatic and leads to the establishment of latency in myeloid lineage cells, where the virus persists for the host's lifetime. Reactivation of latent HCMV can cause severe complications, particularly in immunocompromised individuals such as transplant recipients and people living with HIV. Several factors influence the transition from latent to lytic infection, including signal transduction through the viral G protein-coupled receptors: US27, US28, UL33, and UL78. Using an advanced in vitro model, we show that recombinant viruses lacking UL78 fail to efficiently reactivate from latent infection. Moreover,

we show that UL78 preferentially couples to the $G\alpha_i$ family of G proteins via a conserved DRL motif, and this coupling is required for efficient reactivation. These results were confirmed by proximity-dependent labeling experiments where we identified $G\alpha_i$ and several other proteins involved in trafficking, signaling, transcription, and nuclear localization. Nuclear localization of UL78 was confirmed by cell fractionation, immunofluorescence microscopy, and proximity-dependent labeling in isolated nuclei. Collectively, our results uncover a novel role for UL78 in reactivation from latency and shed new light on its localization and function.

Section 4.3: Introduction

Cytomegaloviruses (CMVs) are species-specific herpesviruses that establish life-long infections in their hosts. Human CMV (HCMV) achieves persistence in part through the ability to establish latent infections in $CD34^+$ hematopoietic progenitor cells (HPCs) and $CD14^+$ monocytes (187,449). Clinical reactivation of latent virus can occur in situations of immunosuppression, such as during allogenic or solid organ transplantation (450). Significant morbidity and mortality is associated with HCMV reactivation following transplantation, and currently available antiviral treatments targeting the DNA replication machinery have toxic side effects that can exacerbate disease and lead to the emergence of drug-resistant variants (64,397,398). Targeting the latent reservoir and/or early reactivation events is an alternative approach that requires detailed knowledge of the viral and cellular factors that regulate these processes.

HCMV encodes four G protein-coupled receptors (US27, US28, UL33, and UL78) that are thought to mimic the functions of cellular chemokine receptors (451). While the functions of US27, US28 and UL33 have been interrogated in the context of lytic and latent infection, much less is known about UL78 (193,210,223,295,303). The UL78 family includes HCMV UL78, rat CMV (RCMV) R78, murine CMV (MCMV) M78 and the human herpesvirus (HHV) -6 and -7 protein U51 (403,452–454). The UL78 family are positionally conserved 7-transmembrane proteins that contain a DRL motif located within the second intracellular loop (ICL2) that is suspected to be necessary for G-protein coupling. UL78 family members undergo endocytosis from the cell surface like many GPCRs; however, only HHV U51 has been shown to bind chemokines and induce migration (287,455–457). UL78, R78, and M78 remain orphan GPCRs with no known ligands and recent

structural analysis suggests that UL78 forms homotrimers that may occlude the putative ligand binding domain (285). A lack of UL78 expression does not impact HCMV lytic replication, however, R78 and M78 are necessary for efficient in vitro replication (286,403,458). RCMV R78 is expressed in many tissues and peripheral blood mononuclear cells in infected rats, and virus lacking R78 does not replicate in the spleen (454,459,460). MCMV M78 is important for transport of virus-infected cells to the salivary glands in part might be due to its ability to participate in the downregulation of MHC-II from the infected cell surface (461,462). In transient transfection assays, UL78 was shown to form heterodimers with the cellular chemokine receptors CXCR4 and CCR5 and reduce their cell surface expression as well as with HCMV vGPCR US28, which affected US28-mediated NF-kB activation, however the mechanism(s) for these findings has yet to be investigated (288,289). Thus, while there are some sequence similarities between the UL78 family members, they may functionally contribute to CMV infection in different ways.

Herein, we investigated the role of HCMV UL78 in latent infection of human embryonic stem cell (hESC) -derived $CD34^+$ HPCs. Our results indicate that $G\alpha_i$ coupling via the DRL motif of UL78 is essential for efficient reactivation from latent infection. To investigate the function of UL78, we performed proximity-dependent labelling experiments utilizing a recombinant virus expressing UL78 containing a C' terminal fusion with TurboID in infected fibroblasts and during reactivation from latency in $CD34^+$ HPCs. We identified a number of cellular and viral proteins as candidate UL78 interactors, including nuclear-localized proteins such as components of the nucleoporin complex, cellular and viral transcriptional regulators, and viral DNA replication machinery, suggesting that UL78 may localize to the nucleus, as has been observed for a number of cellular GPCRs (463–466). We determined that a fraction of both WT and G protein-coupling null mutant UL78 is detected at the nucleus using cell fractionation, luciferase assays, and immunofluorescent approaches. Together, our data indicate that UL78 coupling with $G\alpha_i$ is essential for reactivation from latency and that UL78 localization to the nucleus suggests a novel function for this orphan HCMV GPCR.

Section 4.4: Results

4.4.1 HCMV UL78 is Required for Efficient Viral Reactivation from Latent Infection

Several studies have shown that at least two of the G protein coupled-receptors encoded by HCMV are integral for establishing a latent infection and facilitating viral reactivation (193,194,206,210,430), however, the function of UL78 in this process is still unknown. To evaluate a potential role for UL78 in viral latency or reactivation, we utilized the TB40/E-GFP bacterial artificial chromosome (BAC) to generate a recombinant virus deficient in UL78 protein expression, but not gene expression. GalK-mediated recombination was used to place two contiguous stop codons immediately following the initiating methionine of UL78 (UL78-2XSTOP) (467). To determine the growth kinetics of the recombinant virus, both single and multistep growth kinetics were analyzed in primary human fibroblasts. Similar to previously published studies utilizing recombinant viruses lacking the entire UL78 open reading frame (ORF) (283,286), UL78-2XSTOP replicated with normal growth kinetics in this cell type **(Fig. S4.1)**.

To determine whether UL78 has a role in the establishment of latent infection or the capacity of the virus to reactivate, we infected human embryonic stem cell (hESC)-derived $CD34^+$ HPCs with either WT-HCMV (TB40/E-GFP) or UL78-2XSTOP (TB40/E-GFP-UL78-2XSTOP) viruses. At 48 hours post infection (hpi), viable, infected (GFP^+), $CD34^+$ HPCs were isolated via fluorescence activated cell sorting (FACS) and were seeded into long-term bone marrow culture (LTBMC) above a murine stromal support layer under conditions that favor latent infection, as previously described (211,223,323). After 12 days of LTBMC, half of the infected HPCs from each infection group were lysed by mechanical disruption to serve as a pre-reactivation control. The remaining intact HPCs and lysates were plated over monolayers of fibroblasts in reactivation supportive media supplemented with granulocyte-macrophage colony stimulating factor (GM-CSF) and granulocyte colony stimulating factor (G-CSF) to perform an extreme limiting dilution assay (ELDA) quantifying the frequency of infectious centers at three weeks post-plating (416). Comparable levels of infectious virus were present in lysed cells (pre-reactivation) infected with WT-HCMV or UL78-2XSTOP suggesting that UL78 has no effect on the establishment or maintenance of viral latency **(Fig. 4.1A, Fig. S4.2)**. In contrast, the frequency of infectious centers

for the UL78-2XSTOP-infected cells did not increase in the presence of reactivation stimulus compared to WT-HCMV infected cells suggesting that UL78 is required for efficient reactivation from latency **(Fig 4.1A, Fig. S4.2)**. Since an observed deficit in viral reactivation can be caused by an inability to maintain viral genomes or genome-containing cells throughout latency, we quantified viral genome copies from infected CD34$^+$ HPCs at the end of latent infection via quantitative PCR. A comparable number of viral genomes were present in cells infected with WT-HCMV or UL78-2XSTOP indicating that, despite the presence of viral DNA, viruses lacking UL78 are unable to produce infectious virions in HPCs stimulated to reactivate **(Fig. 4.1B)**. Together, these results indicate that UL78 plays an integral role in the viral reactivation process in CD34$^+$ HPCs.

Figure[4.1] HCMV UL78 is Required for Reactivation from Latent Infection

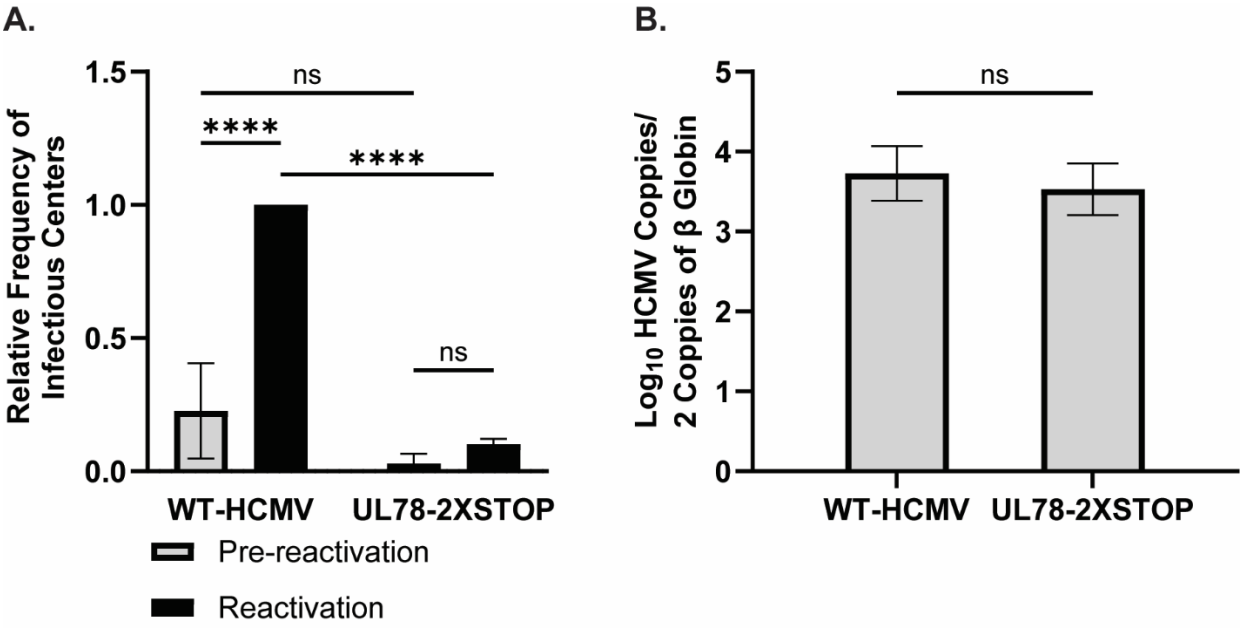

[4.1] Figure legend

hESC-derived CD34$^+$ HPCs were infected with either WT-HCMV (TB40/E-GFP) or UL78-2XSTOP (TB40/E-GFP-UL78-2XSTOP) at a MOI of 2 for 48 hrs. Cells were FACS isolated for viable CD34$^+$/GFP$^+$ HPCs and were cultured above a murine stromal cell support layer for 12 days to establish latent infection. **(A)** At 14-dpi, half of the cells were treated with reactivation cocktail and plated onto a fibroblast monolayer (reactivation). The remaining cells did not receive treatment and were mechanically lysed (pre-reactivation). Reactivation was assessed by the frequency of infectious centers as determined via ELDA and compared to lysed cells (pre-reactivation) at 3 weeks post-plating. Data is shown as fold change in infectious centers, as compared to the WT-HCMV reactivation group, for triplicate experiments. Error bars represent the standard error of the mean. Statistical significance was calculated

using two-way ANOVA followed by Tukey's post-hoc analysis (*****p < 0.0001*). **(B)** At 14-dpi, total DNA was harvested from infected $CD34^+$ HPCs and viral genomes were quantified via qPCR using primers and probes specific for the viral UL141 gene. Viral genomes were normalized to total cell number using human β-globin as a reference gene. Data represents the mean Log_{10} transformed values for triplicate experiments. Error bars represent the standard error of the mean. Statistical significance was calculated using a student's t-test.

4.4.2 HCMV UL78 Coupling to $G\alpha_i$ Heterotrimeric G-proteins via a Conserved DRL Motif is Required for Reactivation from Latency

The DRY motif is a highly conserved sequence found in the second intracellular loop of most Class A GPCRs (468,469). Located at the boundary of transmembrane helix 3 (TM3) and intracellular loop 2 (ICL2), this motif forms an ionic lock to help maintain GPCR conformation and plays a crucial role in receptor activation. Specifically, the arginine residue within this motif stabilizes the receptor to facilitate G protein activation and subsequent signal transduction (470–472). UL78 contains a DRL motif that is conserved across the UL78 family. To identify the complement of G proteins that bind to UL78, we made use of a nLuc-based complementation assay measuring real-time interactions between receptors and heterotrimeric G protein complexes described previously (223,425). In this system, the C' terminus of the GPCR is linked in frame to natural peptide (NP) while the Gα subunit is genetically fused to the complementing Large Bit (LgBiT). Proximity of the complementing fragments reconstitutes a functional luciferase protein whose activity can be measured with addition of substrate. To this end, we engineered an in-frame natural peptide-tag on the C' terminus of the wild-type UL78 receptor. We utilized site directed mutagenesis to make alanine substitutions for the entire motif ($DRL_{133\text{-}135}$ – $AAA_{133\text{-}135}$) and the arginine specifically ($DRL_{133\text{-}135}$ – $DAL_{133\text{-}135}$) to serve as negative controls as these mutations would be predicted to affect G protein coupling. As a positive control, we used US28 as it has been shown to functionally couple to most Gα family members (223,227,370). Equivalent expression of each construct was verified by immunoblot in transiently transfected HEK-293 cells **(Fig. S4.3)**. In live cell GPCR interaction assays with LgBiT-$G\alpha_i$, -$G\alpha_q$, and -$G\alpha_{12}$, the wildtype UL78 receptor exhibited similar $G\alpha_i$ coupling to that of US28 **(Fig. 4.2A,D)**, but did not significantly couple to the other Gα isoforms **(Fig. 4.2B-D)**. Moreover, both UL78 constructs containing mutations within the DRL motif showed significant attenuation of their ability to couple to the

$G\alpha_i$ family of G-proteins and did not show any increase in coupling breadth with LgBiT-$G\alpha_q$ and -$G\alpha_{12}$ **(Fig. 4.2)**. Together, these data indicate that UL78 $G\alpha_i$-specific coupling requires the DRL motif.

Figure[4.2] HCMV UL78 Preferentially Couples to $G\alpha_i$ Isoforms via the DRL Motif

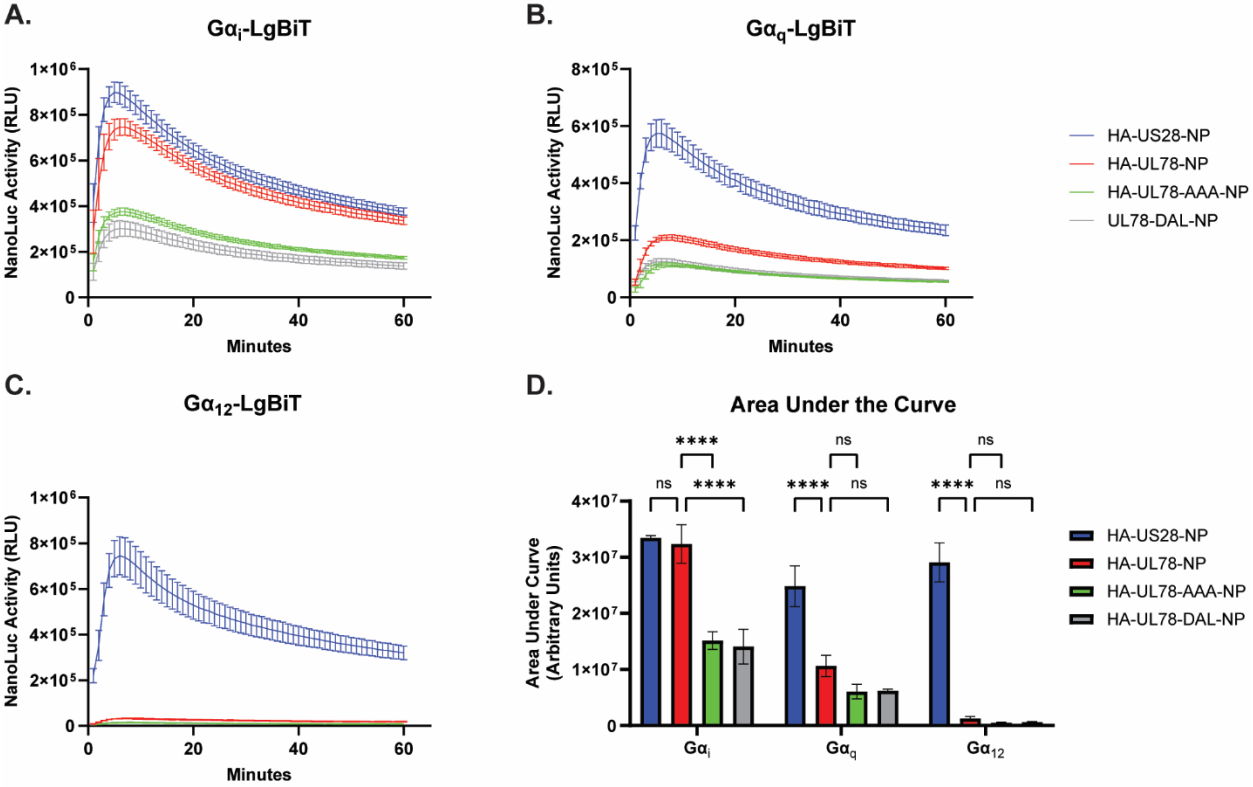

[4.2] Figure legend

HEK-293 cells were transfected with the indicated constructs or the empty vector (EV) and LgBiT tagged **(A)** $G\alpha_i$, **(B)** $G\alpha_q$, or **(C)** $G\alpha_{12}$. At 18 hrs post-transfection, media was exchanged with serum-free DMEM. At 6 hrs post-media replacement, luciferase activity was monitored for 60 min using the Nano-Glo Live Cell Assay System (Promega). Error bars represent the standard error of the mean between technical triplicates. **(D)** The area under the curve was calculated for each profile and plotted. Error bars represent the standard error of the mean between triplicate experiments. Statistical significance was calculated using two-way ANOVA followed by Dunnett's multiple comparison post-hoc analysis *(****$p < 0.001$)*.

To better understand the function of UL78 within the context of viral infection, we generated recombinant viruses using the TB40/E-GFP BAC and engineering the HiBiT tag onto the N' terminus of UL78 (TB40/E-GFP-HB-UL78). An additional recombinant HiBiT tagged virus was generated containing an alanine substitution in the predicted G-protein coupling motif at position R134 (TB40/E-GFP-HB-UL78-DAL). Following reconstitution of these viruses, we

evaluated their growth kinetics via single- and multi-step growth analyses in primary fibroblasts. Both recombinant viruses replicated with similar kinetics to each other, and to the parental TB40/E-GFP virus indicating that the addition of a HiBiT tag to UL78 and the substitution R134A have no effect on lytic replication **(Fig. S4.4)**. Furthermore, both recombinant viruses demonstrated immediate early, early, and late protein expression with similar kinetics **(Fig. 4.3A)**. UL78 protein expression was first observed at 24 hpi with peak expression observed between 72 – 96 hpi **(Fig 4.3A).** To determine whether the DRL motif mutations alter receptor expression at the cell surface, we conducted HiBiT surface vs. total expression assays in infected human fibroblasts (223). In this assay, the total luminescence emitted by HiBiT tagged UL78 in lysed cells is compared with that of live cells where only surface UL78 can interact with the complementing LgBiT. The ratio calculated between the surface and total luminescence indicates the fraction of UL78 that is present at the surface. Consistent with previously published data (287,457), we observed that the majority of UL78 localized intracellularly **(Fig. 4.3B)**. Additionally, no appreciable difference in surface expression was detected between the two recombinant viruses indicating that mutation within the DRL motif of UL78 does not significantly affect cellular surface expression **(Fig. 4.3B)**.

Figure[4.3] HCMV UL78 Expression and Membrane Localization

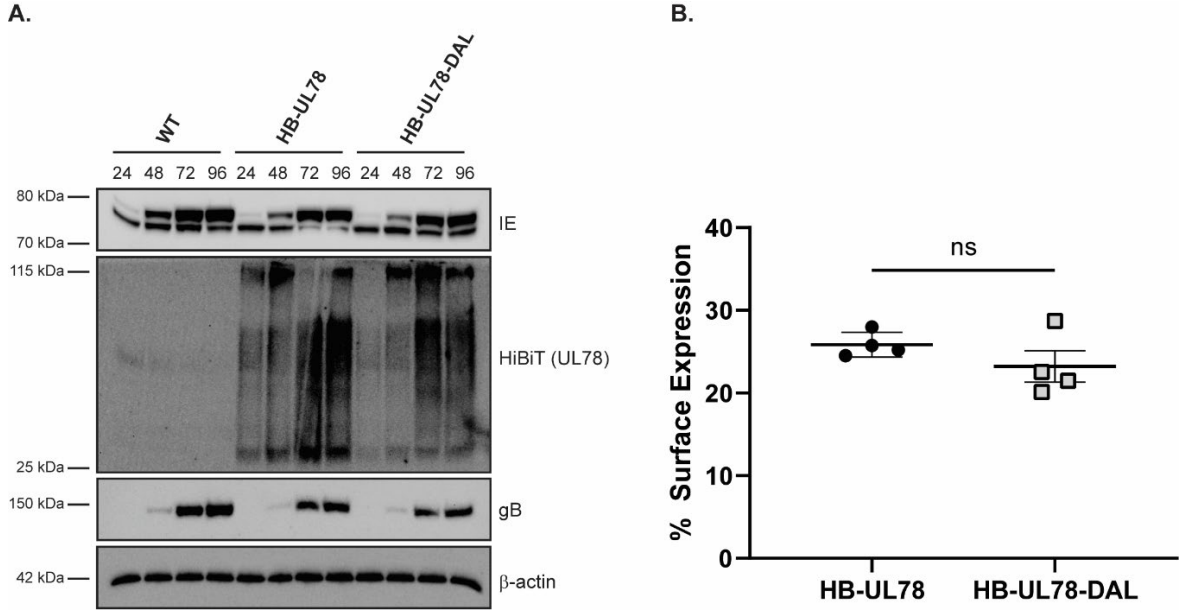

[4.3] Figure legend

(A) NHDFs were infected with the indicated viruses at an MOI of 2 and lysates were harvested at the specified time points post-infection. The presence of the indicated proteins was determined by immunoblot using the indicated antibodies or the Nano-Glo HiBiT Blotting System (Promega). **(B)** NHDFs were infected with the indicated HiBiT-tagged viruses at an MOI of 2. At 72-hpi, surface expression was measured using the Nano-Glo HiBiT Extracellular and Lytic detection Systems (Promega). Error bars represent the standard error of the mean between triplicate experiments. Statistical significance was calculated using one-way ANOVA followed by Dunnett's multiple comparison post-hoc analysis.

To determine whether the observed reactivation deficit with recombinant viruses lacking UL78 protein expression **(Fig. 4.1A)** can be recapitulated with a virus deficient in UL78 $G\alpha_i$ protein coupling, we infected hESC-derived $CD34^+$ HPCs with either WT-HCMV (TB40/E-GFP) or HB-UL78-DAL (TB40/E-GFP-HB-UL78-DAL). Viable, GFP^+, $CD34^+$ HPCs were isolated via FACS and after 12 days of LTBMC, both cells stimulated to reactivate and lysates from unstimulated cells were plated onto fibroblast monolayers to assess infectious center frequency. When compared to infection with WT-HCMV, cells infected with HB-UL78-DAL exhibited major deficits in the ability of the virus to efficiently reactivate from latent infection **(Fig. 4.4A, Fig. S4.5)**. Viral genome copies from infected $CD34^+$ HPCs at the end of LTBMC were comparable in cells infected with WT-HCMV and HB-UL78-DAL suggesting that viral genomes, or genome-containing cells, were not lost over the latency culture period **(Fig. 4.4B)**. Collectively, these results indicate that UL78 – $G\alpha_i$ coupling is not required for the establishment of viral latency in $CD34^+$ HPCs but is required for efficient reactivation from latent infection.

Figure[4.4] Attenuating HCMV UL78 G-Protein Coupling Results in Viral Reactivation Deficits

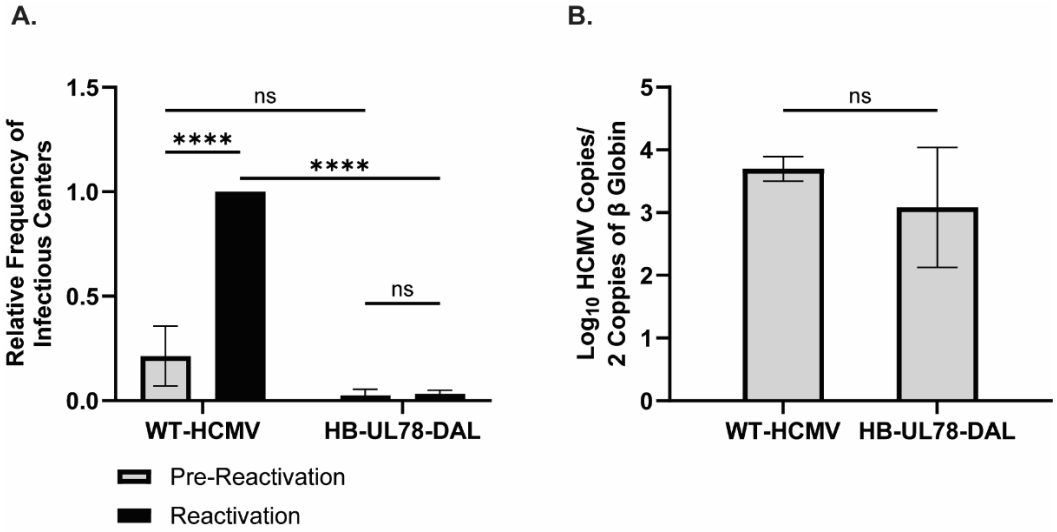

4.4 Figure legend

hESC-derived $CD34^+$ HPCs were infected with either WT-HCMV (TB40/E-GFP) or HB-UL78-DAL (TB40/E-GFP-HB-UL78-DAL) at a MOI of 2 for 48 hrs. Cells were FACS isolated for viable $CD34^+/GFP^+$ HPCs and were cultured above a murine stromal cell support layer for 12 days to establish latent infection. **(A)** At 14-dpi, half of the cells were treated with reactivation cocktail and plated onto a fibroblast monolayer (reactivation). The remaining cells did not receive treatment and were mechanically lysed (pre-reactivation). Reactivation was assessed by the frequency of infectious centers as determined via ELDA and compared to lysed cells (pre-reactivation) at 3 weeks post-plating. Data is shown as fold change in infectious centers, as compared to the WT-HCMV reactivation group, for triplicate experiments. Error bars represent the standard error of the mean. Statistical significance was calculated using two-way ANOVA followed by Tukey's post-hoc analysis (*$****p < 0.0001$*). **(B)** At 14-dpi, total DNA was harvested from infected $CD34^+$ HPCs and viral genomes were quantified via qPCR using primers and probes specific for the viral UL141 gene. Viral genomes were normalized to total cell number using human β-globin as a reference gene. Data represents the mean Log_{10} transformed values for triplicate experiments. Error bars represent the standard error of the mean. Statistical significance was calculated using a student's t-test.

4.4.3 Identification of the HCMV UL78 Interactome During Lytic Infection

A limited number of previous studies have shown that UL78 forms heterodimeric interactions with host (CXCR4 and CCR5) and viral (US28) chemokine receptors to impair or augment surface expression and downstream signaling activity (288,289). While valuable, these overexpression models monitored interactions in transiently transfected cells, which do not recapitulate the conditions of viral infection. Furthermore, UL78 may exhibit additional cell type specific interactions with host and viral proteins to modulate signal transduction that have yet to be captured. To characterize the UL78 interactome during viral infection, a recombinant HCMV was generated containing the biotin ligase TurboID (388) linked in-frame to the C' terminal tail of UL78 (TB40/E-GFP-UL78-TurboID). The recombinant virus replicated with similar growth kinetics in primary fibroblasts relative to the parental virus indicating that the addition of the TurboID enzyme to UL78 has no effect on lytic replication **(Fig. S4.6)**. To identify the UL78 interactome, fibroblasts were mock infected or infected with WT-HCMV (TB40/E-GFP) or UL78-TurboID (TB40/E-GFP-UL78-TurboID). At 72 hpi, exogenous biotin was added to the culture media for an additional six hours. Cellular lysates were harvested, and the resulting biotin-conjugated proteins were purified via streptavidin-mediated bead-based precipitation. Efficient labeling and purification were verified by immunoblot probing for HRP-conjugated streptavidin **(Fig. 4.5A)**. The identity and relative abundance of the purified biotin-conjugated proteins were determined

by label-free quantitative (LFQ) liquid chromatography tandem mass spectrometry (LC-MS/MS). After excluding proteins identified as potential contaminants by comparison against the CRAPome data repository (373), our analysis revealed 1138 host and 32 viral proteins that showed a significant level of enrichment within the dataset **(Fig. 4.5B,C, Data S4.1)**. Interestingly, neither of the previously identified host chemokine receptors reported to interact with UL78 (e.g., CXCR4 and CCR5) (288) were enriched within the dataset, however, the previously identified viral candidate interaction partner (US28) was identified above the significance threshold (206,289). Consistent with a recently published study (285), we identified several $G\alpha_i$ isoforms, but not other G protein families, as candidate interaction partners of UL78 **(Fig. 4.5B, Data S4.1)**, validating the results of our split-nano luciferase assays **(Fig. 4.3)**. Reactome over-representation analysis of the enriched host proteins in proximity to UL78 revealed several cellular processes relating to trafficking, signal transduction, cytoskeletal remodeling, and processes related to nuclear import **(Fig. S7A, Data S4.2)**. Surprisingly, we identified many nuclear-localized cellular proteins as candidate UL78 interactors **(Figs. 4.5B, Data S4.1,2)**, including many of the components of the nuclear pore complex, nuclear membrane proteins, and transcription factors. Additionally, importin, Rab, SNX, and RanGDP proteins were found in proximity to UL78, suggesting a mechanism for translocation to the nucleus. Furthermore, viral proteins, including components of the DNA replication machinery, transcriptional regulators, and proteins that regulate nuclear egress, are candidate interaction partners for UL78 **(Fig. 4.5C, Data S4.1)**. To confirm the candidate UL78 nuclear interaction partners during lytic infection, we performed a second proximity-dependent labeling experiment in which NHDF cells were infected and treated with biotin as previously described, and then cytosolic and nuclear fractions were separated prior to tagged protein purification. Efficient labeling and fractionation were verified by immunoblot prior to LC-MS/MS analysis where we observed visible labeling within the nuclear fraction of cell lysates **(Fig. 4.5D)**. Quantitative mass-spectrometry and downstream analysis revealed 1592 host and 83 viral proteins as candidate interaction partners of UL78 within the nuclear fraction **(Fig. 4.5E, F, Data S4.3)**. Similar to previous experiments, we identified several transcription factors, members of the nuclear pore complex, and $G\alpha_i$ isoforms **(Fig. 4.5E, Data S4.3)**. Reactome over-representation analysis of host candidate interaction partners identified

several previously identified processes such as nuclear import, trafficking, and transcription as well as additional processes involved with RNA biogenesis and chromatin remodeling **(Fig. S4.7B, Data S4.4)**. Moreover, many of the viral proteins enriched within this dataset are known nuclear proteins involved in viral DNA replication, transcription, DNA packaging, encapsidation, and nuclear egress **(Fig. 4.5F, Data S4.3)**. Taken together, our interactome analysis demonstrates that UL78 uniquely interacts with nuclear host and viral proteins during lytic infection conditions and offers novel insight into the function and signal transduction capability of UL78.

Figure[4.5] Interactome Analysis of HCMV UL78

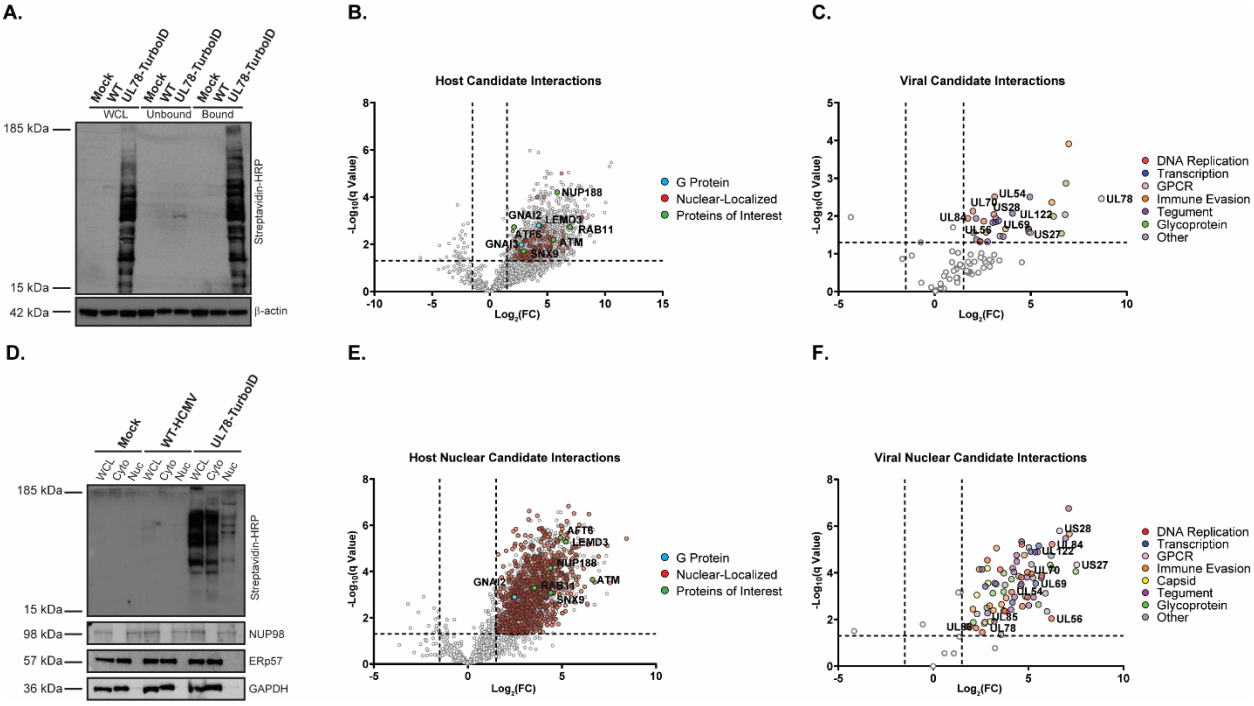

[4.5] Figure legend

(A) NHDF cells were infected with either WT-HCMV (TB40/E-GFP) or UL78-TurboID (TB40/E-GFP-UL78-TurboID) at an MOI of 2 or mock infected. At 72-hpi, the cell culture medium was supplemented with biotin (50 ug/mL) for 6 hrs. Tagged protein were bound to neutravidin beads and were incubated overnight prior to purification. **(A)** Efficient labeling and purification were evaluated by immunoblot using the indicated antibodies on whole cell lysates, unbound fraction, and bound fraction. Purified proteins were subjected to quantitative LC-MS/MS analysis. Representative blot shown for triplicate experiments. **(B)** Volcano plot of host candidate interaction partners of UL78. Red denotes nuclear-localized proteins, blue denotes G proteins, green denotes select proteins of interest. **(C)** Volcano plot of viral candidate interaction partners of UL78. **(D)** NHDF cells were infected and treated under the same conditions as previously described. At 72-hpi, lysates were harvested and were fractionated using the NE-PER extraction kit (ThermoFisher Scientific). Efficient labeling and purification were evaluated by immunoblot using the indicated antibodies on whole cell lysates, cytoplasmic fraction, and nuclear

fraction. Purified proteins were subjected to quantitative LC-MS/MS analysis. Representative blot shown for triplicate experiments. **(E)** Volcano plot of nuclear enriched host candidate interaction partners of UL78. Red denotes nuclear-localized proteins, blue denotes G proteins, green denotes select proteins of interest. **(F)** Volcano plot of nuclear enriched viral candidate interaction partners of UL78.

4.4.4 Examining HCMV UL78 Interactions During Viral Reactivation

Since UL78 is important for reactivation from latency, we wanted to identify host and viral interaction partners of UL78 in the context of HCMV reactivation. To this end, we conducted proximity-dependent labeling experiments in $CD34^+$ HPCs stimulated to reactivate from latent infection. In this experiment, hESC-derived $CD34^+$ HPCs were infected with either WT-HCMV (TB40/E-GFP) or UL78-TurboID (TB40/E-GFP-UL78-TurboID) and were cultured in the same manner as the above experiments **(Fig. 4.6A)**. After 12 days of LTBMC, cells were plated in transwells above a fibroblast monolayer in reactivation supportive media supplemented with exogeneous biotin and incubated for an additional 16 hours prior to cell lysis. Efficient labeling of proteins in proximity of UL78 was confirmed on whole cell lysates via immunoblot probing with HRP-conjugated streptavidin prior to purification and tryptic digestion **(Fig. 4.6B)**. The resultant peptides were subjected to LC-MS/MS analysis. After contaminant filtering, we identified 1075 host and 61 viral proteins as candidate interaction partners of UL78 **(Data S4.5)**. Notably, we again identified $G\alpha_i$ as the only Gα isoform present within this dataset. Additionally, we identified the other viral GPCRs (UL33, US27, and US28), immune evasion proteins (UL40, US23, and US26), and transcriptional activators (UL49, UL69, UL82, and UL122). When compared to our previous proximity-dependent labeling experiments conducted in fibroblasts under lytic conditions **(Fig. 4.5, S4.6)**, a total of 354 common and 721 unique host hits were identified in $CD34^+$ HPCs **(Fig. 4.6C)**. In a similar manner, this dataset contained 54 common and 9 unique viral proteins **(Fig. 4.6D, Table 4.1)**.

Figure[4.6] Comparative Analysis of the HCMV UL78 Interactome During Viral Reactivation

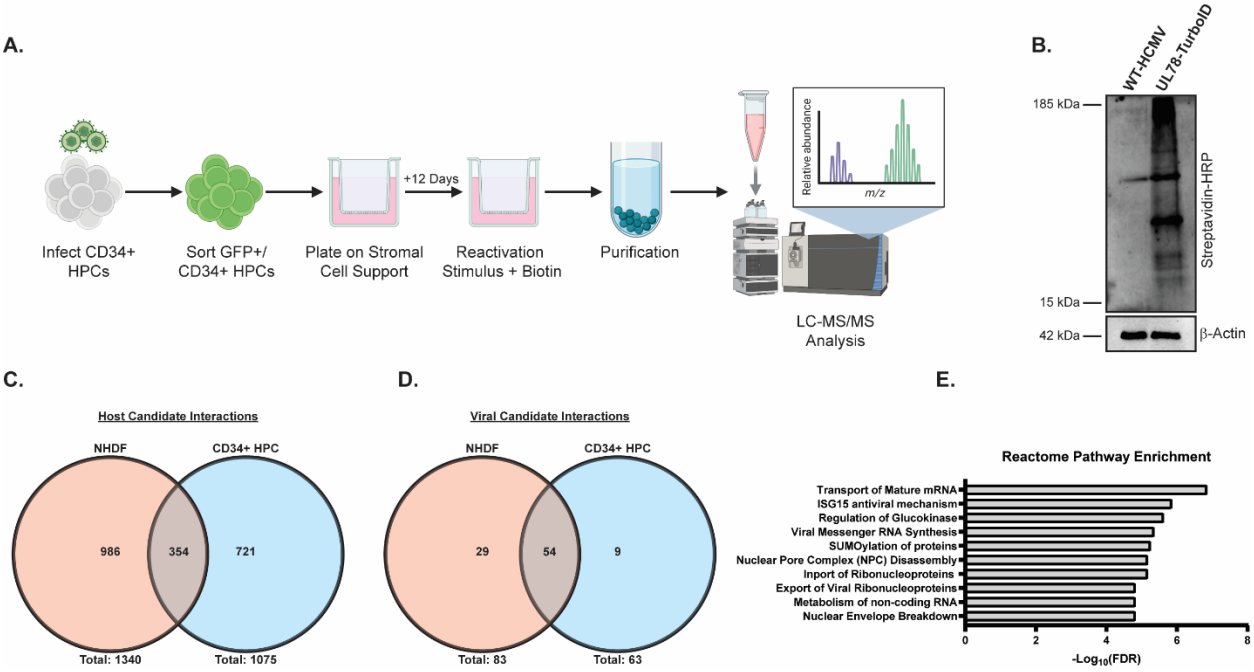

[4.6] Figure legend

(A) hESC-derived CD34$^+$ HPCs were infected with either WT-HCMV (TB40/E-GFP) or UL78-TurboID (TB40/E-GFP-UL78-TurboID) at a MOI of 2 for 48 hrs. Cells were FACS isolated for viable CD34$^+$/GFP$^+$ HPCs and were cultured above a murine stromal cell support layer for 12 days to establish latent infection. At 14-dpi, latently infected cells were plated above a fibroblast monolayer and treated with reactivation cocktail supplemented with biotin (50 ug/mL) for 16 hrs. Biotinylated proteins were purified and were subjected to quantitative LC-MS/MS analysis. Created in BioRender. Medica, S. (2025) https://BioRender.com/hwaox2y **(B)** Efficient labeling was evaluated by immunoblot using the indicated antibodies on whole cell lysates. **(C)** Candidate host UL78 interaction partners were compared between infected NHDFs and CD34$^+$ HPCs. **(D)** Candidate viral UL78 interaction partners were compared between infected NHDFs and CD34$^+$ HPCs. **(E)** Reactome over-representation analysis of high confidence candidate interaction partners.

Finally, Reactome over-representation analysis of the identified host proteins revealed enrichment in several processes related to RNA processing, trafficking, protein post-translational modifications, and members of the nuclear pore complex **(Fig. 4.6E, Data S4.6)**. Together, these results confirm the findings from our previous proximity-dependent labeling experiments in a reactivation model and suggest novel interaction partners and nuclear localization, which will both aid in deciphering the function of UL78 during HCMV pathogenesis.

Table 4.1

Gene Symbol	Fibroblast Lytic Infection		CD34⁺ HPC Reactivation	Function
	Log_{10}(q Value)	Log_2(FC)	Identified	
RL11	1.592	4.898	Peak Found	IgG Fc Binding
RL12	N/A	N/A	High	IgG Fc Binding
UL13	1.660	4.884	Peak Found	Unknown
UL24	N/A	N/A	High	Immune evasion
UL26	N/A	N/A	High	MIEP activator
UL31	N/A	N/A	High	Nucleolar organization
UL32	N/A	N/A	High	Tegument protein, viral DUB main target
UL34	N/A	N/A	High	Transcriptional repressor
UL35	N/A	N/A	High	Tegument protein, viral IE gene expression
UL36	N/A	N/A	High	Anti-apoptotic, inhibits caspase 8 activation
UL40	2.362	6.098	Peak Found	NK cell evasion
UL45	1.376	2.172	High	Immune evasion, blocks NF-kB signaling
UL46	N/A	N/A	High	Capsid protein
UL47	1.320	2.754	N/A	Tegument protein, viral DNA release from capsid
UL48	1.937	2.153	High	Immune evasion, deubiquitin protease
UL49	1.842	3.164	Peak Found	Late viral gene expression, DNA replication
UL50	1.828	3.030	High	Nuclear egress, disruption of nuclear lamina
UL52	2.511	3.124	High	DNA cleavage, packaging
UL53	N/A	N/A	High	Nuclear egress, disruption of nuclear lamina
UL54	2.042	3.084	N/A	DNA polymerase
UL56	1.860	2.560	Peak Found	Terminase subunit
UL57	N/A	N/A	High	ssDNA binding protein
UL69	1.875	3.329	High	mRNA nuclear export, cell cycle block
UL70	2.130	1.992	Peak Found	Primase, DNA synthesis
UL71	2.506	4.957	High	Virus spread and release
UL72	1.457	3.566	Peak Found	Transcription-replication machinery
UL78	2.459	8.683	Peak Found	vGPCR
UL80	N/A	N/A	High	Assembly Protein
UL82	N/A	N/A	High	pp71, MIEP activator, binds Rb
UL84	1.939	1.729	High	UTPase activity, suppresses transcription of IE2
UL85	N/A	N/A	High	Minor capsid protein
UL89	N/A	N/A	High	Terminase ATPase subunit, DNA cleavage
UL95	N/A	N/A	High	Late viral gene expression
UL96	N/A	N/A	High	Nucleocapsid stability

UL97	N/A	N/A	High	Ser-thr kinase, regulates nuclear export, DNA replication
UL98	N/A	N/A	High	Alkaline nuclease
UL100	1.538	6.603	N/A	gM, recruits Rab11
UL102	N/A	N/A	High	DNA helicase-primase
UL112	N/A	N/A	High	Transcriptional activator
UL114	1.319	2.362	N/A	Uracil DNA glycosylase, DNA replication
UL121	1.993	6.190	N/A	Unknown
UL122	2.068	4.053	High	IE2, negative regulator of MIEP
UL132	5.039	6.836	High	Viral glycoprotein
UL138	1.661	3.690	N/A	Silences IE1 transcription, latency
UL140	N/A	N/A	High	Unknown
UL148	N/A	N/A	High	NK cell evasion
UL150	1.660	4.890	N/A	Unknown
US8	1.326	2.368	N/A	Antagonize TLR signaling
US12	1.470	3.402	N/A	NK cell evasion
US22	1.559	2.032	High	Unknown
US23	1.569	2.683	Peak Found	Unknown
US26	3.975	6.977	Peak Found	Unknown
US27	1.562	4.977	Peak Found	vGPCR
US28	1.941	3.181	Peak Found	vGPCR, chemokine receptor
US30	2.038	6.791	N/A	Unknown
TRS1	N/A	N/A	High	Binds UL44, inhibits PKR

4.1 Table legend

Viral Proteins Within the UL78 Interactome in Infected Fibroblasts and CD34⁺ hematopoietic progenitor cells.

4.4.5 HCMV UL78 Localizes to the Nucleus During Infection

A limited number of cellular GPCRs have been detected in the nuclear envelope and nucleus, and have been shown to play an important role in host signaling and cell cycle regulation (463–465). Since UL78 proximity-dependent labelling experiments identified several host and viral nuclear-localized proteins during infection, we next used orthogonal methods to validate whether UL78 is present at the nucleus. Previous studies using transient overexpression and infection models clearly detect UL78 at the cell surface and in cytoplasmic endocytic vesicles (287,457). In addition, **Figure 4.4B** demonstrates cell surface expression of a fraction of UL78. To assess whether UL78 also localizes to the nucleus, we infected fibroblasts with WT-HCMV (TB40/E-GFP), HB-UL78 (TB40/E-GFP-HB-UL78), and HB-UL78-DAL (TB40/E-GFP-HB-UL78-DAL) viruses for 72 hours and performed cell fractionation to separate cytoplasmic and nuclear fractions. As shown by

immunoblots from fractionated lysates, HB-UL78 and HB-UL78-DAL were detected in both the cytoplasmic and nuclear fractions, suggesting that UL78 localizes to the nucleus during lytic infection and that G protein coupling may not be required for translocation or retention at the nucleus **(Fig. 4.7A)**. To confirm the nuclear localization of UL78, we performed HiBiT split luciferase assays on fractionated lysates. In these experiments, we utilized WT-HCMV and a recombinant virus with a HiBiT tag on the N' terminus of the membrane protein UL8 (HB-UL8) as negative controls (205). Similar to observations from immunoblot experiments **(Fig. 4.7A)**, we detected both HB-UL78 and HB-UL78-DAL within the nuclear fraction of these cell lysates **(Fig. 4.7B)**. Moreover, the signal in nuclear extracts obtained from cells infected with virus expressing HB-UL8 was negligible when compared to the background readings from cells infected with WT-HCMV **(Fig. 4.7B)**.

Figure[4.7] A Subset of HCMV UL78 Is Targeted to the Nuclear Envelope During Lytic Replication

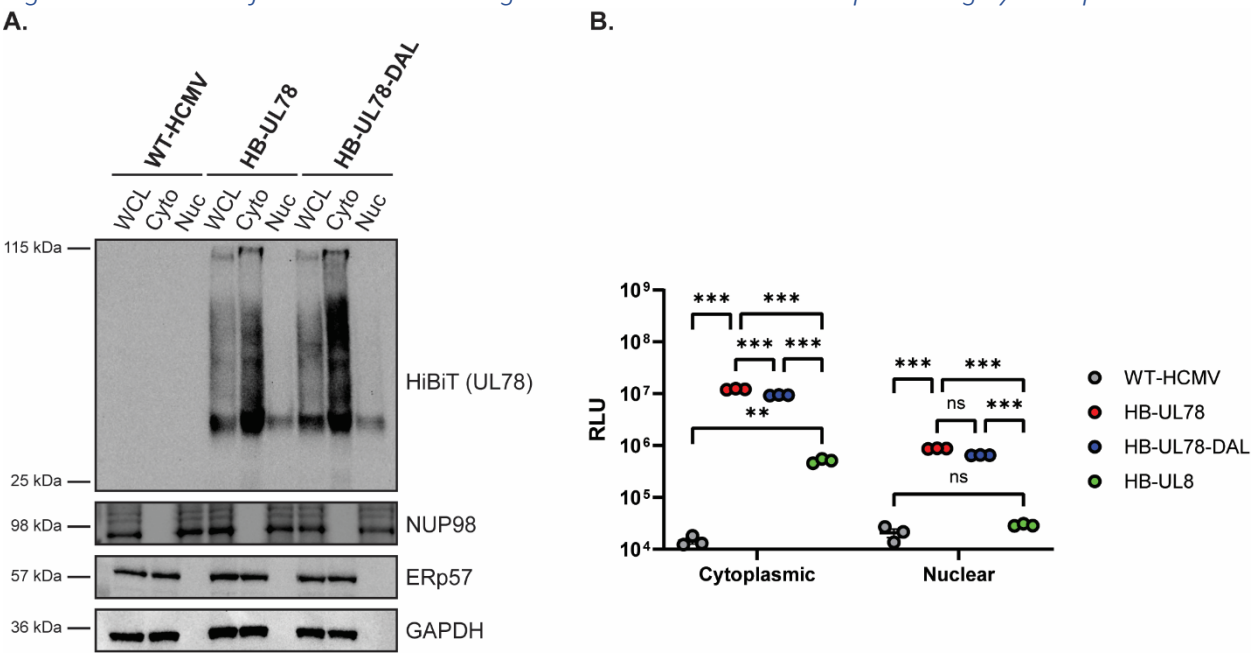

[4.7] Figure legend

(A) NHDFs were infected with the indicated viruses at an MOI of 2. At 72-hpi, whole cell lysates were harvested and were fractionated using the NE-PER extraction kit (ThermoFisher Scientific). The presence of the indicated proteins was determined by immunoblot using the indicated antibodies or the Nano-Glo HiBiT Blotting System (Promega). Representative blot shown from triplicate experiments. **(B)** NHDFs were infected with the indicated viruses at an MOI of 2. At 72-hpi, whole cell lysates were harvested and were fractionated using the NE-PER extraction kit (ThermoFisher Scientific). The presence of the indicated proteins was determined using the Nano-Glo HiBiT Lytic detection Systems (Promega). Error bars represent the standard error of the mean between

triplicate experiments. Statistical significance was calculated using two-way ANOVA followed by Dunnett's multiple comparison post-hoc analysis *(**p < 0.01, ***p < 0.005)*.

We further validated these findings using immunofluorescence in the context of fibroblast infection. WT-HCMV, HB-UL78, and HB-UL78-DAL viruses were used to infect human fibroblasts for 72 hours and UL78 localization was detected by confocal microscopy using an antibody to HiBiT. During HB-UL78 infection, UL78 could be detected in punctate structures consistent with previous reports showing localization in intracellular vesicles. However, HiBiT signal could also be detected at the nuclear membrane of HB-UL78 and HB-UL78-DAL-infected cells **(Fig. 4.8A,B)**, further supporting that a fraction of UL78 is nuclear and that this localization may be independent of G-protein coupling. Together, these data strongly support the nuclear localization of a portion of UL78 and suggest novel intra-nuclear functions for the GPCR.

Figure[4.8] A Fraction of HCMV UL78 Localizes to the Nuclear Envelope During Lytic Infection

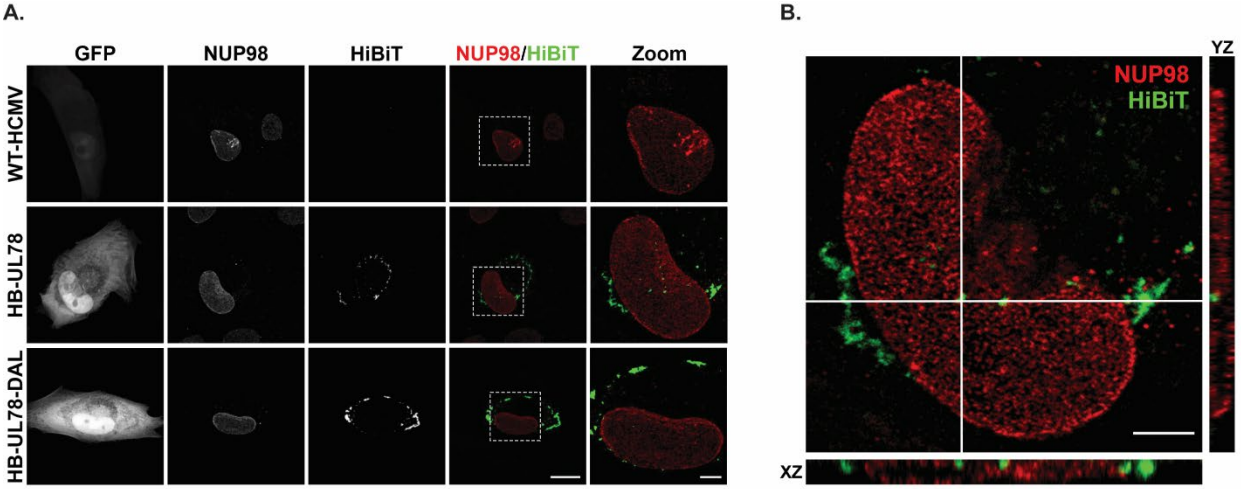

[4.8] Figure legend

NHDF cells were plated on glass coverslips and infected at an MOI of 0.5 with the indicated viruses. Cells were fixed 72-hpi and stained for NUP98 and HiBiT. **(A)** Representative images are shown as the maximum projection from a z-stack. Right panels show overlay of NUP98 (red) and HiBiT (green). White dotted lines indicate region of interest used for magnified images (right panel). Scale bar, 20µm (four left panels) or 5µM (right panel). **(B)** A single z-stack of the HB-UL78-infected cell shown in panel A, along with orthogonal views in XY and XZ planes for the area of interest (indicated by white lines). Scale bar, 5µM.

Section 4.5: Discussion

A mechanistic role for the HCMV-encoded G protein coupled receptor UL78 in viral pathogenesis has remained elusive. In this study, we demonstrate that UL78 joins the viral genes UL7, UL8, UL33, UL81-82ast (LUNA), UL135, UL136, and US28 as well as viral miRNAs (miR-UL36, miR-UL112, and miR-UL148D) as factors required for HCMV reactivation in myeloid lineage cells (193,196,205–211,223). Herein, we establish that recombinant HCMV that lacks UL78 protein expression or contains a single amino acid substitution in the DRL motif (DAL) were both unable to reactivate from latency in $CD34^+$ HPCs. We also demonstrate that while UL78 specifically couples to $G\alpha_i$ heterotrimeric G proteins, the UL78 DAL mutant failed to couple, which is consistent with the role of this motif in G protein coupling for other GPCRs. Combined, these findings suggest that UL78 coupling to $G\alpha_i$ is necessary to promote viral reactivation. $G\alpha_i$ specificity was also observed in UL78-proximity labeling where only $G\alpha_i$ family members were identified as enriched in both HCMV infected human fibroblasts and latently infected $CD34^+$ HPCs undergoing the early stages of viral reactivation. Moreover, an important, and yet unexpected, finding obtained through analysis of the proximity labeling experiments in both cell types positioned UL78 at the nucleus and identified a potential pathway of nuclear translocation for the viral GPCR.

While the role of UL78 and requirement of G protein coupling in the viral reactivation process are both clear, further characterization is needed to determine whether nuclear localization, signaling, and/or interactions with host and viral machinery located in the nucleus are required to promote reactivation. A functional role for nuclear GPCRs has become better appreciated in recent years (473,474). Some cellular GPCRs translocate from the plasma membrane to the nucleus upon ligand binding and activation, whereas others appear resident at the nucleus (475,476). Nuclear-localized GPCRs can activate ‘classical’ signaling cascades within the nucleus as G-proteins, GRKs, b-arrestin and components of many signal transduction pathways are readily detected in the nucleus (477,478) and nuclear GPCR activity can induce the phosphorylation of signaling intermediates as well as Ca^{2+} and cAMP flux (479). Additionally, some cellular GPCRs interact directly with transcriptional regulators and/or host DNA to impact gene expression. For

example, nuclear translocated F2rl1 (PAR2) interacts with the transcription factor Sp1 and enhances expression of the *Vegfa* gene leading to neovascularization during mouse retinal development (480). Intriguingly, this study demonstrated that nuclear-localized PAR2 activated different transcriptional responses from plasma membrane localized PAR2 suggesting a dichotomy of cellular outcomes based on GPCR location.

Based upon our reactivation and proximity labeling data, we hypothesize that UL78 localized at or near the nuclear pore complex (NPC) is acting as a scaffold to help regulate viral genome accessibility and promote viral transcription during reactivation. This hypothesis is well founded in that the NPC plays a critical role in regulating host chromatin state and gene transcription by recruiting and organizing histone regulatory/remodeling complexes as well as by positioning the open chromatin near the NPC opening to facilitate easy access to transcription factors and nucleotide pools (481–484). The UL78 proximity data was enriched for members of the NPC including NUPs (35, 42, 50, 62, 88, 98, 133, 153, 155, 188, 214, 358), transcription factors (ATF6, JUN B, RelA, GTFIIF, SUMO1, YAP1), RNA metabolism (GTF3C1, POLII, SF1, SYMPK), as well as chromatin remodeling proteins (AHCTF1, LEM, LBR, SAP18, TRIM25, TRIM28) **(Fig. 4.5–select proteins in green, 4.6, Data S4.1-6)**. Our UL78 proximity-dependent labelling experiment also identified several viral transcriptional regulators including the activators: UL26, UL35, UL49, UL69, UL72, UL82, UL95, UL112, and UL122; and repressors: UL34, UL84, UL138. Alternatively, it is also possible that UL78 coupling to heterotrimeric G-protein complexes could directly induce signal transduction to activate these transcriptional regulators to stimulate viral reactivation either by $G\alpha_i$ or $G\beta\gamma$. HCMV leverages components of the DNA damage response, particularly the ataxia-telangiectasia mutated (ATM) and ataxia telangiectasia and Rad3-related (ATR) kinase pathways, to facilitate chromatin remodeling and promote the transcriptional activation of the major immediate early promoter (485,486). These kinases phosphorylate downstream effectors such as H2AX and checkpoint kinase 2 (Chk2) to create a permissive environment for viral gene expression (487,488). In parallel, RNA transport and metabolism are tightly regulated during HCMV infection to support the efficient processing and nuclear export of viral transcripts. HCMV lytic infection is associated with altered expression and activity of RNA-binding proteins and splicing factors, such as ribonuclear proteins (RNPs) and serine/arginine-rich (SRs) proteins,

which enhance the stability and translational competence of viral mRNAs (113,489). Furthermore, viral proteins like UL69, identified here as a potential UL78 interactor, mimic host mRNA export factors to promote the nuclear export of viral transcripts, bypassing typical cellular restrictions (490–492). Future studies will aim to determine if UL78 can directly or indirectly modify the viral genome to promote transcription during reactivation.

Work presented here, and by others (286), has identified that the bulk of UL78 protein is localized to the plasma membrane and endosomal pools, but nuclear localization has also been suggested in the context of infection (287). Our biochemical approaches to quantify the sub-cellular localization of UL78 using the HiBiT tag fused to the N' terminus of UL78 determined that between 25-30% of total UL78 (both WT and the DAL mutant) is found at the plasma membrane during infection of human fibroblasts **(Fig. 4.3B)** with a smaller fraction present in nuclear fractions (**Fig. 4.7,4.8**). We also observed a fraction of UL78 associated with the nuclear membrane by confocal microscopy. The capacity to label cellular and viral proteins found within the nucleus as well as the nuclear pore complex suggests that UL78 is oriented such that the C-terminal tail is within the nucleoplasm. There are several ways that GPCRs can traffic to the nucleus including: (1) agonist-dependent or -independent endocytosis from the cell surface and transport to the nucleus mediated by importins, Rabs and sorting nexins (SNX) and (2) agonist-independent translocation from the trans-Golgi network to the nucleus via Rabs and importins. While a specific ligand for UL78 has not been identified to date, a recent structural analysis suggests that the N' terminus of the protein may in fact cover the ligand tunnel area to either self-activate or prevent access of ligands, which makes it currently challenging to assign ligand-dependent vs. ligand-independent nuclear translocation mechanisms for UL78 (285). Our data showing that the UL78-DAL mutant is also found in the nucleus would imply that ligand-dependent signaling may not be required for nuclear localization. Our UL78 proximity-dependent labeling experiments identified several Rab GTPases and SNX proteins as candidate interaction partners that are likely involved in initial endocytosis and recycling (Rabs 3B, 8A, 21, 35 and SNXs 5, 6, 9 and 18). Intriguingly, Rab11a and SNX11 have been implicated in the translocation of cellular GPCRs from the plasma membrane to the nucleus (473,480,493) and were enriched in our datasets. Alternatively, a fraction of UL78 may be transported to the nucleus directly from

the endoplasmic reticulum without trafficking to the cell surface. We identified importin proteins as significantly enriched within our datasets, providing a direct mechanism for the import of UL78 into the host cell nucleus. Two putative classical nuclear localization signals exist within the C' terminal tail of UL78 at positions 328 – 336 and 360 – 365, suggesting candidate interaction sites for import machinery. It is also possible that UL78 interacts with other cellular proteins that facilitate its nuclear localization. While for now the precise mechanisms of UL78 nuclear translocation are unclear, further host and viral genetic studies could uncover how UL78 gets to the nucleus.

Of the four HCMV-encoded GPCRs, two have previously been investigated in the context of latency and reactivation in $CD34^+$ HPCs. UL33 is necessary for virus reactivation through the phosphorylation and activation of the transcription factor CREB (210). We, and others, have shown that US28 expression is necessary for virus latency and reactivation in vitro and in vivo in humanized mice in a ligand-dependent manner that involves signaling through specific G proteins and downstream effectors (193,194,206,430). In fact, the multiple roles for US28 at different stages of HPC infection highlight the complexity of GPCR signaling during viral infection of progenitor cells. Herein we provide a role for UL78 in reactivation from latency in $CD34^+$ HPCs and indicate that Ga_i coupling is important for this phenotype. Our work also uncovers the nuclear localization of a fraction of UL78, although it is still not known whether this process is essential for efficient reactivation from latency. These findings add to the growing appreciation of the role of virally-encoded GPCRs play in latency and reactivation in $CD34^+$ HPCs. UL78 awaits the identification of a ligand, either extracellular or intracellular, and a more mechanistic understanding of its function(s) in different cellular compartments which will lead to a greater understanding into the role played by UL78 in promoting virus reactivation in hematopoietic cells.

Section 4.6: Materials & Methods

Plasmids

Plasmids were generated utilizing traditional cloning methodology as previously described using primers listed in **Table S4.1** (223). Briefly, HA-UL78-NP was generated by cloning the Natural

Peptide (NP) tag (GVTGWRLCERILA) in-frame with the C-term of UL78. HB-UL78 was generated by cloning the HiBiT (HB) tag (VSGWRLFKKIS) in-frame with the N-term of UL78. Fragments were PCR amplified and cloned into the pcDNA3.1- vector. Mutations in the DRL motif of UL78 were generated by site-directed mutagenesis, substituting alanine for the indicated amino acid using the Q5 Mutagenesis Kit (NEB) following the manufacturer's recommended procedure. All constructs were confirmed by sequencing and transformed into TOP10 Escherichia coli cells (Invitrogen). Large-BiT tagged Gα subunits were kindly provided by Julien Hanson (Addgene plasmid ID: 134359, 134360, 134364, and 134363) (425).

Cells and Virus

Normal human dermal fibroblasts (NHDFs) were obtained from ATCC (PCS-2021-010) and human embryonic kidney (HEK) -293 cells were obtained from Microbix. NHDF and HEK-293 cells were maintained in Dulbecco's modified eagle's medium (DMEM) supplemented with 10% fetal bovine serum (FBS), streptomycin, penicillin, and glutamine at 37° C and 5% CO_2. M2-10B4 and S1/S1 stromal cells were obtained from Stem Cell Technologies and cultured as previously described (384). WA01 human embryonic stem cells (hESCs) were obtained from the WiCell Research Institute – National Stem Cell Bank and were cultured as previously described (206,323). The HCMV strain TB40/E-GFP, which constitutively expresses green fluorescent protein under the SV40 promoter (442), was amplified in NHDFs as previously described (196,202). Recombinant viruses were generated using a two-step recombineering procedure utilizing the HCMV TB40/E-GFP bacterial artificial chromosome (BAC). Viral constructs were confirmed by next generation sequencing prior to plaque purification and clonal expansion. Viral titers were determined via plaque assay on NHDF cells and aliquots stored at -80° C. For viral growth analyses, single-step growth curves were carried out at a multiplicity of infection (MOI) of 3.0 PFU/mL, and multi-step growth curves were carried out at a MOI of 0.01 PFU/mL. Supernatant and cell-associated virus were harvested at multiple time points post-infection and titered via limiting dilution plaque assay on NHDF cells.

Immunoblot

Blotting procedures were carried out as previously described (206,223). Briefly, cell lysates were harvested using either RIPA Lysis Buffer (Santa-Cruz Biotechnology) supplemented with HALT

protease inhibitor (Thermo-Fisher Scientific) or utilizing the NE-PER extraction kit (ThermoFisher Scientific). Proteins were separated on a 4-12% SDS-PAGE gel and transferred onto PVDF membranes. Immunoblots were performed using antibodies directed against β-Actin (sc-47778, Santa-Cruz Biotechnology), HCMV IE1/IE2 (MAB8131, Millipore-Sigma), HA (sc-7392, Santa-Cruz Biotechnology), HCMV gB (sc-69742, Santa-Cruz Biotechnology), Streptavidin-HRP (21130, Thermo Scientific), NUP98 (C39A3, Cell Signaling Technology), ERp57 (CL2444, Thermo Scientific), GAPDH (sc-47724, Santa-Cruz Biotechnology), and, if required, the appropriate HRP-conjugated secondary antibody (sc-525409, Santa-Cruz Biotechnology). HiBiT-tagged proteins were visualized using the Nano-Glo HiBiT Blotting System (Promega).

Proximity-Dependent Labeling Experiments

Proximity-dependent labeling experiments were conducted as previously described (206). Briefly, monolayers of NHDF cells or $CD34^+$ HPCs were either mock infected, or infected HCMV TB40/E-GFP-UL78-TurboID or TB40/E-GFP at an MOI of 2. For experiments utilizing NHDFs, at three days post infection, cells were incubated for 6 hours in complete media supplemented with 50µg/mL biotin. Cells were either lysed in RIPA buffer (50 mM Tris pH 8, 150 mM NaCl, 1% triton x-100, 0.1% SDS) and 1x Halt protease inhibitor cocktail (ThermoFisher) and centrifuged at 10,000 relative centrifugal force at 4°C or were processed utilizing the NE-PER extraction kit (ThermoFisher Scientific). For experiments utilizing $CD34^+$ HPCs, cells were cultured in LTBMC as previously described (384). At 14 days post-infection, HPCs were placed into RPMI-1640 medium containing 20% FBS, 2 mM L-glutamine, 100 U/mL penicillin, 100 µg/mL streptomycin, 15 ng/mL granulocyte-colony stimulating factor (G-CSF), 15 ng/mL granulocyte-macrophage colony-stimulating factor (GM-CSF), and 50 µg/mL of biotin and overlaid onto confluent monolayers of NHDFs for 16 hours prior to cell lysis. Resultant lysates were incubated with 250µL Pierce NeutrAvidin Agarose beads (ThermoFisher) overnight at 4°C while rotating. Beads were collected and washed several times using urea wash buffer (PBS pH 7.4, 4 M urea), wash buffer 2 (PBS pH 7.4, 1% triton x-100), 50 mM ammonium bicarbonate, and 6 M urea. Proteins were reduced and alkylated using 0.5 M tris(2-carboxyethyl) phosphine and 0.5 M iodoacetamide prior to tryptic digestion. Digestion was halted by adding 20 µL formic acid to each sample and samples were stored at -80° C until LC-MS/MS.

LC-MS/MS and Data Analysis

LC-MS/MS was performed as previously described by the Fred Hutchinson Proteomics Core (Seattle, WA) (206). Briefly, samples were desalted using ZipTip C18 (Millipore, Billerica, MA) and eluted with 70% acetonitrile/0.1% TFA (Trifluoracetic acid; Sigma) and the desalted material dried in a speed vac. Desalted samples were brought up in 2% acetonitrile in 0.1% formic acid (12 µL) and 10 µL of sample analyzed by LC/ESI MS/MS with a ThermoScientific Easy-nLC II nano HPLC system (Thermo Scientific, Waltham, MA) coupled to a tribrid Orbitrap Fusion mass spectrometer (Thermo Scientific, Waltham, MA). Peptide separations were performed on a reversed-phase column (75 µm × 400 mm) packed with Magic C18AQ (5-µm 100Å resin; Michrom Bioresources, Bruker, Billerica, MA) directly mounted on the electrospray ion source. A 90-minute gradient from 7% to 28% acetonitrile in 0.1% formic acid at a flow rate of 300 nL/minute was used for chromatographic separations. The heated capillary temperature was set to 300°C and a static spray voltage of 2100 V was applied to the electrospray tip. The Orbitrap Fusion instrument was operated in the data-dependent mode, switching automatically between MS survey scans in the Orbitrap (AGC target value 500,000, resolution 120,000, and maximum injection time 50 milliseconds) with MS/MS spectra acquisition in the linear ion trap using quadrupole isolation. A 2 second cycle time was selected between master full scans in the Fourier-transform (FT) and the ions selected for fragmentation in the HCD cell by higher-energy collisional dissociation with a normalized collision energy of 27%. Selected ions were dynamically excluded for 30 seconds and exclusion mass by mass width +/- 10 ppm.

Data analysis was performed using Proteome Discoverer 2.2 (Thermo Scientific, San Jose, CA) searching against the UniProt Human (proteome ID: UP000005640) and HCMV TB40/E (proteome ID, UP000143167) proteomes. Trypsin was set as the enzyme with maximum missed cleavages set to 2. The precursor ion tolerance was set to 10 ppm and the fragment ion tolerance was set to 0.6 Da. Variable modifications included oxidation on methionine, carbamidomethyl on cysteine, and acetylation on protein N-terminus. Normalized LFQ intensities were inputted into Perseus (494) where proteins with greater than 70% missing values were removed. Remaining missing values were imputed from the normal distribution. Protein abundances were Log_2 transformed, and a student's t test corrected for multiple comparisons was performed. Proteins

were considered candidate interaction partners of HCMV UL78 if the CRAPome frequency was <30%, FDR-corrected q value <0.05, and the Log_2 fold change was > 1.5.

Live Cell G-Protein Coupling Assay

Receptor G-protein coupling was assessed as previously described (223,425) using the Nano-Glo Live Cell Assay system (Promega). Briefly, HEK-293 cells were seeded into treated black 96-well plates at a density of $3.0x10^4$ cells per well. The following day, cells were co-transfected in triplicate with a 1:1 ratio of the indicated GPCR constructs or the empty pcDNA3.1- vector, and Large BiT linked Gα subunit using Fugene4K (Promega) following the manufacturer's recommended procedure. At 18 hours post-transfection, the growth medium was replaced with Opti-MEM media (Thermo Fisher Scientific). At 6 hours post media replacement, 25 µL of reconstituted Nano-Glo Live Cell assay reagent was added to each well, and plates were briefly incubated with agitation. Luminescence, indicative of G protein coupling, was measured using a Promega GloMax Navigator luminometer. Assay results were transferred to a Microsoft Excel spreadsheet, backgrounds subtracted and plotted in GraphPad Prism 10.0 software.

HiBiT Split-Luciferase Assay

For surface vs total expression assays, NHDFs were seeded into cell culture-treated black 96-well plates at a density of $1.5x10^4$ cells per well. The following day, triplicate wells were infected with the indicated HiBiT-tagged recombinant viruses at a MOI of 1.0. At 72 hpi, surface vs. total HiBiT expression was evaluated using the Nano-Glo HiBiT Extracellular and Lytic Detection kits (Promega) following the manufacturer's recommended procedure. For nuclear localization assays, NHDFs were seeded into cell culture-treated 6-well plates at a density of $3.0x10^5$ cells per well. The following day, replicate wells were infected with the indicated HiBiT-tagged recombinant viruses at a MOI of 1.0. At 72 hpi, cytoplasmic and nuclear extracts were harvested utilizing the NE-PER extraction kit (ThermoFisher Scientific). Lysates were plated in triplicate into black 96-well plates and HiBiT expression was evaluated using the Nano-Glo HiBiT Lytic Detection kits (Promega) following the manufacturer's recommended procedure. Luminescence was measured using a Promega GloMax Navigator luminometer. Assay results were transferred to a Microsoft Excel spreadsheet, background subtracted, normalized to the HiBiT control protein,

and % surface expression was determined by using the ratio of extracellular vs lytic luminescence. Results were analyzed using GraphPad Prism 10.0 software.

Microscopy

NHDFs were grown on 13mm glass coverslips and infected at an MOI of 0.5 with WT-HCMV, HB-UL78, or HB-UL78-DAL. At 72 hpi, coverslips were washed with PBS and fixed with 4% paraformaldehyde in PBS. Cells were permeablized with 0.25% Triton, blocked with normal goat serum, and stained with the indicated antibodies. Coverslips were then washed with PBS and incubated with the appropriate fluorophore-conjugated secondary antibodies. Fluorescence was visualized using a LEICA Stellaris 8 microscope using a 63x objective with an NA of 1.4. The fluorophores were excited using 405nm and White Light Lasers. The signals were captured using Leica Stellaris 8 and the Leica Application Suite Software. Images were exported as .tiff files and analyzed using ImageJ software.

HCMV Latency and Reactivation Assay

hESC-derived $CD34^+$ HPCs were differentiated from WA01 human embryonic stem cells using the commercial STEMdiff Heme feeder-free hematopoietic differentiation kit (Stem Cell Technologies) as previously described (202,205,323). HPCs were cultured in IMDM with 10% BIT serum replacement, stem cell cytokines (stem cell factor, FLT3L, IL-3, and IL-6 [PeproTech]), and penicillin/streptomycin as previously described (193,196,202). $CD34^+$ HPCs were infected with the indicated viruses at a MOI of 2 for 48 hours prior to isolation by fluorescence-activated cell sorting (FACS) using a FACSAria (BD FACS Aria equipped with 488, 633, and 405 nm lasers, running FACS DIVA software) in order to obtain a pure population of viable, GFP^+, $CD34^+$, HPCs as previously described (384). Infected cells were co-cultured in transwells above monolayers of irradiated M2-10B4 and S1/S1 stromal cells. At 14 days post-infection, HPCs were serially diluted in RPMI-1640 medium containing 20% FBS, 2 mM L-glutamine, 100 U/mL penicillin, 100 µg/mL streptomycin, 15 ng/mL granulocyte-colony stimulating factor (G-CSF), and 15 ng/mL granulocyte-macrophage colony-stimulating factor (GM-CSF) and overlaid onto confluent monolayers of NHDFs cultured in 96-well plates in an extreme limiting dilution assay. To quantify the levels of pre-reactivation infectious virus, a fraction of the HPC cultures were mechanically disrupted and then used in the ELDA. Cell cultures were microscopically visualized for the

presence of GFP^+ weekly, for up to 3 weeks, and the frequency of infectious center production was calculated by ELDA software (416).

Viral DNA Quantification

Primers and probes recognizing HCMV UL141 were used to quantify viral genomes by quantitative real-time PCR (193). Briefly, total DNA was extracted using Trizol (ThermoFisher) according to the manufacturer's recommendations. Dilutions of purified HCMV BAC DNA were used to create a standard curve. Total DNA was added to each reaction well of TaqMan FastAdvance PCR master mix (Applied Biosystems) and samples were analyzed in triplicate on a StepOnePlus TaqMan PCR machine (Applied Biosystems) with an initial activation at 50°C for 2 min and 95°C for 20 s, followed by 40 cycles of 1 s at 95°C and 20 s at 60°C. TaqMan results were analyzed using ABI StepOne software and graphed using GraphPad Prism 10.0 software.

Section 4.7: Acknowledgements

This work was supported by the National Institutes of Health (P01 AI127335 to P.C., M.H.H., and DNS; T32 AI170496-01A1 to S.M.; and R37 AI21640 to P.C. and M.H.H). This research utilized the Integrated Pathology Core at the Oregon National Primate Research Center (ONPRC), which is supported by the National Institutes of Health (P51 OD 011092). The funder had no role in study design, data collection and analysis, decision to publish, or preparation of the manuscript.

Author Contributions: S.M., N.L.D., D.M., P.C., D.N.S. and M.H.H. designed research; S.M., N.L.D., M.D., R.L.T., L.J.P., A.T.M., J.M., L.S., L.H., T.B., G.S., C.N.K., D.M., P.C., D.N.S., and M.H.H. performed research; S.M., N.L.D., M.H.H., P.C., and D.N.S. analyzed data; and S.M., N.L.D., M.D., D.N.S., and M.H.H. wrote the paper with input from all authors. The authors have declared that no competing interests exist.

Section 4.8: Supplemental Figures

Figure[S4.1] HCMV UL78 is Not Required for Lytic Replication

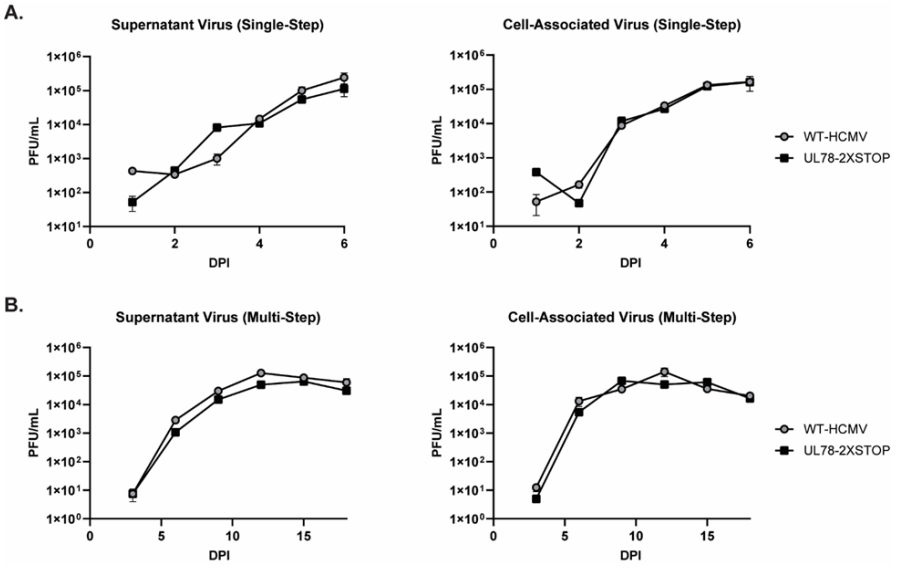

[S4.1] Figure legend

NHDF cells were infected with the indicated viruses at a MOI of **(A)** 3 or **(B)** 0.01. Supernatant and cell-associated virus were harvested at the indicated timepoints post-infection and titered using confluent monolayers of NHDFs. Error bars represent the standard error of the mean between biological triplicates.

Figure[S4.2] Replicate Experiments for HCMV UL78-2XSTOP Latency Assays

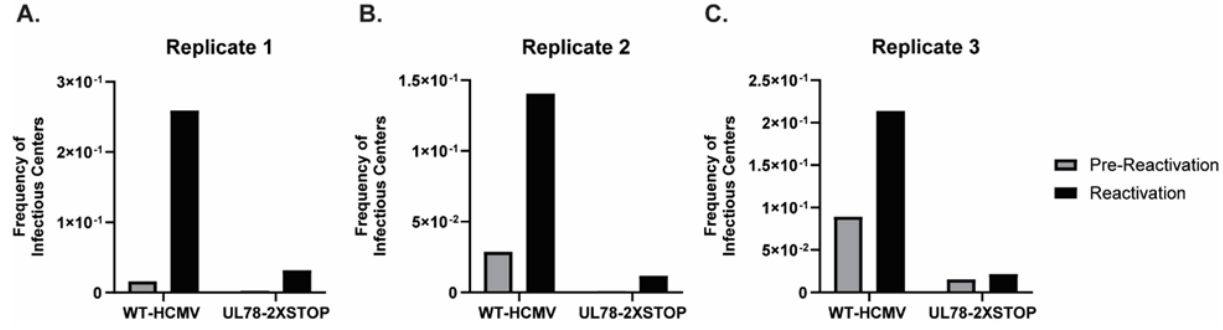

[S4.2] Figure legend

hESC-derived CD34$^+$ HPCs were infected with either TB40/E-GFP (WT-HCMV) or TB40/E-GFP-UL78-2XSTOP (UL78-2XSTOP) at a MOI of 2 for 48 hrs. Cells were FACS isolated for viable CD34$^+$/GFP$^+$ HPCs and were cultured above a murine stromal cell support layer for 12 days to establish latent infection. **(A – C)** At 14-dpi, half of the cells were treated with reactivation cocktail and plated onto a fibroblast monolayer (reactivation). Reactivation was assessed by the frequency of infectious centers as determined via ELDA and compared to lysed cells (pre-reactivation) at 3 weeks post-plating.

Figure[S4.3] Natural Peptide Tagged Constructs are Efficiently Expressed

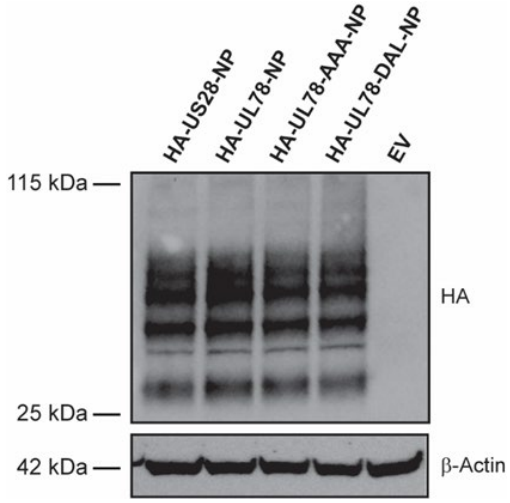

[S4.3] Figure legend

HEK-293 cells were transfected with the indicated constructs. Expression was confirmed via immunoblot using the indicated antibodies on whole lysates harvested 48 hrs post-transfection. Representative blot shown from triplicate experiments.

Figure[S4.4] HCMV UL78 G-Protein Coupling is Not Required for Lytic Replication

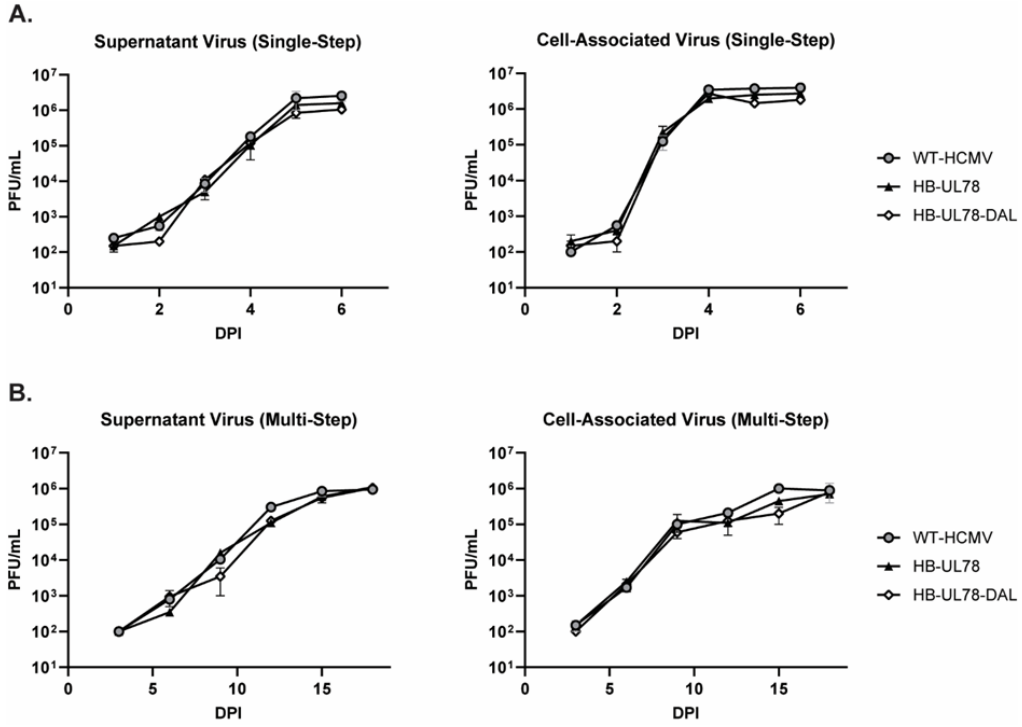

[S4.4] Figure legend

NHDF cells were infected with the indicated viruses at a MOI of **(A)** 3 or **(B)** 0.01. Supernatant and cell-associated virus were harvested at the indicated timepoints post-infection and titered using confluent monolayers of NHDFs. Error bars represent the standard error of the mean between biological triplicates.

Figure[S4.5] Replicate Experiments for HCMV HB-UL78-DAL Latency Assays

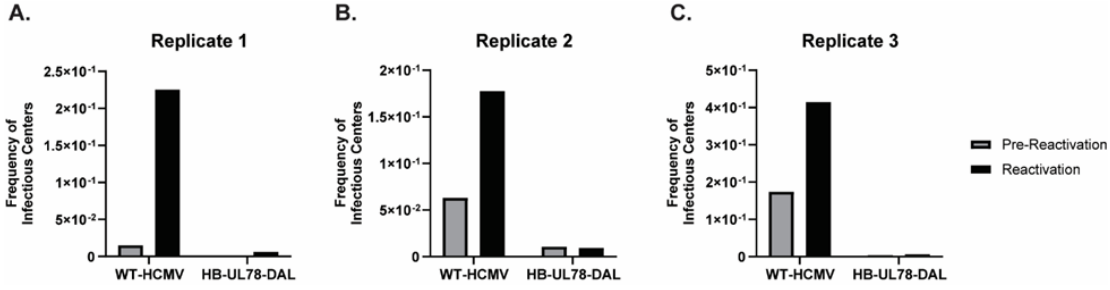

[S4.5] Figure legend

hESC-derived $CD34^+$ HPCs were infected with either TB40/E-GFP (WT-HCMV) or TB40/E-GFP-HB-UL78-DAL (HB-UL78-DAL) at a MOI of 2 for 48 hours. Cells were FACS isolated for viable $CD34^+/GFP^+$ HPCs and were cultured above a murine stromal cell support layer for 12 days to establish latent infection. **(A – C)** At 14 dpi, half of the cells were treated with reactivation cocktail and plated onto a fibroblast monolayer (reactivation). Reactivation was assessed by the frequency of infectious centers as determined via ELDA and compared to lysed cells (pre-reactivation) at 3 weeks post-plating.

Figure[S4.6] Growth Analysis of Recombinant UL78-TurboID Virus

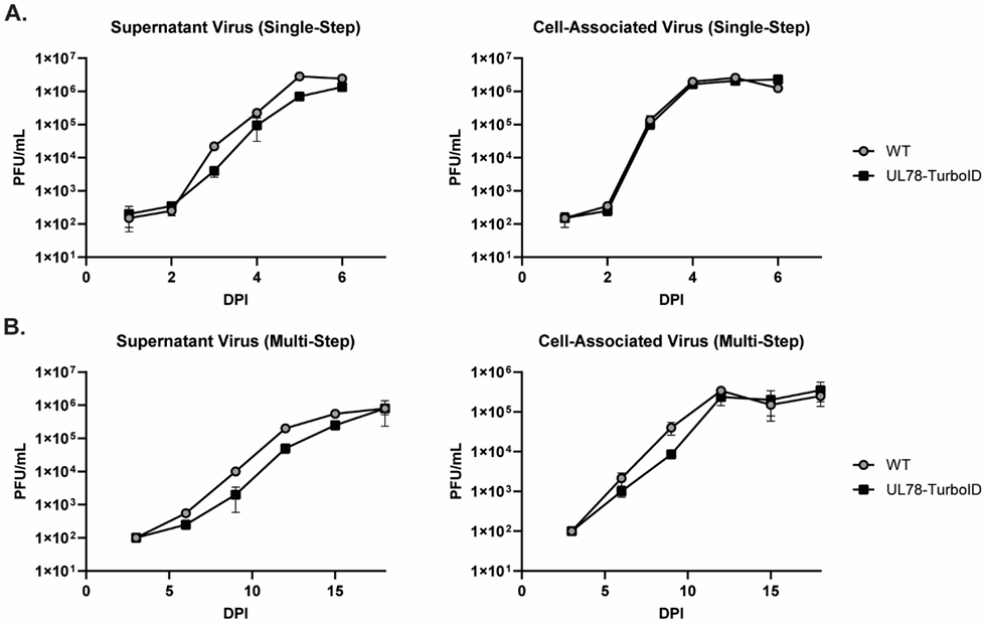

[S4.6] Figure legend

NHDF cells were infected with the indicated viruses at a MOI of **(A)** 3 or **(B)** 0.01. Supernatant and cell-associated virus were harvested at the indicated timepoints post-infection and titered using confluent monolayers of NHDFs. Error bars represent the standard error of the mean between biological triplicates.

Figure[S4.7] Over-Representation Analysis of Candidate UL78 Interaction Partners

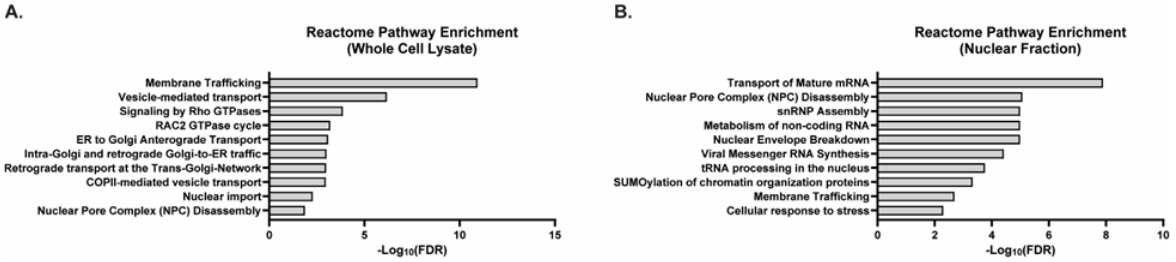

[S4.7] Figure legend

Reactome over-representation analysis on proteins identified through proximity-dependent labeling experiments in NDHF cells utilizing **(A)** whole cell lysates or **(B)** nuclear extracts.

Section 4.9: Data Availability

All data and supplementary material associated with this manuscript is available within the main publication. Doi: [10.1128/jvi.01402-25](https://doi.org/10.1128/jvi.01402-25)

Chapter 5: Summary and Final Perspectives

Section 5.1: Highlights

5.1.1 Chapter 2 Highlights: Proximity-Dependent Mapping of the HCMV US28 Interactome Identifies RhoGEF Signaling as a Requirement for Efficient Viral Reactivation

1. Proximity-dependent mapping of the HCMV US28 interactome identified both previously known and novel host proteins (Src, ERK, PDZ-RhoGEF, p115-RhoGEF) and viral proteins (UL33, UL78, US27, glycoproteins, and tegument proteins) that associate with US28 during infection.
2. Rho guanine nucleotide exchange factors (RhoGEFs), key activators of RhoA, were consistently enriched in the US28 interactome in transiently transfected HEK293 cells, lytically infected fibroblast, and latently infected $CD34^+$ HPCs.
3. RhoGEF inhibitors, Rhosin and Y16, significantly reduced US28-mediated RhoA activation and downstream signaling in vitro.
4. In vitro pharmacological inhibition of RhoGEFs, by Rhosin or Y16, impaired HCMV reactivation from latency, reducing viral progeny post stimulation by ~30–50% in primary $CD34^+$ HPCs.
5. In a humanized mouse model, treatment with Rhosin during reactivation reduced viral genome copies by ~70% post stimulation, preventing efficient reactivation.

We employed a proximity-dependent biotin ligase (TurboID) to comprehensively map the US28 interactome during both latent and lytic modes of HCMV infection. This approach enabled us to capture a broad range of host and viral proteins in close proximity to US28, including those with transient or weak interactions that are often difficult to detect using conventional methods. Our analyses revealed that US28 interfaces with the RhoA signal transduction pathway via the activation of RhoGEFs. To validate these findings, we carried out several functional assays in vitro, where pharmacological inhibition of RhoGEFs using the small-molecule compounds Rhosin and Y16 led to a pronounced reduction in US28-mediated activation of RhoA and its downstream

effectors. Importantly, latency and reactivation assays performed in primary $CD34^+$ HPCs demonstrated that disruption of US28–RhoGEF signaling significantly impaired efficient viral reactivation following reactivation stimuli. These in vitro observations were further confirmed in vivo using a humanized mouse model of HCMV infection, where treatment with Rhosin markedly suppressed HCMV reactivation, resulting in viral loads comparable to those observed during latency. Taken together, these data establish RhoGEFs as essential components of the US28 signaling network and highlight the US28–RhoGEF interaction as a potential therapeutic vulnerability. Our findings not only expand the current understanding of HCMV latency and reactivation mechanisms but also identify a new signaling pathway that could be targeted for the development of next-generation anti-HCMV therapeutics.

5.1.2 Chapter 3 Highlights: Third intracellular loop of HCMV US28 is necessary for signaling and viral reactivation

1. Inhibition of $G\alpha_{q/11}$ signal transduction results in deficit during viral reactivation.
2. Alanine substitutions at positions S218, K223, and R225 in ICL3 significantly impaired US28-mediated activation of MAPK, PCL-β, and RhoA signal transduction pathways.
3. Mutation at positions S218, K223, and R225 in ICL3 significantly reduce the G-protein coupling ability of US28 to multiple Gα isoforms ($G\alpha_{q/11}$, $G\alpha_{i/o}$, $G\alpha_{12/13}$), establishing ICL3 as a major determinant of US28–G-protein interactions.
4. Despite signaling defects, the US28 ICL3 mutant expression constructs displayed normal plasma membrane localization and internalization kinetics.
5. Recombinant viruses with mutations in the ICL3 region of US28 replicated normally in fibroblasts and established latent infections but showed profound defects in reactivation in $CD34^+$ HPCs.
6. In a humanized mouse model of HCMV infection, recombinant viruses with mutations in the ICL3 region of US28 could establish latency but failed to efficiently reactivate after mobilization stimuli.

In this study, we investigated the role of the ICL3 region of the HCMV-encoded chemokine receptor US28. Through a targeted alanine scanning campaign, we identified residues S218, K223, and R225 as critical determinants of US28 function. Substitution at these positions markedly reduced US28-mediated activation of MAPK, PCL-β, and RhoA signal transduction pathways. These deficiencies were not due to recycling and trafficking as mutations at these positions did not affect US28 internalization or membrane localization. Interestingly, mutations within the ICL3 region of US28 resulted in impaired G protein-coupling to multiple Gα isoforms, including $G\alpha_{i/o}$, $G\alpha_{q/11}$, and $G\alpha_{12/13}$. To assess the biological relevance, we engineered recombinant HCMV strains harboring mutations in the ICL3 region of US28 and tested their function in both primary and human embryonic stem cell-derived $CD34^+$ HPCs. Recombinant viruses established and maintained latency at levels similar to wild type infection but displayed profound defects in reactivation capacity following stimulation. These findings were confirmed in vivo using a humanized mouse model of HCMV infection, where ICL3 mutant viruses failed to efficiently reactivate after mobilization despite successfully establishing latency. Collectively, these results demonstrate that specific residues within the ICL3 region of US28 are essential for G protein-coupling and signal transduction and directly link these molecular functions to the ability of HCMV to reactivate from latency. This work provides new mechanistic insights into viral GPCR biology and highlights the ICL3 domain of US28 as a potential target for therapeutic strategies aimed at preventing HCMV reactivation.

5.1.3 Chapter 4 highlights: Human Cytomegalovirus UL78 is a Nuclear-Localized GPCR Necessary for Efficient Reactivation from Latent Infection in $CD34^+$ Hematopoietic Progenitor Cells

1. Recombinant viruses lacking UL78 protein expression replicated normally in fibroblasts and established latent infections but showed profound defects in reactivation in $CD34^+$ HPCs.
2. UL78 preferentially couples to the $G\alpha_i$ family of G proteins through a conserved DRL motif located in the ICL2 region, similar to host chemokine receptors.
3. Mutations within the DRL motif of UL78 do not alter protein expression or membrane localization.

4. Attenuating UL78 G protein-coupling results in deficits in viral reactivation recapitulating data obtained with a functional knock-out recombinant virus.
5. UL78 is in close proximity to host proteins involved in membrane trafficking, intracellular signaling, epigenetic modifiers, and components of the nuclear pore complex and viral proteins involved in DNA replication and transcription during infection.
6. A subset of UL78 is directed to the nucleus during latent and lytic infection.

Utilizing in vitro $CD34^+$ HPCs models, we demonstrate that a recombinant virus lacking UL78 protein expression is unable to efficiently reactivate from latent infection. In addition, we provide evidence that UL78 preferentially interacts with the $G\alpha_i$ family of G-proteins through a conserved DRL motif in the ICL2 region of UL78. Recombinant HCMV harboring mutations in the UL78 G protein-coupling DRL motif similarly fails to efficiently reactivate despite establishing and maintaining latent infection. Collectively, these results indicate that UL78 G protein-coupling plays a critical role in viral reactivation in latently infected $CD34^+$ HPCs. To further elucidate the functional role of UL78, we performed proximity-dependent labeling experiments in lytically infected fibroblasts and $CD34^+$ HPCs undergoing reactivation. Consistent with the results of our G protein-coupling data, $G\alpha_i$ was the only $G\alpha$ isoform significantly enriched within our datasets. Pathway analyses of the UL78 interactome revealed significant enrichment of proteins involved in membrane trafficking, intracellular signaling, and components of the nuclear pore complex in both fibroblasts and HPCs. Moreover, the UL78 interactome included viral proteins with nuclear localization, encompassing factors associated with viral transcription and DNA replication machinery. Nuclear localization of UL78 was further validated using complementary approaches including cell fractionation, immunoblot, immunofluorescence microscopy, and proteomic profiling of isolated nuclei. Overall, these findings provide novel mechanistic insights into both the localization and functional role of UL78, revealing a previously unrecognized contribution of this viral protein to the reactivation process from latent infection.

Section 5.2: Synthesis of Dissertation Chapters

HCMV encodes a set of vGPCRs that subvert host cellular signaling pathways to establish and regulate latency, facilitate reactivation, and ultimately promote persistence within the host. Among these, US28 and UL78 have emerged as central players in shaping the cellular microenvironment during infection of HPCs. Across the three studies presented here, I have examined how US28 and UL78 mediate signaling events, defined critical molecular determinants of their activity, and explored their functional significance in both in vitro and in vivo models of HCMV infection. Taken together, these findings provide mechanistic insights into how HCMV co-opts host signaling networks to regulate the latent-to-lytic switch, while also revealing therapeutic opportunities to target viral persistence.

The work in **Chapters 2 and 3** highlights the multifunctional role of US28 in coordinating signaling pathways required for efficient viral reactivation. **Chapter 2** established the US28 interactome across multiple contexts using proximity-dependent biotinylation to identify a range of host and viral proteins in close association with US28, including members of the Rho guanine nucleotide exchange factor (RhoGEF) family. Functional validation experiments confirmed that inhibition of RhoGEF activity disrupted US28-mediated activation of RhoA, leading to impaired viral reactivation in both primary $CD34^+$ HPCs and a humanized mouse model. These results underscored the requirement for US28–RhoGEF–RhoA signaling in reactivation and emphasized the value of unbiased proteomic approaches in mapping viral protein networks.

Chapter 3 extended this mechanistic dissection by focusing on the structural determinants of US28 required for signal transduction. Specifically, mutational analysis of the ICL3 region of US28 identified residues S218, K223, and R225 as critical for G protein-coupling and downstream activation of MAPK and RhoA pathways. Importantly, recombinant viruses bearing ICL3 mutations established latency but failed to reactivate from $CD34^+$ HPCs in vitro or in humanized mice, mirroring the phenotype observed upon pharmacologic inhibition of US28 signaling. These data confirm that specific structural elements within US28 are indispensable for productive G protein engagement and for the signaling events that drive viral reactivation.

Together, **Chapters 2 and 3** provide complementary perspectives on US28 biology: the former identifies signaling intermediates and pathways engaged by US28, while the latter defines the receptor residues required to initiate those interactions. By linking structural determinants to functional outcomes in primary cells and in vivo models, these findings clarify how US28 integrates into host signaling networks and underscore its role as a signaling hub for reactivation.

While US28 has long been recognized as a key modulator of HCMV latency and reactivation, the role of the related vGPCR UL78 has remained more enigmatic. **Chapter 4** addresses this gap by demonstrating that UL78 is likewise required for efficient reactivation from latency in $CD34^+$ HPCs. Recombinant viruses lacking UL78 expression, or harboring mutations in the conserved DRL motif required for G protein-coupling, were unable to reactivate despite establishing latency. Mechanistically, UL78 specifically coupled to $G\alpha_i$ proteins, implicating this signaling axis as essential for the reactivation process. These results add UL78 to the growing list of viral and cellular factors necessary for efficient HCMV reactivation, highlighting functional redundancy and complexity in the viral toolkit. Unexpectedly, proximity-dependent labeling and downstream functional assays revealed that a significant fraction of UL78 localizes to the nucleus, where it associates with components of the nuclear pore complex, transcription factors, RNA metabolism machinery, chromatin regulators, and viral gene products. This raises the possibility that UL78 plays a scaffolding role at the nuclear periphery, facilitating viral genome accessibility and transcriptional activation during reactivation. Although the functional importance of nuclear localization remains unresolved, these findings open new avenues of investigation into nuclear GPCR signaling and its contribution to viral pathogenesis.

A key outcome of this body of work is the recognition that US28 and UL78, despite differences in signaling specificity, converge on a shared biological role: enabling HCMV to efficiently transition from latent to productive infection. Both receptors engage heterotrimeric G protein complexes, with US28 coupling promiscuously to multiple Gα isoforms and UL78 coupling selectively to $G\alpha_i$. In both cases, disruption of receptor function, whether by pharmacologic inhibition, mutational

inactivation, or deletion, precludes viral reactivation without impacting the establishment of a latent infection.

Mechanistically, the receptors appear to influence distinct but potentially complementary pathways. US28 regulates cytoskeletal dynamics and cellular migration through RhoGEF–RhoA signaling, which may facilitate mobilization of progenitor cells from the bone marrow during reactivation. UL78, by contrast, may function at the nuclear interface, coordinating transcriptional activation of viral immediate-early genes through interactions with nuclear pore components and chromatin modifiers. Together, these findings suggest a model in which US28 and UL78 operate at different cellular compartments and signaling nodes to coordinate the complex cellular remodeling required for viral reactivation.

The identification of both US28 and UL78 as essential regulators of reactivation underscores the multifaceted strategies employed by HCMV to ensure persistence within the host. Latency in HPCs presents a significant barrier to viral clearance, and the ability to periodically reactivate underlies the virus's long-term pathogenesis and clinical impact, particularly in immunocompromised populations. By encoding multiple vGPCRs with distinct signaling properties, HCMV ensures robustness and redundancy in its control over host signaling networks.

These findings also emphasize the cell-type specificity of viral signaling. Both US28 and UL78 appear dispensable for replication in fibroblasts yet are indispensable for reactivation in HPCs. This context dependence highlights the importance of studying viral proteins in physiologically relevant models. The use of primary HPCs and humanized mouse systems in these studies not only validates the relevance of the findings but also provides a platform for translational investigations into therapeutic strategies.

Section 5.3: Future Directions

The work presented here establishes US28 and UL78 as critical regulators of HCMV reactivation, but it also raises a number of unanswered questions that merit further investigation. Addressing

these questions will not only clarify the mechanistic underpinnings of viral persistence but may also inform the development of therapeutic interventions.

Although both US28 and UL78 are required for efficient reactivation, it remains unclear whether they act independently, redundantly, or in a coordinated manner. One possibility is that US28 and UL78 engage parallel signaling pathways that converge on shared transcriptional regulators of immediate-early (IE) gene expression. Alternatively, the receptors may function sequentially, with US28 initiating cellular differentiation, cytoskeletal remodeling, and cellular mobilization while UL78 primes the nuclear environment for viral transcription. To address this, combinatorial mutant viruses lacking one or both receptors, alongside temporal transcriptomic and phosphoproteomic profiling, could delineate whether their signaling outputs intersect or diverge. Complementary single-cell analyses of reactivation events in HPCs would help reveal whether receptor dependence varies across subpopulations, providing insight into cellular heterogeneity in latency models.

One of the most intriguing findings is the enrichment of UL78 at the nuclear periphery, where it interacts with nuclear pore proteins, transcriptional regulators, and viral factors. Future studies should determine whether this localization is essential for viral reactivation or whether it reflects an alternative, noncanonical GPCR function. Generating UL78 mutants with disrupted nuclear localization signals, while preserving G protein-coupling capacity, would provide a direct test of nuclear involvement. Chromatin immunoprecipitation–sequencing (ChIP-seq) or proximity labeling focused on chromatin modifiers could identify whether UL78 influences genome positioning, chromatin accessibility, or the assembly of transcriptional hubs at viral promoters. Such studies would clarify whether UL78 serves as a scaffold that coordinates nuclear signaling events critical for viral reactivation.

HCMV latency and reactivation are tightly linked to the epigenetic status of the viral genome, including histone modifications and chromatin remodeling. It remains to be determined how US28 and UL78 intersect with epigenetic regulation of the viral genome. Mapping changes in

histone markers and chromatin accessibility following pharmacologic inhibition or mutational inactivation of the receptors could reveal direct connections between vGPCR signaling and viral chromatin regulation. CRISPR-based perturbations of key host factors identified in the US28 and UL78 interactomes, such as RhoGEFs, nuclear pore components, or chromatin modifiers, would further refine our understanding of how signal transduction pathways are translated into transcriptional outcomes.

The requirement for US28 and UL78 in reactivation has been established in HPCs, but these receptors appear dispensable for replication in fibroblasts and epithelial cells. This context dependence underscores the need to investigate vGPCR function across additional physiologically relevant cell types, such as monocytes, endothelial cells, and tissue-resident progenitors. Comparative studies could determine whether receptor function is modulated by cell-intrinsic differences in signaling machinery or chromatin environment. In addition, advances in single-cell RNA-seq and ATAC-seq now allow for high-resolution dissection of latency heterogeneity, which could illuminate cell type-specific dependencies and refine models of HCMV persistence.

The precise timing of US28 and UL78 activity during the reactivation process remains unresolved. It is possible that their signaling outputs are required at distinct stages such as chromatin priming, IE gene transcription, or cellular mobilization. Alternatively, it is possible that sustained signaling across multiple phases is necessary. Time-resolved functional studies, using inducible expression systems or pharmacologic inhibitors with precise temporal control, could dissect when each receptor exerts its critical functions. Integration of these data with viral gene expression kinetics would enable construction of a temporal map of vGPCR activity during reactivation.

Given the essential role of US28 and UL78 in reactivation, targeting their signaling pathways presents a compelling therapeutic opportunity. Future studies should test whether antagonists, inverse agonists, or biologics targeting US28 and UL78 can prevent reactivation in clinically relevant latency models. Small-molecule inhibitors of downstream host signaling partners, such

as RhoGEFs or $G\alpha_i$ proteins, could also be explored for antiviral potential. Importantly, efficacy studies in humanized mouse models will be necessary to evaluate the feasibility and safety of targeting vGPCR signaling in vivo. Beyond antiviral therapy, insights into viral manipulation of GPCR signaling cascades could also inform broader pharmacological strategies, given the importance of GPCR pathways in diverse human diseases.

Finally, this work contributes to the emerging paradigm that viral GPCRs may exert functions extending beyond classical cell-surface signaling. The discovery of UL78 at the nuclear periphery suggests that other viral GPCRs could likewise adopt noncanonical localizations and roles. Extending proximity labeling and interactome mapping approaches to the full complement of HCMV vGPCRs, as well as to those encoded by other herpesviruses, could reveal unexpected dimensions of vGPCR biology. Such studies would broaden our understanding of how viruses exploit GPCR signaling across cellular compartments and may uncover novel vulnerabilities for therapeutic intervention.

Section 5.4: References

1. Whitley RJ. Herpesviruses. In: Baron S, editor. Medical Microbiology [Internet]. 4th ed. Galveston (TX): University of Texas Medical Branch at Galveston; 1996 [cited 2025 July 10]. Available from: http://www.ncbi.nlm.nih.gov/books/NBK8157/

2. McGeoch DJ, Rixon FJ, Davison AJ. Topics in herpesvirus genomics and evolution. Virus Res. 2006 Apr;117(1):90–104.

3. Davison AJ. Evolution of the herpesviruses. Veterinary Microbiology. 2002 Apr 22;86(1):69–88.

4. Hu G, Du H, Liu Y, Wu G, Han J. Herpes B virus: History, zoonotic potential, and public health implications. Biosafety and Health. 2022 Aug 1;4(4):213–9.

5. Cohen JI. Herpesvirus latency. J Clin Invest. 130(7):3361–9.

6. Su D, Han L, Shi C, Li Y, Qian S, Feng Z, et al. An updated review of HSV-1 infection-associated diseases and treatment, vaccine development, and vector therapy application. Virulence. 2024 Dec 31;15(1):2425744.

7. Patil A, Goldust M, Wollina U. Herpes zoster: A Review of Clinical Manifestations and Management. Viruses. 2022 Jan 19;14(2):192.

8. Sawtell NM, Thompson RL. Alphaherpesvirus Latency and Reactivation with a Focus on Herpes Simplex Virus. Curr Issues Mol Biol. 2021;41:267–356.

9. Nicoll MP, Proença JT, Efstathiou S. The molecular basis of herpes simplex virus latency. FEMS Microbiol Rev. 2012 May;36(3):684–705.

10. Margolis TP, Imai Y, Yang L, Vallas V, Krause PR. Herpes Simplex Virus Type 2 (HSV-2) Establishes Latent Infection in a Different Population of Ganglionic Neurons than HSV-1: Role of Latency-Associated Transcripts. Journal of Virology. 2007 Feb 15;81(4):1872–8.

11. James C, Harfouche M, Welton NJ, Turner KM, Abu-Raddad LJ, Gottlieb SL, et al. Herpes simplex virus: global infection prevalence and incidence estimates, 2016. Bulletin of the World Health Organization. 2020 May 1;98(5):315–29.

12. Krishnan R, Stuart PM. Developments in Vaccination for Herpes Simplex Virus. Front Microbiol [Internet]. 2021 Dec 7 [cited 2025 July 10];12. Available from: https://www.frontiersin.org/journals/microbiology/articles/10.3389/fmicb.2021.798927/full

13. Stanfield BA, Kousoulas KG, Fernandez A, Gershburg E. Rational Design of Live-Attenuated Vaccines against Herpes Simplex Viruses. Viruses. 2021 Aug 18;13(8):1637.

14. Munoz-Moreno R, Allaj V, Gadee E, Button JM, Diaz F, Maddur MS, et al. A highly stable lyophilized mRNA vaccine for Herpes Zoster provides potent cellular and humoral responses. npj Vaccines. 2025 Mar 14;10(1):49.

15. Eshleman E, Shahzad A, Cohrs RJ. Varicella zoster virus latency. Future Virol. 2011 Mar;6(3):341–55.

16. Syed YY. Recombinant Zoster Vaccine (Shingrix®): A Review in Herpes Zoster. Drugs Aging. 2018 Dec 1;35(12):1031–40.

17. Harder T, Siedler A. Systematic Review and Meta-analysis of Chickenpox Vaccination and Risk of Herpes Zoster: A Quantitative View on the "Exogenous Boosting Hypothesis." Clinical Infectious Diseases. 2019 Sept 27;69(8):1329–38.

18. Ljungman P. β-Herpesvirus Challenges in the Transplant Recipient. The Journal of Infectious Diseases. 2002 Oct 15;186(Supplement_1):S99–109.

19. Marin LJ, Santos de Carvalho Cardoso E, Bispo Sousa SM, Debortoli de Carvalho L, Marques Filho MF, Raiol MR, et al. Prevalence and clinical aspects of CMV congenital Infection in a low-income population. Virol J. 2016 Aug 31;13(1):148.

20. Zuhair M, Smit GSA, Wallis G, Jabbar F, Smith C, Devleesschauwer B, et al. Estimation of the worldwide seroprevalence of cytomegalovirus: A systematic review and meta-analysis. Reviews in Medical Virology. 2019;29(3):e2034.

21. Vanarsdall AL, Johnson DC. Human cytomegalovirus entry into cells. Curr Opin Virol. 2012 Feb;2(1):10.1016/j.coviro.2012.01.001.

22. Mokry RL, Monti CE, Rosas-Rogers S, Schumacher ML, Dash RK, Terhune SS. Replication efficiencies of human cytomegalovirus-infected epithelial cells are dependent on source of virus production. bioRxiv. 2024 Mar 19;2024.03.19.585739.

23. Crawford LB. Hematopoietic stem cells and betaherpesvirus latency. Front Cell Infect Microbiol [Internet]. 2023 June 6 [cited 2024 Oct 4];13. Available from: https://www.frontiersin.org/journals/cellular-and-infection-microbiology/articles/10.3389/fcimb.2023.1189805/full

24. Wu K, Hou YJ, Makrinos D, Liu R, Zhu A, Koch M, et al. Characterization of humoral and cellular immunologic responses to an mRNA-based human cytomegalovirus vaccine from a phase 1 trial of healthy adults. Journal of Virology. 2024 Mar 25;98(4):e01603-23.

25. Hu X, Wang HY, Otero CE, Jenks JA, Permar SR. Lessons from Acquired Natural Immunity and Clinical Trials to Inform Next-Generation Human Cytomegalovirus Vaccine Development. Annual Review of Virology. 2022 Sept 29;9(Volume 9, 2022):491–520.

26. Kondo K, Yamanishi K. HHV-6A, 6B, and 7: molecular basis of latency and reactivation. In: Arvin A, Campadelli-Fiume G, Mocarski E, Moore PS, Roizman B, Whitley R, et al., editors. Human Herpesviruses: Biology, Therapy, and Immunoprophylaxis [Internet]. Cambridge: Cambridge University Press; 2007 [cited 2025 July 10]. Available from: http://www.ncbi.nlm.nih.gov/books/NBK47366/

27. Pantry SN, Medveczky PG. Latency, Integration, and Reactivation of Human Herpesvirus-6. Viruses. 2017 July;9(7):194.

28. Wang B, Hara K, Kawabata A, Nishimura M, Wakata A, Tjan LH, et al. Tetrameric glycoprotein complex gH/gL/gQ1/gQ2 is a promising vaccine candidate for human herpesvirus 6B. PLoS Pathog. 2020 July 23;16(7):e1008609.

29. Longnecker R, Neipel F. Introduction to the human γ-herpesviruses. In: Arvin A, Campadelli-Fiume G, Mocarski E, Moore PS, Roizman B, Whitley R, et al., editors. Human Herpesviruses: Biology, Therapy, and Immunoprophylaxis [Internet]. Cambridge: Cambridge University Press; 2007 [cited 2025 July 18]. Available from: http://www.ncbi.nlm.nih.gov/books/NBK47397/

30. Leung AKC, Lam JM, Barankin B. Infectious Mononucleosis: An Updated Review. Curr Pediatr Rev. 2024;20(3):305–22.

31. Münz C. Epstein–Barr virus pathogenesis and emerging control strategies. Nat Rev Microbiol. 2025 Apr 25;1–13.

32. Tosato G, Cohen JI. Generation of Epstein-Barr Virus (EBV)-immortalized B cell lines. Curr Protoc Immunol. 2007 Feb;Chapter 7:7.22.1-7.22.4.

33. Patel PD, Alghareeb R, Hussain A, Maheshwari MV, Khalid N. The Association of Epstein-Barr Virus With Cancer. Cureus. 14(6):e26314.

34. Lanz TV, Brewer RC, Ho PP, Moon JS, Jude KM, Fernandez D, et al. Clonally expanded B cells in multiple sclerosis bind EBV EBNA1 and GlialCAM. Nature. 2022 Mar;603(7900):321–7.

35. Garg P, Matlani M, Kumar S, Nair D. Seroprevalence and characterization of Epstein-Barr virus exposure among paediatric population. Indian Journal of Medical Microbiology. 2024 July 1;50:100643.

36. Li P, Meng Z, Zhou Z, Zhong Z, Kang M. Therapeutic vaccines for Epstein–Barr virus: a way forward. The Lancet. 2024 June 29;403(10446):2779–80.

37. Huang K, Lin X jun, Hu J chu, Xia T ying, Xu F ping, Huang J dong, et al. Epstein-Barr virus mRNA vaccine synergizes with NK cells to enhance nasopharyngeal carcinoma eradication in humanized mice. Molecular Therapy Oncology. 2025 June 18;33(2):200986.

38. Sun C, Kang YF, Fang XY, Liu YN, Bu GL, Wang AJ, et al. A gB nanoparticle vaccine elicits a protective neutralizing antibody response against EBV. Cell Host Microbe. 2023 Nov 8;31(11):1882-1897.e10.

39. Ganem D. KSHV-induced oncogenesis. In: Arvin A, Campadelli-Fiume G, Mocarski E, Moore PS, Roizman B, Whitley R, et al., editors. Human Herpesviruses: Biology, Therapy, and Immunoprophylaxis [Internet]. Cambridge: Cambridge University Press; 2007 [cited 2025 July 18]. Available from: http://www.ncbi.nlm.nih.gov/books/NBK47373/

40. Purushothaman P, Dabral P, Gupta N, Sarkar R, Verma SC. KSHV Genome Replication and Maintenance. Front Microbiol [Internet]. 2016 Feb 1 [cited 2025 July 18];7. Available from: https://www.frontiersin.org/journals/microbiology/articles/10.3389/fmicb.2016.00054/full

41. Kim KY, Huerta SB, Izumiya C, Wang DH, Martinez A, Shevchenko B, et al. Kaposi's Sarcoma-Associated Herpesvirus (KSHV) Latency-Associated Nuclear Antigen Regulates the KSHV Epigenome by Association with the Histone Demethylase KDM3A. Journal of Virology. 2013 June 15;87(12):6782–93.

42. Cesarman E, Damania B, Krown SE, Martin J, Bower M, Whitby D. Kaposi sarcoma. Nat Rev Dis Primers. 2019 Jan 31;5(1):9.

43. Knights SM, Salyards M, Kendall N, Lazarte SM, Kainthla R, Miley W, et al. High Seroprevalence of Kaposi Sarcoma–Associated Herpesvirus in Men Who Have Sex With Men With HIV in the Southern United States. Open Forum Infect Dis. 2023 Mar 24;10(4):ofad160.

44. Butler LM, Dorsey G, Hladik W, Rosenthal PJ, Brander C, Neilands TB, et al. Kaposi Sarcoma–Associated Herpesvirus (KSHV) Seroprevalence in Population-Based Samples of African Children: Evidence for At Least 2 Patterns of KSHV Transmission. J Infect Dis. 2009 Aug 1;200(3):430–8.

45. Manicklal S, Emery VC, Lazzarotto T, Boppana SB, Gupta RK. The "silent" global burden of congenital cytomegalovirus. Clin Microbiol Rev. 2013 Jan;26(1):86–102.

46. Bate SL, Dollard SC, Cannon MJ. Cytomegalovirus Seroprevalence in the United States: The National Health and Nutrition Examination Surveys, 1988–2004. Clin Infect Dis. 2010 June 1;50(11):1439–47.

47. Rico A, Dollard SC, Valencia D, Corchuelo S, Tong VT, Laiton-Donato K, et al. Epidemiology of cytomegalovirus Infection among mothers and infants in Colombia. J Med Virol. 2021 Nov;93(11):6393–7.

48. Schottstedt V, Blümel J, Burger R, Drosten C, Gröner A, Gürtler L, et al. Human Cytomegalovirus (HCMV) – Revised*. Transfus Med Hemother. 2010 Dec;37(6):365–75.

49. Wang C, Zhu Y, Chen P, Wang C, Zhou W, Zhang C, et al. Altered serum human cytomegalovirus microRNA levels are common and closely associated with the inflammatory status in patients with fever. Front Immunol [Internet]. 2022 Dec 14 [cited 2025 July 18];13. Available from: https://www.frontiersin.org/journals/immunology/articles/10.3389/fimmu.2022.1079259/full

50. Sindre H, Tjoonnfjord G, Rollag H, Ranneberg-Nilsen T, Veiby O, Beck S, et al. Human cytomegalovirus suppression of and latency in early hematopoietic progenitor cells. Blood. 1996 Dec 15;88(12):4526–33.

51. Mena Lora A, Khine J, Khosrodad N, Yeldandi V. Unusual Manifestations of Acute Cytomegalovirus Infection in Solid Organ Transplant Hosts: A Report of Two Cases. Case Rep Transplant. 2017;2017:4916973.

52. Zhang J, Kamoi K, Zong Y, Yang M, Zou Y, Miyagaki M, et al. Cytomegalovirus Retinitis: Clinical Manifestations, Diagnosis and Treatment. Viruses. 2024 Sept 7;16(9):1427.

53. Abu-Omar A, Mihm J, Bronder S, Schmidt T, Sester M, Sester U. CMV management of patients with leukopenia after CMV high-risk kidney transplantation. Transpl Immunol. 2025 Mar;89:102188.

54. Gerna G, Fornara C, Furione M, Lilleri D. Congenital Human Cytomegalovirus Infection: A Narrative Review of Maternal Immune Response and Diagnosis in View of the Development of a Vaccine and Prevention of Primary and Non-Primary Infections in Pregnancy. Microorganisms. 2021 Aug 16;9(8):1749.

55. Malm G, Engman ML. Congenital cytomegalovirus infections. Seminars in Fetal and Neonatal Medicine. 2007 June 1;12(3):154–9.

56. Hui L, Wood G. Perinatal outcome after maternal primary cytomegalovirus infection in the first trimester: a practical update and counseling aid. Prenatal Diagnosis. 2015;35(1):1–7.

57. Pass RF, Fowler KB, Boppana SB, Britt WJ, Stagno S. Congenital cytomegalovirus infection following first trimester maternal infection: Symptoms at birth and outcome. Journal of Clinical Virology. 2006 Feb 1;35(2):216–20.

58. Cheeran MCJ, Lokensgard JR, Schleiss MR. Neuropathogenesis of Congenital Cytomegalovirus Infection: Disease Mechanisms and Prospects for Intervention. Clin Microbiol Rev. 2009 Jan;22(1):99–126.

59. Erice A, Tierney C, Hirsch M, Caliendo AM, Weinberg A, Kendall MA, et al. Cytomegalovirus (CMV) and Human Immunodeficiency Virus (HIV) Burden, CMV End-Organ Disease, and Survival in Subjects with Advanced HIV Infection (AIDS Clinical Trials Group Protocol 360). Clinical Infectious Diseases. 2003 Aug 15;37(4):567–78.

60. Stewart MW. Optimal management of cytomegalovirus retinitis in patients with AIDS. Clinical Ophthalmology. 2010 Apr 26;4:285–99.

61. Sheth A, Boktor M, Diamond K, Lavu K, Sangster G. Complete esophageal obliteration secondary to cytomegalovirus in AIDS patient. Dis Esophagus. 2010 Aug;23(6):E32-34.

62. Pergam SA, Xie H, Sandhu R, Pollack M, Smith J, Stevens-Ayers T, et al. Efficiency and Risk Factors for CMV Transmission in Seronegative Hematopoietic Stem Cell Recipients. Biol Blood Marrow Transplant. 2012 Sept;18(9):1391–400.

63. Hodowanec AC, Pikis A, Singer ME. The Development of Therapeutics for the Treatment and Prevention of CMV Disease in the Transplant Population: A Regulatory Perspective. The Journal of Infectious Diseases. 2020 Mar 5;221(Supplement_1):S109–12.

64. Gilbert C, Boivin G. Human Cytomegalovirus Resistance to Antiviral Drugs. Antimicrob Agents Chemother. 2005 Mar;49(3):873–83.

65. Zhang P, Fleming P, Andoniou CE, Waltner OG, Bhise SS, Martins JP, et al. IL-6-mediated endothelial injury impairs antiviral humoral immunity after bone marrow transplantation. J Clin Invest. 2024 Apr 1;134(7):e174184.

66. Haese NN, Burg JM, Andoh TF, Jones IKA, Kreklywich CN, Smith PP, et al. Macrophage Depletion Of CMV-Latently Infected Donor Hearts Ameliorates Recipient Accelerated Chronic Rejection. Transpl Infect Dis. 2021 Apr;23(2):e13514.

67. Yu C, He S, Zhu W, Ru P, Ge X, Govindasamy K. Human cytomegalovirus in cancer: the mechanism of HCMV-induced carcinogenesis and its therapeutic potential. Front Cell Infect Microbiol. 2023 June 23;13:1202138.

68. Cinatl J, Cinatl J, Vogel JU, Rabenau H, Kornhuber B, Doerr HW. Modulatory effects of human cytomegalovirus infection on malignant properties of cancer cells. Intervirology. 1996;39(4):259–69.

69. Galloway DA, McDougall JK. The oncogenic potential of herpes simplex viruses: evidence for a “hit-and-run” mechanism. Nature. 1983 Mar 3;302(5903):21–4.

70. Michaelis M, Doerr HW, Cinatl J. The Story of Human Cytomegalovirus and Cancer: Increasing Evidence and Open Questions. Neoplasia. 2009 Jan;11(1):1–9.

71. Chen SJ, Wang SC, Chen YC. Challenges, Recent Advances and Perspectives in the Treatment of Human Cytomegalovirus Infections. Tropical Medicine and Infectious Disease. 2022 Dec;7(12):439.

72. Matthews T, Boehme R. Antiviral activity and mechanism of action of ganciclovir. Rev Infect Dis. 1988;10 Suppl 3:S490-494.

73. Chung H. CMV infections after HSCT: prophylaxis and treatment. Blood Res. 2025 June 3;60(1):33.

74. Clinical Overview of CMV and Congenital CMV | Cytomegalovirus (CMV) and Congenital CMV Infection | CDC [Internet]. [cited 2025 Sept 8]. Available from: https://www.cdc.gov/cytomegalovirus/hcp/clinical-overview/index.html

75. Andrei G, Topalis D, De Schutter T, Snoeck R. Insights into the mechanism of action of cidofovir and other acyclic nucleoside phosphonates against polyoma- and papillomaviruses and non-viral induced neoplasia. Antiviral Research. 2015 Feb 1;114:21–46.

76. Crumpacker CS. Mechanism of action of foscarnet against viral polymerases. The American Journal of Medicine. 1992 Feb 14;92(2, Supplement 1):S3–7.

77. Kendle JB, Fan-Havard P. Cidofovir in the Treatment of Cytomegaloviral Disease. Ann Pharmacother. 1998 Nov 1;32(11):1181–92.

78. Gérard L, Salmon-Céron D. Pharmacology and clinical use of foscarnet. International Journal of Antimicrobial Agents. 1995 July 1;5(4):209–17.

79. Ronchi A, Pietrasanta C, Binda S, Mosca F, Pugni L. Congenital Cytomegalovirus Infection and Antiviral Therapy: How to Manage Neutropenia Properly? The Pediatric Infectious Disease Journal. 2019 Aug;38(8):e190.

80. Papaevangelou V, Pedrero-Tomé R, Syridou G, Baquero-Artigao F, Rodríguez-Molino P, Del Rosal T, et al. Severe Neutropenia in Infants With Congenital Cytomegalovirus on Antiviral Therapy. Pediatr Infect Dis J. 2025 July 4;

81. Mehta Steinke SA, Alfares M, Valsamakis A, Shoham S, Arav-Boger R, Lees L, et al. Outcomes of transplant recipients treated with cidofovir for resistant or refractory cytomegalovirus infection. Transpl Infect Dis. 2021 June;23(3):e13521.

82. Upadhyayula S, Michaels MG. Ganciclovir, Foscarnet, and Cidofovir: Antiviral Drugs Not Just for Cytomegalovirus. J Pediatric Infect Dis Soc. 2013 Sept 1;2(3):286–90.

83. Reusser P, Einsele H, Lee J, Volin L, Rovira M, Engelhard D, et al. Randomized multicenter trial of foscarnet versus ganciclovir for preemptive therapy of cytomegalovirus infection after allogeneic stem cell transplantation. Blood. 2002 Feb 15;99(4):1159–64.

84. Sun K, Fournier M, Sundberg AK, Song IH. Maribavir: Mechanism of action, clinical, and translational science. Clinical and Translational Science. 2024;17(1):e13696.

85. Goldner T, Hewlett G, Ettischer N, Ruebsamen-Schaeff H, Zimmermann H, Lischka P. The Novel Anticytomegalovirus Compound AIC246 (Letermovir) Inhibits Human Cytomegalovirus Replication through a Specific Antiviral Mechanism That Involves the Viral Terminase. Journal of Virology. 2011 Oct 15;85(20):10884–93.

86. Komatsu TE, Hodowanec AC, Colberg-Poley AM, Pikis A, Singer ME, O'Rear JJ, et al. In-depth genomic analyses identified novel letermovir resistance-associated substitutions in the cytomegalovirus UL56 and UL89 gene products. Antiviral Res. 2019 Sept;169:104549.

87. Muller C, Tilloy V, Frobert E, Feghoul L, Garrigue I, Lepiller Q, et al. First clinical description of letermovir resistance mutation in cytomegalovirus UL51 gene and potential impact on the terminase complex structure. Antiviral Res. 2022 Aug;204:105361.

88. Doshi S, Dassner A, Hanisch B. Maribavir use in pediatric immunocompromised hosts: A case series to talk about real-world experience. J Pediatric Infect Dis Soc. 2024 Oct 1;13(Supplement_4):26–7.

89. Zhang Y, Chen X, Zhou M, Zhang Y, Chen C, Zhou R, et al. Letermovir Effectively Prevents Cytomegalovirus Infection in Patients with Aplastic Anemia After Hematopoietic Stem Cell Transplantation: A Real-World Retrospective Cohort Study. Infect Dis Ther. 2024 Feb 1;13(2):345–59.

90. Oxman MN. Zoster Vaccine: Current Status and Future Prospects. Clin Infect Dis. 2010 July 15;51(2):197–213.

91. Neff BJ, Weibel RE, Buynak EB, McLean AA, Hilleman MR. Clinical and Laboratory Studies of Live Cytomegalovirus Vaccine Ad-169. Proceedings of the Society for Experimental Biology and Medicine. 1979 Jan 1;160(1):32–7.

92. Elek SD, Stern H. DEVELOPMENT OF A VACCINE AGAINST MENTAL RETARDATION CAUSED BY CYTOMEGALOVIRUS INFECTION IN UTERO. The Lancet. 1974 Jan 5;303(7845):1–5.

93. Cox KS, Zhang L, Freed DC, Tang A, Zhang S, Zhou Y, et al. Functional Evaluation and Genetic Evolution of Human T-Cell Responses After Vaccination With a Conditionally Replication-Defective Cytomegalovirus Vaccine. J Infect Dis. 2021 June 1;223(11):2001–12.

94. Bernstein DI, Munoz FM, Callahan ST, Rupp R, Wootton SH, Edwards KM, et al. Safety and efficacy of a cytomegalovirus glycoprotein B (gB) vaccine in adolescent girls: A randomized clinical trial. Vaccine. 2016 Jan 12;34(3):313–9.

95. Adler SP, Starr SE, Plotkin SA, Hempfling SH, Buis J, Manning ML, et al. Immunity Induced By Primary Human Cytomegalovirus Infection Protects Against Secondary Infection Among Women Of Childbearing Age. J Infect Dis. 1995 Jan 1;171(1):26–32.

96. Adler SP, Manganello AM, Lee R, McVoy MA, Nixon DE, Plotkin S, et al. A Phase 1 Study of 4 Live, Recombinant Human Cytomegalovirus Towne/Toledo Chimera Vaccines in Cytomegalovirus–Seronegative Men. J Infect Dis. 2016 Nov 1;214(9):1341–8.

97. Das R, Blázquez-Gamero D, Bernstein DI, Gantt S, Bautista O, Beck K, et al. Safety, efficacy, and immunogenicity of a replication-defective human cytomegalovirus vaccine, V160, in

cytomegalovirus-seronegative women: a double-blind, randomised, placebo-controlled, phase 2b trial. The Lancet Infectious Diseases. 2023 Dec 1;23(12):1383–94.

98. Pass RF, Duliegè AM, Boppana S, Sekulovich R, Percell S, Britt W, et al. A Subunit Cytomegalovirus Vaccine Based on Recombinant Envelope Glycoprotein B and a New Adjuvant. J Infect Dis. 1999 Oct 1;180(4):970–5.

99. Chiuppesi F, Wussow F, Scharf L, Contreras H, Gao H, Meng Z, et al. Comparison of homologous and heterologous prime-boost vaccine approaches using Modified Vaccinia Ankara and soluble protein to induce neutralizing antibodies by the human cytomegalovirus pentamer complex in mice. PLOS ONE. 2017 Aug 16;12(8):e0183377.

100. Contreras H, Wussow F, Fernández-Alarcón C, Bierle C, Nguyen J, Diamond DJ, et al. MVA-Vectored Pentameric Complex (PC) and gB Vaccines Improve Pregnancy Outcome after Guinea Pig CMV Challenge, but Only gB Vaccine Reduces Vertical Transmission. Vaccines. 2019 Dec;7(4):182.

101. Halsey G. Investigational mRNA CMV Vaccine Ready for Phase 3 Clinical Trial, Based on Results of Phase 2 Safety, Efficacy and Dose-Finding Study. Patient Care (Online). 2023 Oct 11;NA-NA.

102. Aldoss I, La Rosa C, Baden LR, Longmate J, Ariza-Heredia EJ, Rida WN, et al. Poxvirus Vectored Cytomegalovirus Vaccine to Prevent Cytomegalovirus Viremia in Transplant Recipients. Ann Intern Med. 2020 Mar 3;172(5):306–16.

103. Rosa CL, Park Y, Yang D, Zhou Q, Kaltcheva T, Karras N, et al. Cytomegalovirus Triplex vaccine in pediatric hematopoietic stem cell transplant patients at high risk for cytomegalovirus complications: evaluation of vaccine safety, immunogenicity and impact on viremia requiring antivirals. Haematologica. 2024 Feb 29;109(7):2303–8.

104. La Rosa C, Longmate J, Martinez J, Zhou Q, Kaltcheva TI, Tsai W, et al. MVA vaccine encoding CMV antigens safely induces durable expansion of CMV-specific T cells in healthy adults. Blood. 2017 Jan 5;129(1):114–25.

105. Sarov I, Abady I. The morphogenesis of human cytomegalovirus: Isolation and polypeptide characterization of cytomegalovirions and dense bodies. Virology. 1975 Aug 1;66(2):464–73.

106. Irmiere A, Gibson W. Isolation and characterization of a noninfectious virion-like particle released from cells infected with human strains of cytomegalovirus. Virology. 1983 Oct 15;130(1):118–33.

107. Jih J, Liu YT, Liu W, Zhou ZH. The incredible bulk: Human cytomegalovirus tegument architectures uncovered by AI-empowered cryo-EM. Science Advances. 2024 Feb 23;10(8):eadj1640.

108. Schneider-Ohrum K, Cayatte C, Liu Y, Wang Z, Irrinki A, Cataniag F, et al. Production of Cytomegalovirus Dense Bodies by Scalable Bioprocess Methods Maintains Immunogenicity and Improves Neutralizing Antibody Titers. Journal of Virology. 2016 Oct 28;90(22):10133–44.

109. Penner I, Büscher N, Dejung M, Freiwald A, Butter F, Plachter B. Subviral Dense Bodies of Human Cytomegalovirus Induce an Antiviral Type I Interferon Response. Cells. 2022 Dec 13;11(24):4028.

110. Penner I, Büscher N, Krauter S, Plachter B. Subviral Dense Bodies of Human Cytomegalovirus Enhance Interferon-Beta Responses in Infected Cells and Impair Progeny Production. Viruses. 2023 June 7;15(6):1333.

111. Xi Y, Lindenmayer L, Kline I, von Einem J, Purdy JG. Human Cytomegalovirus Uses a Host Stress Response To Balance the Elongation of Saturated/Monounsaturated and Polyunsaturated Very-Long-Chain Fatty Acids. mBio. 2021 May 4;12(3):10.1128/mbio.00167-21.

112. Koyuncu E, Purdy JG, Rabinowitz JD, Shenk T. Saturated Very Long Chain Fatty Acids Are Required for the Production of Infectious Human Cytomegalovirus Progeny. PLoS Pathog. 2013 May 16;9(5):e1003333.

113. Varnum SM, Streblow DN, Monroe ME, Smith P, Auberry KJ, Paša-Tolić L, et al. Identification of Proteins in Human Cytomegalovirus (HCMV) Particles: the HCMV Proteome. J Virol. 2004 Oct;78(20):10960–6.

114. Nguyen CC, Kamil JP. Pathogen at the Gates: Human Cytomegalovirus Entry and Cell Tropism. Viruses. 2018 Dec 11;10(12):704.

115. Yu X, Shah S, Lee M, Dai W, Lo P, Britt W, et al. Biochemical and Structural Characterization of the Capsid-Bound Tegument Proteins of Human Cytomegalovirus. J Struct Biol. 2011 June;174(3):451–60.

116. Browne EP, Shenk T. Human cytomegalovirus UL83-coded pp65 virion protein inhibits antiviral gene expression in infected cells. Proc Natl Acad Sci U S A. 2003 Sept 30;100(20):11439–44.

117. Silva MC, Yu QC, Enquist L, Shenk T. Human Cytomegalovirus UL99-Encoded pp28 Is Required for the Cytoplasmic Envelopment of Tegument-Associated Capsids. J Virol. 2003 Oct;77(19):10594–605.

118. Chen DH, Jiang H, Lee M, Liu F, Zhou ZH. Three-Dimensional Visualization of Tegument/Capsid Interactions in the Intact Human Cytomegalovirus. Virology. 1999 July 20;260(1):10–6.

119. Yu X, Jih J, Jiang J, Zhou ZH. Atomic structure of the human cytomegalovirus capsid with its securing tegument layer of pp150. Science. 2017 June 30;356(6345):eaam6892.

120. Dittmer A, Bogner E. Analysis of the quaternary structure of the putative HCMV portal protein PUL104. Biochemistry. 2005 Jan 18;44(2):759–65.

121. Dolan A, Cunningham C, Hector RD, Hassan-Walker AF, Lee L, Addison C, et al. Genetic content of wild-type human cytomegalovirus. J Gen Virol. 2004 May;85(Pt 5):1301–12.

122. Zeng J, Cao D, Yang S, Jaijyan DK, Liu X, Wu S, et al. Insights into the Transcriptome of Human Cytomegalovirus: A Comprehensive Review. Viruses. 2023 Aug 8;15(8):1703.

123. Dunn W, Chou C, Li H, Hai R, Patterson D, Stolc V, et al. Functional profiling of a human cytomegalovirus genome. Proc Natl Acad Sci U S A. 2003 Nov 25;100(24):14223–8.

124. Tamashiro JC, Spector DH. Terminal structure and heterogeneity in human cytomegalovirus strain AD169. Journal of Virology. 1986 Sept;59(3):591–604.

125. Boyle KA, Compton T. Receptor-Binding Properties of a Soluble Form of Human Cytomegalovirus Glycoprotein B. J Virol. 1998 Mar;72(3):1826–33.

126. Compton T, Nowlin DM, Cooper NR. Initiation of Human Cytomegalovirus Infection Requires Initial Interaction with Cell Surface Heparan Sulfate. Virology. 1993 Apr 1;193(2):834–41.

127. Kari B, Gehrz R. A human cytomegalovirus glycoprotein complex designated gC-II is a major heparin-binding component of the envelope. J Virol. 1992 Mar;66(3):1761–4.

128. Kschonsak M, Rougé L, Arthur CP, Hoangdung H, Patel N, Kim I, et al. Structures of HCMV Trimer reveal the basis for receptor recognition and cell entry. Cell. 2021 Mar 4;184(5):1232-1244.e16.

129. Compton T, Nepomuceno RR, Nowlin DM. Human cytomegalovirus penetrates host cells by PH-independent fusion at the cell surface. Virology. 1992 Nov 1;191(1):387–95.

130. Sinzger C. Entry route of HCMV into endothelial cells. Journal of Clinical Virology. 2008 Mar 1;41(3):174–9.

131. Ryckman BJ, Jarvis MA, Drummond DD, Nelson JA, Johnson DC. Human cytomegalovirus entry into epithelial and endothelial cells depends on genes UL128 to UL150 and occurs by endocytosis and low-pH fusion. J Virol. 2006 Jan;80(2):710–22.

132. Ryckman BJ, Chase MC, Johnson DC. HCMV gH/gL/UL128-131 interferes with virus entry into epithelial cells: evidence for cell type-specific receptors. Proc Natl Acad Sci U S A. 2008 Sept 16;105(37):14118–23.

133. Cha TA, Tom E, Kemble GW, Duke GM, Mocarski ES, Spaete RR. Human cytomegalovirus clinical isolates carry at least 19 genes not found in laboratory strains. J Virol. 1996 Jan;70(1):78–83.

134. Vanarsdall AL, Pritchard SR, Wisner TW, Liu J, Jardetzky TS, Johnson DC. CD147 Promotes Entry of Pentamer-Expressing Human Cytomegalovirus into Epithelial and Endothelial Cells. mBio. 2018 May 8;9(3):10.1128/mbio.00781-18.

135. Wang D, Shenk T. Human cytomegalovirus virion protein complex required for epithelial and endothelial cell tropism. Proc Natl Acad Sci U S A. 2005 Dec 13;102(50):18153–8.

136. Vanarsdall AL, Wisner TW, Lei H, Kazlauskas A, Johnson DC. PDGF receptor-α does not promote HCMV entry into epithelial and endothelial cells but increased quantities stimulate entry by an abnormal pathway. PLoS Pathog. 2012 Sept;8(9):e1002905.

137. Liu Y, Heim KP, Che Y, Chi X, Qiu X, Han S, et al. Prefusion structure of human cytomegalovirus glycoprotein B and structural basis for membrane fusion. Sci Adv. 2021 Mar 5;7(10):eabf3178.

138. Si Z, Zhang J, Shivakoti S, Atanasov I, Tao CL, Hui WH, et al. Different functional states of fusion protein gB revealed on human cytomegalovirus by cryo electron tomography with Volta phase plate. PLOS Pathogens. 2018 Dec 3;14(12):e1007452.

139. Park A, Ra EA, Lee TA, Choi H jin, Lee E, Kang S, et al. HCMV-encoded US7 and US8 act as antagonists of innate immunity by distinctively targeting TLR-signaling pathways. Nat Commun. 2019 Oct 11;10(1):4670.

140. Sampaio KL, Cavignac Y, Stierhof YD, Sinzger C. Human Cytomegalovirus Labeled with Green Fluorescent Protein for Live Analysis of Intracellular Particle Movements. Journal of Virology. 2005 Mar;79(5):2754–67.

141. Tandon R, Mocarski ES. Cytomegalovirus pUL96 Is Critical for the Stability of pp150-Associated Nucleocapsids ▿. J Virol. 2011 July;85(14):7129–41.

142. Ogawa-Goto K, Tanaka K, Gibson W, Moriishi E, Miura Y, Kurata T, et al. Microtubule Network Facilitates Nuclear Targeting of Human Cytomegalovirus Capsid. Journal of Virology. 2003 Aug;77(15):8541–7.

143. Ahn JH, Hayward GS. Disruption of PML-Associated Nuclear Bodies by IE1 Correlates with Efficient Early Stages of Viral Gene Expression and DNA Replication in Human Cytomegalovirus Infection. Virology. 2000 Aug 15;274(1):39–55.

144. Tavalai N, Papior P, Rechter S, Stamminger T. Nuclear domain 10 components promyelocytic leukemia protein and hDaxx independently contribute to an intrinsic antiviral defense against human cytomegalovirus infection. J Virol. 2008 Jan;82(1):126–37.

145. Saffert RT, Kalejta RF. Human cytomegalovirus gene expression is silenced by Daxx-mediated intrinsic immune defense in model latent infections established in vitro. J Virol. 2007 Sept;81(17):9109–20.

146. Cantrell SR, Bresnahan WA. Human Cytomegalovirus (HCMV) UL82 Gene Product (pp71) Relieves hDaxx-Mediated Repression of HCMV Replication. J Virol. 2006 June;80(12):6188–91.

147. Scherer M, Schilling EM, Stamminger T. The Human CMV IE1 Protein: An Offender of PML Nuclear Bodies. Adv Anat Embryol Cell Biol. 2017;223:77–94.

148. Wiebusch L, Hagemeier C. The human cytomegalovirus immediate early 2 protein dissociates cellular DNA synthesis from cyclin-dependent kinase activation. The EMBO Journal. 2001 Mar;20(5):1086–98.

149. Lee SB, Lee CF, Ou DSC, Dulal K, Chang LH, Ma CH, et al. Host-viral effects of chromatin assembly factor 1 interaction with HCMV IE2. Cell Res. 2011 Aug;21(8):1230–47.

150. Ball CB, Li M, Parida M, Hu Q, Ince D, Collins GS, et al. Human Cytomegalovirus IE2 Both Activates and Represses Initiation and Modulates Elongation in a Context-Dependent Manner. mBio. 2022 May 17;13(3):e00337-22.

151. Wiebusch L, Neuwirth A, Grabenhenrich L, Voigt S, Hagemeier C. Cell Cycle-Independent Expression of Immediate-Early Gene 3 Results in G1 and G2 Arrest in Murine Cytomegalovirus-Infected Cells. Journal of Virology. 2008 Oct 15;82(20):10188–98.

152. Wiebusch L, Hagemeier C. Human Cytomegalovirus 86-Kilodalton IE2 Protein Blocks Cell Cycle Progression in G1. J Virol. 1999 Nov;73(11):9274–83.

153. Zhang X, Jiang S, Zhou X, Yu Z, Han S, Nan F, et al. Human Cytomegalovirus-IE2 Affects Embryonic Liver Development and Survival in Transgenic Mouse. Cellular and Molecular Gastroenterology and Hepatology. 2022 Jan 1;14(2):494–511.

154. Xu Y, Colletti KS, Pari GS. Human Cytomegalovirus UL84 Localizes to the Cell Nucleus via a Nuclear Localization Signal and Is a Component of Viral Replication Compartments. J Virol. 2002 Sept;76(17):8931–8.

155. Colletti KS, Smallenburg KE, Xu Y, Pari GS. Human cytomegalovirus UL84 interacts with an RNA stem-loop sequence found within the RNA/DNA hybrid region of oriLyt. J Virol. 2007 July;81(13):7077–85.

156. Vornhagen R, Hinderer W, Sonneborn HH, Bein G, Matter L, The TH, et al. The DNA-binding protein pUL57 of human cytomegalovirus is a major target antigen for the immunoglobulin M antibody response during acute infection. Journal of Clinical Microbiology. 1995 July;33(7):1927–30.

157. Smith JA, Pari GS. Human cytomegalovirus UL102 gene. Journal of Virology. 1995 Mar;69(3):1734–40.

158. Kerry JA, Priddy MA, Jervey TY, Kohler CP, Staley TL, Vanson CD, et al. Multiple regulatory events influence human cytomegalovirus DNA polymerase (UL54) expression during viral infection. Journal of Virology. 1996 Jan;70(1):373–82.

159. Timmoneri M. Inhibition of HCMV replication by small molecules interfering with the dimerization of the DNA polymerase processivity factor UL44. 2018 [cited 2025 Sept 9]; Available from: https://tesidottorato.depositolegale.it/handle/20.500.14242/83972

160. Smith JA, Jairath S, Crute JJ, Pari GS. Characterization of the human cytomegalovirus UL105 gene and identification of the putative helicase protein. Virology. 1996 June 1;220(1):251–5.

161. Shen A, Lei J, Yang E, Pei Y, Chen YC, Gong H, et al. Human Cytomegalovirus Primase UL70 Specifically Interacts with Cellular Factor Snapin ▿. J Virol. 2011 Nov;85(22):11732–41.

162. Muller C, Alain S, Baumert TF, Ligat G, Hantz S. Structures and Divergent Mechanisms in Capsid Maturation and Stabilization Following Genome Packaging of Human Cytomegalovirus and Herpesviruses. Life. 2021 Feb;11(2):150.

163. Gibson W. Structure and Assembly of the Virion. Intervirology. 2008 July 30;39(5–6):389–400.

164. Borst EM, Harmening S, Sanders S, Caragliano E, Wagner K, Lenac Roviš T, et al. A Unique Role of the Human Cytomegalovirus Small Capsid Protein in Capsid Assembly. mBio. 2022 Oct 26;13(5):e0100722.

165. Wood LJ, Baxter MK, Plafker SM, Gibson W. Human cytomegalovirus capsid assembly protein precursor (pUL80.5) interacts with itself and with the major capsid protein (pUL86) through two different domains. J Virol. 1997 Jan;71(1):179–90.

166. Loveland AN, Nguyen NL, Brignole EJ, Gibson W. The Amino-Conserved Domain of Human Cytomegalovirus UL80a Proteins Is Required for Key Interactions during Early Stages of Capsid Formation and Virus Production. Journal of Virology. 2007 Jan 15;81(2):620–8.

167. Neuber S, Wagner K, Goldner T, Lischka P, Steinbrueck L, Messerle M, et al. Mutual Interplay between the Human Cytomegalovirus Terminase Subunits pUL51, pUL56, and pUL89 Promotes Terminase Complex Formation. Journal of Virology. 2017 May 26;91(12):10.1128/jvi.02384-16.

168. Marschall M, Muller YA, Diewald B, Sticht H, Milbradt J. The human cytomegalovirus nuclear egress complex unites multiple functions: Recruitment of effectors, nuclear envelope rearrangement, and docking to nuclear capsids. Rev Med Virol. 2017 July;27(4).

169. Buser C, Walther P, Mertens T, Michel D. Cytomegalovirus Primary Envelopment Occurs at Large Infoldings of the Inner Nuclear Membrane. Journal of Virology. 2007 Mar 15;81(6):3042–8.

170. Sharma M, Kamil JP, Coughlin M, Reim NI, Coen DM. Human Cytomegalovirus UL50 and UL53 Recruit Viral Protein Kinase UL97, Not Protein Kinase C, for Disruption of Nuclear Lamina and Nuclear Egress in Infected Cells. Journal of Virology. 2014 Jan;88(1):249–62.

171. Mettenleiter TC. Herpesvirus Assembly and Egress. Journal of Virology. 2002 Feb 15;76(4):1537–47.

172. Kalejta RF. Tegument Proteins of Human Cytomegalovirus. Microbiology and Molecular Biology Reviews. 2008 June;72(2):249–65.

173. Ahlqvist J, Mocarski E. Cytomegalovirus UL103 Controls Virion and Dense Body Egress ▿ . J Virol. 2011 May;85(10):5125–35.

174. Britt W. Manifestations of human cytomegalovirus infection: proposed mechanisms of acute and chronic disease. Curr Top Microbiol Immunol. 2008;325:417–70.

175. Stagno S, Reynolds DW, Pass RF, Alford CA. Breast milk and the risk of cytomegalovirus infection. N Engl J Med. 1980 May 8;302(19):1073–6.

176. Sinclair J, Sissons P. Latent and persistent infections of monocytes and macrophages. Intervirology. 1996;39(5–6):293–301.

177. von Laer D, Meyer-Koenig U, Serr A, Finke J, Kanz L, Fauser AA, et al. Detection of cytomegalovirus DNA in CD34+ cells from blood and bone marrow. Blood. 1995 Dec 1;86(11):4086–90.

178. Mendelson M, Monard S, Sissons P, Sinclair J. Detection of endogenous human cytomegalovirus in CD34+ bone marrow progenitors. J Gen Virol. 1996 Dec;77 (Pt 12):3099–102.

179. Smith MS, Goldman DC, Bailey AS, Pfaffle DL, Kreklywich CN, Spencer DB, et al. Granulocyte-colony stimulating factor reactivates human cytomegalovirus in a latently infected humanized mouse model. Cell Host Microbe. 2010 Sept 16;8(3):284–91.

180. Sinclair J. Human cytomegalovirus: Latency and reactivation in the myeloid lineage. J Clin Virol. 2008 Mar;41(3):180–5.

181. Reeves MB, MacAry PA, Lehner PJ, Sissons JGP, Sinclair JH. Latency, chromatin remodeling, and reactivation of human cytomegalovirus in the dendritic cells of healthy carriers. Proceedings of the National Academy of Sciences. 2005 Mar 15;102(11):4140–5.

182. Dooley AL, O'Connor CM. Regulation of the MIE Locus During HCMV Latency and Reactivation. Pathogens. 2020 Oct 23;9(11):869.

183. Rossetto CC, Tarrant-Elorza M, Pari GS. Cis and Trans Acting Factors Involved in Human Cytomegalovirus Experimental and Natural Latent Infection of CD14 (+) Monocytes and CD34 (+) Cells. PLOS Pathogens. 2013 May 23;9(5):e1003366.

184. Lee SH, Albright ER, Lee JH, Jacobs D, Kalejta RF. Cellular defense against latent colonization foiled by human cytomegalovirus UL138 protein. Sci Adv. 2015 Nov 27;1(10):e1501164.

185. Buehler J, Zeltzer S, Reitsma J, Petrucelli A, Umashankar M, Rak M, et al. Opposing Regulation of the EGF Receptor: A Molecular Switch Controlling Cytomegalovirus Latency and Replication. PLoS Pathog. 2016 May 24;12(5):e1005655.

186. Montag C, Wagner JA, Gruska I, Vetter B, Wiebusch L, Hagemeier C. The Latency-Associated UL138 Gene Product of Human Cytomegalovirus Sensitizes Cells to Tumor Necrosis Factor Alpha (TNF-α) Signaling by Upregulating TNF-α Receptor 1 Cell Surface Expression. Journal of Virology. 2011 Nov;85(21):11409–21.

187. Goodrum F. HUMAN CYTOMEGALOVIRUS LATENCY: Approaching the Gordian Knot. Annu Rev Virol. 2016 Sept 29;3(1):333–57.

188. Dutta N, Lashmit P, Yuan J, Meier J, Stinski MF. The human cytomegalovirus UL133-138 gene locus attenuates the lytic viral cycle in fibroblasts. PLoS One. 2015;10(3):e0120946.

189. Petrucelli A, Umashankar M, Zagallo P, Rak M, Goodrum F. Interactions between proteins encoded within the human cytomegalovirus UL133-UL138 locus. J Virol. 2012 Aug;86(16):8653–62.

190. Umashankar M, Petrucelli A, Cicchini L, Caposio P, Kreklywich CN, Rak M, et al. A novel human cytomegalovirus locus modulates cell type-specific outcomes of infection. PLoS Pathog. 2011 Dec;7(12):e1002444.

191. Humby MS, O'Connor CM. Human Cytomegalovirus US28 Is Important for Latent Infection of Hematopoietic Progenitor Cells. J Virol. 2015 Dec 30;90(6):2959–70.

192. Krishna BA, Poole EL, Jackson SE, Smit MJ, Wills MR, Sinclair JH. Latency-Associated Expression of Human Cytomegalovirus US28 Attenuates Cell Signaling Pathways To Maintain Latent Infection. mBio. 2017 Dec 5;8(6):e01754-17.

193. Crawford LB, Caposio P, Kreklywich C, Pham AH, Hancock MH, Jones TA, et al. Human Cytomegalovirus US28 Ligand Binding Activity Is Required for Latency in CD34+ Hematopoietic Progenitor Cells and Humanized NSG Mice. mBio. 2019 Aug 20;10(4):e01889-19.

194. Krishna BA, Wass AB, Sridharan R, O'Connor CM. The Requirement for US28 During Cytomegalovirus Latency Is Independent of US27 and US29 Gene Expression. Frontiers in Cellular and Infection Microbiology [Internet]. 2020 [cited 2022 July 4];10. Available from: https://www.frontiersin.org/articles/10.3389/fcimb.2020.00186

195. Zhu D, Pan C, Sheng J, Liang H, Bian Z, Liu Y, et al. Human cytomegalovirus reprogrammes haematopoietic progenitor cells into immunosuppressive monocytes to achieve latency. Nat Microbiol. 2018 Apr;3(4):503–13.

196. Crawford LB, Kim JH, Collins-McMillen D, Lee BJ, Landais I, Held C, et al. Human Cytomegalovirus Encodes a Novel FLT3 Receptor Ligand Necessary for Hematopoietic Cell Differentiation and Viral Reactivation. mBio. 2018 Apr 24;9(2):e00682-18.

197. Human Cytomegalovirus UL7, miR-US5-1, and miR-UL112-3p Inactivation of FOXO3a Protects CD34+ Hematopoietic Progenitor Cells from Apoptosis | mSphere [Internet]. [cited 2025 Sept 11]. Available from: https://journals.asm.org/doi/10.1128/msphere.00986-20

198. Lau B, Poole E, Van Damme E, Bunkens L, Sowash M, King H, et al. Human cytomegalovirus miR-UL112-1 promotes the down-regulation of viral immediate early-gene expression during latency to prevent T-cell recognition of latently infected cells. J Gen Virol. 2016 Sept;97(9):2387–98.

199. Murphy E, Vanícek J, Robins H, Shenk T, Levine AJ. Suppression of immediate-early viral gene expression by herpesvirus-coded microRNAs: implications for latency. Proc Natl Acad Sci U S A. 2008 Apr 8;105(14):5453–8.

200. Grey F, Meyers H, White EA, Spector DH, Nelson J. A Human Cytomegalovirus-Encoded microRNA Regulates Expression of Multiple Viral Genes Involved in Replication. PLOS Pathogens. 2007 Nov 2;3(11):e163.

201. Pan C, Zhu D, Wang Y, Li L, Li D, Liu F, et al. Human Cytomegalovirus miR-UL148D Facilitates Latent Viral Infection by Targeting Host Cell Immediate Early Response Gene 5. PLOS Pathogens. 2016 Nov 8;12(11):e1006007.

202. Hancock MH, Crawford LB, Perez W, Struthers HM, Mitchell J, Caposio P. Human Cytomegalovirus UL7, miR-US5-1, and miR-UL112-3p Inactivation of FOXO3a Protects CD34+ Hematopoietic Progenitor Cells from Apoptosis. mSphere. 2021 Jan 6;6(1):10.1128/msphere.00986-20.

203. Diggins NL, Crawford LB, Hancock MH, Mitchell J, Nelson JA. Human Cytomegalovirus miR-US25-1 Targets the GTPase RhoA To Inhibit CD34+ Hematopoietic Progenitor Cell Proliferation To Maintain the Latent Viral Genome. mBio. 2021 Apr 6;12(2):e00621-21.

204. Jiang S, Qi Y, He R, Huang Y, Liu Z, Ma Y, et al. Human cytomegalovirus microRNA miR-US25-1-5p inhibits viral replication by targeting multiple cellular genes during infection. Gene. 2015 Oct 1;570(1):108–14.

205. Dirck A, Diggins NL, Crawford LB, Perez WD, Parkins CJ, Struthers HH, et al. HCMV UL8 interaction with β-catenin and DVL2 regulates viral reactivation in CD34+ hematopoietic progenitor cells. J Virol. 2023 Oct 31;97(10):e0124123.

206. Medica S, Crawford LB, Denton M, Min CK, Jones TA, Alexander T, et al. Proximity-dependent mapping of the HCMV US28 interactome identifies RhoGEF signaling as a requirement for efficient viral reactivation. PLOS Pathogens. 2023 Oct 2;19(10):e1011682.

207. Keyes LR, Hargett D, Soland M, Bego MG, Rossetto CC, Almeida-Porada G, et al. HCMV protein LUNA is required for viral reactivation from latently infected primary $CD14^+$ cells. PLoS One. 2012;7(12):e52827.

208. Moy MA, Collins-McMillen D, Crawford L, Parkins C, Zeltzer S, Caviness K, et al. UL135 and UL136 Epistasis Controls Reactivation of Human Cytomegalovirus. bioRxiv. 2023 Jan 24;2023.01.24.525282.

209. Rak MA, Buehler J, Zeltzer S, Reitsma J, Molina B, Terhune S, et al. Human Cytomegalovirus UL135 Interacts with Host Adaptor Proteins To Regulate Epidermal Growth Factor Receptor and Reactivation from Latency. J Virol. 2018 Oct 15;92(20):e00919-18.

210. Krishna BA, Wass AB, Dooley AL, O'Connor CM. CMV-encoded GPCR pUL33 activates CREB and facilitates its recruitment to the MIE locus for efficient viral reactivation. J Cell Sci. 2021 Jan 25;134(5):jcs254268.

211. Diggins NL, Pham AH, Mitchell J, Parkins CJ, Slind L, Turner R, et al. Viral microRNA regulation of Akt is necessary for reactivation of Human Cytomegalovirus from latency in CD34+ hematopoietic progenitor cells and humanized mice. PLOS Pathogens. 2024 Dec 11;20(12):e1012285.

212. Mlera L, Moy M, Maness K, Tran LN, Goodrum FD. The Role of the Human Cytomegalovirus UL133-UL138 Gene Locus in Latency and Reactivation. Viruses. 2020 July 1;12(7):714.

213. Rønning SB, Pedersen NM, Madshus IH, Stang E. CIN85 regulates ubiquitination and degradative endosomal sorting of the EGF receptor. Exp Cell Res. 2011 Aug 1;317(13):1804–16.

214. Stanton RJ, Prod'homme V, Purbhoo MA, Moore M, Aicheler RJ, Heinzmann M, et al. HCMV pUL135 remodels the actin cytoskeleton to impair immune recognition of infected cells. Cell Host Microbe. 2014 Aug 13;16(2):201–14.

215. Tanos BE, Pendergast AM. Abi-1 forms an epidermal growth factor-inducible complex with Cbl: role in receptor endocytosis. Cell Signal. 2007 July;19(7):1602–9.

216. Wang D, Li G, Schauflinger M, Nguyen CC, Hall ED, Yurochko AD, et al. The ULb' region of the human cytomegalovirus genome confers an increased requirement for the viral protein kinase UL97. J Virol. 2013 June;87(11):6359–76.

217. Li G, Rak M, Nguyen CC, Umashankar M, Goodrum FD, Kamil JP. An epistatic relationship between the viral protein kinase UL97 and the UL133-UL138 latency locus during the human cytomegalovirus lytic cycle. J Virol. 2014 June;88(11):6047–60.

218. Caviness K, Cicchini L, Rak M, Umashankar M, Goodrum F. Complex expression of the UL136 gene of human cytomegalovirus results in multiple protein isoforms with unique roles in replication. J Virol. 2014 Dec;88(24):14412–25.

219. Poole EL, Kew VG, Lau JCH, Murray MJ, Stamminger T, Sinclair JH, et al. A Virally Encoded DeSUMOylase Activity Is Required for Cytomegalovirus Reactivation from Latency. Cell Rep. 2018 July 17;24(3):594–606.

220. van Senten JR, Bebelman MP, van Gasselt P, Bergkamp ND, van den Bor J, Siderius M, et al. Human Cytomegalovirus-Encoded G Protein-Coupled Receptor UL33 Facilitates Virus Dissemination via the Extracellular and Cell-to-Cell Route. Viruses. 2020 May 30;12(6):594.

221. Davis-Poynter N, Farrell HE. Constitutive Signaling by the Human Cytomegalovirus G Protein Coupled Receptor Homologs US28 and UL33 Enables Trophoblast Migration In Vitro. Viruses. 2022 Feb;14(2):391.

222. Wass AB, Krishna BA, Herring LE, Gilbert TSK, Nukui M, Groves IJ, et al. Cytomegalovirus US28 regulates cellular EphA2 to maintain viral latency. Sci Adv. 2022 Oct 28;8(43):eadd1168.

223. Medica S, Denton M, Diggins NL, Kramer-Hansen O, Crawford LB, Mayo AT, et al. Third intracellular loop of HCMV US28 is necessary for signaling and viral reactivation. Journal of Virology. 2024 Dec 10;0(0):e01801-24.

224. Wu S en, Miller WE. The HCMV US28 vGPCR induces potent Gαq/PLC-β signaling in monocytes leading to increased adhesion to endothelial cells. Virology. 2016 Oct;497:233–43.

225. Miller WE, Zagorski WA, Brenneman JD, Avery D, Miller JLC, O'Connor CM. US28 is a potent activator of phospholipase C during HCMV infection of clinically relevant target cells. PLoS One. 2012;7(11):e50524.

226. Dumortier J, Streblow DN, Moses AV, Jacobs JM, Kreklywich CN, Camp D, et al. Human cytomegalovirus secretome contains factors that induce angiogenesis and wound healing. J Virol. 2008 July;82(13):6524–35.

227. Vomaske J, Melnychuk RM, Smith PP, Powell J, Hall L, DeFilippis V, et al. Differential ligand binding to a human cytomegalovirus chemokine receptor determines cell type-specific motility. PLoS Pathog. 2009 Feb;5(2):e1000304.

228. Osanyinlusi SA, Baruah V, Groves IJ, Kulp KH, Krishna BA, O'Connor CM. Human cytomegalovirus-encoded G protein-coupled receptor (GPCR) UL78 regulates viral reactivation. J Virol. 2025 Aug 27;e0105725.

229. Medica S, Diggins NL, Denton M, Turner RL, Pung LJ, Mayo AT, et al. Human Cytomegalovirus UL78 is a Nuclear-Localized GPCR Necessary for Efficient Reactivation from Latent Infection in CD34+ Hematopoietic Progenitor Cells [Internet]. bioRxiv; 2025 [cited 2025 Sept 11]. p. 2025.06.02.657350. Available from: https://www.biorxiv.org/content/10.1101/2025.06.02.657350v1

230. Buehler J, Carpenter E, Zeltzer S, Igarashi S, Rak M, Mikell I, et al. Host signaling and EGR1 transcriptional control of human cytomegalovirus replication and latency. PLoS Pathog. 2019 Nov;15(11):e1008037.

231. Mikell I, Crawford LB, Hancock MH, Mitchell J, Buehler J, Goodrum F, et al. HCMV miR-US22 down-regulation of EGR-1 regulates CD34+ hematopoietic progenitor cell proliferation and viral reactivation. PLoS Pathog. 2019 Nov;15(11):e1007854.

232. Hancock MH, Mitchell J, Goodrum FD, Nelson JA. Human Cytomegalovirus miR-US5-2 Downregulation of GAB1 Regulates Cellular Proliferation and UL138 Expression through Modulation of Epidermal Growth Factor Receptor Signaling Pathways. mSphere. 2020 Aug 5;5(4):e00582-20.

233. Ono SJ, Nakamura T, Miyazaki D, Ohbayashi M, Dawson M, Toda M. Chemokines: Roles in leukocyte development, trafficking, and effector function. Journal of Allergy and Clinical Immunology. 2003 June 1;111(6):1185–99.

234. Zlotnik A, Yoshie O. The Chemokine Superfamily Revisited. Immunity. 2012 May 25;36(5):705–16.

235. Palomino DCT, Marti LC. Chemokines and immunity. Einstein (Sao Paulo). 2015;13(3):469–73.

236. Raman D, Sobolik-Delmaire T, Richmond A. Chemokines in health and disease. Experimental Cell Research. 2011 Mar 10;317(5):575–89.

237. Hughes CE, Nibbs RJB. A guide to chemokines and their receptors. FEBS J. 2018 Aug;285(16):2944–71.

238. Stievano L, Piovan E, Amadori A. C and CX3C chemokines: cell sources and physiopathological implications. Crit Rev Immunol. 2004;24(3):205–28.

239. Kelner GS, Kennedy J, Bacon KB, Kleyensteuber S, Largaespada DA, Jenkins NA, et al. Lymphotactin: a cytokine that represents a new class of chemokine. Science. 1994 Nov 25;266(5189):1395–9.

240. Clark AK, Staniland AA, Malcangio M. Fractalkine/CX3CR1 signalling in chronic pain and inflammation. Curr Pharm Biotechnol. 2011 Oct;12(10):1707–14.

241. Marsland BJ, Bättig P, Bauer M, Ruedl C, Lässing U, Beerli RR, et al. CCL19 and CCL21 Induce a Potent Proinflammatory Differentiation Program in Licensed Dendritic Cells. Immunity. 2005 Apr 1;22(4):493–505.

242. Singh P, Mohammad KS, Pelus LM. CXCR4 expression in the bone marrow microenvironment is required for hematopoietic stem and progenitor cell maintenance and early hematopoietic regeneration after myeloablation. Stem Cells. 2020 July;38(7):849–59.

243. Schyrr F, Alonso-Calleja A, Vijaykumar A, Sordet-Dessimoz J, Gebhard S, Sarkis R, et al. Inducible CXCL12/CXCR4–dependent extramedullary hematopoietic niches in the adrenal gland. Blood. 2024 Aug 29;144(9):964–76.

244. Basith S, Cui M, Macalino SJY, Park J, Clavio NAB, Kang S, et al. Exploring G Protein-Coupled Receptors (GPCRs) Ligand Space via Cheminformatics Approaches: Impact on Rational Drug Design. Front Pharmacol [Internet]. 2018 Mar 9 [cited 2025 Sept 11];9. Available from: https://www.frontiersin.org/journals/pharmacology/articles/10.3389/fphar.2018.00128/full

245. Yang D, Zhou Q, Labroska V, Qin S, Darbalaei S, Wu Y, et al. G protein-coupled receptors: structure- and function-based drug discovery. Sig Transduct Target Ther. 2021 Jan 8;6(1):1–27.

246. Masuho I, Kise R, Gainza P, Von Moo E, Li X, Tany R, et al. Rules and mechanisms governing G protein coupling selectivity of GPCRs. Cell Rep. 2023 Oct 31;42(10):113173.

247. Kufareva I, Salanga CL, Handel TM. Chemokine and chemokine receptor structure and interactions: implications for therapeutic strategies. Immunol Cell Biol. 2015 Apr;93(4):372–83.

248. Bonecchi R, Graham GJ. Atypical Chemokine Receptors and Their Roles in the Resolution of the Inflammatory Response. Front Immunol. 2016 June 10;7:224.

249. Horuk R. The Duffy Antigen Receptor for Chemokines DARC/ACKR1. Front Immunol. 2015 June 5;6:279.

250. Lin Y, Chai Y, Gao A, Han J, Guo Y, Lin Y, et al. CXCL13/CXCR5 axis mediates IgM+ B cell migration through AKT and STAT3 signaling pathways in Nile tilapia (*Oreochromis niloticus*). Aquaculture. 2024 Oct 15;591:741109.

251. Yan Y, Chen R, Wang X, Hu K, Huang L, Lu M, et al. CCL19 and CCR7 Expression, Signaling Pathways, and Adjuvant Functions in Viral Infection and Prevention. Front Cell Dev Biol [Internet]. 2019 Oct 1 [cited 2025 Sept 11];7. Available from:

https://www.frontiersin.org/journals/cell-and-developmental-biology/articles/10.3389/fcell.2019.00212/full

252. Meloun A, León B. Beyond CCR7: dendritic cell migration in type 2 inflammation. Front Immunol. 2025 Feb 28;16:1558228.

253. Heng AHS, Han CW, Abbott C, McColl SR, Comerford I. Chemokine-Driven Migration of Pro-Inflammatory CD4+ T Cells in CNS Autoimmune Disease. Front Immunol. 2022 Feb 16;13:817473.

254. Chow MT, Luster AD. Chemokines in Cancer. Cancer Immunol Res. 2014 Dec;2(12):1125–31.

255. Li H, Wu M, Zhao X. Role of chemokine systems in cancer and inflammatory diseases. MedComm (2020). 2022 June 8;3(2):e147.

256. Choi J, Selmi C, Leung P, Kenny TP, Roskams T, Gershwin ME. Chemokine and chemokine receptors in autoimmunity: the case of primary biliary cholangitis. Expert Rev Clin Immunol. 2016 June;12(6):661–72.

257. Rosenkilde MM, Kledal TN. Targeting Herpesvirus Reliance of the Chemokine System. Current Drug Targets. 2006 Jan 1;7(1):103–18.

258. Bleul CC, Wu L, Hoxie JA, Springer TA, Mackay CR. The HIV coreceptors CXCR4 and CCR5 are differentially expressed and regulated on human T lymphocytes. Proceedings of the National Academy of Sciences. 1997 Mar 4;94(5):1925–30.

259. Proudfoot AEI. Chemokine receptors: multifaceted therapeutic targets. Nat Rev Immunol. 2002 Feb;2(2):106–15.

260. Gulick RM, Fatkenheuer G, Burnside R, Hardy WD, Nelson MR, Goodrich J, et al. Five-Year Safety Evaluation of Maraviroc in HIV-1–Infected Treatment-Experienced Patients. J Acquir Immune Defic Syndr. 2014 Jan 1;65(1):78–81.

261. Schneider EH, Schnell D, Strasser A, Dove S, Seifert R. Impact of the DRY motif and the missing “ionic lock” on constitutive activity and G-protein coupling of the human histamine H4 receptor. J Pharmacol Exp Ther. 2010 May;333(2):382–92.

262. Pietraszewska-Bogiel A, Joosen L, Chertkova AO, Goedhart J. Not So Dry After All: DRY Mutants of the AT1A Receptor and H1 Receptor Can Induce G-Protein-Dependent Signaling. ACS Omega. 2020 Feb 18;5(6):2648–59.

263. Syrovatkina V, Alegre KO, Dey R, Huang XY. Regulation, Signaling and Physiological Functions of G-proteins. J Mol Biol. 2016 Sept 25;428(19):3850–68.

264. Zhang M, Chen T, Lu X, Lan X, Chen Z, Lu S. G protein-coupled receptors (GPCRs): advances in structures, mechanisms and drug discovery. Sig Transduct Target Ther. 2024 Apr 10;9(1):88.

265. Khater M, Wei Z, Xu X, Huang W, Lokeshwar BL, Lambert NA, et al. G protein βγ translocation to the Golgi apparatus activates MAPK via p110γ-p101 heterodimers. J Biol Chem. 2021 Jan 23;296:100325.

266. Brock C, Schaefer M, Reusch HP, Czupalla C, Michalke M, Spicher K, et al. Roles of Gβγ in membrane recruitment and activation of p110γ/p101 phosphoinositide 3-kinase γ. J Cell Biol. 2003 Jan 6;160(1):89–99.

267. De Vries L, Zheng B, Fischer T, Elenko E, Farquhar MG. The regulator of G protein signaling family. Annu Rev Pharmacol Toxicol. 2000;40:235–71.

268. Reiter E, Lefkowitz RJ. GRKs and β-arrestins: roles in receptor silencing, trafficking and signaling. Trends in Endocrinology & Metabolism. 2006 May 1;17(4):159–65.

269. Chen Q, Tesmer JJG. G protein–coupled receptor interactions with arrestins and GPCR kinases: The unresolved issue of signal bias. J Biol Chem. 2022 July 19;298(9):102279.

270. Kovacs JJ, Hara MR, Davenport CL, Kim J, Lefkowitz RJ. Arrestin Development: Emerging Roles for β-arrestins in Developmental Signaling Pathways. Developmental Cell. 2009 Oct 20;17(4):443–58.

271. Neel NF, Schutyser E, Sai J, Fan GH, Richmond A. Chemokine receptor internalization and intracellular trafficking. Cytokine Growth Factor Rev. 2005 Dec;16(6):637–58.

272. Alkhatib G. The biology of CCR5 and CXCR4. Curr Opin HIV AIDS. 2009 Mar;4(2):96–103.

273. He R, Ruan Q, Qi Y, Ma YP, Huang YJ, Sun ZR, et al. Sequence variability of human cytomegalovirus UL146 and UL147 genes in low-passage clinical isolates. Intervirology. 2006;49(4):215–23.

274. Lüttichau HR. The Cytomegalovirus UL146 Gene Product vCXCL1 Targets Both CXCR1 and CXCR2 as an Agonist*. Journal of Biological Chemistry. 2010 Mar 19;285(12):9137–46.

275. Penfold MET, Dairaghi DJ, Duke GM, Saederup N, Mocarski ES, Kemble GW, et al. Cytomegalovirus encodes a potent α chemokine. Proc Natl Acad Sci U S A. 1999 Aug 17;96(17):9839–44.

276. Seidel E, Dassa L, Schuler C, Oiknine-Djian E, Wolf DG, Le-Trilling VTK, et al. The human cytomegalovirus protein UL147A downregulates the most prevalent MICA allele: MICA*008, to evade NK cell-mediated killing. PLoS Pathog. 2021 May 3;17(5):e1008807.

277. Lurain NS, Fox AM, Lichy HM, Bhorade SM, Ware CF, Huang DD, et al. Analysis of the human cytomegalovirus genomic region from UL146 through UL147A reveals sequence hypervariability, genotypic stability, and overlapping transcripts. Virology Journal. 2006 Jan 12;3(1):4.

278. Tao R, Xu J, Gao HH, Zhao WT, Shang SQ. Characteristics and functions of human cytomegalovirus UL128 gene/protein. Acta Virol. 2014;58(2):103–7.

279. Patrone M, Secchi M, Fiorina L, Ierardi M, Milanesi G, Gallina A. Human Cytomegalovirus UL130 Protein Promotes Endothelial Cell Infection through a Producer Cell Modification of the Virion. Journal of Virology. 2005 July;79(13):8361–73.

280. Freeman MR, Dooley AL, Beucler MJ, Sanders W, Moorman NJ, O'Connor CM, et al. The Human Cytomegalovirus vGPCR UL33 is Essential for Efficient Lytic Replication in Epithelial Cells [Internet]. bioRxiv; 2024 [cited 2025 Sept 12]. p. 2024.09.18.609710. Available from: https://www.biorxiv.org/content/10.1101/2024.09.18.609710v1

281. Fraile-Ramos A, Pelchen-Matthews A, Kledal TN, Browne H, Schwartz TW, Marsh M. Localization of HCMV UL33 and US27 in endocytic compartments and viral membranes. Traffic. 2002 Mar;3(3):218–32.

282. Casarosa P, Gruijthuijsen YK, Michel D, Beisser PS, Holl J, Fitzsimons CP, et al. Constitutive Signaling of the Human Cytomegalovirus-encoded Receptor UL33 Differs from That of Its Rat Cytomegalovirus Homolog R33 by Promiscuous Activation of G Proteins of the Gq, Gi, and Gs Classes*. Journal of Biological Chemistry. 2003 Dec 12;278(50):50010–23.

283. Michel D, Milotić I, Wagner M, Vaida B, Holl J, Ansorge R, et al. The human cytomegalovirus UL78 gene is highly conserved among clinical isolates, but is dispensable for replication in fibroblasts and a renal artery organ-culture system. Journal of General Virology. 2005;86(2):297–306.

284. Frank T, Niemann I, Reichel A, Stamminger T. Emerging roles of cytomegalovirus-encoded G protein-coupled receptors during lytic and latent infection. Med Microbiol Immunol. 2019 Aug 1;208(3):447–56.

285. Chen Y, Li Y, Zhou Q, Cong Z, Lin S, Yan J, et al. A homotrimeric GPCR architecture of the human cytomegalovirus revealed by cryo-EM. Cell Discov. 2024 May 16;10(1):1–4.

286. O'Connor CM, Shenk T. Human Cytomegalovirus pUL78 G Protein-Coupled Receptor Homologue Is Required for Timely Cell Entry in Epithelial Cells but Not Fibroblasts. J Virol. 2012 Nov;86(21):11425–33.

287. Niemann I, Reichel A, Stamminger T. Intracellular Trafficking of the Human Cytomegalovirus-Encoded 7-trans-Membrane Protein Homologs pUS27 and pUL78 during Viral Infection: A Comparative Analysis. Viruses. 2014 Feb 10;6(2):661–82.

288. Tadagaki K, Tudor D, Gbahou F, Tschische P, Waldhoer M, Bomsel M, et al. Human cytomegalovirus-encoded UL33 and UL78 heteromerize with host CCR5 and CXCR4 impairing their HIV coreceptor activity. Blood. 2012 May 24;119(21):4908–18.

289. Tschische P, Tadagaki K, Kamal M, Jockers R, Waldhoer M. Heteromerization of human cytomegalovirus encoded chemokine receptors. Biochemical Pharmacology. 2011 Sept 15;82(6):610–9.

290. Schwartz M, Stern-Ginossar N. The Transcriptome of Latent Human Cytomegalovirus. J Virol. 2019 May 15;93(11):e00047-19.

291. Cheng S, Caviness K, Buehler J, Smithey M, Nikolich-Žugich J, Goodrum F. Transcriptome-wide characterization of human cytomegalovirus in natural infection and experimental latency. Proceedings of the National Academy of Sciences. 2017 Dec 5;114(49):E10586–95.

292. Scarborough JA, Paul JR, Spencer JV. Evolution of the ability to modulate host chemokine networks via gene duplication in Human Cytomegalovirus (HCMV). Infect Genet Evol. 2017 July;51:46–53.

293. Lares AP, Tu CC, Spencer JV. The Human Cytomegalovirus US27 gene product enhances cell proliferation and alters cellular gene expression. Virus Res. 2013 Sept;176(0):312–20.

294. Arnolds KL, Lares AP, Spencer JV. The US27 Gene Product of Human Cytomegalovirus Enhances Signaling of Host Chemokine Receptor CXCR4. Virology. 2013 May 10;439(2):122–31.

295. Boeck JM, Stowell GA, O'Connor CM, Spencer JV. The Human Cytomegalovirus US27 Gene Product Constitutively Activates Antioxidant Response Element-Mediated Transcription through Gβγ, Phosphoinositide 3-Kinase, and Nuclear Respiratory Factor 1. J Virol. 2018 Dec 1;92(23):e00644-18.

296. Krishna BA, Miller WE, O'Connor CM. US28: HCMV's Swiss Army Knife. Viruses. 2018 Aug 20;10(8):445.

297. Billstrom MA, Johnson GL, Avdi NJ, Worthen GS. Intracellular Signaling by the Chemokine Receptor US28 during Human Cytomegalovirus Infection. J Virol. 1998 July;72(7):5535–44.

298. Bongers G, Maussang D, Muniz LR, Noriega VM, Fraile-Ramos A, Barker N, et al. The cytomegalovirus-encoded chemokine receptor US28 promotes intestinal neoplasia in transgenic mice. J Clin Invest. 2010 Nov;120(11):3969–78.

299. Amărandi RM, Lückmann M, Melynis M, Jakobsen MH, Fallah Z, Spiess K, et al. Ligand-selective small molecule modulators of the constitutively active vGPCR US28. European Journal of Medicinal Chemistry. 2018 July 15;155:244–54.

300. Fraile-Ramos A, Kledal TN, Pelchen-Matthews A, Bowers K, Schwartz TW, Marsh M. The Human Cytomegalovirus US28 Protein Is Located in Endocytic Vesicles and Undergoes Constitutive Endocytosis and Recycling. MBoC. 2001 June;12(6):1737–49.

301. Daly CA, Smit MJ, Plouffe B. The constitutive activity of the viral-encoded G protein-coupled receptor US28 supports a complex signalling network contributing to cancer development. Biochemical Society Transactions. 2020 Aug 11;48(4):1493–504.

302. Vieira J, Schall TJ, Corey L, Geballe AP. Functional Analysis of the Human Cytomegalovirus US28 Gene by Insertion Mutagenesis with the Green Fluorescent Protein Gene. J Virol. 1998 Oct;72(10):8158–65.

303. Streblow DN, Soderberg-Naucler C, Vieira J, Smith P, Wakabayashi E, Ruchti F, et al. The Human Cytomegalovirus Chemokine Receptor US28 Mediates Vascular Smooth Muscle Cell Migration. Cell. 1999 Nov 24;99(5):511–20.

304. Streblow DN, Vomaske J, Smith P, Melnychuk R, Hall L, Pancheva D, et al. Human Cytomegalovirus Chemokine Receptor US28-induced Smooth Muscle Cell Migration Is Mediated by Focal Adhesion Kinase and Src*. Journal of Biological Chemistry. 2003 Dec 12;278(50):50456–65.

305. Vomaske J, Varnum S, Melnychuk R, Smith P, Pasa-Tolic L, Shutthanandan JI, et al. HCMV pUS28 initiates pro-migratory signaling via activation of Pyk2 kinase. Herpesviridae. 2010 Dec 7;1:2.

306. Vomaske J, Nelson JA, Streblow DN. Human Cytomegalovirus US28: a functionally selective chemokine binding receptor. Infect Disord Drug Targets. 2009 Nov;9(5):548–56.

307. Langemeijer EV, Slinger E, de Munnik S, Schreiber A, Maussang D, Vischer H, et al. Constitutive ß-Catenin Signaling by the Viral Chemokine Receptor US28. PLoS One. 2012 Nov 8;7(11):e48935.

308. Maussang D, Verzijl D, van Walsum M, Leurs R, Holl J, Pleskoff O, et al. Human cytomegalovirus-encoded chemokine receptor US28 promotes tumorigenesis. Proc Natl Acad Sci U S A. 2006 Aug 29;103(35):13068–73.

309. Moepps B, Tulone C, Kern C, Minisini R, Michels G, Vatter P, et al. Constitutive serum response factor activation by the viral chemokine receptor homologue pUS28 is differentially regulated by Gαq/11 and Gα16. Cellular Signalling. 2008 Aug 1;20(8):1528–37.

310. Slinger E, Maussang D, Schreiber A, Siderius M, Rahbar A, Fraile-Ramos A, et al. HCMV-encoded chemokine receptor US28 mediates proliferative signaling through the IL-6-STAT3 axis. Sci Signal. 2010 Aug 3;3(133):ra58.

311. Bodaghi B, Jones TR, Zipeto D, Vita C, Sun L, Laurent L, et al. Chemokine Sequestration by Viral Chemoreceptors as a Novel Viral Escape Strategy: Withdrawal of Chemokines from the Environment of Cytomegalovirus-infected Cells. J Exp Med. 1998 Sept 7;188(5):855–66.

312. Yang Z, Bjorkman PJ. Structure of UL18, a peptide-binding viral MHC mimic, bound to a host inhibitory receptor. Proceedings of the National Academy of Sciences. 2008 July 22;105(29):10095–100.

313. Prod'homme V, Griffin C, Aicheler RJ, Wang ECY, McSharry BP, Rickards CR, et al. The Human Cytomegalovirus MHC Class I Homolog UL18 Inhibits LIR-1+ but Activates LIR-1− NK Cells. J Immunol. 2007 Apr 1;178(7):4473–81.

314. Cosman D, Fanger N, Borges L, Kubin M, Chin W, Peterson L, et al. A Novel Immunoglobulin Superfamily Receptor for Cellular and Viral MHC Class I Molecules. Immunity. 1997 Aug 1;7(2):273–82.

315. Hewitt EW, Gupta SS, Lehner PJ. The human cytomegalovirus gene product US6 inhibits ATP binding by TAP. EMBO J. 2001 Feb 1;20(3):387–96.

316. Misaghi S, Sun ZYJ, Stern P, Gaudet R, Wagner G, Ploegh H. Structural and functional analysis of human cytomegalovirus US3 protein. J Virol. 2004 Jan;78(1):413–23.

317. Kim Y, Park B, Cho S, Shin J, Cho K, Jun Y, et al. Human Cytomegalovirus UL18 Utilizes US6 for Evading the NK and T-Cell Responses. PLoS Pathog. 2008 Aug 8;4(8):e1000123.

318. Poole E, Neves TC, Oliveira MT, Sinclair J, da Silva MCC. Human Cytomegalovirus Interleukin 10 Homologs: Facing the Immune System. Front Cell Infect Microbiol. 2020 June 9;10:245.

319. Avdic S, McSharry BP, Steain M, Poole E, Sinclair J, Abendroth A, et al. Human Cytomegalovirus-Encoded Human Interleukin-10 (IL-10) Homolog Amplifies Its Immunomodulatory Potential by Upregulating Human IL-10 in Monocytes. J Virol. 2016 Mar 28;90(8):3819–27.

320. Poole E, Avdic S, Hodkinson J, Jackson S, Wills M, Slobedman B, et al. Latency-associated viral interleukin-10 (IL-10) encoded by human cytomegalovirus modulates cellular IL-10 and CCL8 Secretion during latent infection through changes in the cellular microRNA hsa-miR-92a. J Virol. 2014 Dec;88(24):13947–55.

321. Chang WLW, Baumgarth N, Yu D, Barry PA. Human Cytomegalovirus-Encoded Interleukin-10 Homolog Inhibits Maturation of Dendritic Cells and Alters Their Functionality. J Virol. 2004 Aug;78(16):8720–31.

322. Peppenelli M, Buehler J, Goodrum F. Human Hematopoietic Long-Term Culture (hLTC) for Human Cytomegalovirus Latency and Reactivation. Methods Mol Biol. 2021;2244:83–101.

323. Crawford LB. Human Embryonic Stem Cells as a Model for Hematopoietic Stem Cell Differentiation and Viral Infection. Current Protocols. 2022;2(12):e622.

324. Goodrum FD, Jordan CT, High K, Shenk T. Human cytomegalovirus gene expression during infection of primary hematopoietic progenitor cells: A model for latency. Proceedings of the National Academy of Sciences. 2002 Dec 10;99(25):16255–60.

325. Hakki M, Goldman DC, Streblow DN, Hamlin KL, Krekylwich CN, Fleming WH, et al. HCMV infection of humanized mice after transplantation of G-CSF-mobilized peripheral blood stem cells from HCMV-seropositive donors. Biol Blood Marrow Transplant. 2014 Jan;20(1):132–5.

326. Crawford LB, Hancock MH, Struthers HM, Streblow DN, Yurochko AD, Caposio P, et al. CD34+ Hematopoietic Progenitor Cell Subsets Exhibit Differential Ability To Maintain Human Cytomegalovirus Latency and Persistence. J Virol. 2021 Jan 13;95(3):e02105-20.

327. Smith MS, Bentz GL, Alexander JS, Yurochko AD. Human cytomegalovirus induces monocyte differentiation and migration as a strategy for dissemination and persistence. J Virol. 2004 May;78(9):4444–53.

328. Collins-McMillen D, Chesnokova L, Lee BJ, Fulkerson HL, Brooks R, Mosher BS, et al. HCMV Infection and Apoptosis: How Do Monocytes Survive HCMV Infection? Viruses. 2018 Sept 29;10(10):533.

329. Lin YP, Frye AM, Nowak TA, Kraiczy P. New Insights Into CRASP-Mediated Complement Evasion in the Lyme Disease Enzootic Cycle. Front Cell Infect Microbiol. 2020;10:1.

330. Chesnokova LS, Mosher BS, Fulkerson HL, Nam HW, Shakya AK, Yurochko AD. Distinct early role of PTEN regulation during HCMV infection of monocytes. Proc Natl Acad Sci U S A. 2024 Mar 19;121(12):e2312290121.

331. Kim JH, Collins-McMillen D, Caposio P, Yurochko AD. Viral binding-induced signaling drives a unique and extended intracellular trafficking pattern during infection of primary monocytes. Proceedings of the National Academy of Sciences of the United States of America. 2016 Aug 8;113(31):8819.

332. Collins-McMillen D, Rak M, Buehler JC, Igarashi-Hayes S, Kamil JP, Moorman NJ, et al. Alternative promoters drive human cytomegalovirus reactivation from latency. Proc Natl Acad Sci U S A. 2019 Aug 27;116(35):17492–7.

333. Shultz LD, Lyons BL, Burzenski LM, Gott B, Chen X, Chaleff S, et al. Human lymphoid and myeloid cell development in NOD/LtSz-scid IL2R gamma null mice engrafted with mobilized human hemopoietic stem cells. J Immunol. 2005 May 15;174(10):6477–89.

334. Brehm MA, Wiles MV, Greiner DL, Shultz LD. Generation of improved humanized mouse models for human infectious diseases. J Immunol Methods. 2014 Aug;410:3–17.

335. Crawford LB, Tempel R, Streblow DN, Kreklywich C, Smith P, Picker LJ, et al. Human Cytomegalovirus Induces Cellular and Humoral Virus-specific Immune Responses in Humanized BLT Mice. Sci Rep. 2017 Apr 20;7:937.

336. Seckert CK, Renzaho A, Tervo HM, Krause C, Deegen P, Kühnapfel B, et al. Liver sinusoidal endothelial cells are a site of murine cytomegalovirus latency and reactivation. J Virol. 2009 Sept;83(17):8869–84.

337. Liu XF, Swaminathan S, Yan S, Engelmann F, Abbott DA, VanOsdol LA, et al. A novel murine model of differentiation-mediated cytomegalovirus reactivation from latently infected bone marrow haematopoietic cells. J Gen Virol. 2019 Dec;100(12):1680–94.

338. Munks MW, Rott K, Nesterenko PA, Smart SM, Williams V, Tatum A, et al. Latent CMV infection of Lymphatic endothelial cells is sufficient to drive CD8 T cell memory inflation. PLoS Pathog. 2023 Jan;19(1):e1010351.

339. Smith LM, McWhorter AR, Masters LL, Shellam GR, Redwood AJ. Laboratory Strains of Murine Cytomegalovirus Are Genetically Similar to but Phenotypically Distinct from Wild Strains of Virus. J Virol. 2008 July;82(13):6689–96.

340. Loh HS, Mohd-Lila MA, Abdul-Rahman SO, Kiew LJ. Pathogenesis and vertical transmission of a transplacental rat cytomegalovirus. Virol J. 2006 June 1;3:42.

341. Kilham L, Ferm VH. RAT VIRUS (RV) INFECTIONS OF PREGNANT, FETAL AND NEWBORN RATS. Proc Soc Exp Biol Med. 1964 Dec;117:874–9.

342. Bruggeman CA, Meijer H, Bosman F, van Boven CP. Biology of rat cytomegalovirus infection. Intervirology. 1985;24(1):1–9.

343. Oxford KL, Strelow L, Yue Y, Chang WLW, Schmidt KA, Diamond DJ, et al. Open reading frames carried on UL/b' are implicated in shedding and horizontal transmission of rhesus cytomegalovirus in rhesus monkeys. J Virol. 2011 May;85(10):5105–14.

344. Wussow F, Yue Y, Martinez J, Deere JD, Longmate J, Herrmann A, et al. A vaccine based on the rhesus cytomegalovirus UL128 complex induces broadly neutralizing antibodies in rhesus macaques. J Virol. 2013 Feb;87(3):1322–32.

345. Pande NT, Powers C, Ahn K, Früh K. Rhesus cytomegalovirus contains functional homologues of US2, US3, US6, and US11. J Virol. 2005 May;79(9):5786–98.

346. Hansen SG, Marshall EE, Malouli D, Ventura AB, Hughes CM, Ainslie E, et al. A live-attenuated RhCMV/SIV vaccine shows long-term efficacy against heterologous SIV challenge. Sci Transl Med. 2019 July 17;11(501):eaaw2607.

347. Hansen SG, Womack JL, Perez W, Schmidt KA, Marshall E, Iyer RF, et al. Late gene expression–deficient cytomegalovirus vectors elicit conventional T cells that do not protect

against SIV. JCI Insight [Internet]. 2023 Mar 22 [cited 2025 Sept 12];8(6). Available from: https://insight.jci.org/articles/view/164692

348. Malouli D, Hansen SG, Hancock MH, Hughes CM, Ford JC, Gilbride RM, et al. Cytomegaloviral Determinants of CD8+ T Cell Programming and RhCMV/SIV Vaccine Efficacy. Sci Immunol. 2021 Mar 25;6(57):eabg5413.

349. Fowler K, Mucha J, Neumann M, Lewandowski W, Kaczanowska M, Grys M, et al. A systematic literature review of the global seroprevalence of cytomegalovirus: possible implications for treatment, screening, and vaccine development. BMC Public Health. 2022 Sept 1;22(1):1659.

350. Lachmann R, Loenenbach A, Waterboer T, Brenner N, Pawlita M, Michel A, et al. Cytomegalovirus (CMV) seroprevalence in the adult population of Germany. PLoS One. 2018;13(7):e0200267.

351. Goodrum F, Jordan CT, Terhune SS, High K, Shenk T. Differential outcomes of human cytomegalovirus infection in primitive hematopoietic cell subpopulations. Blood. 2004 Aug 1;104(3):687–95.

352. Boström L, Ringdén O, Jacobsen N, Zwaan F, Nilsson B. A European multicenter study of chronic graft-versus-host disease. The role of cytomegalovirus serology in recipients and donors--acute graft-versus-host disease, and splenectomy. Transplantation. 1990 June 1;49(6):1100–5.

353. Fishman JA. Infection in Organ Transplantation. Am J Transplant. 2017 Apr;17(4):856–79.

354. Grattan MT, Moreno-Cabral CE, Starnes VA, Oyer PE, Stinson EB, Shumway NE. Cytomegalovirus infection is associated with cardiac allograft rejection and atherosclerosis. JAMA. 1989 June 23;261(24):3561–6.

355. Lao WC, Lee D, Burroughs AK, Lanzani G, Rolles K, Emery VC, et al. Use of polymerase chain reaction to provide prognostic information on human cytomegalovirus disease after liver transplantation. J Med Virol. 1997 Mar;51(3):152–8.

356. Lautenschlager I, Höckerstedt K, Jalanko H, Loginov R, Salmela K, Taskinen E, et al. Persistent cytomegalovirus in liver allografts with chronic rejection. Hepatology. 1997 Jan;25(1):190–4.

357. Lönnqvist B, Ringdén O, Wahren B, Gahrton G, Lundgren G. Cytomegalovirus infection associated with and preceding chronic graft-versus-host disease. Transplantation. 1984 Nov;38(5):465–8.

358. Meyers JD, Flournoy N, Thomas ED. Risk factors for cytomegalovirus infection after human marrow transplantation. J Infect Dis. 1986 Mar;153(3):478–88.

359. Reinke P, Fietze E, Ode-Hakim S, Prösch S, Lippert J, Ewert R, et al. Late-acute renal allograft rejection and symptomless cytomegalovirus infection. Lancet. 1994 Dec 24;344(8939–8940):1737–8.

360. Casarosa P, Bakker RA, Verzijl D, Navis M, Timmerman H, Leurs R, et al. Constitutive signaling of the human cytomegalovirus-encoded chemokine receptor US28. J Biol Chem. 2001 Jan 12;276(2):1133–7.

361. Maussang D, Langemeijer E, Fitzsimons CP, Stigter-van Walsum M, Dijkman R, Borg MK, et al. The Human Cytomegalovirus–Encoded Chemokine Receptor US28 Promotes Angiogenesis and Tumor Formation via Cyclooxygenase-2. Cancer Research. 2009 Apr 1;69(7):2861–9.

362. McLean KA, Holst PJ, Martini L, Schwartz TW, Rosenkilde MM. Similar activation of signal transduction pathways by the herpesvirus-encoded chemokine receptors US28 and ORF74. Virology. 2004 Aug 1;325(2):241–51.

363. Vischer HF, Siderius M, Leurs R, Smit MJ. Herpesvirus-encoded GPCRs: neglected players in inflammatory and proliferative diseases? Nat Rev Drug Discov. 2014 Feb;13(2):123–39.

364. Patterson BK, Landay A, Andersson J, Brown C, Behbahani H, Jiyamapa D, et al. Repertoire of chemokine receptor expression in the female genital tract: implications for human immunodeficiency virus transmission. Am J Pathol. 1998 Aug;153(2):481–90.

365. Boomker JM, Verschuuren EAM, Brinker MGL, de Leij LFMH, The TH, Harmsen MC. Kinetics of US28 gene expression during active human cytomegalovirus infection in lung-transplant recipients. J Infect Dis. 2006 June 1;193(11):1552–6.

366. Lollinga WT, de Wit RH, Rahbar A, Vasse GF, Davoudi B, Diepstra A, et al. Human Cytomegalovirus-Encoded Receptor US28 Is Expressed in Renal Allografts and Facilitates Viral Spreading In Vitro. Transplantation. 2017 Mar;101(3):531–40.

367. Gao JL, Murphy PM. Human cytomegalovirus open reading frame US28 encodes a functional beta chemokine receptor. Journal of Biological Chemistry. 1994 Nov 18;269(46):28539–42.

368. Kledal TN, Rosenkilde MM, Schwartz TW. Selective recognition of the membrane-bound CX3C chemokine, fractalkine, by the human cytomegalovirus-encoded broad-spectrum receptor US28. FEBS Lett. 1998 Dec 18;441(2):209–14.

369. Kuhn DE, Beall CJ, Kolattukudy PE. The Cytomegalovirus US28 Protein Binds Multiple CC Chemokines with High Affinity. Biochemical and Biophysical Research Communications. 1995 June 6;211(1):325–30.

370. Melnychuk RM, Streblow DN, Smith PP, Hirsch AJ, Pancheva D, Nelson JA. Human cytomegalovirus-encoded G protein-coupled receptor US28 mediates smooth muscle cell migration through Galpha12. J Virol. 2004 Aug;78(15):8382–91.

371. Azoitei ML, Noh J, Marston DJ, Roudot P, Marshall CB, Daugird TA, et al. Spatiotemporal dynamics of GEF-H1 activation controlled by microtubule- and Src-mediated pathways. J Cell Biol. 2019 Sept 2;218(9):3077–97.

372. Ridley AJ. Rho GTPase signalling in cell migration. Curr Opin Cell Biol. 2015 Oct;36:103–12.

373. Mellacheruvu D, Wright Z, Couzens AL, Lambert JP, St-Denis NA, Li T, et al. The CRAPome: a contaminant repository for affinity purification-mass spectrometry data. Nat Methods. 2013 Aug;10(8):730–6.

374. Fabregat A, Korninger F, Viteri G, Sidiropoulos K, Marin-Garcia P, Ping P, et al. Reactome graph database: Efficient access to complex pathway data. PLoS Comput Biol. 2018 Jan;14(1):e1005968.

375. Nobre LV, Nightingale K, Ravenhill BJ, Antrobus R, Soday L, Nichols J, et al. Human cytomegalovirus interactome analysis identifies degradation hubs, domain associations and viral protein functions. Garrett WS, Maes P, Maes P, Szpara ML, editors. eLife. 2019 Dec 24;8:e49894.

376. Aoyagi M, Gaspar M, Shenk TE. Human cytomegalovirus UL69 protein facilitates translation by associating with the mRNA cap-binding complex and excluding 4EBP1. Proc Natl Acad Sci U S A. 2010 Feb 9;107(6):2640–5.

377. Kronemann D, Hagemeier SR, Cygnar D, Phillips S, Bresnahan WA. Binding of the human cytomegalovirus (HCMV) tegument protein UL69 to UAP56/URH49 is not required for efficient replication of HCMV. J Virol. 2010 Sept;84(18):9649–54.

378. Shang X, Marchioni F, Sipes N, Evelyn CR, Jerabek-Willemsen M, Duhr S, et al. Rational design of small molecule inhibitors targeting RhoA subfamily Rho GTPases. Chem Biol. 2012 June 22;19(6):699–710.

379. Shang X, Marchioni F, Evelyn CR, Sipes N, Zhou X, Seibel W, et al. Small-molecule inhibitors targeting G-protein–coupled Rho guanine nucleotide exchange factors. Proc Natl Acad Sci U S A. 2013 Feb 19;110(8):3155–60.

380. Lu H, Zhou Q, He J, Jiang Z, Peng C, Tong R, et al. Recent advances in the development of protein–protein interactions modulators: mechanisms and clinical trials. Sig Transduct Target Ther. 2020 Sept 23;5(1):1–23.

381. Nguyen TN, Goodrich JA. Protein-protein interaction assays: eliminating false positive interactions. Nat Methods. 2006 Feb;3(2):135–9.

382. Rao VS, Srinivas K, Sujini GN, Kumar GNS. Protein-Protein Interaction Detection: Methods and Analysis. Int J Proteomics. 2014;2014:147648.

383. Diggins NL, Skalsky RL, Hancock MH. Regulation of Latency and Reactivation by Human Cytomegalovirus miRNAs. Pathogens. 2021 Feb;10(2):200.

384. Umashankar M, Goodrum F. Hematopoietic long-term culture (hLTC) for human cytomegalovirus latency and reactivation. Methods Mol Biol. 2014;1119:99–112.

385. Chen W, Zhao Y, Li XC, Kubiak JZ, Ghobrial RM, Kloc M. Rho-specific Guanine nucleotide exchange factors (Rho-GEFs) inhibition affects macrophage phenotype and disrupts Golgi complex. Int J Biochem Cell Biol. 2017 Dec;93:12–24.

386. Singh NK, Janjanam J, Rao GN. p115 RhoGEF activates the Rac1 GTPase signaling cascade in MCP1 chemokine-induced vascular smooth muscle cell migration and proliferation. J Biol Chem. 2017 Aug 25;292(34):14080–91.

387. Cervantes-Villagrana RD, Color-Aparicio VM, Reyes-Cruz G, Vázquez-Prado J. Protumoral bone marrow-derived cells migrate via Gβγ-dependent signaling pathways and exhibit a complex repertoire of RhoGEFs. J Cell Commun Signal. 2019 June;13(2):179–91.

388. Branon TC, Bosch JA, Sanchez AD, Udeshi ND, Svinkina T, Carr SA, et al. Efficient proximity labeling in living cells and organisms with TurboID. Nat Biotechnol. 2018 Oct;36(9):880–7.

389. Eng JK, McCormack AL, Yates JR. An approach to correlate tandem mass spectral data of peptides with amino acid sequences in a protein database. J Am Soc Mass Spectrom. 1994 Nov;5(11):976–89.

390. The M, MacCoss MJ, Noble WS, Käll L. Fast and Accurate Protein False Discovery Rates on Large-Scale Proteomics Data Sets with Percolator 3.0. J Am Soc Mass Spectrom. 2016 Nov;27(11):1719–27.

391. Szklarczyk D, Gable AL, Nastou KC, Lyon D, Kirsch R, Pyysalo S, et al. The STRING database in 2021: customizable protein-protein networks, and functional characterization of user-uploaded gene/measurement sets. Nucleic Acids Res. 2021 Jan 8;49(D1):D605–12.

392. Livak KJ, Schmittgen TD. Analysis of relative gene expression data using real-time quantitative PCR and the 2(-Delta Delta C(T)) Method. Methods. 2001 Dec;25(4):402–8.

393. Griffiths P, Reeves M. Pathogenesis of human cytomegalovirus in the immunocompromised host. Nat Rev Microbiol. 2021 Dec;19(12):759–73.

394. Poole E, Sinclair J. Latency-associated upregulation of SERBP1 is important for the recruitment of transcriptional repressors to the viral major immediate early promoter of human cytomegalovirus during latent carriage. Frontiers in Microbiology [Internet]. 2022 [cited 2023 July 8];13. Available from: https://www.frontiersin.org/articles/10.3389/fmicb.2022.999290

395. Zhuravskaya T, Maciejewski JP, Netski DM, Bruening E, Mackintosh FR, St Jeor S. Spread of Human Cytomegalovirus (HCMV) After Infection of Human Hematopoietic Progenitor Cells: Model of HCMV Latency. Blood. 1997 Sept 15;90(6):2482–91.

396. Farrell HE, Bruce K, Lawler C, Oliveira M, Cardin R, Davis-Poynter N, et al. Murine Cytomegalovirus Spreads by Dendritic Cell Recirculation. mBio. 2017 Oct 3;8(5):10.1128/mbio.01264-17.

397. Panda K, Parashar D, Viswanathan R. An Update on Current Antiviral Strategies to Combat Human Cytomegalovirus Infection. Viruses. 2023 June;15(6):1358.

398. Perera MR, Wills MR, Sinclair JH. HCMV Antivirals and Strategies to Target the Latent Reservoir. Viruses. 2021 May 1;13(5):817.

399. Overington JP, Al-Lazikani B, Hopkins AL. How many drug targets are there? Nat Rev Drug Discov. 2006 Dec;5(12):993–6.

400. Wettschureck N, Offermanns S. Mammalian G proteins and their cell type specific functions. Physiol Rev. 2005 Oct;85(4):1159–204.

401. Jones EM, Lubock NB, Venkatakrishnan A, Wang J, Tseng AM, Paggi JM, et al. Structural and functional characterization of G protein–coupled receptors with deep mutational scanning. Larhammar D, Aldrich RW, Fraser JS, Manglik A, editors. eLife. 2020 Oct 21;9:e54895.

402. Nygaard R, Frimurer TM, Holst B, Rosenkilde MM, Schwartz TW. Ligand binding and micro-switches in 7TM receptor structures. Trends Pharmacol Sci. 2009 May;30(5):249–59.

403. Oliveira SA, Shenk TE. Murine cytomegalovirus M78 protein, a G protein-coupled receptor homologue, is a constituent of the virion and facilitates accumulation of immediate-early viral mRNA. Proc Natl Acad Sci U S A. 2001 Mar 13;98(6):3237–42.

404. Miller WE, Houtz DA, Nelson CD, Kolattukudy PE, Lefkowitz RJ. G-protein-coupled Receptor (GPCR) Kinase Phosphorylation and β-Arrestin Recruitment Regulate the Constitutive Signaling Activity of the Human Cytomegalovirus US28 GPCR *. Journal of Biological Chemistry. 2003 June 13;278(24):21663–71.

405. Waldhoer M, Kledal TN, Farrell H, Schwartz TW. Murine Cytomegalovirus (CMV) M33 and Human CMV US28 Receptors Exhibit Similar Constitutive Signaling Activities. Journal of Virology. 2002 Aug 15;76(16):8161–8.

406. Cambien B, Pomeranz M, Schmid-Antomarchi H, Millet MA, Breittmayer V, Rossi B, et al. Signal transduction pathways involved in soluble fractalkine-induced monocytic cell adhesion. Blood. 2001 Apr 1;97(7):2031–7.

407. Kledal TN, Rosenkilde MM, Coulin F, Simmons G, Johnsen AH, Alouani S, et al. A Broad-Spectrum Chemokine Antagonist Encoded by Kaposi's Sarcoma-Associated Herpesvirus. Science. 1997 Sept 12;277(5332):1656–9.

408. Teo WH, Chen HP, Huang JC, Chan YJ. Human cytomegalovirus infection enhances cell proliferation, migration and upregulation of EMT markers in colorectal cancer-derived stem cell-like cells. International Journal of Oncology. 2017 Nov 1;51(5):1415–26.

409. Goodrum F. The complex biology of human cytomegalovirus latency. Adv Virus Res. 2022;112:31–85.

410. Hancock MH, Nelson JA. Modulation of the NFκb Signalling Pathway by Human Cytomegalovirus. Virology (Hyderabad). 2017 Aug;1(1):104.

411. Dupont L, Reeves MB. Cytomegalovirus latency and reactivation: Recent insights into an age old problem. Rev Med Virol. 2016 Mar;26(2):75–89.

412. Forte E, Zhang Z, Thorp EB, Hummel M. Cytomegalovirus Latency and Reactivation: An Intricate Interplay With the Host Immune Response. Frontiers in Cellular and Infection Microbiology [Internet]. 2020 [cited 2023 Mar 13];10. Available from: https://www.frontiersin.org/articles/10.3389/fcimb.2020.00130

413. Forte E, Swaminathan S, Schroeder MW, Kim JY, Terhune SS, Hummel M. Tumor Necrosis Factor Alpha Induces Reactivation of Human Cytomegalovirus Independently of Myeloid Cell Differentiation following Posttranscriptional Establishment of Latency. mBio. 2018 Sept 11;9(5):e01560-18.

414. Taniguchi M, Suzumura K ichi, Nagai K, Kawasaki T, Takasaki J, Sekiguchi M, et al. YM-254890 analogues, novel cyclic depsipeptides with Gαq/11 inhibitory activity from Chromobacterium sp. QS3666. Bioorganic & Medicinal Chemistry. 2004 June 15;12(12):3125–33.

415. Yurochko AD, editor. Human Cytomegaloviruses: Methods and Protocols [Internet]. New York, NY: Springer US; 2021 [cited 2023 May 31]. (Methods in Molecular Biology; vol. 2244). Available from: https://link.springer.com/10.1007/978-1-0716-1111-1

416. Hu Y, Smyth GK. ELDA: extreme limiting dilution analysis for comparing depleted and enriched populations in stem cell and other assays. J Immunol Methods. 2009 Aug 15;347(1–2):70–8.

417. Chee MJS, Mörl K, Lindner D, Merten N, Zamponi GW, Light PE, et al. The Third Intracellular Loop Stabilizes the Inactive State of the Neuropeptide Y1 Receptor. J Biol Chem. 2008 Nov 28;283(48):33337–46.

418. DeGraff JL, Gurevich VV, Benovic JL. The Third Intracellular Loop of α2-Adrenergic Receptors Determines Subtype Specificity of Arrestin Interaction*. Journal of Biological Chemistry. 2002 Nov 8;277(45):43247–52.

419. Prasad Pydi S, Singh N, Upadhyaya J, Pal Bhullar R, Chelikani P. The third intracellular loop plays a critical role in bitter taste receptor activation. Biochimica et Biophysica Acta (BBA) - Biomembranes. 2014 Jan 1;1838(1, Part B):231–6.

420. Sadler F, Ma N, Ritt M, Sharma Y, Vaidehi N, Sivaramakrishnan S. Autoregulation of GPCR signalling through the third intracellular loop. Nature. 2023 Mar 8;1–8.

421. Timossi C, Ortiz-Elizondo C, Pineda DB, Dias JA, Conn PM, Ulloa-Aguirre A. Functional significance of the BBXXB motif reversed present in the cytoplasmic domains of the human follicle-stimulating hormone receptor. Molecular and Cellular Endocrinology. 2004 Aug 31;223(1):17–26.

422. Wess J. The third intracellular loop of GPCRs: size matters. Trends in Pharmacological Sciences. 2023 Aug 1;44(8):492–4.

423. Miles TF, Spiess K, Jude KM, Tsutsumi N, Burg JS, Ingram JR, et al. Viral GPCR US28 can signal in response to chemokine agonists of nearly unlimited structural degeneracy. Kuriyan J, editor. eLife. 2018 June 8;7:e35850.

424. Boomker JM, The TH, de Leij LFMH, Harmsen MC. The human cytomegalovirus-encoded receptor US28 increases the activity of the major immediate-early promoter/enhancer. Virus Res. 2006 June;118(1–2):196–200.

425. Laschet C, Dupuis N, Hanson J. A dynamic and screening-compatible nanoluciferase-based complementation assay enables profiling of individual GPCR–G protein interactions. Journal of Biological Chemistry. 2019 Mar 15;294(11):4079–90.

426. Pleskoff O, Casarosa P, Verneuil L, Ainoun F, Beisser P, Smit M, et al. The human cytomegalovirus-encoded chemokine receptor US28 induces caspase-dependent apoptosis. The FEBS Journal. 2005;272(16):4163–77.

427. Minisini R, Tulone C, Lüske A, Michel D, Mertens T, Gierschik P, et al. Constitutive inositol phosphate formation in cytomegalovirus-infected human fibroblasts is due to expression of the chemokine receptor homologue pUS28. J Virol. 2003 Apr;77(8):4489–501.

428. Inoue A, Raimondi F, Kadji FMN, Singh G, Kishi T, Uwamizu A, et al. Illuminating G-Protein-Coupling Selectivity of GPCRs. Cell. 2019 June 13;177(7):1933-1947.e25.

429. De Groof TWM, Bergkamp ND, Heukers R, Giap T, Bebelman MP, Goeij-de Haas R, et al. Selective targeting of ligand-dependent and -independent signaling by GPCR conformation-specific anti-US28 intrabodies. Nat Commun. 2021 July 16;12(1):4357.

430. Krishna BA, Humby MS, Miller WE, O'Connor CM. Human cytomegalovirus G protein-coupled receptor US28 promotes latency by attenuating c-fos. Proceedings of the National Academy of Sciences. 2019 Jan 29;116(5):1755–64.

431. Crawford LB, Diggins NL, Caposio P, Hancock MH. Advances in Model Systems for Human Cytomegalovirus Latency and Reactivation. mBio. 2022 Jan 11;13(1):e01724-21.

432. Liu A, Liu Y, Masachs CL del T, Zhang W, Pardo L, Ye RD. Structural basis for constitutive activation and CXCL1 recognition of human herpesvirus 8-encoded G protein-coupled receptor KSHV-GPCR [Internet]. bioRxiv; 2023 [cited 2024 June 25]. p. 2023.12.27.573477. Available from: https://www.biorxiv.org/content/10.1101/2023.12.27.573477v1

433. Tsutsumi N, Qu Q, Mavri M, Baggesen MS, Maeda S, Waghray D, et al. Structural basis for the constitutive activity and immunomodulatory properties of the Epstein-Barr virus-encoded G protein-coupled receptor BILF1. Immunity. 2021 July 13;54(7):1405-1416.e7.

434. Liu C, Sandford G, Fei G, Nicholas J. Gα Protein Selectivity Determinant Specified by a Viral Chemokine Receptor-Conserved Region in the C Tail of the Human Herpesvirus 8 G Protein-Coupled Receptor. Journal of Virology. 2004 Mar;78(5):2460–71.

435. Zuo J, Quinn LL, Tamblyn J, Thomas WA, Feederle R, Delecluse HJ, et al. The Epstein-Barr Virus-Encoded BILF1 Protein Modulates Immune Recognition of Endogenously Processed Antigen by Targeting Major Histocompatibility Complex Class I Molecules Trafficking on both the Exocytic and Endocytic Pathways. Journal of Virology. 2011 Feb 15;85(4):1604–14.

436. Zuo J, Currin A, Griffin BD, Shannon-Lowe C, Thomas WA, Ressing ME, et al. The Epstein-Barr Virus G-Protein-Coupled Receptor Contributes to Immune Evasion by Targeting MHC Class I Molecules for Degradation. PLOS Pathogens. 2009 Jan 2;5(1):e1000255.

437. Pati S, Cavrois M, Guo HG, Foulke JS, Kim J, Feldman RA, et al. Activation of NF-κB by the Human Herpesvirus 8 Chemokine Receptor ORF74: Evidence for a Paracrine Model of Kaposi's Sarcoma Pathogenesis. Journal of Virology. 2001 Sept 15;75(18):8660–73.

438. Smit MJ, Verzijl D, Casarosa P, Navis M, Timmerman H, Leurs R. Kaposi's Sarcoma-Associated Herpesvirus-Encoded G Protein-Coupled Receptor ORF74 Constitutively Activates p44/p42 MAPK and Akt via Gi and Phospholipase C-Dependent Signaling Pathways. Journal of Virology. 2002 Feb 15;76(4):1744–52.

439. Madrid AS, Ganem D. Kaposi's Sarcoma-Associated Herpesvirus ORF54/dUTPase Downregulates a Ligand for the NK Activating Receptor NKp44. Journal of Virology. 2012 Aug 15;86(16):8693–704.

440. Berg C, Rosenkilde MM. Therapeutic targeting of HCMV-encoded chemokine receptor US28: Progress and challenges. Front Immunol. 2023 Feb 13;14:1135280.

441. Thomson JA, Itskovitz-Eldor J, Shapiro SS, Waknitz MA, Swiergiel JJ, Marshall VS, et al. Embryonic Stem Cell Lines Derived from Human Blastocysts. Science. 1998 Nov 6;282(5391):1145–7.

442. Sinzger C, Hahn G, Digel M, Katona R, Sampaio KL, Messerle M, et al. Cloning and sequencing of a highly productive, endotheliotropic virus strain derived from human cytomegalovirus TB40/E. Journal of General Virology. 2008;89(2):359–68.

443. Hancock MH, Hook LM, Mitchell J, Nelson JA. Human Cytomegalovirus MicroRNAs miR-US5-1 and miR-UL112-3p Block Proinflammatory Cytokine Production in Response to NF-κB-Activating Factors through Direct Downregulation of IKKα and IKKβ. mBio. 2017 Mar 7;8(2):e00109-17.

444. Haese NN, May NA, Taft-Benz S, Moukha-Chafiq O, Madadi N, Zhang S, et al. Identification of Quinolinones as Antivirals against Venezuelan Equine Encephalitis Virus. Antimicrob Agents Chemother. 65(9):e00244-21.

445. Thiele S, Mungalpara J, Steen A, Rosenkilde MM, Våbenø J. Determination of the binding mode for the cyclopentapeptide CXCR4 antagonist FC131 using a dual approach of ligand modifications and receptor mutagenesis. British Journal of Pharmacology. 2014;171(23):5313–29.

446. Mavri M, Glišić S, Senćanski M, Vrecl M, Rosenkilde MM, Spiess K, et al. Patterns of human and porcine gammaherpesvirus-encoded BILF1 receptor endocytosis. Cell Mol Biol Lett. 2023 Feb 21;28(1):14.

447. Sundqvist M, Holdfeldt A, Wright SC, Møller TC, Siaw E, Jennbacken K, et al. Barbadin selectively modulates FPR2-mediated neutrophil functions independent of receptor endocytosis. Biochimica et Biophysica Acta (BBA) - Molecular Cell Research. 2020 Dec 1;1867(12):118849.

448. Crawford LB, Tempel R, Streblow DN, Yurochko AD, Goodrum FD, Nelson JA, et al. Human Cytomegalovirus Infection Suppresses CD34+ Progenitor Cell Engraftment in Humanized Mice. Microorganisms. 2020 Apr 6;8(4):525.

449. Söderberg-Nauclér C, Streblow DN, Fish KN, Allan-Yorke J, Smith PP, Nelson JA. Reactivation of latent human cytomegalovirus in CD14(+) monocytes is differentiation dependent. J Virol. 2001 Aug;75(16):7543–54.

450. Söderberg-Nauclér C, Fish KN, Nelson JA. Reactivation of Latent Human Cytomegalovirus by Allogeneic Stimulation of Blood Cells from Healthy Donors. Cell. 1997 Oct 3;91(1):119–26.

451. McSharry BP, Avdic S, Slobedman B. Human Cytomegalovirus Encoded Homologs of Cytokines, Chemokines and their Receptors: Roles in Immunomodulation. Viruses. 2012 Oct 25;4(11):2448–70.

452. Tadagaki K, Nakano K, Yamanishi K. Human Herpesvirus 7 Open Reading Frames U12 and U51 Encode Functional β-Chemokine Receptors. J Virol. 2005 June;79(11):7068–76.

453. Zhen Z, Bradel-Tretheway B, Sumagin S, Bidlack JM, Dewhurst S. The Human Herpesvirus 6 G Protein-Coupled Receptor Homolog U51 Positively Regulates Virus Replication and Enhances Cell-Cell Fusion In Vitro. J Virol. 2005 Sept;79(18):11914–24.

454. Kaptein SJF, Beisser PS, Gruijthuijsen YK, Savelkouls KGM, van Cleef KWR, Beuken E, et al. The rat cytomegalovirus R78 G protein-coupled receptor gene is required for production of infectious virus in the spleen. Journal of General Virology. 2003;84(9):2517–30.

455. Milne RS, Mattick C, Nicholson L, Devaraj P, Alcami A, Gompels UA. RANTES binding and down-regulation by a novel human herpesvirus-6 beta chemokine receptor. J Immunol. 2000 Mar 1;164(5):2396–404.

456. Sharp EL, Davis-Poynter NJ, Farrell HE. Analysis of the subcellular trafficking properties of murine cytomegalovirus M78, a 7 transmembrane receptor homologue. Journal of General Virology. 2009;90(1):59–68.

457. Wagner S, Arnold F, Wu Z, Schubert A, Walliser C, Tadagaki K, et al. The 7-transmembrane protein homologue UL78 of the human cytomegalovirus forms oligomers and traffics between the plasma membrane and different intracellular compartments. Arch Virol. 2012 May;157(5):935–49.

458. Beisser PS, Grauls G, Bruggeman CA, Vink C. Deletion of the R78 G Protein-Coupled Receptor Gene from Rat Cytomegalovirus Results in an Attenuated, Syncytium-Inducing Mutant Strain. Journal of Virology. 1999 Sept;73(9):7218–30.

459. Kreklywich CN, Smith PP, Jones CB, Cornea A, Orloff SL, Streblow DN. Fluorescence-based laser capture microscopy technology facilitates identification of critical in vivo cytomegalovirus transcriptional programs. Methods Mol Biol. 2014;1119:217–37.

460. Streblow DN, van Cleef KWR, Kreklywich CN, Meyer C, Smith P, Defilippis V, et al. Rat Cytomegalovirus Gene Expression in Cardiac Allograft Recipients Is Tissue Specific and Does Not Parallel the Profiles Detected In Vitro. J Virol. 2007 Apr;81(8):3816–26.

461. Bittencourt FM, Wu SE, Bridges JP, Miller WE. The M33 G Protein-Coupled Receptor Encoded by Murine Cytomegalovirus Is Dispensable for Hematogenous Dissemination but Is Required for Growth within the Salivary Gland. Journal of Virology. 2014 Oct 15;88(20):11811–24.

462. Yunis J, Farrell HE, Bruce K, Lawler C, Sidenius S, Wyer O, et al. Murine cytomegalovirus degrades MHC class II to colonize the salivary glands. PLOS Pathogens. 2018 Feb 15;14(2):e1006905.

463. Buxton BF, Jones CR, Molenaar P, Summers RJ. Characterization and autoradiographic localization of beta-adrenoceptor subtypes in human cardiac tissues. Br J Pharmacol. 1987 Oct;92(2):299–310.

464. Cheng F, McLaughlin PJ, Verderame MF, Zagon IS. Dependence on Nuclear Localization Signals of the Opioid Growth Factor Receptor in the Regulation of Cell Proliferation. Exp Biol Med (Maywood). 2009 May 1;234(5):532–41.

465. Wang L, Wang Z, Yang B, Yang Q, Wang L, Sun Y. CXCR4 nuclear localization follows binding of its ligand SDF-1 and occurs in metastatic but not primary renal cell carcinoma. Oncology Reports. 2009 Dec 1;22(6):1333–9.

466. Speetjens FM, Liefers GJ, Korbee CJ, Mesker WE, van de Velde CJH, van Vlierberghe RL, et al. Nuclear Localization of CXCR4 Determines Prognosis for Colorectal Cancer Patients. Cancer Microenvironment. 2009 Dec 1;2(1):1–7.

467. Jones IKA, Haese NN, Gatault P, Streblow ZJ, Andoh TF, Denton M, et al. Rat Cytomegalovirus Virion-Associated Proteins R131 and R129 Are Necessary for Infection of Macrophages and Dendritic Cells. Pathogens. 2020 Nov;9(11):963.

468. Rovati GE, Capra V, Neubig RR. The highly conserved DRY motif of class A G protein-coupled receptors: beyond the ground state. Mol Pharmacol. 2007 Apr;71(4):959–64.

469. Saidak Z, Blake-Palmer K, Hay DL, Northup JK, Glass M. Differential activation of G-proteins by mu-opioid receptor agonists. Br J Pharmacol. 2006 Mar;147(6):671–80.

470. Tobin AB, Butcher AJ, Kong KC. Location, location, location...site-specific GPCR phosphorylation offers a mechanism for cell-type-specific signalling. Trends Pharmacol Sci. 2008 Aug;29(8):413–20.

471. Schwartz TW, Frimurer TM, Holst B, Rosenkilde MM, Elling CE. Molecular mechanism of 7TM receptor activation--a global toggle switch model. Annu Rev Pharmacol Toxicol. 2006;46:481–519.

472. Auger GA, Pease JE, Shen X, Xanthou G, Barker MD. Alanine scanning mutagenesis of CCR3 reveals that the three intracellular loops are essential for functional receptor expression. European Journal of Immunology. 2002;32(4):1052–8.

473. Bhosle VK, Rivera JC, Chemtob S. New insights into mechanisms of nuclear translocation of G-protein coupled receptors. Small GTPases. 2017 Feb 10;10(4):254–63.

474. Allen BG, Merlen C, Branco AF, Pétrin D, Hébert TE. Understanding the impact of nuclear-localized GPCRs on cellular signalling. Cellular Signalling. 2024 Nov 1;123:111358.

475. Xu Z, Li P, Wei D, Wang Z, Bao Y, Sun J, et al. NMMHC-IIA-dependent nuclear location of CXCR4 promotes migration and invasion in renal cell carcinoma. Oncology Reports. 2016 Nov 1;36(5):2681–8.

476. Jensen D, Zhang Z, Flynn FW. Trafficking of tachykinin neurokinin 3 receptor to nuclei of neurons in the paraventricular nucleus of the hypothalamus following osmotic challenge. Neuroscience. 2008 July 31;155(1):308–16.

477. Kang J, Shi Y, Xiang B, Qu B, Su W, Zhu M, et al. A Nuclear Function of β-Arrestin1 in GPCR Signaling: Regulation of Histone Acetylation and Gene Transcription. Cell. 2005 Dec 2;123(5):833–47.

478. Vaniotis G, Allen BG, Hébert TE. Nuclear GPCRs in cardiomyocytes: an insider's view of β-adrenergic receptor signaling. American Journal of Physiology-Heart and Circulatory Physiology. 2011 Nov;301(5):H1754–64.

479. Tadevosyan A, Vaniotis G, Allen BG, Hébert TE, Nattel S. G protein-coupled receptor signalling in the cardiac nuclear membrane: evidence and possible roles in physiological and pathophysiological function. The Journal of Physiology. 2012;590(6):1313–30.

480. Joyal JS, Nim S, Zhu T, Sitaras N, Rivera JC, Shao Z, et al. Subcellular localization of coagulation factor II receptor-like 1 in neurons governs angiogenesis. Nat Med. 2014 Oct;20(10):1165–73.

481. Kadota S, Ou J, Shi Y, Lee JT, Sun J, Yildirim E. Nucleoporin 153 links nuclear pore complex to chromatin architecture by mediating CTCF and cohesin binding. Nat Commun. 2020 May 25;11(1):2606.

482. Huang P, Zhang X, Cheng Z, Wang X, Miao Y, Huang G, et al. The nuclear pore Y-complex functions as a platform for transcriptional regulation of FLOWERING LOCUS C in Arabidopsis. Plant Cell. 2023 Oct 25;36(2):346–66.

483. Kuhn TM, Capelson M. Nuclear Pore Proteins in Regulation of Chromatin State. Cells. 2019 Nov 9;8(11):1414.

484. Brickner JH. The nuclear pore complex as a platform for epigenetic regulation. Journal of Cell Biology. 2023 Aug 21;222(9):e202307078.

485. Luo MH, Rosenke K, Czornak K, Fortunato EA. Human Cytomegalovirus Disrupts both Ataxia Telangiectasia Mutated Protein (ATM)- and ATM-Rad3-Related Kinase-Mediated DNA Damage Responses during Lytic Infection. Journal of Virology. 2007 Feb 15;81(4):1934–50.

486. Shen YH, Utama B, Wang J, Raveendran M, Senthil D, Waldman WJ, et al. Human Cytomegalovirus Causes Endothelial Injury Through the Ataxia Telangiectasia Mutant and p53 DNA Damage Signaling Pathways. Circulation Research. 2004 May 28;94(10):1310–7.

487. van Domselaar R, de Poot S a. H, Remmerswaal EBM, Lai KW, ten Berge IJM, Bovenschen N. Granzyme M targets host cell hnRNP K that is essential for human cytomegalovirus replication. Cell Death Differ. 2013 Mar;20(3):419–29.

488. Pastor F, Shkreta L, Chabot B, Durantel D, Salvetti A. Interplay Between CMGC Kinases Targeting SR Proteins and Viral Replication: Splicing and Beyond. Front Microbiol [Internet]. 2021 Mar 29 [cited 2025 May 13];12. Available from: https://www.frontiersin.org/journals/microbiology/articles/10.3389/fmicb.2021.658721/full

489. Gaddy CE, Wong DS, Markowitz-Shulman A, Colberg-Poley AM. Regulation of the subcellular distribution of key cellular RNA-processing factors during permissive human cytomegalovirus infection. Journal of General Virology. 2010;91(6):1547–59.

490. Lischka P, Toth ,Zsolt, Thomas ,Marco, Mueller ,Regina, and Stamminger T. The UL69 Transactivator Protein of Human Cytomegalovirus Interacts with DEXD/H-Box RNA Helicase UAP56 To Promote Cytoplasmic Accumulation of Unspliced RNA. Molecular and Cellular Biology. 2006 Mar 1;26(5):1631–43.

491. Toth Z, Lischka P, Stamminger T. RNA-binding of the human cytomegalovirus transactivator protein UL69, mediated by arginine-rich motifs, is not required for nuclear export of unspliced RNA. Nucleic Acids Research. 2006 Feb 1;34(4):1237–49.

492. Winkler M, Rice SA, Stamminger T. UL69 of human cytomegalovirus, an open reading frame with homology to ICP27 of herpes simplex virus, encodes a transactivator of gene expression. Journal of Virology. 1994 June;68(6):3943–54.

493. Bhosle VK, Rivera JC, Zhou TE, Omri S, Sanchez M, Hamel D, et al. Erratum: Nuclear localization of platelet-activating factor receptor controls retinal neovascularization. Cell Discov. 2016;2:16034.

494. Tyanova S, Temu T, Sinitcyn P, Carlson A, Hein MY, Geiger T, et al. The Perseus computational platform for comprehensive analysis of (prote)omics data. Nat Methods. 2016 Sept;13(9):731–40.